CURTIN UNIVERSITY

Modelling Metal Complexation in Solvent Extraction Systems

by

Sergey Lunkov

A thesis submitted in partial fulfillment for the
degree of Doctor of Philosophy

in the
Faculty of Science and Engineering
Department of Chemistry

October 2013

Declaration of Authorship

I, Sergey Lunkov, declare that this thesis titled, 'Modelling Metal Complexation in Synergistic Solvent Extraction Systems' and the work presented in it are my own. To the best of my knowledge and belief this thesis contains no material previously published by any other person except where due acknowledgement has been made. This thesis contains no material which has been accepted for the award of any other degree or diploma in any university. I confirm that:

- This work was done wholly or mainly while in candidature for a research degree at this University.
- Where any part of this thesis has previously been submitted for a degree or any other qualification at this University or any other institution, this has been clearly stated.
- Where I have consulted the published work of others, this is always clearly attributed.
- Where I have quoted from the work of others, the source is always given. With the exception of such quotations, this thesis is entirely my own work.
- I have acknowledged all main sources of help.
- Where the thesis is based on work done by myself jointly with others, I have made clear exactly what was done by others and what I have contributed myself.

Signed: _____

Date: _____

"Knowledge is knowing a tomato is a fruit; Wisdom is not putting it in a fruit salad."

Brian Gerald O'Driscoll

CURTIN UNIVERSITY

Abstract

Faculty of Science and Engineering

Department of Chemistry

Doctor of Philosophy

by Sergey Lunkov

Quantum mechanical studies of the Z/E acetoin oxime interconversion have been conducted using both density functional theory (DFT) and *ab initio* post-Hartree-Fock methods in order to understand the thermodynamic and kinetic properties of the *syn/anti* isomerisation of 5,8-diethyl-7-hydroxydodecan-6-oxime. This molecule is the active reagent in LIX63, a commercial material used in hydrometallurgical solvent extraction (SX). Based on calculated data and experimental results, for Z/E 5,8-diethyl-7-hydroxydodecan-6-oxime interconversion and the IR spectra of its pure *anti* isomer, it has been shown that the active reagent in LIX63 favours an oligomeric form. Theoretically, it has been found that higher order oligomers are energetically more favourable. Based on this it has been suggested that at high concentrations hydroxyoximes exist in the form of polymeric rings and/or chains.

The effect of different R groups on the thermodynamic and kinetic properties of aliphatic α-hydroxyoxime *syn/anti* interconversion has also been studied. Theoretically, it has been shown that using R=C_3H_8 on both ends of the oxime is the minimum substituent size required to obtain a good description of thermodynamics and kinetics in comparison to experimental data for LIX63. Further increases in the size of the R group does not have any significant effect on either thermodynamics or kinetics of the *syn/anti* isomerisation (except via an inversion mechanism, where the effect of the size of the hydrocarbon side-chain is still quite significant in going from R=C_2H_5 to R=C_3H_8).

Lastly, potential energy surfaces of Ni^{2+}, Co^{2+}, Cu^{2+}, Zn^{2+} and Mn^{2+} transition metal complexes with acetoin oxime and acetic acid have been studied at the M06/6-31G(d,p)/LanL2DZ level of theory using different stoichiometries. The theoretically determined order in which metal ions are extracted agrees well with experiment for the case when 1:2:2 metal:hydroxyoxime:carboxylic acid complexes are formed. The synergistic effect of addition of hydroxyoxime to the system of metal ions and carboxylic acid has been shown. The theoretically determined lowest energy conformation for the Ni:hydroxyoxime:carboxylic acid 1:2:2 stoichiometry complex agrees well with that observed experimentally.

Acknowledgements

This thesis is built on the shoulders of more people than I could ever name in this space, for I feel I should thank all of the people who have had a hand in shaping my intellectual and personal growth to this point. However, I would be remiss if I did not single out a few people for special thanks.

I thank my main supervisor and first reader, Prof. Julian Gale from the Department of Chemistry at Curtin University, for encouraging me to be strategic at all times, for constantly feeding me with the most useful ideas and advice without which my thesis would not be even half as good as it is and for inviting me to be part of the project that introduced me to The Parker Cooperative Research Centre for Integrated Hydrometallurgy Solutions in the first place. Thank you to Prof. Kate Wright, my co-supervisor, for putting me on a track that turned scattered ideas and observations into a single thesis. To Dr. Keith Barnard, my associate supervisor and second reader from the Parker Centre, who provided us with the latest experimental data on the synergistic solvent extraction of transition metal ions with the mixture of LIX63 hydroxyoxime and Versatic10 carboxylic acid. To Prof. Mark Ogden, my chairperson from the Department of Chemistry at Curtin University, who pointed out some key points in studying hydroxyoxime oligomerisation and provided me with the facilities for analysing the IR spectra of the *anti* isomer of LIX63 hydroxyoximme. A big thank you to the iVEC and National Computational Infrastructure (NCI) for giving me chance to use their facilities and providing me with an impressive amount of computing time without which it would not be possible to perform all these calculations.

I would like to express my great appreciations to my family and friends for their inspiration and support. I gratefully acknowledge the financial support from Curtin University and Parker Centre.

Finally I would like to thank Curtin University for its existence as without it I would not have met all these great people and spent this wonderful time of conducting such exciting research.

Contents

List of Figures

List of Tables

Abbreviations

ACM	**A**diabatic **C**onnection **M**ethod
B3LYP	**B**ecke **3**-parameter **L**ee, **Y**ang and **P**arr
CC	**C**oupled-**C**luster
CI	**C**onfiguration-**I**nteraction
CSIRO	**C**ommonwealth **S**cientific and **I**ndustrial **R**esearch **O**rganisation
DFT	**D**ensity **F**unctional **T**heory
FF	**F**orce **F**ields
GGA	**G**eneralised **G**radient **A**pproximation
HF	**H**artree-**F**ock
HOMO	**H**ighest **O**ccupied **M**olecular **O**ebital
IRC	**I**ntrinsic **R**eaction **C**oordinates
LDA	**L**ocal **D**ensity **A**pproximation
LSDA	**L**ocal **S**pin **D**ensity **A**pproximation
LUMO	**L**owest **U**noccupied **M**olecular **O**ebital
MM	**M**olecular **M**echanics
MPn	**M**øller-**P**lesset
NCI	**N**ational **C**omputational **I**nfrastructure
PCM	**P**olarisable **C**ontinuum **M**odel
PES	**P**otential **E**nergy **S**urface
QM	**Q**uantum **M**echanics
SCF	**S**elf-**C**onsistent **F**ield
SX	**S**olvent **E**xtraction
SSX	**S**ynergistic **S**olvent **E**xtraction
TS	**T**ransition **S**tate
UEG	**U**niform **E**lectron **G**as
VWN	**V**osko **W**ilk **N**usair
ZPE	**Z**ero-**P**oint **E**nergy

Physical Constants

Bohr Radius	a_0	$\approx$	0.52917725 Å
Boltzmann's Constant	k_B	$=$	$1.3806503 \times 10^{-23}$ $m^2 kg\ s^{-2} K^{-1}$
Electron Rest Mass	m_e	$=$	$9.10938291(40) \times 10^{-31}$ kg
Elementary Charge	e	$=$	$1.602176565(35) \times 10^{-19}$ C
Gas Constant	R	$\approx$	8.3144621(75) J $mol^{-1} K^{-1}$
Planck's Constant	h	$=$	6.626068×10^{-34} $m^2 kg\ s^{-1}$
Pi	π	$=$	3.14159265359

Symbols

E^o	Total electronic energy	a.u.
G_v^T	Vibrational Gibbs free energy correction at temperature T	a.u.
$\Delta \mathrm{G}^{\mathrm{T}}$	Gibbs free energy difference at temperature T	kJ mol^{-1}
H_v^T	Vibrational enthalpy correction at temperature T	a.u.
$\Delta \mathrm{H}^{\mathrm{T}}$	Enthalpy difference at temperature T	kJ mol^{-1}
k_b	Rate constant for backward reaction	s^{-1}
K_{eq}	Equilibrium constant	
k_f	Rate constant for forward reaction	s^{-1}
P	Probability distribution	%
S_v^T	Vibrational entropy correction at temperature T	cal $\mathrm{mol}^{-1}\mathrm{K}^{-1}$
$\Delta \mathrm{S}^{\mathrm{T}}$	Entropy difference at temperature T	kJ $\mathrm{mol}^{-1}\mathrm{K}^{-1}$
T	Temperature	K
ZPE_v	Zero-point vibrational energy	a.u.

Dedicated to my grandmother, Anna Sirotkina, who was giving me the best possible life education and experience throughout the first twelve years of my life...

Chapter 1

Solvent Extraction

1.1 Introduction

The first ever metals produced by humans were tin and lead, followed by copper, bronze (copper with tin and/or arsenic) and iron (Radivojevic *et al.*, 2010). The ability to produce metals from their ores resulted in a serious impact on the evolution of mankind by giving a fantastic opportunity to produce better construction materials, tools used in everyday life, weapons etc. Co and Ni, in particular, are highly consumed transition metals in modern heavy industry due to their ferromagnetic properties and catalytic behaviour. The area of consumption of these metals is very broad, which includes applications in catalysis, production of building materials and electronics, the petroleum industry etc. It is interesting to note, that the biggest natural source for industrial nickel and cobalt production is laterite ore, followed by sulphide ore and sea nodules[1] (Moskalyk and Alfantazi, 2002). Laterite ore can be found in many different places around the world. The largest lateritic deposits are located in New Caledonia, Cuba, Indonesia, the Philippines and Australia (mostly in the western part of the continent). However, this type of ore has a complicated multi-component composition including salts and oxides of many different metal species, which makes the separation of specific metal ions extremely challenging. The field of science studying the processes of metal extraction from its natural sources and its following recovery is called extractive metallurgy (Ray and Ghosh, 1991). Mastering metallurgy processes made it possible to produce a large range of different metals. Constantly rising demand for the high purity of these metals became a driving force for the future development of extractive metallurgy in general (Seetharaman, 2005).

[1]Note that the sea nodules is the potential source for industrial nickel and cobalt production and not necessarily the one which is currently being exploited.

1.2 Overview of Extractive Metallurgy

Ore is the main natural source for the industrial production of metals (Fuerstenau and Han, 2003). Ore can be defined as the rocky material containing oxides, carbonates, sulphides, silicates and/or arsenides of different metal species. Briefly describing the process of metal recovery from the ore/gangue one could say that the metal species (oxides, sulphides and/or carbonates) of interest must be first purified/separated and then reduced to a pure metal species using chemical, physical or electro-winning reduction processes. The area of extractive metallurgy that achieves the first part of metal recovery when the desired metal compounds need to be purified/separated is called minerals processing (Napier-Munn, 1997; Seetharaman, 2005). It should be stressed here that ore is a complex mixture of solid compounds and may contain combinations of them; however, it is well known (Seetharaman, 2005) that it is easier to process metal compounds and to free the metal when this compound presents itself as an oxide. Generally there are two main metal recovery routes available in extractive metallurgy. These differ from each other in the way the metal ores are converted into a form for which further treatment is more straightforward and how they are purified/separated (see below - refining and extraction). It should be noted that there is no clear distinction between some sub-categories of these two methods and some industrial processes of extractive metallurgy may contain both hydrometallurgical and pyrometallurgical processes.

In minerals processing the ore is first crushed into small pieces. This stage of a process is called comminution (Fuerstenan and Han, 2003). Comminution is a physical process achieved using different types of crushing/grinding equipment, such as a jaw crusher, ball mill etc., therefore the chemical composition during the crushing stage is not being changed. In the next stage of minerals processing, which is called sizing, ore pieces of a certain size are separated from the others. After sizing each of the small ore pieces produced contains a higher percentage of oxide or sulphide of a metal species. Sizing can be performed using either a dry method or in aqueous solution. Screening is one of the most general dry ways of sizing ore pieces. The most common way to concentrate the ore particles from solution is based on the differences in their physical properties such as density or mass[2], for example. Along with physical properties, this stage of the concentration in minerals processing can also be based on surface properties (froth flotation[3]) or electrostatic (high tension rollers or electrostatic separators) and/or magnetic separation (high gradient magnetic separation or high/low intensity magnetic separation) of ore particles (Meloy, 1983; Seetharaman, 2005).

[2]Denser particles will settle quicker than the lighter ones.

[3]The hydrophobic particles mixed in water are attracted to the surface of bubbles introduced to the system. In order to improve the selectivity of froth flotation, different chemicals (collectors) are often used.

In pyrometallurgy, thermal treatment is used in order to extract metals from minerals. The pyrometallurgical process of metals' recovery from ores normally consists of the following stages (Ray and Ghosh, 1991):

1. Drying. At this stage the input minerals are dried using hot air.
2. Calcining. At the calcining stage, dry materials, such as carbonates or hydrated minerals (if present) are decomposed using thermal treatment[4]. Originally the calcining process was used to decompose limestone (calcium carbonate) to lime (calcium oxide) and carbon dioxide; however, in ore processing it is normally applied in order to get rid of crystalline water.
3. Roasting. Depending on the nature of the ore, different types of gas-solid reactions (pyrohydrolysis, oxidation, reduction, sulphation etc.) are involved in order to purify metal compounds. Generally roasting is applied in order to purify the sulphides of different metals, which is achieved via an oxidation gas-solid reaction at a certain temperature[5]. A balanced equation for metal (M^{2+}) sulphide roasting (oxidation) can be represented as follows:

$$2MS_{(s)} + 3O_{2(g)} \rightarrow 2MO_{(s)} + 2SO_{2(g)}$$

As can be seen from the above equation, sulphur dioxide is emitted as a co-product in roasting. This gas is harmful for the environment and usually absorbed using limestone (Fuerstenan and Han, 2003; Roy and Weisweiler, 1982):
Calcination

$$CaCO_{3(s)} \rightleftarrows CaO_{(s)} + CO_{2(g)}$$

Sulphation

$$CaO_{(s)} + SO_{2(g)} \rightleftarrows CaSO_{3(s)}$$

$$4CaO_{(s)} + 4SO_{2(g)} \rightleftarrows CaS_{(s)} + 3CaSO_{4(s)}$$

However, in some cases the sulphur dioxide produced is used directly for sulphuric acid production (King, 1950).
4. Smelting. Metal oxides are reduced to pure metals in this type of pyrometallurgical process using thermal treatment at temperatures usually, but not always, above the melting points of some metals, at a very low partial pressure of oxygen (in an air-starved environment) and in the presence of carbon monoxide as the reducing agent.
5. Refining. Refining is a method of purification of metal compounds that can be based on either pyrometallurgical or hydrometallurgical techniques. The choice

[4]The temperature is usually set below the melting point of the material
[5]The choice of temperature is normally defined by the kind of metal compound to be purified.

of technique may vary with respect to the metal compound to be purified. For instance, in order to clean up copper containing compounds, fire refining and/or electrolytic refining can be used (Ibl, 1977).

In Figure 1.1 a schematic sequence of processes used in pyrometallurgical recovery of FeNi from laterite ore is depicted.

FIGURE 1.1: Schematic representation of a typical pyrometallurgical process for ferronickel recovery from laterite ore.

The first row transition metals, in particular chromium, manganese, cobalt, nickel, copper and zinc, are heavily consumed in industry due to their ferromagnetic properties and catalytic behaviour (Deeth, 1995; Gibson, 1997; House, 2008). In general, pyro routes are chosen when the source of metals corresponds to the system of metal sulphides, while metal oxides are preferably treated by hydrometallurgical techniques. Hydrometallurgical techniques are more effective and environmentally friendly, however, in some cases may be not as economic as the pyrometallurgical ones. In hydrometallurgy the ore is collected and treated to liberate the metal ion(s) of interest into an aqueous solution before subsequent recovery. The stage of the hydrometallurgical process during which metal compounds contained in the ore are dissolved in aqueous solution is called leaching. Depending on the ore composition (the nature of metal compounds) different types of leaching agents (solvents) can be used. On an industrial scale the most commonly used solvents are sulphuric and hydrochloric acids, sodium and aluminium carbonates, sodium hydroxide, ammonia and cyanides (Bouffard and Dixon, 2007; Luo *et al.*, 2010; Mattus and Torma, 1980; Santos *et al.*, 2010). It is important to note, however, that ore

consisting of metal sulphides is either not or hardly dissolved by these solvents. Therefore, for this type of ore, roasting or pressure oxidation is normally performed prior to the leaching stage in order to convert metal sulphides to the metal oxides (Habashi, 2005).

There are many different types of leaching process available in hydrometallurgy such us thin layer, dump, heap, *in-situ* leaching etc (Dutrizac, 1992; Ray and Ghosh, 1991). In general, looking at the conditions at which all these types of leaching are carried out, they can be divided into two main groups; simple leaching operated at normal conditions and pressure leaching (Dutrizac, 1992)[6].

Metal salts (sulphates in the case of sulphuric acid aqueous solution being used for ore leaching) dissolved in aqueous solution are then separated prior to the electrowinning process (the stage of pure metal recovery) using one of the available techniques, such as solvent extraction or ion exchange (Mooiman *et al.*, 2005). A schematic representation of the hydrometallurgical metal recovery process, including the stage of solvent extraction[7] for metal cation separation, is depicted in Figure 1.2.

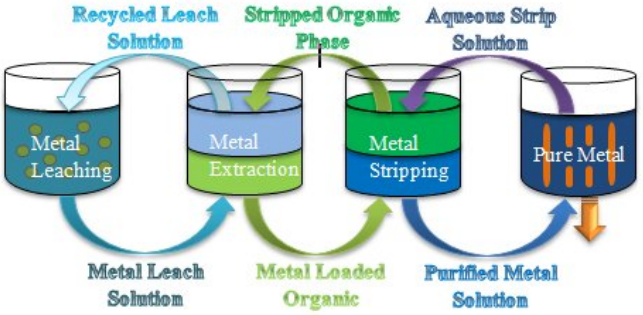

FIGURE 1.2: Hydrometallurgical scheme for the metal recovery process incorporating the stage of solvent extraction for metal cation purification.

Solvent extraction is hydrometallurgical process of metal recovery and it is the main focus of the current study; therefore, further discussion of the background will be focussed on this specific aspect in order to better understand the specificity of metal complexation processes towards which our theoretical investigation is targeted.

[6]Pressure leaching is operated in autoclaves and normally used in order to improve the solubility of hardly soluble metal compounds.

[7]The solvent extraction stage is composed of two sub-stages: metal extraction and metal stripping.

1.3 Solvent Extraction

Solvent extraction is a method for compound separation based on their relative solubility in two different immiscible liquids (Rydberg *et al.*, 2004). As stated above, in hydrometallurgy this process is used in order to separate/purify desired metal species from gangue by extracting them from the aqueous into the organic phase[8]. During the leaching stage, metal compounds contained in the ore are transferred into aqueous solution and in order to separate metal ions from each other this aqueous solution is contacted with an organic phase (usually kerosene-based) containing an extractant that selectively extracts one or more of the metal ions from the aqueous solution. Metal extraction from the aqueous into the organic phase is achieved via metal complex formation between the metal cation(s) of interest and the extractant.

To be able to model the process of metal complexation we have to understand the mechanism of metal extraction and the first thing to do in order to achieve this goal would be to look at how the solvation of the metal cations is achieved in aqueous solution. In particular, we need to know the forms of these metal cations present in aqueous solution at the molecular level.

Let us consider the situation when the ore compounds have been leached with sulphuric acid solution converting metal oxides into the metal sulphates. Metal sulphates are electrolytes which means that they dissociate in water producing metal cations and sulphate anions. This leads us to consider the process of solvation of each ion separately, so that when the metal sulphate is dissolved in water each ion of this electrolyte has its own hydration shell (Wander *et al.*, 2010). Let us now consider the structure of hydrated metal cations in more detail. Water molecules directly bond to the metal cation via dative covalent bonding to form the first solvation shell[9]. The second solvation shell is formed by other water molecules (up to 12 water molecules for the metal cations with a coordination number of 6 in the first shell) attached to the coordinated water molecules via hydrogen bonding. A graphical representation of the first and second solvation shells of an M^{3+} cation dissolved in water is depicted in Figure 1.3

[8]Note that the opposite process, when the metal species of interest are left in aqueous solution and undesired ones extracted into the organic phase, is also possible and quite often applied at the industrial scale of metal recovery.

[9]The first solvation shell of all 2+ and 3+ first row transition elements has a regular octahedral structure except Cu^{2+} and high-spin Cr^{2+} complexes where the Jahn-Teller distortion takes place (Burdett, 1981).

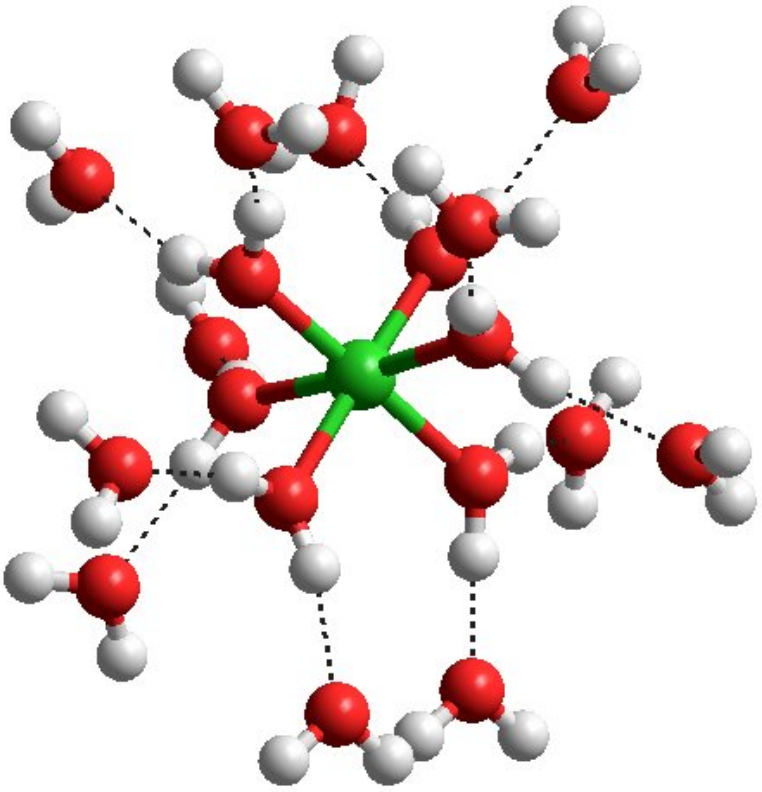

FIGURE 1.3: First and second solvation shells of M^{3+} cation dissolved in water. Atom colours: oxygen (O) - red; hydrogen (H) - white and metal cation (M) - green.

It is very important to note that the formation of the second solvation shell may be different from that presented in Figure 1.3 for metal cations with a charge of +1 and/or +2. Water molecules in the first hydration shell may not be sufficiently polarised by these charges (+1 or +2) in order to form strong hydrogen bonds with the second layer water molecules and a certain level of disorder in hydrogen bonding between first and second solvation shells should be expected for hydrated +1 and/or +2 metal cations (Atta-Fynn *et al.*, 2011; Sakane *et al.*, 1998). In general it could be stated that the larger the charge on a metal cation, the stronger the water molecules from the first hydration shell are coordinated to it and the stronger the hydrogen bonding between these water molecules and those from the second hydration shells or bulk water will be. Experimentally it was derived (Kristiansson, 1989) that the strength of coordination between the metal cation and the oxygen of a water molecule is proportional to the ratio of $\frac{Z}{r}$, where Z is the effective charge and r is the effective radius of a metal cation. A list of experimental hydration enthalpies (kJ/mol) of the first row transition metal cations (Uudsemaa and

Tamm, 2004) is shown in Table 1.1.

TABLE 1.1: Experimental hydration enthalpies (kJ/mol) for selected oxidation states of the first row transition metal cations. Modified from Uudsemaa and Tamm (2004).

Ti^{2+}	V^{2+}	Cr^{2+}	Mn^{2+}	Fe^{2+}	Co^{2+}	Ni^{2+}	Cu^{2+}
1862	-1918	-1904	-1841	-1946	-1996	-2105	-2100

Sc^{3+}	Ti^{3+}	V^{3+}	Cr^{3+}	Mn^{3+}	Fe^{3+}	Co^{3+}
-3960	-4154	-4375	-4560	-4544	-4430	-4651

It is also interesting to note that the water molecules directly bonded to the metal cation are not always held in one position and often are exchanged with the water molecules from the second hydration shell or with the bulk solvent, which may not be necessarily the water, and the rate of this exchange also depends on the $\frac{Z}{r}$ ratio.

According to solvation theory (Birkholz, 1992), the process of metal salt dissolution consists of three stages; in two stages free energy is consumed and from one stage free energy is released. First of all some energy is required in order to free the ions from the crystalline salt. This energy is called the lattice Gibbs free energy and it is equal to the free energy of salt dissociation into ions in the gas phase. Secondly, a certain amount of free energy should be spent in order to create a large enough cavity in the water for the solute ions to be accommodated. In other words, this energy is required for breaking the solvent-solvent attraction, which in case of hydration is usually related to the Gibbs free energy required for breaking hydrogen bonds and for covering the entropic penalty for ordering of solvent molecules. Lastly, free energy is released when the ions are introduced to the cavity and bound to water. To estimate the Gibbs free energy required for metal salt dissolution we need to sum up all three values of the free energy. The resulting energy is called the standard molar Gibbs free energy change of solution, which is usually measured in kJ/mol and has a large negative value for readily soluble compounds. In order to determine the standard molar Gibbs free energy of hydration of a given metal cation experimentally one must compare the thermodynamics for the hydration of salts with different cations and the same anion and vice versa, because it is impossible to measure the free energy of hydration for each ion separately by direct means. However, in order to estimate it theoretically we only need to consider the thermodynamics of the following single reaction;

$$M^{x+}_{(g)} \rightleftarrows M^{x+}_{(aq)}$$

In this reaction a gaseous metal cation is transferred into the aqueous phase.

It is well known that in solvent extraction, metal extraction is achieved via metal complexation with the extractant introduced into the system. In general, the process of inner-sphere metal complex formation can be described as a substitution reaction where the water molecules from the first hydration shell of a metal cation are replaced with extractant molecules (Fishtik, 1989; Rydberg *et al.*, 2004). This mechanism can be represented by the following reaction;

$$\mathrm{M}^{x+}_{(aq)} + \mathrm{nL}^{y-}_{(aq)} \rightleftarrows [\mathrm{ML_n}]^{(x-ny)+}_{(aq)}$$
$$[\mathrm{ML_n}]^{(x-ny)+}_{(aq)} \rightleftarrows [\mathrm{ML_n}]^{(x-ny)+}_{(org)}$$

As will be shown in latter results sections, it is possible to estimate the change of the standard Gibbs free energy for complex formation by comparing the corrected Gibbs free energies of the reagents (M and L) and product(s) (ML_n), calculated using modern computational chemistry methods based on the laws of quantum mechanics (for more background information see the following chapter) and statistical thermodynamics. Knowing the change of the standard Gibbs free energy for the metal complexation process, an equilibrium constant can be estimated using the following equation[10];

$$\Delta \mathrm{G}^o = -2.303 \cdot RT \cdot \log_{10} K_{eq} \tag{1.1}$$

where R - is the universal gas constant, T is the temperature and K_{eq} is an equilibrium constant which has the form of;

$$K_{eq} = \frac{[\mathrm{ML_n}]}{[\mathrm{M}][\mathrm{L}]^n} \tag{1.2}$$

for the metal extraction equilibrium given above. It should be noted that this equilibrium for product formation is simplified and in comprehensive form should be written as a multi stage process (Rydberg *et al.*, 2004). This includes the stage of extractant deprotonation, because, according to Bjerrum (1941), the process of metal complexation should be considered as a form of acid-base equilibrium where the metal cation substitutes for the hydrogen atom of an extractant (ligand L):

[10] In $\frac{\mathrm{kJ}}{\mathrm{mol}}$ $\Delta \mathrm{G}^o = -5.708 \cdot \log_{10} K_{eq}$ at $T = 298.15\mathrm{K}$.

$$\begin{array}{ccc} \mathrm{LH}_{(org)} & \rightleftarrows & \mathrm{L}^{-}_{(aq)} + \mathrm{H}^{+}_{(aq)} \\ [\mathrm{M(H_2O)_{n(}}_{aq)}] + \mathrm{L}^{-}_{(aq)} & \rightleftarrows & [\mathrm{M(H_2O)_{n\text{-}1}L}_{(aq)}] + \mathrm{H_2O}_{(aq)} \\ & \vdots & \\ [\mathrm{M(H_2O)L_{n\text{-}1(}}_{aq)}] + \mathrm{L}^{-}_{(aq)} & \rightleftarrows & [\mathrm{ML_{n(}}_{aq)}] + \mathrm{H_2O}_{(aq)} \\ [\mathrm{ML_{n(}}_{aq)}] & \rightleftarrows & [\mathrm{ML_{n(}}_{org)}] \end{array} \tag{1.3}$$

Sometimes in order to improve the efficiency of the metal selectivity and increase the value of an equilibrium constant two or more different kinds of ligands are introduced (see subsection 1.3.2 on synergistic solvent extraction). However, in some cases (like for instance in case of LIX63/Versatic10 SSX) it is unclear even experimentally how the metal complexation is achieved (which component loses its proton and plays the role of an extractant and which is a synergist). Molecular modelling, in this case, allows us to inspect the change of the standard Gibbs free energy for each stage of the complex formation with different types of ligands (synergist/extractant) being put in different geometrical positions, which may provide us with some valuable insights as to the mechanism of metal complexation.

From an industrial perspective, it is also important to understand the chemistry of an extraction process with selected extractant(s) in order to find the optimal conditions for the process. The conditions of a solvent extraction process are acceptable if the chosen reagent(s) is(are) selective enough, relatively inexpensive and not being decomposed to a great extent, and the level of equipment corrosion is acceptable (Ray and Ghosh, 1991).

1.3.1 Extractants available for the Solvent Extraction of Transition Metals

There is a finite variety of metal extractants available for commercial use for effective metals separation in modern solvent extraction (Rydberg *et al.*, 2004). Nowadays, solvent extraction makes it possible to separate almost any type of metal present in aqueous solution, practically in any combination and any proportion. It is important to note, however, that in some cases even though the technical criteria for the process are achievable due to the large variety of different types of extractants available, there still could be some major drawbacks (related to environmental problems, economical reasons etc.), in which case a more detailed investigation of the process or even the development of a new extractant needs to be undertaken[11]. For example, in one particular case there

[11] The development of a new extractant, which as a matter of fact is supposed to be effective, non-toxic and economically stable, is usually a quite costly process and normally considered as the last resort.

could be a set of suitable extractants available in order to achieve the required goals for metal extraction; however, at the same time it might be impossible to realise solvent extraction with any of these extractants on the industrial scale.

This large variety of different types of metal extractants can be divided into five different classes depending on their nature, the range of extractable metal species and the mechanism of extraction (the structures of both metal compounds and metal extractants are important). These classes are: ion pairing, chelation reagents, solvating, organic acids and ligand substitution (Rydberg *et al.*, 2004).

In ion-pair metal extraction anionic forms of metal compounds $ML_n^{(z-n)}$, where (z-n) ≤ -1, are extracted with various organic amines R_kN (primary - R_1, secondary - R_2, tertiary - R_3 or quaternary - R_4). Anionic metal complexes are formed in aqueous solution of HL, where HL could be $HClO_4, HNO_3, HCl, H_2SO_4, HF$ etc., according to the following equation:

$$\begin{array}{rcl} LH_{(aq)} & \rightleftarrows & L^-_{(aq)} + H^+_{(aq)} \\ M^{z+}_{(aq)} + nL^-_{(aq)} & \rightleftarrows & ML^{(z-n)}_{n(aq)} \end{array} \tag{1.4}$$

It should be noted here that the equilibrium constant for $ML^{(z-n)}_{n(aq)}$ formation depends on the nature of L^- and increases in the order $ClO_4^- < NO_3^- < Cl^- < HSO_4^- < F^-$; therefore, in order to improve the ion-pair extraction of metal ions it is often recommended to substitute less active anions in anionic metal salts with more active ones according to the above sequence. Amine bases R_kN with large linear or branched aliphatic or aromatic R group(s) ($C_8 - C_{12}$) are highly soluble in organic phases and almost insoluble in water. In contact with aqueous solution of HL acid, the organic amines R_kN tend to form $R_kNH^+L^-$ ion-pair salts. Formed anionic metal compound is completed with positively charged ion of the large organic ion-pair compound R_kNH^+ in order to be transferred into the organic phase as a $[ML_n]R_kNH_{(z-n)}$ complex (Kislik, 2011). The order of extraction of anionic metal complexes by amines is decreased in going from quaternary to primary amines[12]. It should be noted, however, that even though ion-pair metal extraction is quite simple and an easy process to operate it is not highly selective.

Chelating reagents are different from the other types of ligands in the way they bind to a metal cation. The Greek translation of the word "chele", from which chelation is derived, is "claw". The extractants of this type are polydentate so that there are at least two ligating atoms bonded to the metal ion (Ferreiros-Martinez *et al.*, 2009). Examples of bi-, tri- and tetra-dentate chelating ligands are depicted in Figure 1.4.

[12]The tertiary and quaternary amines are the most frequently used amines by the industry.

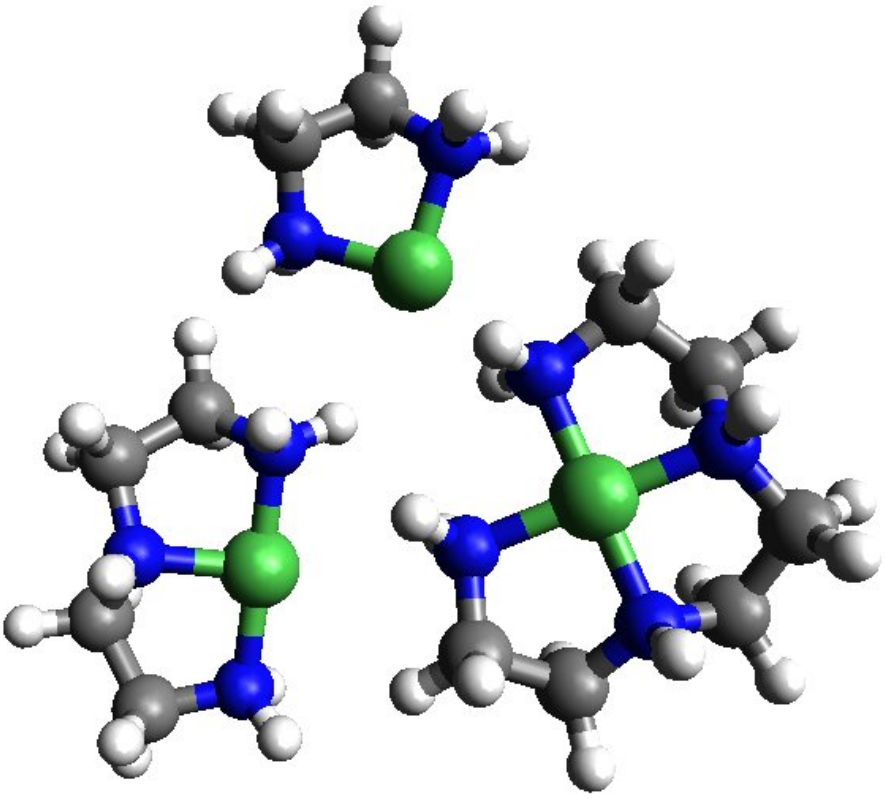

FIGURE 1.4: Examples of binding by polydentate ligands (ethylenediamine - top structure; diethylenetriamine - left bottom structure and triethylenetetramine - right bottom structure) to the metal cation. Metal cation is coloured green, carbon atoms are grey, nitrogen - blue and hydrogen - white.

Bidentate chelating agents were found to perform well in the highly selective separation of transition metal cations. BASF (formerly Cognis Corporation) has developed a whole range of bidentate chelating agents that are commercially available for metal ion solvent extraction (MCT Redbook, 2007), which are well-known under the trade mark of LIX® reagents. These include LIX54/LIX55 (beta-diketone reagents used for copper extraction), LIX63 (aliphatic hydroxyoxime, which can be used in synergistic solvent extraction of transition metals like Co and Ni), LIX26 (alkylated 8-hydroxyquinoline based reagents used for gallium extraction from Bayer liquors), LIX84-I (ketoximes used for copper extraction), LIX84-INS (ketoximes used for nickel extraction from ammonia solutions), LIX87QN (similar to LIX84-INS), LIX860-I (aldoximes used to co-extract copper and zinc), LIX6422-LV (group of extractants based on 5-dodecylsalicylaldoxime used for copper extraction) and LIX 612N-LV and LIX 616N-LV (salicylaldoxime-based extractants used for copper extraction from acidic solutions). The selectivity of different metal extractants with respect to a range of selected metal ions is usually shown by pH isotherms (Figure 1.5).

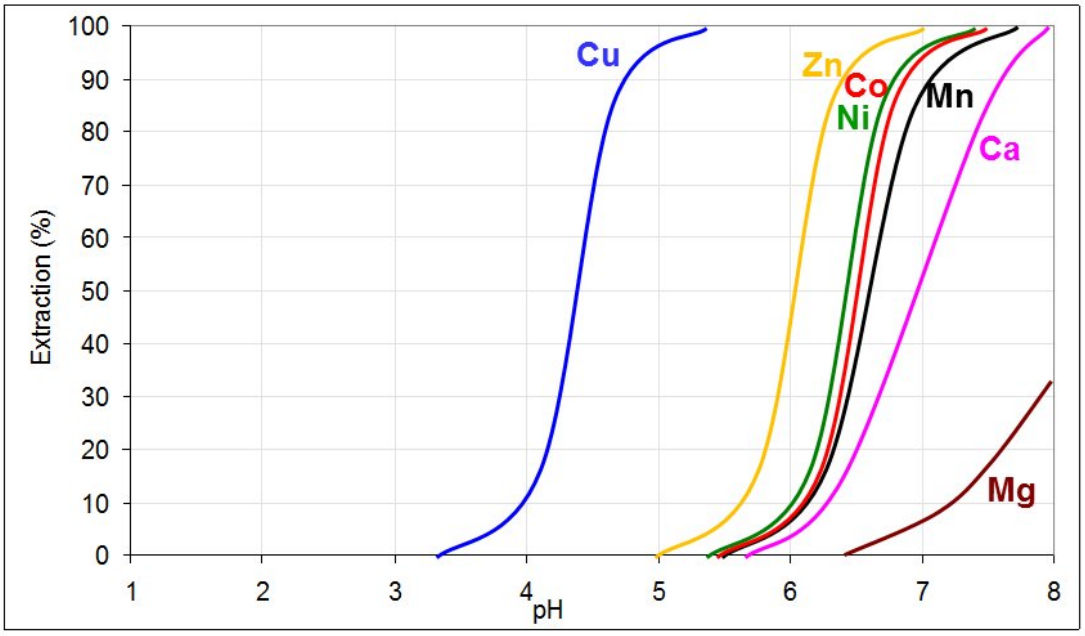

FIGURE 1.5: Extraction pH isotherms of metals with 0.5M Versatic10 acid in Shellsol 2046 and the synthetic laterite leach solution at an aqueous/organic phase ratio of 1:1 and 40^{o}C (modified from Cheng (2006)).

These isotherms are determined at constant temperature operating the extraction process of different metal ions at different pH values[13]. They tell us which metal species and what percentage of them will be extracted from the aqueous into the organic phase if the system is being operated under the chosen level of acidity (pH). It should be noted, however, that the knowledge of initial composition (list of metal species present in aqueous solution) and of the stabilities of each metal complex with respect to others is very important. For instance, if there are two different metal ions X^{n+} and Y^{k+}, and separately each of them is easily extracted using the same reagent at the same pH when they are present together in aqueous solution, it may be possible that only one of the metal ions, say X^{n+}, will be extracted at a chosen pH because it forms a more stable complex with the chosen reagent. For instance, this is seen for Ni extraction over Co in the synergistic system studied by Mayhew *et al.* (2011). In the case when metal ions are co-extracted and they are both needed, but separately, the stripping stage can be adjusted in such a way so that the metal species are stripped and recovered one by one.

[13]It should be noted that the contact time between aqueous and organic phases, as well as the initial concentrations of metal ions and reagent(s)/extractant(s), should be fixed in each run for experimental determination of pH isotherms (MCT Redbook, 2007).

1.3.2 Synergistic Solvent Extraction

In 'normal' solvent extraction (SX) a single active agent is used to separate the metal ions via metal complexation. This active agent is called an extractant or sometimes just a reagent. However, as it was stated above, in case when none of the available reagents perform well enough in separation/purification of some particular metal ions, it could be very difficult and quite costly to develop a new effective extractant. Even if such a component was developed, the market for it may not be great, or the metallurgical industry may be reluctant to modify plants to use it.

Synergistic Solvent Extraction (SSX) is one possible way out of this situation. SSX is the use of one or more additional reagents to improve the selectivity of an existing extractant. If the choice of additional component (synergist) is successful, SSX could have the potential to recover metal ions of interest from aqueous leach solution via Direct Solvent Extraction (DSX), avoiding the need for intermediate precipitation and re-leach steps which are normally done in order to overcome metal selectivity issues in the SX stage (Barnard, 2008; Barnard and Turner, 2008; Cheng, 2006).

The current study will be mostly focussed on the theoretical investigation of the processes occurring in the synergistic solvent extraction/purification of transition metals, in particular cobalt and nickel, from a gangue including magnesium and calcium. As was stated above, the majority of known metal separation processes, such as solvent extraction, ion exchange, pyrolytic extraction, normal/pressure acid leach and solvent extraction/electrowinning processes, suffer from disadvantages including low selectivity, high cost of the extractant and/or precipitation agent used, or the use of harsh conditions (high pressure, high temperature and high acidity). In contrast to all these methods, the newly proposed synergistic solvent extraction technique, consisting of the combined use of LIX63 hydroxyoxime and Versatic10 carboxylic acid, guarantees a high yield and selective extraction of Co, Ni and other transition metals with a lower capital cost (Cheng and Urbani, 2005a,b).

Graphical representation of the synergistic effect of the LIX63/Versatic10 mixture is depicted in Figure 1.6. From the pH isotherms it can be clearly seen that in contrast to SX (Figure 1.5) when an additional component (synergist) is added to the system, the pH isotherms of all elements present in the system are shifted to the left. This makes the process separation of Zn, Cu, Co, and Ni metal ions from Mn, Mg and Ca cations more selective.

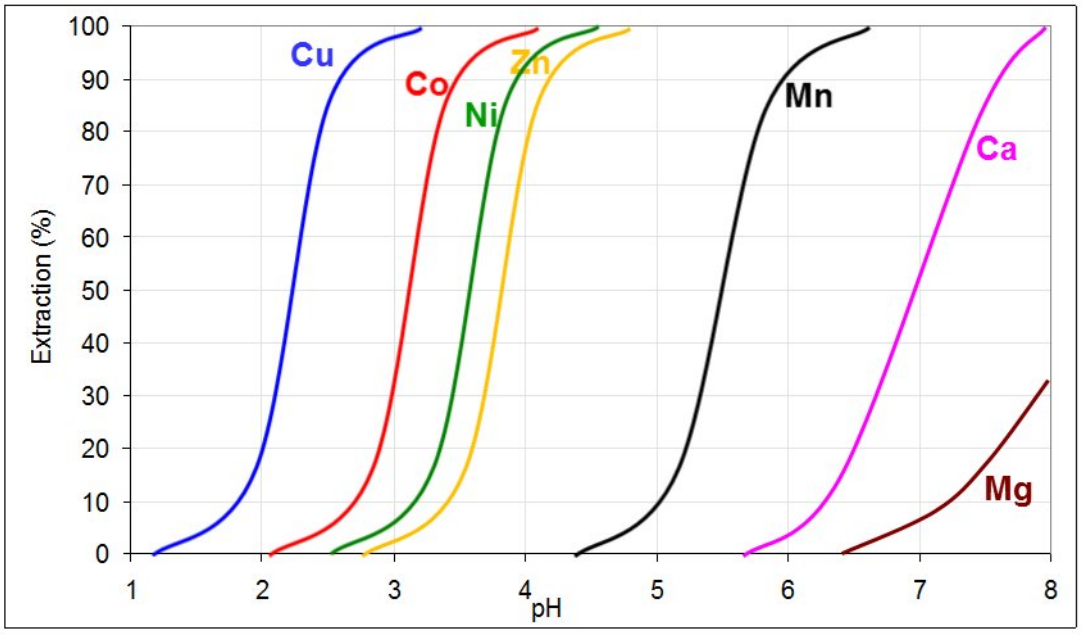

FIGURE 1.6: Extraction pH isotherms of metals with 0.5M Versatic10 acid/0.35M LIX63 in Shellsol 2046 and the synthetic laterite leach solution at an aqueous/organic phase ratio of 1:1 and 40°C (modified from Cheng (2006)).

From the thermodynamic point of view, the synergistic effect can be explained by comparing the equilibrium parameters of metal complexation before and after the synergist is added to the system. Coordinating to the metal ion along with an extractant, synergists make the formed complex more stable, which shifts the equilibrium for metal complexation in SSX more to the right compared to the SX case. It is interesting to note that chelating agents are the most commonly used synergistic components that usually do not deprotonate during metal extraction and are present in neutral form (Flett *et al.*, 1974). Earlier it was reported by Flett *et al.* (1974) that when Ni is extracted by the synergistic solvent extraction mixture of α-hydroxyoxime (HOx) and carboxylic acid (RH) the $Ni(Ox)_2(RH)_2$ complex is formed, where α-hydroxyoxime plays the role of an extractant (it is deprotonated) and carboxylic acid is a synergistic agent. However, the latest experimental results of Barnard *et al.* (2010) have shown that the $Ni(HOx)_2(R)_2$ complex is formed in this mixture, where hydroxyoxime stays neutral and the carboxylic acid deprotonates.

Even though the synergistic solvent extraction system, consisting of LIX63 aliphatic α-hydroxyoxime and Versatic10 carboxylic acid, secures highly selective separation of Co and Ni from gangue materials including Mg and Ca, it suffers from several drawbacks. First of all the kinetics of Ni extraction and stripping were found to be very slow compared to the extraction and stripping of other metal cations present in the system. It

was then shown by Cheng (2006) that the kinetics of both these processes can be significantly improved by adding a kinetic accelerator such as tributylphosphate (TBP) to the organic phase of the extraction mixture. Secondly, some losses of the expensive LIX63 α-hydroxyoxime were registered under the proposed extraction and stripping conditions (Barnard, 2008). These losses are mainly due to the hydroxyoxime degradation process, which is associated with the presence of carboxylic acid during the stripping process and/or with the oxidation process catalyzed by cobalt and/or manganese-complexes under the extraction conditions (Barnard, 2008; Barnard and Turner, 2008; Barnard and Urbani, 2007). The two main conclusions that can be drawn from the investigation of the role of carboxylic acid in SSX are;

1) the more sterically hindered the carboxylic acid, the greater the synergism (Castresana *et al.*, 1988; Preston and du Preez, 1996);

2) the speed of hydroxyoxime degradation process is higher when a stronger acid is used (Barnard and Urbani, 2007; Castresana *et al.*, 1988).

It is possible, however, to slow the process of hydroxyoxime degradation by using different stabilizers, such as 2,6-bis-1,1-dimethyl-4-methylphenol (Cheng and Urbani, 2005a,b) or trichloroethylene (Castresana *et al.*, 1988). The process of hydroxyoxime degradation mainly goes through the oxidation and hydrolysis processes; therefore, it is preferable to use the anti-oxidant reagent as the stabilizer for hydroxyoxime (Cheng and Urbani, 2005a,b). It was also found by Barnard (2008) that LIX63 hydroxyoxime can be recovered from the main degradation product (keto-oxime) by borohydride-based regeneration. In addition, further investigation of Barnard and Turner (2008) has clarified that the hydroxyoxime degradation does not affect significantly the metal selectivity due to interconversion of "inactive" *syn*-hydroxyoxime to the active *anti*- form under extraction conditions. It is important to note here that the nature of the carboxylic acid affects both the complex formation and the degradation process of hydroxyoxime.

Despite this system being widely studied experimentally there are still many unexplored properties which can be investigated in order to improve the selectivity for the removal of specific metal ions. Therefore, aside from available experimental data, it is valuable to use computational chemistry in order to build a high quality theoretical model of this intriguing system.

1.4 References

Atta-Fynn R., Bylaska E.J., Schenter G.K. and de Jong W.A. (2011) Hydration shell structure and dynamics of curium(III) in aqueous solution: first principles and empirical studies. *Journal of Physical Chemistry A* **115**, 4665-4677.

Barnard K.R. (2008) LIX63 stability in the presence of Versatic 10 under proposed commercial extract and strip conditions, part I: operation at high temperature. *Hydrometallurgy* **91**, 1-10.

Barnard K.R. (2008) Isolation and characterisation of the LIX63 degradation products 5,8-diethyl-6,7-dodecanedione monooxime (keto-oxime) and 5,8-diethyl-6,7-dodecanediol (diol) and regeneration of oxime from keto-oxime. *Hydrometallurgy* **90**, 147-153.

Barnard K.R., Nealon G.L., Ogden M.I. and Skelton B.W. (2010) Crystallographic determination of three Ni-α-hydroxyoxime-carboxylic acid synergist complexes. *Solvent Extraction and Ion exchange* **28**, 778-792.

Barnard K.R. and Turner N.L. (2008) LIX63 stability in the presence of Versatic 10 under proposed commercial extract and strip conditions, part II: oxime isomer interconversion and the effect of oxime degradation products on selected physical properties. *Hydrometallurgy* **91**, 11-19.

Barnard K.R. and Urbani M.D. (2007) The effect of organic acids on LIX63 stability under harsh strip conditions and isolation of a diketone degradation product. *Hydrometallurgy* **89**, 40-51.

Birkholz M. (1992) The crystal energy of pyrite. *Journal of Physics: Condensed Matter* **4**, 6227-6240.

Bjerrum J. (1941) *Metal ammine formation in aqueous solution: theory of the reversible step reaction.* Copenhagen, Denmark: P.Haase and Son.

Bouffard S.C. and Dixon D.G. (2007) Evaluation of kinetic and diffusion phenomena in cyanide leaching of crushed and run-of-mine gold ores. *Hydrometallurgy* **86**, 63-71.

Burdett J.K. (1981) Use of the Jahn-Teller Theorem in inorganic chemistry. *Journal of Inorganic Chemistry* **20**, 1959-1962.

Castresana J.M., Elizalde M.P., Aguilar M. and Cox M. (1988) Synergistic extraction of nickel by mixtures of alpha-hydroxyoximes and carboxylic acids. *Solvent Extraction and Ion Exchange* **6**(2), 265-274.

Cheng C.Y. and Urbani M.D. (2005a) *Solvent extraction process for separation cobalt and/or manganese from impurities in leach solutions.* Patent Application No PCT/AU2005/000088 and Patent Publication No. WO 2005/073415 A1.

Cheng C.Y. and Urbani M.D. (2005b) *Solvent extraction process for separation cobalt and/or nickel from impurities in leach solutions.* Patent Application No PCT/AU2005/000099 and Patent Publication No. WO 2005/073416 A1.

Cheng C.Y. (2006) Solvent extraction of nickel and cobalt with synergistic systems consisting of carboxylic acid and aliphatic hydroxyoxime. *Hydrometallurgy* **84**, 109-117.

Deeth R.J. (1995) Computational modelling of transition metal centers. *Structure and Bonding* **82**, 1-42.

Dutrizac J.E. (1992) The leaching of sulphide minerals in chloride media. *Hydrometallurgy* **29**, 1-45.

Ferreiros-Martinez R., Esteban-Gomez D., Platas-Iglesias, de Blas A. and Rodriguez-Blas T. (2009) Selective chelation of Cd(II) and Pd(II) versus Ca(II) and Zn(II) by using octadentate ligands containing pyridinecarboxylate and pyridyl pendants. *Journal of Inorganic Chemistry* **48**, 10976-10987.

Fishtik I.F. (1989) Thermodynamics of the complex formation reactions. 1. mononuclear complexes. *Journal of Physical Chemistry* **93**, 4928-4930.

Flett D.S., Cox M. and Heels J.D. (1974) Extraction of nickel by α-hydroxy oxime/lauric acid mixtures. Proceeding of ISEC '74. *Society of Chemical Industry, London* **3**, 2560-2575.

Flett D.S. (2005) Solvent extraction in hydrometallurgy: the role of organophosphorus extractants. *Journal of Organometallic Chemistry* **690**, 2426-2438.

Fuerstenan M.C. and Han K.N. (2003) *Principles of mineral processing.* Littleton: Society For Mining, Metallurgy and Exploration.

Gibson S.E. (1997) *Transition metals in organic synthesis: a practical approach.* New York: Oxford Univercity Press.

Habashi F. (2005) A short history of hydrometallurgy. *Hydrometallurgy* **79**, 15-22.

House J.E. (2008) *Inorganic Chemistry.* Canada: Academic Press, Elsevier.

Ibl N. (1977) Optimization of copper refining. *Electrochimica Acta* **22**, 465-477.

King R.A. (1950) Economic utilization of sulfur dioxide from metallurgical gases. *Industrial and engineering chemistry* **42**(11), 2241-2248.

Kislik V.S.I (2011) *Solvent Extraction. Classical and Novel Approaches.* United Kingdom: Elsevier Science Ltd.

Kristiansson O. (1989) *Hydration of ions in aqueous solution studied by infrared spectroscopy.* Doctoral Thesis: University of Uppsala. ISBN 91-554-2356-6.

Luo W., Feng Q., Ou L., Zhang G. and Chen Y. (2010) Kinetics of saprolitic laterite leaching by sulfuric acid at atmospheric pressure. *Minerals Engineering* **23**, 458-462.

Mattus A.J. and Torma A.E. (1980) A comparison of carbonate leaching of a low-grade uranium ore at atmospheric and increased pressures. *Hydrometallurgy* **5**, 179-190.

MCT Redbook (2007) *Solvent extraction reagents and applications.* Cognis Group: Mining Chemicals Technology.

Mayhew K., McCoy T., Jones D., Barnard K., Cheng C.Y., Zhang W. and Robinson D. (2011) Kinetic separation of Co from Ni, Mg, Mn and Ca via synergistic solvent extraction. *Solvent Extraction and Ion Exchange* **29** 755-781.

Meloy T.P. (1983) Analysis and optimization of mineral processing and coal-cleaning circuits - circuit analysis. *International Journal of Mineral Processing* **10**, 61-80.

Mooiman M.B., Sole K.C. and Kinneberg D.J. (2005) Challenging the traditional hydrometallurgy curriculum - an industry perspective. *Hydrometallurgy* **79**, 80-88.

Moskalyk R.R. and Alfantazi A.M. (2002) Nickel laterite processing and electrowinning practice. *Minerals Engineering* **15**, 593-605.

Napier-Munn T.J. (1997) Invention and innovation in mineral processing. *Minerals Engineering* **8**(10), 757-773.

Preston J.S. and Preez A.C. (1996) Synergistic effects in solvent-extraction systems based on alkylsalicylic acids. Part 2. Extraction of nickel, cobalt, cadmium and zinc in the presence of some neutral N-, O- and S-donor compounds. *Solvent Extraction and Ion Exchange* **14**(2), 179-201.

Radivojevic M., Rehen T., Pernicka E., Sljivar D., Brauns M. and Boric D. (2010) On the origins of extractive metallurgy: new evidence from Europe. *Journal of Archaeological Science* **37**, 2775-2787.

Ray H.S. and Ghosh A. (1991) *Principles of extractve metallurgy.* New Delhi: New Age International (P)Ltd.

Roy G.K. and Weisweiler W. (1982) Absorption of sulfur dioxide by limestone in a high temperature fluidized bed. *Journal of the Institution of Engineers (India)* **62**, 33-36.

Rydberg J., Cox M., Musikas C. and Choppin G.R. (2004) *Solvent extraction principles and practice.* New York: Taylor and Francis Press.

Sakane H., Munoz-Paez A., Diaz-Moreno S., Martinez J.M., Pappalardo R.R. and Marcos E.S. (1998) Second hydration shell single scattering versus first hydration shell multiple scattering in $M(H_2O)_6^{3+}$ EXAFS spectra. *Journal of the American Chemical Society* **120**, 10397-10401.

Santos F.M.F., Pina P.S., Porcaro R., Oliveira V.A., Silva C.A. and Leao V.A. (2010) The kinetics of zinc silicate leaching in sodium hydroxide. *Hydrometallurgy* **102**, 43-49.

Seetharaman S. (2005) *Fundamentals of metallurgy.* New York: Woodhead Publishing Limited and CRC Press LLC.

Uudsemaa M. and Tamm T. (2004) Calculation of hydration enthalpies of aqueous transition metal cations using two coordination shells and central ion substitution. *Chemical Physics Letters* **400**, 54-58.

Wander M.C.F., Rustad J.R. and Casey W.H. (2010) Influence of explicit hydration waters in calculating the hydrolysis constatns for geochemically relevant metals. *Journal of Physical Chemistry A* **114**(4), 1917-1925.

Chapter 2

Computational Chemistry

2.1 Introduction to Quantum Mechanics

The main purpose of the current study consists of investigating the stability of different conformations of chemicals involved in metal complexation. Specifically the thermodynamics and kinetics of some processes occurring in synergistic solvent extraction of transition metals will be studied. Most of the calculations will be performed on single molecules of either the extractant/synergist or transition metal complex with a number of atoms typically not exceeding one hundred. This makes it affordable to use quantum mechanical methods as an appropriate level of theory.

Before introducing different computational chemistry methods based on quantum mechanics and talking about their weaknesses and strengths we should first briefly remind ourselves of the very basic postulates of quantum mechanics in order to be able to understand the nature of these methods.

The core equation of quantum mechanics is the Schrödinger equation (Schrödinger, 1926), which can be generally written as:

$$\hat{\mathbf{H}}\Psi = i\hbar\frac{\partial}{\partial t}\Psi \tag{2.1}$$

This form of Schrödinger equation is time-dependent. $i\hbar\frac{\partial}{\partial t}$ is the energy operator (where i is $\sqrt{-1}$ and $\hbar$ is Planck constant divided by 2π) and $\hat{\mathbf{H}}$ is the Hamiltonian operator. Ψ is the time-dependent wavefunction which can be written for N particles using either the "*position-space*" representation, ignoring spin, $\Psi(r_1, r_2, \ldots, r_N, t)$, where r_N stands for the position of the N^{th} particle in three dimensions. Alternatively the "*position-spin-space*" representation for the N particles with spin can be used, $\Psi(r_1, r_2, \ldots, r_N, s_{z1}, s_{z2}, \ldots, s_{zN}, t)$, where s_z is the quantum number for the spin projection along the z axis.

The Schrödinger equation can also be called an eigenvalue equation (Mueller, 2002). Using the terminology of linear algebra, an equation is an eigenvalue problem if the action of some operator $\hat{A}$ (which could be integration, differentiation or any other type of operator) on some function, f, can be substituted by multiplication of that function by some constant, ω, so that $\hat{A}f = \omega f$. The constant in this case is called an eigenvalue and the function is an eigenfunction of the operator $\hat{A}$. Given this definition, as the Hamiltonian $\hat{\mathbf{H}}$ in the Schrödinger equation 2.1 is an operator, then the total energy of a system, E, and the wave function, Ψ, are the eigenvalue and eigenfunction, respectively.

In order to understand how and why the Schrödinger equation works, we need to look at the way it was derived. For simplicity let us consider the case of a single particle. In classical physics, the motion of a particle in space can be either described by Newtonian or Hamiltonian mechanics. In Newtonian mechanics the change of particle motion depends directly on the applied force. The direction of the change of motion is exactly the same as the direction of the force vector (Mueller, 2002); therefore, in order to describe the trajectory of motion of a single particle we need to know the force acting on it;

$$\overrightarrow{F} = m \cdot \overrightarrow{a} \tag{2.2}$$

where m - is the mass of the particle and $\overrightarrow{F}$ and $\overrightarrow{a}$ are the force and acceleration vectors, respectively[1].

In 1834 the Scottish mathematician R. Hamilton introduced an alternative way of describing the motion of a single particle. Hamilton suggested to determine the equation of motion by finding the simultaneous solution of the following equations;

$$\begin{aligned} \left(\frac{\partial \hat{\mathbf{H}}}{\partial q_i}\right)_{P_i} &= -\frac{\mathrm{d}p_i}{\mathrm{d}t} \\ \left(\frac{\partial \hat{\mathbf{H}}}{\partial p_i}\right)_{q_i} &= \frac{\mathrm{d}q_i}{\mathrm{d}t} \end{aligned} \tag{2.3}$$

where i is the dimension in which the motion is described (the motion of a single particle must be described in three dimensions - x, y and z), q and p are the position and the momentum of a particle respectively and $\hat{\mathbf{H}}$ is the Hamiltonian which is characterised as a sum of the kinetic and potential energies of a particle in a conservative system[2]:

[1] This method of describing a particle's trajectory has found its practical application first in theoretical physics and then in materials science and molecular modelling, which is now known as molecular dynamics. In molecular dynamics the forces between interacting particles are typically described by a force field and the simulations are based on finding the numerical solution to Newton's equations of motion. Note that quantum mechanical forces can also be used in molecular dynamics in order to describe the forces between interacting particles.

[2] The system is called conservative if the force acting on it depends only on the position and non-conservative if the force depends on both position and time

$$\hat{\mathbf{H}} = \hat{\mathrm{T}} + \hat{\mathrm{V}} = \sum_{i=1,\ldots,n} \frac{p_i^2}{2m} + \hat{\mathrm{V}}(\mathrm{r}) \tag{2.4}$$

Hamiltonian mechanics played a significant role in the development of quantum mechanics (Esposito *et al.*, 2004). At the beginning of the 20^{th} century, it was proved that a beam of electrons can be diffracted just like light. It was concluded then that particles as small as nuclei and/or electrons behave not just like a classical particle in Newtonian and Hamiltonian mechanics but also like a wave (the theory of wave-particle duality)[3].

The relation between particle-like and wave-like properties of a particle, i.e. momentum (p) and wavelength (λ), respectively, was derived by de Broglie in 1924:

$$p = \frac{h}{\lambda} \tag{2.5}$$

where h is Planck's constant. It was then proved mathematically that the nature of any particle can be described by some function which was called the *wave function* and if it is known then any observable of a particle can be obtained mathematically by applying a certain operator to this function (Schrödinger, 1926). The Schrödinger equation can now be derived by applying the Hamiltonian operator to the wave function of a single particle. This will give us the energy (E) as an observable (eigenvalue). For the Hamiltonian a more convenient way to write the momentum is using the position representation;

$$p \rightarrow \frac{\hbar}{i}\nabla \tag{2.6}$$

where ∇ (del) is the gradient operator. For a single particle moving in a three-dimensional space the kinetic energy operator would look as follows:

$$\hat{\mathrm{T}} = \frac{p^2}{2m} = -\frac{\hbar^2}{2m}\nabla^2 = -\frac{\hbar^2}{2m}\Big\{\frac{\partial^2}{\partial x^2} + \frac{\partial^2}{\partial y^2} + \frac{\partial^2}{\partial z^2}\Big\} \tag{2.7}$$

$$\hat{\mathbf{H}} = -\frac{\hbar^2}{2m}\Big\{\frac{\partial^2}{\partial x^2} + \frac{\partial^2}{\partial y^2} + \frac{\partial^2}{\partial z^2}\Big\} + V(r) \tag{2.8}$$

Now we can write the Schrödinger equation as follows:

$$\Big\{-\frac{\hbar^2}{2m}\Big\{\frac{\partial^2}{\partial x^2} + \frac{\partial^2}{\partial y^2} + \frac{\partial^2}{\partial z^2}\Big\} + V(r)\Big\}\Psi(r,t) = \mathrm{i}\hbar\frac{\partial\Psi(r,t)}{\partial t} \tag{2.9}$$

In this study we are interested in finding the solution to the time-independent Schrödinger equation for various types of systems. In order to simplify the problem we can use the

[3]Note that not just light and particles as small as electrons have wave-particle duality; it is still applicable to macroscopic bodies also; it is just that their wave-like properties are insignificant and therefore can be neglected.

technique of separation of variables in the Schrödinger equation 2.9 (Atkins and Friedman, 2004; Fitts, 2002):

$$\Psi(r,t) = \psi(r)\Theta(t) = \psi(r)e^{-\frac{iEt}{\hbar}} \tag{2.10}$$

From now-on all further discussion will be related to finding solution for the time-independent Schrödinger equation;

$$\hat{\mathbf{H}}\psi = E\psi \tag{2.11}$$

which describes only the stationary state of a system. Here lower case ψ is used for the time-independent wavefunction $\psi(r)$.

The physical meaning of the wavefunction was not clear until in 1926 Max Born showed that the probability of finding a particle in the volume of a infinitesimal region at a position r is represented by;

$$\int \psi(r)^2 \mathrm{d}\tau < \infty \tag{2.12}$$

where $\mathrm{d}\tau$ is a region of space ($\mathrm{d}x$ in one dimension and $\mathrm{d}x\mathrm{d}y\mathrm{d}z$ in three dimensions). In this case $\psi(r)^2$ can be called the probability density (the probability of finding a particle in a unit of space) and $\psi(r)$ is the probability amplitude (Fitts, 2002). The meaning of the above expression is that in the finite volume the wavefunction cannot be infinite (the exception is a Dirac δ function). The probability density should have a direct meaning or, in other words, it has to be a real number. However, time-dependent or periodic wavefunctions can be complex and to make the probability density of such functions real they must be multiplied by their complex conjugates $\psi^*(r)$, therefore, it is more correct to write $\psi^*(r)\psi(r)$ or $|\psi(r)|^2$ instead of just $\psi(r)^2$.

Born also specified that the probability of finding a particle integrated over all space must be equal to unity. This property is known as the normalisation condition of the wavefunction and is written as follows:

$$\int_{-\infty}^{\infty} |\psi(r)|^2 \mathrm{d}\tau = 1 \tag{2.13}$$

The wavefunction is a solution of a second-order differential equation which implies the condition that it should be continuous everywhere in order for its second derivative to be valid. In fact its first derivative should also be continuous, although, it has some exceptions for ill-behaved regions (e.g. where the particle touches the wall of the box in the "Particle-in-a-Box" model) (Atkins and Friedman, 2004). Lastly, the wavefunction

must be single-valued, otherwise multiple probabilities would be available for the particle at the same point in space.

The next important requirement for the Schrödinger equation states that the Hamiltonian operator, $\hat{\mathrm{H}}$, be Hermitian so that its corresponding eigenvalues are real and not complex (Mueller, 2002; Rae, 2002). An operator, $\hat{\mathrm{A}}$, is called Hermitian if it satisfies the following condition;

$$\int f_m^* \hat{\mathrm{A}} f_n \mathrm{d}\tau = \left\{ \int f_n^* \hat{\mathrm{A}} f_m \mathrm{d}\tau \right\}^* \tag{2.14}$$

or using Dirac bracket notation;

$$\langle \mathrm{m}|\hat{\mathrm{A}}|\mathrm{n}\rangle = \langle \mathrm{n}|\hat{\mathrm{A}}|\mathrm{m}\rangle^* \tag{2.15}$$

where f_m ($|\mathrm{m}\rangle$) and f_n ($|\mathrm{n}\rangle$)are the eigenfunctions of the operator $\hat{\mathrm{A}}$ and f_m^* ($\langle \mathrm{m}|$) and f_n^* ($\langle \mathrm{n}|$) are their complex conjugates. This is very important property of quantum mechanical operators because in most cases the order in which they act on functions is important.

Another condition is that all Hermitian operators must satisfy the following commutation relations;

$$[\hat{\mathrm{A}},\hat{\mathrm{B}}] \neq 0 \qquad [\hat{\mathrm{A}},\hat{\mathrm{A}}'] = 0 \qquad [\hat{\mathrm{B}},\hat{\mathrm{B}}'] = 0$$

where $\hat{\mathrm{A}}(\hat{\mathrm{B}})$ and $\hat{\mathrm{A}}'(\hat{\mathrm{B}}')$ are operators of a similar kind, $[\hat{\mathrm{A}},\hat{\mathrm{B}}]$, $[\hat{\mathrm{A}},\hat{\mathrm{A}}']$ and $[\hat{\mathrm{B}},\hat{\mathrm{B}}']$ are the commutators of $\hat{\mathrm{A}}$ and $\hat{\mathrm{B}}$, $\hat{\mathrm{A}}$ and $\hat{\mathrm{A}}'$, and $\hat{\mathrm{B}}$ and $\hat{\mathrm{B}}'$ which can also be written as $\hat{\mathrm{A}}\hat{\mathrm{B}} - \hat{\mathrm{B}}\hat{\mathrm{A}}$, $\hat{\mathrm{A}}\hat{\mathrm{A}}' - \hat{\mathrm{A}}'\hat{\mathrm{A}}$ and $\hat{\mathrm{B}}\hat{\mathrm{B}}' - \hat{\mathrm{B}}'\hat{\mathrm{B}}$, respectively. The physical meaning of this is that if observables commute with each other ($[\hat{\mathrm{A}},\hat{\mathrm{B}}] = 0$) they can be simultaneously specified for the same eigenstate. Pairs of observables that do not commute with each other are called complementary observables. Complementary observables are governed by the uncertainty principle, which was described in 1927 by Werner Heisenberg and further developed by H.P. Robertson in 1929. The uncertainty principle for two complementary operators $\hat{\mathrm{A}}$ and $\hat{\mathrm{B}}$ is represented as following;

$$\Delta\hat{\mathrm{A}}\Delta\hat{\mathrm{B}} \geq \frac{1}{2}|\langle[\hat{\mathrm{A}},\hat{\mathrm{B}}]\rangle|$$

where $\Delta\hat{\mathrm{A}}$ and $\Delta\hat{\mathrm{B}}$ are the root mean square deviations defined as:

$$\Delta\hat{\mathrm{A}} = \{\langle\hat{\mathrm{A}}^2\rangle - \langle\hat{\mathrm{A}}\rangle^2\}^{\frac{1}{2}} \qquad \text{and} \qquad \Delta\hat{\mathrm{B}} = \{\langle\hat{\mathrm{B}}^2\rangle - \langle\hat{\mathrm{B}}\rangle^2\}^{\frac{1}{2}}$$

According to the next postulate (Atkins and Friedman, 2004; Jensen, 1999), if the wavefunction describing the state of a system is known, then the average value of the

observable ω corresponds to the expectation value of a relevant operator $\langle\Omega\rangle$ which is given by:

$$\omega = \frac{\int \psi^* \Omega \psi \mathrm{d}\tau}{\int \psi^* \psi \mathrm{d}\tau} = \frac{\langle\psi|\Omega|\psi\rangle}{\langle\psi|\psi\rangle} \tag{2.16}$$

If the wavefunction and its complex conjugate describe the same system and are normalised, then the overlap integral $\mathrm{S} = \int \psi^* \psi \mathrm{d}\tau$ must be equal to unity. The expectation value of the Ω operator, would then be:

$$\omega = \int \psi^* \Omega \psi \mathrm{d}\tau = \langle\psi|\Omega|\psi\rangle \tag{2.17}$$

In the case when ψ is an eigenfunction of some other operator (different from Ω), it still can be represented as a linear combination of Ω eigenfunctions (Hameka, 2004):

$$\psi = \sum_n c_n \psi_n \qquad \Omega\psi_n = \omega_n \psi_n$$

This will give us the following expectation value:

$$\langle\Omega\rangle = \int (\sum_m c_m \psi_m)^* \Omega (\sum_n c_n \psi_n) \mathrm{d}\tau = \sum_{m,n} c_m^* c_n \int \psi_m^* \Omega \psi_n \mathrm{d}\tau = \sum_{m,n} c_m^* c_n \omega_n \int \psi_m^* \psi_n \mathrm{d}\tau$$

The overlap integral $\int \psi_m^* \psi_n \mathrm{d}\tau$ for an orthonormal set of wavefunctions (when $\mathrm{n} \neq \mathrm{m}$) is equal to 0. For the normalised eigenfunctions the expectation value will then look as follows;

$$\langle\Omega\rangle = \sum_n |c_n|^2 \omega_n \tag{2.18}$$

where c_n is the coefficient of a wavefunction ψ_n and $|c_n|^2$ gives the probability of the case that the ω_n eigenvalue is measured.

Mathematically the solution to the Schrödinger equation is found using methods of approximation such as the variational and perturbation theories (Cramer 2004; Foresman, 1996). Variational theory finds the solution by varying the coefficients of a trial wavefunction which is constructed based on an initial guess. The expectation value of energy is obtained using equation 2.16 listed above. The optimisation is continued until the first derivative of the energy with respect to each coefficient of the wavefunction is equal to 0. It is interesting to note that in variational theory the expectation value of energy (ε) will be equal to the true ground-state energy of the system (E_0) only if the trial wavefunction is the same as the true ground-state wavefunction, but otherwise it is always greater ($\varepsilon > E_0$). With a higher number of coefficients, the expectation

value of energy will be closer to the true ground-state energy. However, the number of differential equations will be increased equally, which means that it will be more time consuming.

In perturbation theory the starting point is another system that is similar in nature and for which the solution is already known. In this case the Hamiltonian is constructed from several parts; one part describes the system with the known solution and the other additional Hamiltonians describe the changes ("*perturbations*") between the system of interest and that for which solution is already known. The number of additional Hamiltonian parts corresponds to the order of perturbation (one - for first order perturbation, two - for second order perturbation and so on);

$$\hat{\mathbf{H}} = \lambda^0 \hat{\mathbf{H}}^{(0)} + \lambda^1 \hat{\mathbf{H}}^{(1)} + \lambda^2 \hat{\mathbf{H}}^{(2)} + ... \tag{2.19}$$

where λ is the parameter which may vary in order to "tune" the level of perturbation, $\hat{\mathbf{H}}^{(0)}$ is the Hamiltonian for the system with known solution and $\hat{\mathbf{H}}^{(1)}$ and $\hat{\mathbf{H}}^{(2)}$ are the Hamiltonians for the first and second orders of perturbation, respectively.

Earlier we introduced the Hamiltonian as a sum of the kinetic and potential energy operators. Any molecular system can be represented as a collection of nuclei and electrons. Therefore, to describe the Hamiltonian operator for a molecule in more specific form we must introduce the motions of, and interactions between, the nuclei and electrons. Specifically terms for the kinetic energy operators for nuclei ($\mathbf{T}_n$) and electrons ($\mathbf{T}_e$) and the potential energy operators for electron-nuclear attraction ($\mathbf{U}_{en}$), nuclear-nuclear repulsion ($\mathbf{U}_{nn}$) and electron-electron repulsion ($\mathbf{U}_{ee}$) form the Hamiltonian:

$$\hat{\mathbf{H}} = \mathbf{T}_n + \mathbf{T}_e + \mathbf{U}_{en} + \mathbf{U}_{ee} + \mathbf{U}_{nn}$$

$$= -\sum_{i}^{nuclei} \frac{\hbar^2}{2M_i}\nabla^2(R_i) - \sum_{i}^{electrons} \frac{\hbar^2}{2m_e}\nabla^2(r_i) - \sum_i \sum_j \frac{Z_i e^2}{4\pi\epsilon_0 \mid R_i - r_j \mid}$$

$$+ \sum_i \sum_{j>i} \frac{e^2}{4\pi\epsilon_0 \mid r_i - r_j \mid} + \sum_i \sum_{j>i} \frac{Z_i Z_j e^2}{4\pi\epsilon_0 \mid R_i - R_j \mid} \tag{2.20}$$

Here Z and e are the nucleus and electron charges respectively.

Prior to the introduction of any approximations to the time-independent Schrödinger equation we need to specify the units for the energy. For simplicity, the energy is often expressed in *Hartrees* (atomic units). Hartrees are defined by setting Planck's constant, the electron mass and charge to one so that one *Hartree* is equal to the potential energy between two electrons (Coulomb repulsion) at a distance of 1 Bohr from each other (Jensen, 1999). The Bohr radius is determined according to the following equation:

$$a_0 = \frac{h^2}{4\pi^2 m_e e^2} \approx 0.52917725\text{Å} \tag{2.21}$$

Using atomic units, we can rewrite the molecular Hamiltonian as follows:

$$\hat{H} = -\sum_{i}^{nuclei} \frac{\nabla^2(R_i)}{2M_i} - \sum_{i}^{electrons} \frac{\nabla^2(r_i)}{2}$$

$$-\sum_{i}^{nuclei}\sum_{j}^{electrons} \frac{Z_i}{\mid R_i - r_j \mid} + \sum_{i}^{electrons}\sum_{j>i}^{} \frac{1}{\mid r_i - r_j \mid} + \sum_{i}^{nuclei}\sum_{j>i}^{} \frac{Z_i Z_j}{\mid R_i - R_j \mid} \tag{2.22}$$

Now we are ready to talk about the key approximations used in quantum mechanics in order to simplify the solution of the Schrödinger equation.

2.2 The Born-Oppenheimer Approximation

It is extremely difficult and time consuming to solve the time-independent Schrödinger equation analytically for any type of molecular system bigger than H_2^+, even if the size of the wavefunction is finite. Fortunately in 1927 Born and Oppenheimer proposed a way of finding the solution to the Schrödinger equation for systems bigger than H_2^+ by using a reasonable approximation. The Born-Oppenheimer approximation is based on the well-known observation that the speed of an electron is typically much higher than that of a nucleus due to the large difference in their masses so that the electron positions are instantly adjusted to each new configuration of the nuclei. Therefore, the electron distribution does not often depend on the nuclear velocities (Fitts, 2002; Mueller, 2002). According to this approximation, the nuclear kinetic energy operator ($\mathbf{T}_n$) can be treated classically in the Hamiltonian. Under these circumstances we can separate the Hamiltonian operator into nuclear and electronic parts. The total wavefunction of a system can now be rewritten as a product of electronic and nuclear terms, $\psi(r, R) = \psi^{elec}(r, R)\chi^{nucl}(R)$, where the electronic term $\psi^{elec}(r, R)$ depends parametrically on the nuclei coordinates, R. All this gives us the following form of the Hamiltonian:

$$\hat{\mathbf{H}}^{elec} = \mathbf{T}_e + \mathbf{U}_{en} + \mathbf{U}_{ee} + \mathbf{U}_{nn} = -\sum_{i}^{electrons} \frac{\nabla^2(r_i)}{2}$$

$$-\sum_{i}^{nuclei}\sum_{j}^{electrons} \frac{Z_i}{\mid R_i - r_j \mid} + \sum_{i}^{electrons}\sum_{j>i}^{} \frac{1}{\mid r_i - r_j \mid} + \sum_{i}^{nuclei}\sum_{j>i}^{} \frac{Z_i Z_j}{\mid R_i - R_j \mid} \tag{2.23}$$

Note that in this case the nuclear-nuclear potential energy term ($\mathbf{U}_{nn}$) is a constant being equal to the total energy of a system for a certain (fixed) set of nuclear positions and usually is added to the total energy at the end of the electronic calculation.
The motion of nuclei is described by the potential energy surface which can be obtained by solving the Schrödinger equation for a range of nuclear coordinates R. The translational, vibrational and rotational motions of the nuclei are therefore described classically.

2.3 Hartree-Fock Theory

As mentioned before, it is rarely possible to find an analytic solution to the Schrödinger equation for any system larger than the H_2^+ molecule or similar one-electron systems. In order to find a solution for larger molecules, a number of approximations beyond that of Born-Oppenheimer must be made.

It is important to note that when we attempt to describe molecular systems with more than one electron we need to introduce electron spin (Cramer, 2004). An electron can either have a positive (spin up) or negative (spin down) spin quantum number of 1/2. The direction of an electron spin is usually defined by the spin functions, α and β as follows:

$$\begin{aligned} \alpha(\uparrow) &= 1 \qquad \alpha(\downarrow) = 0 \\ \beta(\uparrow) &= 0 \qquad \beta(\downarrow) = 1 \end{aligned} \tag{2.24}$$

Similarly to the wavefunction, the spin functions obey orthonormality conditions:

$$\begin{aligned} \langle\alpha|\alpha\rangle &= \langle\beta|\beta\rangle = 1 \\ \langle\alpha|\beta\rangle &= \langle\beta|\alpha\rangle = 0 \end{aligned} \tag{2.25}$$

According to Hartree-Fock theory, the total electronic wavefunction of a many electron system $\psi(r_1, r_2, \ldots, r_N)$ can be represented as a combination of single-electron wavefunctions that are called *(Molecular) Orbitals*, $\psi_i(r_i)$ assuming that the electrons interact with each other only in a mean field way. This assumption can be expressed through the so called *Hartree Product*:

$$\psi_{HP}(r_1, r_2, \ldots, r_N) = \psi_1(r_1)\psi_2(r_2)\ldots\psi_N(r_N)$$

Molecular orbitals $\psi_i(r)$ are constructed as a linear combination of basis functions (for example, a pre-defined basis set of atomic one-electron functions) as follows (Cramer, 2004; Foresman, 1996);

$$\psi_i(r) = \sum_{j=1}^{n_{basis}} c_{ij}\phi_i(r) \tag{2.26}$$

for closed shell systems, and;

$$\psi_i^{\alpha}(r) = \sum_{j=1}^{n_{basis}} c_{ij}^{\alpha}\phi_i(r) \qquad \psi_i^{\beta}(r) = \sum_{j=1}^{n_{basis}} c_{ij}^{\beta}\phi_i(r) \tag{2.27}$$

for open shell systems.

To make the *Hartree Product* allow for electron spin we need to multiply it by the α and/or β spin functions, which will give us $\psi(r_1, r_2, \ldots, r_N, x_1, x_2, \ldots, x_N)$ expressed as a product of a so-called *spin orbitals* $\chi_i(r_i, x_i)$ where x is a generic spin coordinate (either α or β):

$$\psi_{HP}(r_1, r_2, \ldots, r_N, x_1, x_2, \ldots, x_N) = \chi_1(r_1, x_1)\chi_2(r_2, x_2)\ldots\chi_N(r_N, x_N)$$

Unfortunately, this resulting wavefunction does not satisfy the antisymmetry principle and to make it do so we need to construct a Slater determinant (Jensen, 1999). For simplicity let us write $\chi_i(r_i, x_i)$ as $\chi_i(q_i)$:

$$\psi(q_1, q_2, \ldots, q_N) = \frac{1}{\sqrt{N!}} \begin{vmatrix} \chi_1(q_1) & \chi_2(q_1) & \cdots & \chi_N(q_1) \\ \chi_1(q_2) & \chi_2(q_2) & \cdots & \chi_N(q_2) \\ \vdots & \vdots & \ddots & \vdots \\ \chi_1(q_N) & \chi_2(q_N) & \cdots & \chi_N(q_N) \end{vmatrix} \tag{2.28}$$

Having constructed such a determinant we can easily prove that it is impossible to find two electrons at the same point unless they have opposite spin.

Now that we have the molecular wavefunction set up in form of a Slater determinant we can finally solve the electronic Schrödinger equation for each electron. By looking at the electronic Hamiltonian in 2.23 one could figure-out that in order to calculate the electron repulsion potential for each electron the wavefunction for the system of all electrons must be known and vice versa. One of the solutions to this is the self-consistent field (SCF) theory, first introduced by Hartree in 1927 and then further developed by Fock and Slater. Let us consider an example of a closed-shell system when all electrons are paired in the molecular orbitals. In SCF theory the motion of each electron in the electronic Schrödinger equation is described by the *effective one-electron*

Hamiltonian;

$$\hat{\mathbf{H}}^{eff}(1) = -\frac{\nabla^2(r_1)}{2} - \sum_{i}^{nuclei} \frac{Z_i}{\mid R_i - r_1 \mid} + \sum_{j}^{N/2}[2J_j(1) - K_j(1)] \tag{2.29}$$

where $J_j(1)$ is the Coulomb operator and $K_j(1)$ is the exchange operator. The potential due to the nuclei is determined from the initial configuration and that of the electrons from the approximate trial wavefunction. It is now required to find the solution to the following Schrödinger equation:

$$\hat{\mathbf{H}}^{eff}(x)\psi^{elec}(x) = \varepsilon\psi^{elec}(x) \tag{2.30}$$

As was shown above, all the single-electron molecular orbitals $\psi_i(r)$ are represented as a linear combinations of the atomic orbitals $\phi_j(r)$ multiplied by the coefficient c_{ij}, where j goes from 1 to n_{basis}[4] It is clear now that the wavefunction depends directly on the c_{ij} coefficients according to the variational principle and the "best" wavefunction should correspond to the lowest possible value of energy. Therefore, in the Hartree-Fock-Roothaan method the energy is minimised by finding an appropriate set of c_{ij} coefficients[5].

When the solution to the Schrödinger equation 2.30 for each electron is found, the new improved set of wavefunctions is created and the Schrödinger equation 2.30 is solved again for each electron using the improved set of wavefunctions. The results are used to construct another set of wavefunctions, which is then compared with the previous set and if the differences in these are insignificant then the wavefunctions are assumed to be self-consistent and the energy of the molecule is converged. If the differences are too large, then the cycle is continued until self-consistency of the wavefunctions is reached.

2.3.1 Electron Correlation Methods

The electron correlation energy (E_c) corresponds to difference between the exact (E_{exact}) and Hartree-Fock (E_{HF}) energies. Often it is not possible to achieve results of high accuracy for most organic systems and especially for systems containing organometallic compounds without electron correlation (Raghavachari and Anderson, 1996). The biggest disadvantage of the Hartree-Fock method is that the antisymmetric wavefunction is expressed by a single Slater determinant. This error is corrected to varying degrees

[4]The bigger n_{basis} is, the better the shape of the molecular orbitals can be reproduced. Ideally n_{basis} is infinite; however, practically this is not achievable.

[5]An initial set of coefficients is usually generated using semi-empirical methods, which will be discussed later on.

in the *post*-Hartree-Fock methods, which are also called *electron correlation* methods (Foresman 1996; Jensen, 1999). *Configuration Interaction* (CI), *Coupled Cluster* (CC) and *Møller-Plesset* (MPn) are amongst the most commonly used *post*-SCF methods to correct for electron correlation. In CI, the correlation effect is included by expanding the molecular wavefunction as a linear combination of Slater determinants. In order to find the solution for the CI wavefunction all the coefficients of the Slater determinants are optimised using the variational principle. Any possible electronic state of a system is computed by the full CI method; therefore, it is one of the most complete and time consuming methods in quantum mechanics. In order to minimise the computational cost, the calculation is usually started from the Hartree-Fock wavefunction and then Slater determinants are added progressively[6]. It should be stressed; however, that truncated CI methods are not size consistent and in order to fix this the *Quadratic Configuration Interaction* (QCIS, QCISD etc.) or *Coupled Cluster* (CCSD) methods can be used.

Møller-Plesset (MPn) methods are based on many body perturbation theory (Mueller, 2002). In contrast to CI, a non-iterative correction to the Hartree-Fock theory is used in MPn methods, where n stands for the order of applied perturbation. When the order of perturbation is increased it should be taken into account that the computational cost of *Møller-Plesset* method increases according to N^{n+3}, where N is the total number of basis functions in the system and n is the order of perturbation. While the results derived from calculations with the full CI method are more accurate, the calculations with high order *Møller-Plesset* methods are significantly faster than calculations using the full CI method (with the same size of a basis set).

Concluding this part, we note that overall *ab initio* Hartree-Fock theory is able to provide a good approximation that can be systematically improved by introducing different levels of electron correlation corrections with post-SCF methods. However, the computational cost of this improvement can be very high.

2.4 Density Functional Theory

The concept of Density Functional Theory is different from that of *ab initio* types of calculation. It states, contrary to the Hartree-Fock method, that the energy can be derived from the electron density (Hohenberg and Kohn, 1964). Hohenberg and Kohn were the first to prove that the external potential is a function of electron density, ρ_0, and therefore if the latter is known, $v_{ext}(\rho_0)$, can be defined along with ground state

[6]In the first Slater determinant only one occupied orbital is replaced with a virtual orbital within the Hartree-Fock determinant (CIS - CI with a single excitation to the Hartree-Fock determinant), in the second - two (CISD - CI with a single and double excitations), and so on.

energy, E_0. However its mathematical dependence on electron density is still not known. Hohenberg and Kohn proved that any *approximate* electron density, ρ_{approx}, should lead to an *approximate* energy $E_{0,approx}$ which is always higher than or equal to the exact ground state energy ($E_{0,approx} \geqslant E_0$). The main assumption in this approach is that the nuclear positions of the reference system with the *approximate* density are identical to those with the exact ρ_0. In other words the external potential is expected to be the same for both systems. This is analogous to the variational principle. Now if the expression for the energy as a function of density was known, the ground state value could be determined by minimising $E_{0,approx}$ with respect to ρ_{approx}. The energy as a function of density $E(\rho)$ can be separated into three different contributions: electronic kinetic energy, $T(\rho)$, nuclear-electron attraction, $E_{ne}(\rho)$, and electron-electron repulsion $E_{ee}(\rho)$. Note that $E_{ee}(\rho)$ is usually written as a sum of Coulomb, $J(\rho)$, and exchange, $K(\rho)$, terms. If $E_{ne}(\rho)$ and $J(\rho)$ are defined using classical expressions from *ab initio* methods, in order to define the electronic kinetic energy we have to differentiate our wavefunction. Practical implementations of Density Functional Theory were first developed by Kohn and Sham (1965) who defined an effective wavefunction which is different in its interpretation to the one used in Hartree-Fock theory. The Kohn-Sham kinetic energy term T_s within a single Slater determinant framework is given by:

$$T_s(\rho) = \sum_{i=1}^{N} -\frac{1}{2} \int \psi_i^*(r) \nabla^2 \psi_i(r) dr \tag{2.31}$$

The electron density of the non-interacting electron gas is derived from a determinant of the Kohn-Sham orbitals, which are linear combinations of basis functions. The ground-state electron probability density ρ of a non-interacting system is then given by:

$$\rho_s(r) = \sum_{i=1}^{N} |\psi_i(r)|^2 \tag{2.32}$$

where ψ_i are the Kohn-Sham orbitals and N is the number of electrons. Accounting for all of this the final energy defined by the Density Functional Theory can be written as follows:

$$E_{DFT}(\rho) = T_s(\rho) + E_{ne}(\rho) + J(\rho) + E_{xc}(\rho) \tag{2.33}$$

where $E_{xc}(\rho)$ is the *exchange-correlation* energy. An exact expression for $E_{xc}(\rho)$ is not known; however, different approximations have been suggested within Density Functional Theory in order to estimate the *exchange-correlation* energy.

Looking at the advantages of Density Functional Theory over Hartree-Fock theory the dimensionality should be noted first (Koch and Holthausen, 2001). Generally,

when the density fitting techniques are used in the DFT functionals (Reine *et al.*, 2010), the Coulomb repulsion integrals are only calculated over the three-dimensional electron density, scaling therefore as N^3 where N is the total number of basis functions. This saves quite a bit of computing time compared to the HF method, which scales as N^4. Secondly the results derived from DFT methods using approximate electron correlation can be comparable with results obtained from some post Hartree-Fock methods but at a significantly lower computational expense.

In DFT methods the procedure for calculating the total energy of a system is quite similar to the one used in HF methods, except that the exchange term in the HF energy is replaced with an effective exchange-correlation term, E_{xc}. This term is unknown and its dependence on the Kohn-Sham density is approximated differently by various methods.

2.4.1 Local Density Approximation

The Local Density Approximation (LDA) and the Local Spin Density Approximation (LSDA) are the methods of DFT that use the simplest approximation to the electron correlation (Cramer, 2004). They are based on the assumption introduced by Kohn and Sham that the local exchange-correlation energy can be estimated in the same way as if a system was a uniform electron gas;

$$E_{xc}^{LDA}(\rho) = \int \rho(r)\epsilon_{xc}(\rho)\mathrm{d}r \tag{2.34}$$

where ρ is the density of an uniform electron gas and ϵ_{xc} is the exchange-correlation potential. As can be seen, the exchange-correlation term in LDA depends exclusively upon the density which for a union electron gas of N electrons is given by;

$$\rho = \frac{N}{V} \tag{2.35}$$

The exchange-correlation energy density of a uniform electron gas is usually split into two terms; the exchange ϵ_x and correlation ϵ_c energies per particle:

$$\epsilon_{xc} = \epsilon_x + \epsilon_c \tag{2.36}$$

The exchange potential is known explicitly for a uniform electron gas:

$$\epsilon_x(\rho(r)) = -\frac{3}{4}\Big(\rho(r)\frac{3}{\pi}\Big)^{1/3} \tag{2.37}$$

This is then integrated over all space in order to calculate the exchange energy of a system:

$$E_x^{LDA}(\rho) = -\frac{3}{4}\Big(\frac{3}{\pi}\Big)^{1/3} \int \rho(r)^{4/3} dr \tag{2.38}$$

In the *local* density approximation it is assumed that if considered locally, then any system behaves identically to the uniform electron gas. For open-shell systems, the local-spin-density approximation (LSDA) is used where the electron density is represented as a sum of ρ_α and ρ_β spin-densities.

Unfortunately, the correlation potential of a uniform electron gas is only known for the extreme limits where the correlation is either extremely weak or extremely strong (Parr and Yang, 1994). The high-density limit corresponds to the limit with infinitely strong correlation and the low-density limit conforms to the weak correlation limit. Accurate results for the values of correlation energies of the uniform electron gas (UEG) have been determined numerically using quantum Monte Carlo calculations. There are a number of LDA correlation functionals available where different techniques for interpolation of these intermediate ϵ_c values derived from quantum Monte Carlo simulations are used (Cramer, 2004). Some of the most accurate analytic interpolation formulae were suggested by Vosko, Wilk and Nusair and commonly known as the VWN correlation functional (Vosko *et al.*, 1980)

Although the correlation energy term is included in LDA/LSDA methods, there is always a systematic underestimation of the exchange energy and overestimation of the correlation energy (Parr and Yang, 1994). This occurs due to the fast decay of the LDA *exchange-correlation* potential which is supposed to decay much slower in a Coulombic manner. As a result, the energy of the Highest Occupied Molecular Orbital (HOMO) increases in value (Perdew and Zunger, 1981). Fortunately, a significant improvement over LDA at least for many properties was made by the development of *Gradient Corrected* methods, which are also known as *Generalised Gradient Approximation* (GGA) methods.

2.4.2 Generalised Gradient Approximation Methods

In the GGA methods both exchange and correlation energies depend not only on the electron density, but also on the gradient of the electron density. One of the simplest modifications of the LDA exchange-energy density was suggested by Perdew and Wang in 1986 (PW86);

$$\epsilon_x^{PW86} = \epsilon_x^{LDA}(\rho)(1 + ax^2 + bx^4 + cx^6)^{1/15} \tag{2.39}$$

where a, b and c are constants and x is the dimensionless reduced gradient variable represented as:

$$x = \frac{|\nabla\rho|}{\rho^{4/3}}$$

Although in a majority of cases the PW86 correction produces more accurate results than L(S)DA, the level of improvement is not significant (Juan and Kaxiras, 1993). A better correction to the LDA exchange-energy was introduced by Becke in 1988 (B or B88) which is still widely used nowadays;

$$\epsilon_x^{B88} = \epsilon_x^{LDA} - \beta\rho^{1/3}\frac{x^2}{1 + 6\beta\sin^{-1}x} \tag{2.40}$$

where x is the dimensionless gradient variable above and β is a parameter derived from fitting to experimental atomic data. Even though the exchange potential given by the Becke correction is an underestimate in most cases, the mathematical description of the asymptotic behaviour of the exchange-energy density is very accurate at long range. Following the B88 correction, there was a number of GGA exchange functionals developed in a similar manner including CAM, FT97, PW91 (Jensen, 1999) and a combination of B and PW which is commonly referred to as the X functional. One of the most popular gradient corrected correlation functionals is the one derived by Lee, Yang and Parr (LYP). The popularity of the LYP functional is due to its ability to cancel the self-interaction error in a system with single electron. As a disadvantage, it should be noted that no parallel spin correlation can be estimated by this method (Juan and Kaxiras, 1993; Jensen, 1999).

In general, the GGA functionals provide a good description of covalent, ionic and/or hydrogen bonds; however, there is still missing a long range part in the description of van der Waal's interaction by this type of DFT functional.

2.4.3 Meta-GGA Methods

As the next level of improvement in density functional theory the Meta-Generalised Gradient Approximation (meta-GGA) functionals should be introduced in which either the second derivative of the electron density is included or the Kohn-Sham kinetic-energy density $\tau(r)$ or both (Jensen, 1999). The kinetic-energy density is usually used in Meta-GGAs in order to overcome the time consuming problem related to the calculation of the

second derivative (Zhao and Truhlar 2008). In regard to this kind of DFT methods' efficiency it should be highlighted that although the functionals with the second derivative of the density show a small improvement over most of the GGA functionals they are significantly more expensive with respect to computing time (Simon amd Goodman, 2010).

2.4.4 Hybrid Methods

All GGA functionals have both exchange and correlation parts and it is quite common to use *Hybrid* functionals in order to achieve better results (Simon amd Goodman, 2010). In the hybrid methods Density Functional Theory is combined with a partial contribution from Hartree-Fock exchange. It has been shown using the Adiabatic Connection Method (ACM) that it is possible to control the level of the electron-electron interaction by introducing a universal parameter for the interelectronic interaction, λ (Becke, 1993a; Baker *et al.*, 1996). The exchange-correlation energy in this case should be computed then as;

$$E_{xc} = \int_0^1 \psi^*(\lambda) V_{xc}(\lambda) \psi(\lambda) d\lambda \tag{2.41}$$

where the lower bound of the integral (0) corresponds to the non-interacting system and the upper one (1) to the real, interacting system. However, it is not known how exactly the exchange-correlation potential (V_{xc}) and wave function (ψ) depend on λ. Therefore, the exchange energy is evaluated from the wave function in the same way as done in HF methods (E_x^{HF}), but using Kohn-Sham orbitals instead, while the correlation term is then given by DFT. This gives us (Koch and Holthausen 2001);

$$E_{xc} = (1-a)E_{xc}^{DFT} + aE_x^{HF} \tag{2.42}$$

where a is now a parameter fitted empirically. In the *"half-and-half"* method, for instance, the expectation value of the exchange-correlation within a range of $\lambda(0,1)$ is approximated to a straight line which gives $a = 0.5$.

The Becke 3-parameter exchange functional (Becke, 1993a) can be listed here as an example of a successful method providing a very good approximation in many cases (Kim and Jordan, 1994; Murashov and Leszczynski, 2000). This functional is often used in combination with the LYP correlation-energy functional producing the B3LYP functional. According to Simon and Goodman (2010) B3LYP is one of the most successful examples of *Hybrid* DFT functionals. The exchange-correlation energy is calculated in the B3LYP method as follows;

$$E_{xc}^{B3LYP} = (1-a)E_x^{LSDA} + aE_x^{HF} + b\Delta E_x^B + (1-c)E_c^{LSDA} + cE_c^{LYP} \tag{2.43}$$

where a, b and c were estimated to be equal to 0.20, 0.72 and 0.81 respectively (Becke, 1993b). To improve the high/low spin state energy separations for the first-row transition metal complexes, the value of parameter a in the above equation should be changed from 0.20 to 0.15.

In general, the hybrid exchange-correlation energy can be written as follows:

$$E_{xc}^{hyb} = \frac{X}{100}E_x^{HF} + (1 - \frac{X}{100})E_x^{DFT} + E_c^{DFT} \tag{2.44}$$

where E_x^{HF} is the non-local Hartree-Fock exchange energy, X is the percentage of Hartree-Fock exchange in the hybrid functional and E_x^{DFT} and E_c^{DFT} are the exchange and correlation DFT energies, respectively. It is interesting to note that performance of hybrid methods can be tuned for a particular system by changing the percentage of included HF exchange energy, X, (Baker *et al.*, 1996). It is known that when studying the kinetics of a chemical reaction, for instance, the barrier heights are usually underestimated by the GGA functionals and a bit overestimated by the HF method; therefore, inclusion of HF exchange will generally lead to better kinetics. It is known that in general, hybrid methods also improve band-gap energies. However, it is quite common for the hybrid methods with a high percentage of HF exchange energy to provide less accurate molecular geometries (Cramer and Truhlar, 2009; Zhao and Truhlar, 2008).

2.4.5 Hybrid-Meta-GGA Methods

As can be deduced from the name of this type of DFT method, a certain part of Hartree-Fock exchange is added to the meta-GGA approximation. For many types of systems, including transition metal complexes, the performance of the so-called M06-family of hybrid-meta-GGA methods is known to be significantly better than that of the well-known B3LYP hybrid-GGA DFT functional (Cramer and Truhlar, 2009). It is important to specify that for the current study the M06 functional is the most attractive due to its ability to perform well in the modelling of organometallic systems (Zhao and Truhlar, 2008). The form of the M06 correlation functional is derived from the M05 and VSXC correlation functionals and is identical to the M06-L or M06-HF functionals. The mathematical expression for M06 exchange functional is as follows:

$$E_X^{M06} = \sum_\sigma \int (F_{X_\sigma}^{PBE}(\rho_\sigma, \nabla\rho_\sigma) f(w_\sigma) + \varepsilon_{X_\sigma}^{LSDA} h\chi(x_\sigma, z_\sigma))dr \tag{2.45}$$

where $h\chi(x_\sigma, z_\sigma)$ is the so-called working function defined by Zhao and Truhlar (2008), x_σ is the reduced spin density gradient, z_σ is a working variable, $F_{X_\sigma}^{PBE}(\rho_\sigma, \nabla\rho_\sigma)$ is the PBE exchange energy density[7], ρ_σ is a spin density $\varepsilon_{X_\sigma}^{LSDA}$ is the exchange local spin density approximation, $f(w_\sigma)$ is the enhancement factor of the spin kinetic energy density and w_σ is a function of the spin kinetic energy density and spin density. It is very important to note that opposite-spin $E_C^{\alpha\beta}$ and parallel-spin correlation $E_C^{\sigma\sigma}$ energies have different expressions, which can be written as;

$$E_C^{\alpha\beta} = \int e_{\alpha\beta}^{UEG}(g_{\alpha\beta}(x_\alpha, x_\beta) + h_{\alpha\beta}(x_{\alpha\beta}, z_{\alpha\beta}))dr \tag{2.46}$$

and

$$E_C^{\sigma\sigma} = \int e_{\sigma\sigma}^{UEG}(g_{\sigma\sigma}(x_\sigma) + h_{\sigma\sigma}(x_\sigma, z_\sigma))dr \tag{2.47}$$

respectively, where $e_{\sigma\sigma}^{UEG}$ and $e_{\alpha\beta}^{UEG}$ are the universal electron gas correlation energy densities for the parallel and anti-parallel spin cases, respectively, and g and h are the working functions also defined by Zhao and Truhlar (2008). The final expression for the M06 correlation functional should therefore include all three terms:

$$E_C^{M06} = E_C^{\alpha\beta} + E_C^{\alpha\alpha} + E_C^{\beta\beta} \tag{2.48}$$

Metal-metal, metal-ligand bonding, as well as non-bonded interactions and especially the energetics of open-shell systems, are very accurately described by the M06 hybrid-meta-GGA functional (Cramer and Truhlar, 2009). It was parameterised for both transition metals and non-metals and is highly recommended for modelling inorganic salts and organometallic systems and for modelling of non-covalent interactions. The M06-2X functional with doubled non-local Hartree-Fock exchange term was specifically parameterised for non-metals only; therefore, it is highly recommended for molecular modelling of systems consisting of main group elements (Zhao and Truhlar 2008).

2.5 Semi-empirical Methods

Generally, semi-empirical methods are quicker but less accurate than *ab initio*/DFT methods. In modern computationally chemistry semi-empirical methods like AM1 (Dewar and Thiel, 1977) or PM3 (Stewart, 1989) and PM6 for systems including transition

[7]Note that PBE exchange functional itself represents a modified version of the B86 one.

metals (Stewart, 2007) are mostly used only when it is needed to set up an initial guess for an *ab initio* geometry optimisation or transition state search of a system if the geometry of that system is unknown or poorly characterised experimentally. The reason why semi-empirical methods demand so much less computer resources than *ab initio* electronic structure methods is that the most of the integrals are neglected or simplified and parametrised using experimental data (Dewar and Thiel, 1977; Stewart, 1989). Furthermore it is common to use minimal basis sets in semi-empirical methods which also accelerates the calculations. It is reasonable to conclude here that if the set of parameters is closely related to the nature of molecule being investigated, the results derived from semi-empirical methods might be very good. Hence, it is even possible to get valuable results like thermodynamic data or electronic spectra if the method is well parametrised (Fitts, 2002; Mueller, 2002). Still it is highly recommended to check the results with *ab initio* methods.

2.6 Molecular Mechanics

In Molecular Mechanics (MM) the atomic particles are treated as charged spheres. The interactions between these charged spheres are described by classical potentials such as models of springs, for instance. The total energy of a system corresponds to the sum of the bond stretching energy (E_{str}), the bending energy (E_{bend}), the torsion (or twisting) energy (E_{tor}) and the energy of non-bonded interaction (E_{nb}). The energy of interaction between the atoms which are not bonded chemically consists of van der Waals, repulsive and electrostatic contributions[8].

Each component of the total potential energy contains a set of parameters and equations which is generally called the Force Field (FF). The choice of the force field is based on the nature of the system being studied so that such commonly known FF as AMBER and CHARMM (Brooks *et al.*, 1983; Cornell *et al.*, 1995) are generally chosen for studying biomolecules (such as proteins and/or nucleic acids) while N.L. Allingers MM2 (Allinger, 1977) can be recommended for organic compounds and polymers.

Molecular mechanics is generally used only for studying the potential energy surfaces of large molecular systems. In contrast to quantum mechanics, in molecular mechanics, each atom is not considered as a nucleus and associated electrons (where each component is treated explicitly) but as a single particle (Atkins and Friedman, 2004). Therefore, MM is not very useful for modelling chemical processes involving bond-breaking or bond-forming where electronic effects are important. As accuracy was

[8]Note that other contributions of interaction energy between non-bonded atoms such as stretchbend coupling interactions and special treatment of hydrogen bonding, for instance, might also appear in MM.

chosen to be a criterion in the selection of the theoretical methods in the current study, MM methods were not considered within the scope of this project. However molecular mechanics can still be very useful for studying large metal complexes with LIX63 hydroxyoxime and Versatic10 carboxylic acid when used in combination with quantum mechanics. In particular, metal complexes could be partitioned into two regions: the centre of the metal complex in which all the functional groups of the ligands and metal cation are treated with *ab initio* methods and the R groups of the ligands, which are optimised using molecular mechanics. Therefore, it can be recommended to apply QM/MM methods for future studies of metal complexation with LIX63 and Versatic10.

2.7 Methods Selection

In conclusion, the great interest in development and application of Density Functional Theory (DFT) methods in recent years is due to its acceptable accuracy and relatively low computational cost as compared to *ab initio* methods. All the modelling involved in the current study can be divided in two parts. In the first part we are going to study the stabilities of organic compounds, in particular carboxylic acids and hydroxyoximes, including both the kinetics and thermodynamics of processes in which these compounds are involved. In the second part we are going to perform a theoretical study of Ni^{2+}, Co^{2+}, Cu^{2+}, Mn^{2+} and Zn^{2+} metal complexation in the system of carboxylic acid and hydroxyoxime. According to Zhao and Truhlar (2008) and Simon and Goodman (2010), the M06-2X and B3LYP functionals are expected to be the most successful in modelling organic systems like hydroxyoxime and carboxylic acid containing O and N atoms in their functional groups, while the M06 functional is recommended by Zhao and Truhlar (2008) as the most appropriate method for modelling metal complexetion processes as it was specifically parametrised for studying the properties of organometallic systems. However, in order to select the most optimal (considering both: computational cost and accuracy) method for poorly investigated systems like ours it is highly recommended to test the accuracy of each method as a function of a basis set size prior to their application for studying molecular properties. Although the MP2 method has a very high computational cost it provides some of the most reliable thermodynamic data according to Mueller (2002). Therefore, in order to select an optimal method we can use a comparison of the thermodynamics and kinetics estimated by each method as a function of a basis set to the data received from MP2 calculations with the aug-cc-pVTZ basis set (Kendall *et al.*, 1992). This is the largest basis set that we could afford as we were limited in both time and computer resources. In addition, we were able to compare the performance of each method with experimental data kindly provided to us by Keith

Barnard and co-workers from the solvent extraction chemistry group, CSIRO Process Science and Engineering.

2.8 Thermochemistry

In this study we will be mostly focussed on studying the potential energies surfaces (PES) of different compounds in order to locate their global minima and determining the kinetics and thermodynamics of processes in which these minima are involved. The thermochemistry for each structure is automatically calculated by most of the quantum chemical software at the end of a frequency analysis. It is also very important to perform this analysis in order to understand whether the optimised structure[9] corresponds to a minimum or saddle point on the PES (Ochterski, 1999).

When calculating the frequencies of the molecule it is important to remember that the frequencies for translational motion should be close to zero. In order to calculate the frequencies, which correspond to the square roots of the eigenvalues, the Hessian matrix needs to be converted to mass-weighted Cartesian coordinates and then diagonalised in order to get 3N eigenvectors and 3N eigenvalues (Ochterski, 1999).

After the frequencies of a molecule are computed the thermochemical values arising from translation, rotational and vibrational motions are determined using standard formulae for statistical thermodynamics (McQuarrie and Simon, 1999). Note that in contributions from electrons the electronic partition function is set to the spin multiplicity of the molecule and therefore the electronic heat capacity and the internal thermal energy equal zero as the electronic partition function does not depend on temperature. The entropy arising from the electronic motion is equal to $\mathrm{Rln}q_e$, where q_e is the electronic partition function or spin multiplicity of the molecule. For most organic molecules the spin multiplicity is equal to unity. Therefore the electronic entropy equals zero for this case. General expressions which are used to calculate the entropy (S), thermal energy (U) and the heat capacity (C_v) contributions are as follows:

$$S = Rlnq(V,T) + RT\Big(\frac{\partial lnq(V,T)}{\partial T}\Big)_V \tag{2.49}$$

$$U = Nk_BT^2\Big(\frac{\partial lnq(V,T)}{\partial T}\Big)_V + U_0 \tag{2.50}$$

[9]Note that geometry optimisation followed by the frequency analysis must be performed at the same level of theory using the same basis set too.

$$C_v = \left(\frac{\partial U}{\partial T}\right)_{N,V} \tag{2.51}$$

where $q(V,T)$ is the partition function which has different forms for the translational, rotational and vibrational motions (McQuarrie and Simon, 1999). Formally, in quantum mechanics, the partition function can be expressed as follows;

$$q(V,T) = \sum_{i=1}^{n} \left(e^{-\beta H_i}\right) \tag{2.52}$$

where H_i is the quantum Hamiltonian operator and β is the inverse temperature which can be defined as $\frac{1}{k_B T}$.

In some computational chemistry software, like Gaussian09, there are zero point energy, enthalpy, entropy and Gibbs free energy corrections given at the end of the frequency calculations and include contributions of all three types of motion: rotational, translational and vibrational. This is fine if we want to estimate the thermodynamics of processes occurring in the gas phase, however, in this study all the compounds are in liquid state, therefore, before calculating the thermodynamics or kinetics, the rotational and translational contributions must be excluded from the enthalpy and entropy corrections. When the enthalpies and/or Gibbs free energies are calculated for a chemical reaction, zero point energy corrections must be added to the electronic energy along with the enthalpy and/or Gibbs free energy corrections for each component participating in the considered reaction. The more detailed procedure of calculating both the thermodynamics and kinetics of some chemical processes, based on the thermochemistry estimated individually for each component at different levels of theory, is explained in following chapters.

2.9 References

Allinger N.L. (1977) Conformational Analysis 130. MM2. A Hydrocarbon Force Field Utilizing V1 and V2 Torsional Terms. *Journal of the American Chemical Society* **99**, 8127-8134.

Atkins P.W. and Friedman R.S. (2004) *Molecular quantum mechanics, 4th edition.* New York: Oxford University Press.

Baker J., Muir M., Andzelm J. and Scheiner A. (1996) Hybrid HartreeFock Density-Functional Theory Functionals: The Adiabatic Connection Method. *Journal of the American Chemical Society* **629**(24), 342-367.

Becke A.D. (1993a) A new mixing of Hartree-Fock and local density-functional theories. *Journal of Chemical Physics* **98**(2), 13721377.

Becke, Axel D. (1993b) Density-functional thermochemistry. III. The role of exact exchange. *Journal of Chemical Physics* **98**(7), 56485652.

Brooks B.R., Bruccoleri R.E., Olafson B.D., States D.J., Swaminathan S. and Karplus M. (1983) CHARMM: A program for macromolecular energy, minimization, and dynamics calculations. *Journal of Computational Chemistry* **4**(2), 187217.

Cornell W.D., Cieplak P., Bayly C.I., Gould I.R., Merz K.M. Jr., Ferguson D.M., Spellmeyer D.C., Fox T., Caldwell J.W. and Kollman P.A. (1995) A Second Generation Force Field for the Simulation of Proteins, Nucleic Acids, and Organic Molecules. *Journal of the American Chemical Society* **117**, 51795197.

Cramer C.J. (2004) *Essentials of computational chemistry. Theories and Models. 2nd edition.* San Francisco: A John Wiley and Sons, Inc.

Cramer C.J. and Truhlar D.G. (2009) Density functional theory for transition metals and transition metal chemistry. *Physical Chemistry Chemical Physics* **11**, 10757-10816.

Dewar M.J.S. and Thiel W. (1977) Ground-States of Molecules. 38. The MNDO Method: Approximations and Parameters. *Journal of the American Chemical Society* **99**, 4899-907.

Esposito G., Marmo G. and Sudarshan G. (2004) *From classical to quantum mechanics. An introduction to the formalism, foundations and applications.* New York: Cambridge University Press.

Fitts D.D. (2002) *Principles of quantum mechanics: as applied to chemistry and chemical physics.* New York, Melbourne, Cambridge: Cambridge University Press.

Foresman J.B. (1996) *Exploring chemistry with electronic structure methods. 2nd edition.* Pittsburgh: Gaussian, Inc.

Hameka H.F. (2004) *Quantum mechanics. A conceptual approach.* New Jersey: A John Wiley and Sons, Inc. Publication.

Hohenberg P. and Kohn W. (1964) Inhomogeneous Electron Gas. *Physical Review* **136**(3B), B864-B871.

Jensen F. (1999) *Introduction to computational chemistry.* New York: A John Wiley and Sons, Inc.

Juan Y.M. and Kaxiras E. (1993) Application of gradient corrections to density functional theory for atoms and solids. *Physical Review B* **48**(20), 14944-14952.

Kim K. and Jordan K.D. (1994) Comparison of Density Functional and MP2 Calculations on the Water Monomer and Dimer. *Journal of Physical Chemistry* **98**(40): 1008910094.

Koch W. and Holthausen M.C. (2001) *A chemist's guide to density functional theory. 2nd edition.* New York: Wiley-VCH Verlag GmbH.

Kohn W. and Sham L.J. (1965) Self-Consistent Equations Including Exchange and Correlation Effects. *Physical Review* **140**(4A), A1133-A1138.

McQuarrie D. and Simon J.D. (1999) *Molecular Thermodynamics.* Sausalito, California: University Science Books.

Mueller M. (2002) *Fundamentals of quantum chemistry. Molecular spectroscopy and modern electronic structure computations.* New York, Boston, Dordrecht, London, Moscow: Kluwer Academic Publishers.

Murashov V.V. and Leszczynski J. (2000) A comparison of the B3LYP and MP2 methods in the calculation of phosphate complexes. *Journal of Molecular Structure (Theochem)* **529**, 1-14.

Ochterski J.W. 1999 Vibrational Analysis in Gaussian. *Gaussian, Inc*, 1-10.

Ochterski J.W. 2000 Thermochemistry in Gaussian. *Gaussian, Inc*, 2-19.

Parr R. G., Yang W. (1994) *Density-Functional Theory of Atoms and Molecules.* Oxford: Oxford University Press.

Perdew J.P., Zunger A. (1981) Self-interaction correction to density-functional approximations for many-electron systems. *Physical Review B* **23**(10), 50485079.

Rae A.I.M. (2002) *Quantum mechanics. 4th edition.* London: Institute of Physics Publishing.

Raghavachari K. and Anderson J.B. (1996) Electron Correlation Effects in Molecules. *Journal of Physical Chemistry* **100**, 12960-12973.

Reine S., Krapp A., Iozzi M.F., Bakken V., Helgaker T., Pawlowski F. and Salek P. (2010) An efficient density-functional-theory force evaluation for large molecular systems. *Journal of Chemical Physics* **133**, 1-9.

Schrödinger E. (1926) An Undulatory Theory of the Mechanics of Atoms and Molecules. *Physical Review* **28**(6), 10491070.

Schrödinger E. (1926) *Quantisierung als Eigenwertproblem; von Erwin Schrödingerr.* Leipzig: Annalen der Physik, 361377.

Simon L. amd Goodman J.M. (2010) How reliable are DFT transition structures? Comparison of GGA, hybrid-meta-GGA and meta-GGA functionals. *Organic and Biomolecular Chemistry* **9**, 689-700.

Stewart J.J.P. (1989) Optimization of parameters for semiempirical methods. I. Method. *Journal of Computational Chemistry* **10**, 209-220.

Stewart J.J.P. (1989) Optimization of parameters for semiempirical methods. II. Method. *Journal of Computational Chemistry* **10**, 221-264.

Stewart J.J.P. (2007) Optimization of parameters for semiempirical methods. V. Modification of NDDO approximations and application to 70 elements. *Journal of Molecular Modeling* **13**, 1173-213.

Vosko S.N., Wilk L. and Nusair M (1980) Accurate spin-dependent electron liquid correlation energies for local spin density calculations: a critical analysis. *Canadian Journal of Physics* **58**(8), 1200-1211.

Zhao Y. and Truhlar D.G. (2008) The M06 suite of density functionals for main group thermochemistry, thermochemical kinetics, noncovalent interactions, excited states, and transition elements: two new functionals and systematic testing of four M06-class functionals and 12 other functionals. *Theoretical Chemistry Accounts* **120**, 215-241.

Chapter 3

Syn/anti Isomerisation of a Model Hydroxyoxime

3.1 Introduction

Hydroxyoximes are organic compounds used industrially in the area of hydrometallurgy for metals separation/purification. As was described previously in the "Extractive Metallurgy" chapter, hydroxyoximes are able to extract selected transition metals by forming organometallic complexes via chelation of a metal cation leading to transfer from the aqueous to organic phase.

CSIRO Minerals (now CSIRO Process Science and Engineering) has recently submitted a patent for (Cheng and Urbani, 2005ab) a "synergistic solvent extraction" (SSX) system consisting of Versatic10 (a C10 carboxylic acid) and 5,8-diethyl-7-hydroxydodecan-6-oxime (main component of LIX63) metal extractants (Figure 3.1) available commercially. This system has the potential to extract Cu, Co, Ni and Zn over Mn, Mg and Ca from nickel laterite leach solutions via direct solvent extraction avoiding intermediate precipitation/releach processes as used at the Murrin Murrin, Ravensthorpe and Cawse operations (Barnard and Urbani, 2007).

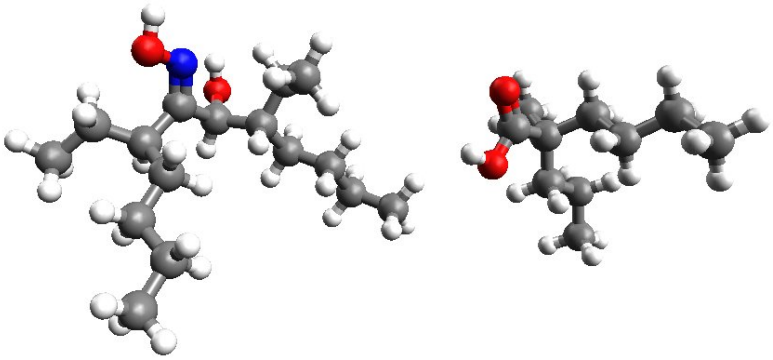

FIGURE 3.1: Structures of the two organic reagents used in the SSX system: the hydroxyoxime LIX63 (left) and carboxylic acid - Versatic 10 (right). Grey coloured atoms represent carbon, red - oxygen, dark blue - nitrogen and white - hydrogen.

Synergistic solvent extraction of transition metals with the LIX63 and Versatic10 active reagents appears to be very attractive for application in the copper/cobalt project at Baja Mining Corporation's proposed El Boleo project in Mexico (Cheng *et al.*, 2005; Cheng 2006). One of the key requirements for this process to be economically attractive is that both LIX63 and Versatic10 can achieve the desired metal separation (which they can) but also be chemically stable under the relevant operating conditions. A comprehensive experimental study of both the physical and chemical properties of LIX63 under conditions relevant to the El Boleo operation has been conducted by Barnard and co-workers (Barnard, 2008; Barnard and Turner, 2008; Barnard *et. al*, 2010) and two main weaknesses were identified. First of all, according to the experimental results, commercial 5,8-diethyl-7-hydroxydodecan-6-oxime contains both *anti* and *syn* isomers in an approximate 3:2 ratio (Barnard and Turner, 2008) and it is well known that when used on its own only the *anti* form extracts metal ions via chelation (Castresana *et al.*, 1988; Barnard and Tsuntsaeva, 2012). Structures of *anti* and *syn* 5,8-diethyl-7-hydroxydodecan-6-oxime are shown in Figure 3.2.

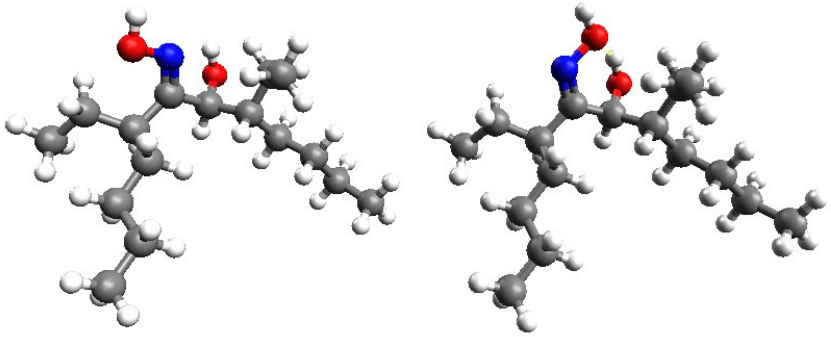

FIGURE 3.2: Graphical representation of *anti*- (left) and *syn*- (right) isomers of LIX63 hydroxyoxime. Grey coloured atoms represent carbon, red - oxygen, dark blue - nitrogen and white - hydrogen.

Another weakness of LIX63 is that it undergoes a degradation process, decomposing to 5,8-diethyl-6,7-dodecanedione (diketone), 5,8-diethyl-7-hydroxydodecan-6-one (acyloin) and 5,8-diethyl-6,7-dodecanedione monooxime (ketooxime) under operating conditions similar to those expected at Boleo. Fortunately, it has been shown (Barnard, 2008; Barnard and Turner, 2008) that these degradation products do not have an adverse effect on the process selectivity. The ability of hydroxyoxime to undergo *syn/anti* isomerism does provide a degree of "buffering" to compensate for degradation of the active *anti* isomeric form of hydroxyoxime. However, even though it is likely that *syn/anti* hydroxyoxime isomerisation leads to maintenance of a high level of metal selectivity, given that LIX63 is a very expensive reagent, this means that there are economic consequences associated with one of the two isomers not assisting in metal complexation. Although metal complexation as occurs during the extraction stage of SX facilitates the desired inter-conversion process (Barnard *et al.*, 2010), subsequent operation under stripping conditions is conducive to the inherent equilibrium being achieved. This results in reverse *anti* to *syn* inter-conversion process being favoured, an undesired outcome. Therefore, the thermodynamic and kinetic properties of the inherent (i.e. metal-free) hydroxyoxime *anti/syn* (also known as E/Z) interconversion should be investigated in order to understand the process and try to make some suggestions as to how this equilibrium 3:2 *anti:syn* ratio could possibly be changed to increase the fraction of the active isomer.

According to the literature there are a number of different mechanisms suggested for the Z(*syn*)/E(*anti*) isomerisation of oximes, including:

1. Photoisomerisation mechanism (Figure 3.3). Interconversion through rotation about the C = N double bond following excitation to the triplet state (Padwa

and Aldrecht, 1974; Blanco *et al.*, 2009).

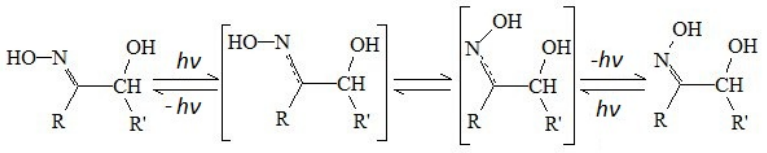

FIGURE 3.3: Photoisomerisation mechanism of Z/E aliphatic-α-hydroxyoxime interconversion.

2. Tautomerisation via an enamine compound (Figure 3.4). In this mechanism, hydrogen is migrated from the carbon atom to the nitrogen leading to formation of a double bond between two carbon atoms C=C and a single C-N bond. This allows facile rotation of the NOH group about the C-N bond, which leads to the process of isomerisation (Jennings and Boyd, 1972).

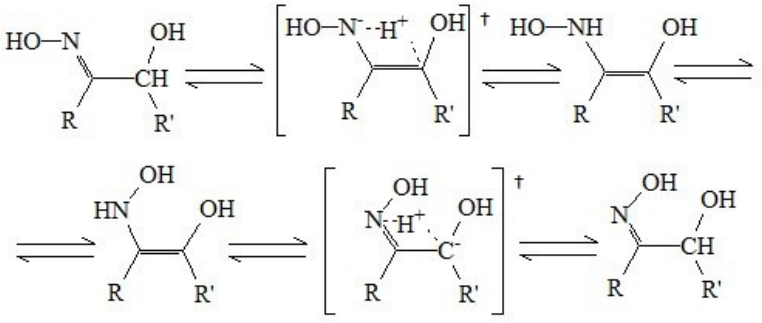

FIGURE 3.4: Tautomerisation mechanism of Z/E aliphatic-α-hydroxyoxime isomerisation via an enamine compound. Note that compound represented in the square brackets with a "†" symbol in the top right corner corresponds to a transition state.

3. Tautomerisation via a nitroso compound (Figure 3.5). In this mechanism, hydrogen is transferred from the oxime oxygen to the carbon atom of the oxime group (C=NOH) leading to formation of a double bond between the oxygen and nitrogen atoms and a single bond between the nitrogen and carbon atoms. This allows easy rotation of the N=O group about the single C-N bond, leading to Z/E isomerisation (Glaser *et al.*, 1996; Long *et al.*, 2001).

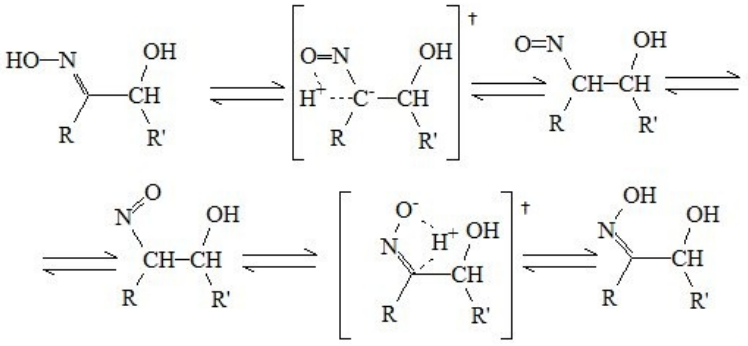

FIGURE 3.5: Tautomerisation mechanism of Z/E aliphatic-α-hydroxyoxime isomerisation via a nitroso compound. Note that compound represented in the square brackets with a "†" symbol in the top right corner corresponds to a transition state.

4. Inversion mechanism (Figure 3.6). Z/E hydroxyoxime isomerisation is achieved via flipping of the -OH group over the C=N double bond in the C=NOH oxime group (Blanco *et al.*, 2009; Marriott *et al.*, 2004).

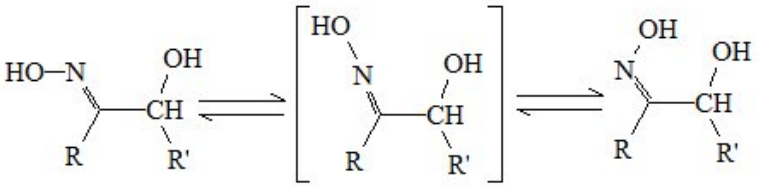

FIGURE 3.6: Inversion mechanism of Z/E aliphatic-α-hydroxyoxime interconversion.

5. Keto-enol tautomerisation (Figure 3.7). Isomerisation of the oxime anion through C-N bond rotation(Dobashi *et al.*, 1977; Glaser and Streitwieser, 1989).

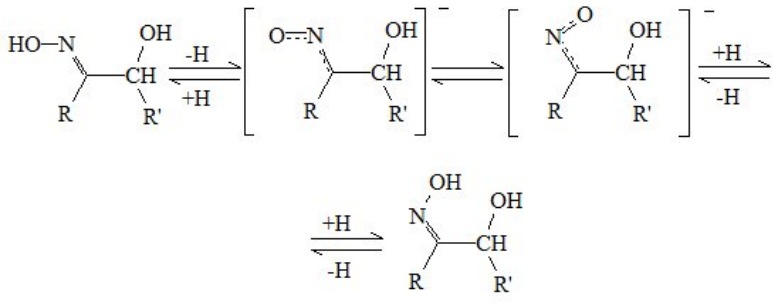

FIGURE 3.7: Anionic Z/E isomerisation of an aliphatic-α-hydroxyoxime.

6. Isomerisation of an oxime cation through C=N bond rotation in the presence of acid (Johnson *et al.*, 2001; Vasiltsov *et al.* 2009). An example of this mechanism is represented in Figure 3.8.

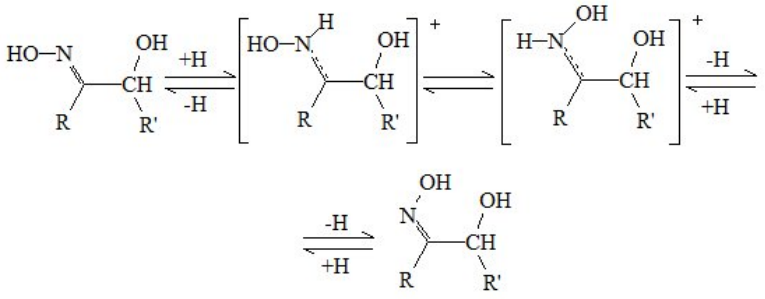

FIGURE 3.8: Acidic Z/E isomerisation of an aliphatic-α-hydroxyoxime cation.

7. The acid promoted Z/E isomerisation of oximes in aqueous solution (Nsikabaka *et al.*, 2006). A schematic representation of this mechanism is depicted in Figure 3.9.

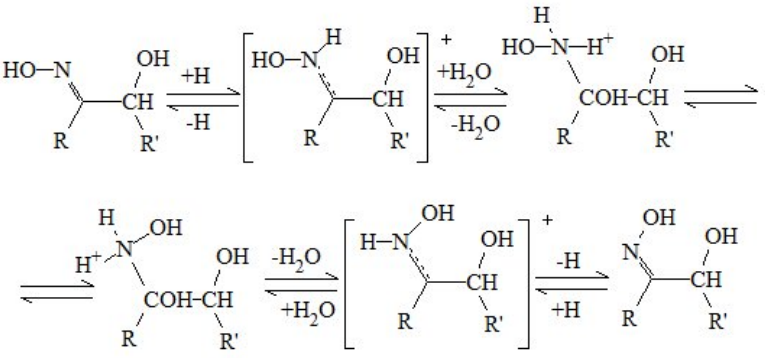

FIGURE 3.9: Z/E isomerisation of an aliphatic-α-hydroxyoxime in aqueous solution in the presence of acid.

All of the above mechanisms need to be studied theoretically in order to determine the one which has the lowest energy barrier and as a result has the fastest rate, assuming the pre-factors to be comparable.

Quantum mechanics was chosen as the most appropriate methodology for the current theoretical investigation. The range of *ab initio* theoretical methods based on both post Hartree-Fock and Density Functional Theory (DFT) was first examined with respect to the recommendations made in the literature regarding the choice of methods for modelling similar types of systems (Georgieva and Trendafilova, 2006; Ronchin *et*

al., 2008; Zhao and Truhlar, 2008). For compounds of a similar nature to aliphatic α-hydroxyoxime and carboxylic acid, the Configuration Interaction (CI) and Møller-Plesset (MPn) post Hartree-Fock methods are known to provide the most reliable thermodynamics (Mueller, 2002). The results derived from calculations with these methods can be improved systematically by introducing a higher degree of electron correlation (in case of MPn) and/or by increasing the size of the basis set. In order to calculate thermodynamic data we would ideally include the maximum possible level of electron correlation with the largest possible basis set and most extended sets of diffuse/polarisation functions. However, in practice for the present system this would be hard to achieve because of the enormous computing time required for each job and the large number of configurations to explore. It is therefore important to find a method giving similar thermodynamics and kinetics to the post Hartree-Fock methods at the highest level of theory, but at significantly lower computational expense.

3.2 Methodology

Based on a review of the literature (Georgieva and Trendafilova, 2006; Ronchin *et al.*, 2008; Zhao and Truhlar, 2008) we have selected the B3LYP, M06 and M06-2X methods as the most promising for modelling of molecular systems similar to those of interest. According to Mueller (2002) the MP2 method provides some of the most reliable thermodynamic data[1]. Therefore, as the first criterion in method selection we have chosen comparison to the thermodynamics and kinetics estimated at the highest level of theory that we could afford, accounting for its future possible application in modelling larger molecules, such as organometallic complexes, which was MP2 with the aug-cc-pVTZ basis set (Kendall *et al.*, 1992). It should be noted that calculations at the MP2/aug-cc-pVTZ level of theory are not expected to be entirely reliable due to both method and basis set limitations described elsewhere (Csaszar *et al.*, 1998; Usvyat *et al.*, 2011). Therefore, as the second criterion in method selection we have used comparison of our theoretical results with the available experimental data provided by Keith Barnard and co-workers from the solvent extraction chemistry group, CSIRO Process Science and Engineering.

All possible structures of different oxime conformers were constructed using the Avogadro[2] molecular visualisation software and then optimised using each of the chosen methods utilising different basis sets. Convergence criteria were chosen to be "tight"

[1] Note that the core orbitals were frozen during the MP2 calculations

[2] Avogadro: an open-source molecular builder and visualization tool. Version 1.0.3/April 25, 2011 http://avogadro.openmolecules.net/

for geometry optimisation, that is: the maximum and root mean square gradient in Cartesian coordinates are set to 0.00001 a.u. and the maximum and root mean square of the Cartesian step - to 0.00005 a.u. The Berny algorithm (which is set by default in Gaussian09) was used in geometry optimisation.

For practical reasons, all preliminary calculations of the minima and the first order saddle points for mechanisms considered have been performed using the semi-empirical PM6 method (Stewart, 2007) as implemented in the Gamess (Schmidt *et al.*, 1993) program and then the resulting structures were re-optimised at higher levels of theory using the Gaussian09 program (Frisch *et al.*, 2009).

Vibrational frequencies were evaluated in order to determine the nature of each stationary point, as well as to estimate the thermochemistry. Thermal corrections to the enthalpy and Gibbs free energy were used in order to calculate the thermodynamics (Ochterski, 2000).

The search for the first-order saddle points was performed by using two different methods. The first approach is based on the eigenvector following algorithm (Peng *et al.*, 1996), while the second method is via the Growing String Method (GSM) (Peters *et al.*, 2004). The main advantage of the GSM is that it allows one to find the transition state without an initial guess if the structures of the reagents and products are known. There are a number of papers where the comprehensive description of the Growing String Method (GSM) and its successful application can be found (Maeda and Ohno, 2005; Quapp, 2005; Quapp, 2007; Goodrow *et al.*, 2009).

Describing the underlying principles of finding the first-order saddle point by the eigenvector following algorithm, it should be clarified that an educated guess for the transition state (TS) structure is required in this case (Mueller, 2002); therefore, the general procedure for the TS search was as follows:

1. Locate a TS-like structure by constraining a chosen reaction coordinate during a sequence of energy minimisations;
2. Check whether the constrained optimised structure has an imaginary frequency that looks like the reaction coordinate;
3. If it does, use it as a starting point for the TS search.

The Intrinsic Reaction Coordinates (IRCs) were computed to see how the transition states found connect the reactants and products. IRC computing is analogous to geometry optimisation initiated near the transition state and then following the gradient down-hill leading to products and reactants.

3.3 Results and Discussion

Before studying the equilibrium between *syn* and *anti* isomers of our target hydoxyoxime molecule we have to make sure that the structure (molecular geometry) of each isomer corresponds to the global minima. In order to determine the minimum for each isomer we had to scan the potential energy surface for our target molecule, which means optimising all its possible conformers. Unfortunately, if we look at the structure of 5,8-diethyl-7-hydroxydodecan-6-oxime in Figure 3.10 we will see that there is an enormous number of different conformers that can be constructed just by changing the torsion angles of the carbon atoms in the R groups. The scanning of the potential energy surface of the main component of LIX63 seems to be even less feasible when we count the number of atoms in this system, as in order to find a reliable ground state we would have to use one of the DFT methods recommended in the literature (Georgieva and Trendafilova, 2006; Ronchin *et al.*, 2008; Zhao and Truhlar, 2008) ideally with a large basis set. It would require significant amount of computer resource to perform optimisation of a single 52 atom conformer and we will need to scan the whole potential energy surface in order to locate the true ground state (total of 708588 conformations for each isomer of 5,8-diethyl-7-hydroxydodecan-6-oxime).

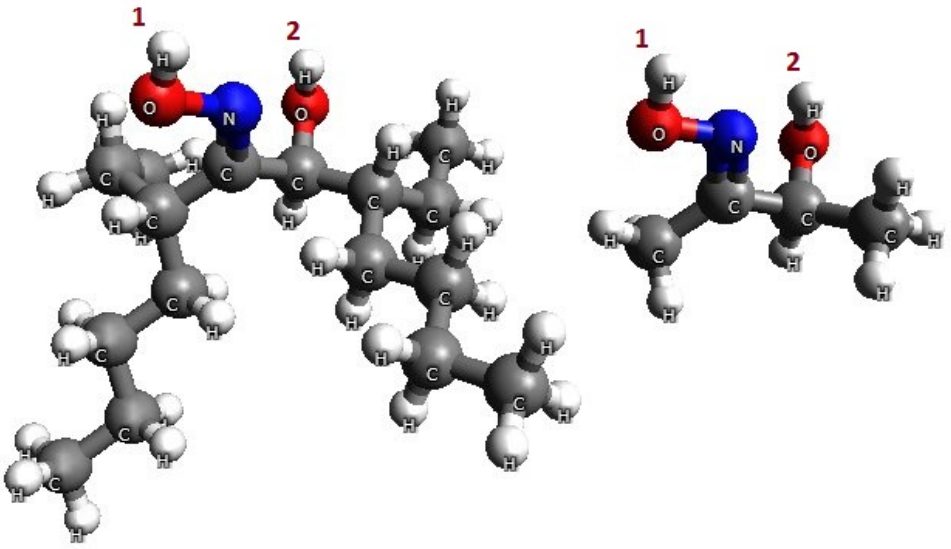

FIGURE 3.10: Structures of the *anti* isomer of the main component of LIX63 - 5,8-diethyl-7-hydroxydodecan-6-oxime (left) and the *anti* isomer of the LIX63 progenitor - acetoin oxime (right) pre-optimised using the semi-empirical PM6 method. Grey coloured atoms represent carbon, red - oxygen, dark blue - nitrogen and white - hydrogen.

In order to decrease the computational cost of the theoretical investigation of hydroxyoxime isomerisation, its progenitor acetoin oxime has been used instead of the actual target molecule LIX63[3]. As can be seen from the structures of *anti*-LIX63 and *anti*-acetoin oxime, represented in Figure 3.10, the relevant functional groups of these two molecules are identical, which implies they should have similar properties with respect to metal complexation. As was discussed earlier, the metal complexes with hydroxyoxime molecules are formed via chelation of the hydroxyoxime functional group with the metal cation and, therefore it would be reasonable to suggest the stabilities of different types of organometallic complexes with hydroxyoxime and a carboxylic acid mostly depend on the way in which the functional groups of the ligands are located around the metal centre. It was also hoped that both thermodynamic and kinetic properties derived from the LIX63 progenitor would provide insights that are relevant to the original LIX63 hydroxyoxime. The validity of this assumption will be examined later in this chapter.

The above approximation narrows down the number of conformers significantly. For each of the two isomers (*syn* and *anti*) we can divide all possible conformers into three groups: In the first one the hydrogens of both hydroxyl groups are pointing up (the -C=NOH torsion angle is close to or equal to 180^o and the HCOH one is close to or equal to 180^o); in the second one, both of these hydrogens are pointing down (the -C=NOH torsion angle is close to or equal to 0^o and the HCOH one is close to or equal to 0^o), in the third - the first hydrogen is up and the second is down, and in the fourth group - the first hydrogen is down and the second is up. For each of these four groups we can construct three different conformers of each isomer by changing the -NCCO- torsion angle (0^o, 120^o and 240^o). This will yield 12 conformers for each isomer or a total number of 24 conformers to optimise in order to find the global minimum for both *syn* and *anti* acetoin oxime.

3.3.1 Thermodynamics of *Syn/Anti* Acetoin Oxime Equilibrium

All possible conformers of acetoin oxime were optimised using methods selected previously based on the literature review of the accuracy of different levels of theory (B3LYP, M06, M06-2X and MP2) as a function of a basis set size. The full list of considered basis sets is as follows: 6-31G, 6-31G(d,p), 6-31++G(d,p) (Ditchfield *et al.*, 1971; Gordon, 1980; Rassolov *et al.*, 2001), 6-311G, 6-311G(d,p), 6-311++G(d,p) (Raghavachari *et al.*, 1980), cc-pVDZ, cc-pVTZ, aug-cc-pVDZ and aug-cc-pVTZ (Peterson *et al.*, 1994). In order to avoid overwhelming this chapter with massive tables, the potential energy surface of acetoin oxime scanned with each method as a function of a basis set size are

[3]Please note that to the best of our knowledge the use of acetoin oxime as a progenitor of LIX63 hydroxyoxime was first introduced by Rusinska-Roszak *et al.* (1995) and Rusinska-Roszak *et al.* (1997).

not included in the main text of the current thesis. However, the interested reader can find the data in the Appendix section. It is most important to note that the selected methods located the same global minima for both *syn* and *anti* acetoin oxime. One of the possible reasons why there is no effect of method type and basis set size on locating the acetoin oxime global minima (for both isomers) is due to the small size of studied system (only 16 atoms). It should also be noted that no thermochemical corrections were included for the structures optimised at different levels of theory at this stage (i.e. zero point and thermal energy corrections were not included in relative stabilities of different acetoin oxime conformers with respect to the lowest energy structure). The thermochemistry could have an impact on the relative stabilities of different conformers. Therefore future studies should verify that the inclusion of such corrections does not alter this conclusion. The global minima for the *syn* and *anti* isomers optimised at the B3LYP/6-31G(d,p) level of theory are shown in Figure 3.11.

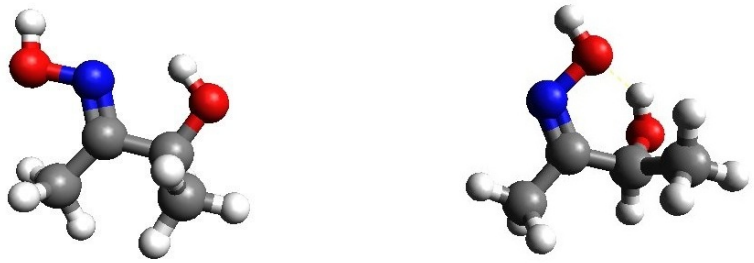

FIGURE 3.11: Graphical representation of the optimised global minima for *anti-* and *syn-* isomers of acetoin oxime at the B3LYP/6-31G(d,p) level. Grey coloured atoms represent carbon, red - oxygen, dark blue - nitrogen and white - hydrogen.

Now that the lowest energy structures are known for both *syn* and *anti* acetoin oxime we can study the thermodynamics of the equilibrium between them using all selected methods as a function of basis set size. As was discussed in the introduction, to estimate the thermodynamics we had to calculate the frequencies in order to find the sum of the electronic energy and the thermal correction to the Gibbs free energy. Calculated free energy differences at 298.15 K using selected methods with different basis sets for the *syn* $\rightleftarrows$ *anti* equilibrium are given in Table 3.1. As can be seen from Table 3.1, the trend of the basis set size effect on the thermodynamics of *syn/anti* equilibrium is very similar for each of the four methods considered. As was expected, the addition of polarisation functions to both hydrogen (p) and heavy atoms (d) has the most significant effect on the calculated free energy differences of the *syn/anti* acetoin oxime equilibrium, followed by addition of diffuse functions to both hydrogen (+) and heavy atoms (+).

Free energy differences calculated with the B3LYP, M06-2X and MP2 methods

TABLE 3.1: Free energy difference between the lowest energy structures of *anti* and *syn* acetoin oxime isomers at 298.15 K, $\Delta G^{298.15}_{(Syn/Anti)}$ (kJ/mol), as a function of method and basis set.

Basis Set	Theoretical Method			
	B3LYP	M06	M06-2X	MP2
6-31G	-4.0	-4.6	-2.8	-2.7
6-31G(d,p)	-8.9	-8.7	-9.5	-9.1
6-31G(3df,3pd)	-11.3	-13.8	-12.3	-10.5
6-31++G(d,p)	-10.7	-12.8	-10.9	-8.5
6-31++G(3df,3pd)	-12.2	-15.2	-13.0	-11.2
6-311G	-4.1	-5.0	-2.9	-2.6
6-311G(d,p)	-8.7	-9.4	-8.8	-7.8
6-311G(3df,3pd)	-11.4	-12.9	-13.2	-10.8
6-311++G(d,p)	-11.2	-12.8	-11.1	-9.6
6-311++G(3df,3pd)	-12.4	-15.4	-12.7	-11.8
cc-pVDZ	-7.9	-8.8	-9.4	-7.3
aug-cc-pVDZ	-12.3	-14.9	-12.1	-9.8
cc-pVTZ	-11.1	-14.1	-11.8	-10.7
aug-cc-pVTZ	-12.6	-15.6	-12.8	-11.7

using triple-zeta basis sets are slightly higher in absolute magnitude compared to those calculated using double-zeta basis sets, while the M06 method gives a larger increase in $\Delta G^{298.15}_{(Syn/Anti)}$. If we compare the values of $\Delta G^{298.15}_{(Syn/Anti)}$ calculated using each of the four methods with the same basis set we find that the B3LYP, M06-2X and MP2 methods provide similar results, though $\Delta G^{298.15}_{(Syn/Anti)}$ calculated using B3LYP and M06-2X tends to be slightly larger in magnitude than those for the MP2 method (with the difference not exceeding 2.5 kJ/mol). In contrast, the M06 method calculates higher $\Delta G^{298.15}_{(Syn/Anti)}$ values by more than 2.5 kJ/mol in most cases compared to those estimated using MP2. The reason for this is that both B3LYP and M06-2X DFT functionals were parametrised specifically for the main group elements, while M06 was designed for modelling organometallic systems containing transition metal elements (Zhao *et al.*, 2004; Zhao and Truhlar, 2008).

As discussed previously, the results derived at the MP2/aug-cc-pVTZ level of theory were chosen to be a reference for method selection. The compromise DFT method should provide the closest results to those derived at the MP2/aug-cc-pVTZ level of

TABLE 3.2: Mean time needed for geometry optimisation of acetoin oxime and frequency calculation using 4 cpus with different types of theoretical method (min). All optimisations were performed on the XE machine available via the NCI National Facility (xe.nci.org.au) which is a cluster based on two socket quad-core Intel Xeon E5462 nodes.

Basis Set	Theoretical Method			
	B3LYP	M06	M06-2X	MP2
6-31G	2	3	3	3
6-31G(d,p)	7	10	10	30
6-31G(3df,3pd)	165	185	180	2670
6-31++G(d,p)	14	20	20	76
6-31++G(3df,3pd)	230	285	275	4050
6-311G	4	6	6	11
6-311G(d,p)	12	17	17	72
6-311G(3df,3pd)	220	265	260	4000
6-311++G(d,p)	21	30	30	175
6-311++G(3df,3pd)	300	365	355	5650
cc-pVDZ	8	11	11	30
aug-cc-pVDZ	40	60	60	320
cc-pVTZ	125	150	150	1850
aug-cc-pVTZ	910	1150	1050	18350

theory at the lowest possible computational expense. The mean time required for the geometry optimisation and frequency calculation of this 16 atom system with each of the considered methods is given in Table 3.2.

At this stage we could select the B3LYP functional as the most appropriate for modelling *syn/anti* acetoin oxime equilibrium as it provides the closest results to the MP2 method and is least demanding in terms of the computer resources. It also gives the best compromise between expense and reproduction of the $\Delta G^{298.15}_{Anti/Syn}$ value as compared to the MP2/aug-cc-pVTZ level of theory: -10.7 kJ/mol at B3LYP/6-31++G(d,p) in 14 minutes vs -11.7 kJ/mol at MP2/aug-cc-pVTZ in 18350 minutes. However, this similarity of B3LYP/6-31++G(d,p) with MP2/aug-cc-pVTZ will need further checking since it is not guaranteed to be true for all cases. It should be noted, however, that the $\Delta G^{298.15}_{Anti/Syn}$ values calculated at the M06/6-31G(d,p) and M06/6-31++G(d,p) levels of theory are also very close to the MP2/aug-cc-pVTZ results, except that the optimisation routine takes a little bit longer to complete as compared to the B3LYP with the same

basis set due to the M06 functional being a meta-hybrid one.
It is also worth noting that for this particular system there is only a small benefit in adding more flexibility to the 6-31G-group of basis sets by using 6-311G ones, because the results are virtually identical for modelling hydroxyoxime equilibria, while being more time consuming. Another important observation to highlight is that the thermodynamics are described very similarly by the functionals using the 6-31G-group of basis sets (Ditchfield *et al.*, 1971; Gordon, 1980; Rassolov *et al.*, 2001) and those using correlation consistent basis sets cc-pVxZ (Dunning Jr., 1989), while the first type of basis set is known to be less expensive in terms of computing time due to the use of common exponents within a shell.

Now that we have computed the thermodynamics, it is important to see if the results derived are at all close to experiment. The experimental data for the *syn/anti* isomerisation of the full LIX63 main component were obtained and kindly provided by the solvent extraction chemistry group based at CSIRO Process Science and Engineering (Barnard and co-workers). The numerical data for reaching *syn/anti* 5,8-diethyl-7-hydroxydodecan-6-oxime equilibrium using 97% pure *anti* isomer as a starting point are given in Table 3.3 and the corresponding graphical representation is depicted in Figure 3.12. Note that in the last column of Table 3.3, C_{antiX} corresponds to percentage of *anti* isomer in the previous step and C_{antiY} corresponds to the current percentage of *anti* LIX63 hydroxyoxime. Also note that the ShellSol D70 solvent mentioned in the title of Table 3.3 is a very low aromatic content, inert hydrocarbon solvent produced by "Shell Chemicals" company. It consists predominantly of C_{11}-C_{14} paraffins and naphthenes.

The kinetics of *anti* to *syn*-hydroxyoxime interconversion can be simply estimated using the data of Table 3.3. The rate for a simple equilibrium reaction;

$$A \rightleftarrows B$$

where A is an *anti* isomer of hydroxyoxime and B is its *syn* form, can be represented as follows;

$$\frac{d[A]}{dt} = -k_f[A] + k_b[B] \tag{3.1}$$

where k_f and k_b are rate constants for "forward" and "backward" reactions, respectively. When equilibrium is reached and the concentration of the A component becomes constant this equation can be rewritten as;

$$\frac{k_f}{k_b} = \frac{[B]_e}{[A]_e} = K_e \tag{3.2}$$

TABLE 3.3: Experimental data for *anti/syn* oxime conversion corresponding to the change in percentage of *syn* (C_{syn}) and *anti* (C_{anti}) isomers of 5,8-diethyl-7-hydroxydodecan-6-oxime with time (hrs) in ShellSol D70 at constant pressure (1 atm) and temperature (363K) provided by Keith Barnard and co-workers, solvent extraction chemistry group, CSIRO Process Science and Engineering.

Time, hrs	C_{anti}, %	C_{syn}, %	$\lvert C_{antiX}\text{-}C_{antiY}\rvert$, %
0.0	96.9	3.1	
0.5	88.5	11.5	8.3
1.0	83.0	17.0	5.5
2.0	74.8	25.2	8.2
3.0	70.0	30.0	4.8
3.5	68.4	31.6	1.6
4.0	67.3	32.7	1.1
4.5	66.5	33.5	0.9
5.0	65.8	34.2	0.6
5.5	65.4	34.6	0.4
6.0	65.1	34.9	0.3
7.0	64.9	35.1	0.2
8.0	64.6	35.4	0.2
9.0	64.4	35.6	0.2
10.0	64.3	35.7	0.1
11.0	64.3	35.7	0.0
12.0	64.2	35.8	0.1
13.0	64.1	35.9	0.1
15.0	64.2	35.8	0.1
18.0	63.7	36.3	0.4
36.0	64.4	35.6	0.7
42.0	64.8	35.2	0.3

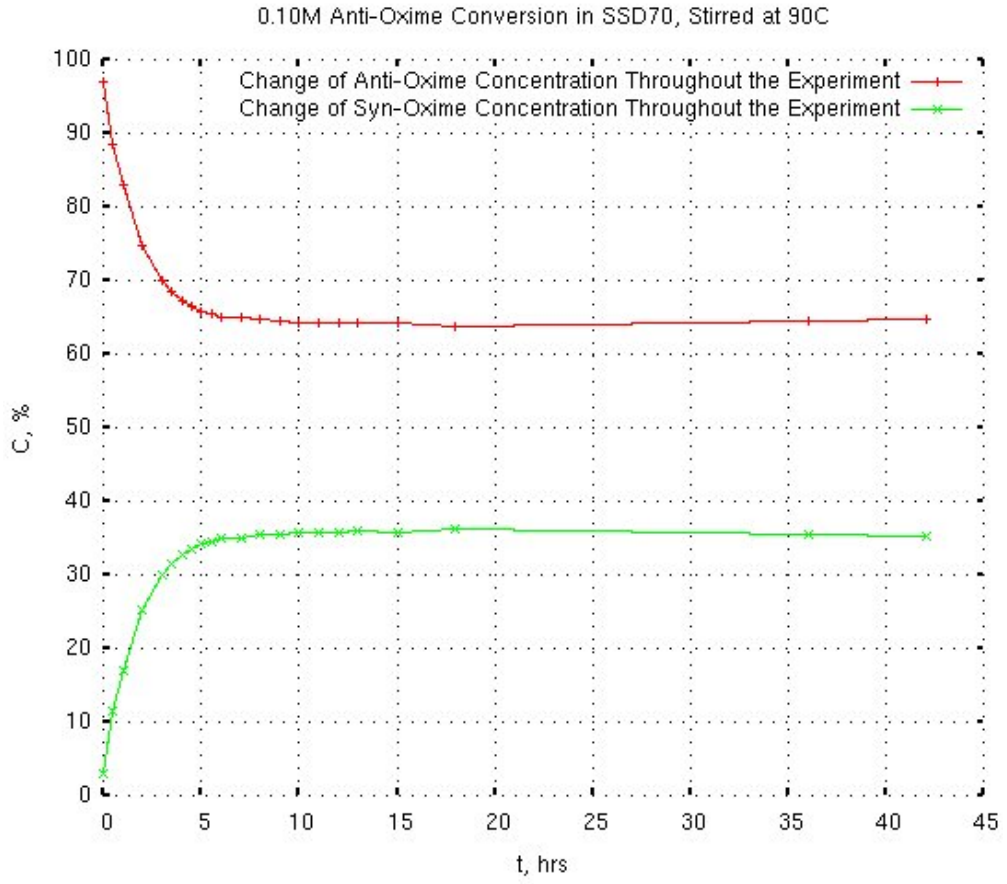

FIGURE 3.12: *Anti/syn* hydroxyoxime conversion operated at constant pressure (1 atm) and temperature (363K) in ShellSol D70 solvent. Data provided by Dr. Keith Barnard and co-workers, solvent extraction chemistry group, CSIRO Process Science and Engineering. Here C, % is the percentage of *syn* and *anti* isomers of 5,8-diethyl-7-hydroxydodecan-6-oxime with time, t, hrs.

where K_e is the equilibrium constant.

If we consider the process before equilibrium is reached and rewrite $[A]$ in equation 3.1 as $[A]_e + x$ and $[B]$ as $[B]_e - x$ we will get;

$$\frac{d[A]}{dt} = -k_f([A]_e + x) + k_b([B]_e - x) = -(k_f + k_b)x \tag{3.3}$$

which shows that the rate of change of concentration A is exactly the same as the rate of change of x; therefore, integration of the above equation will give us;

$$ln(\frac{[A]_0 - [A]_e}{[A]_t - [A]_e}) = (k_f + k_b)t \tag{3.4}$$

where $[A]_t$ is the concentration of a component A at time t. In order to find the sum of $k_f + k_b$ we need to plot the left hand side of the above equation versus t using the experimental data from Table 3.3 to get a straight line with a slope of $k_f + k_b$. This plot is given in Figure 3.13.

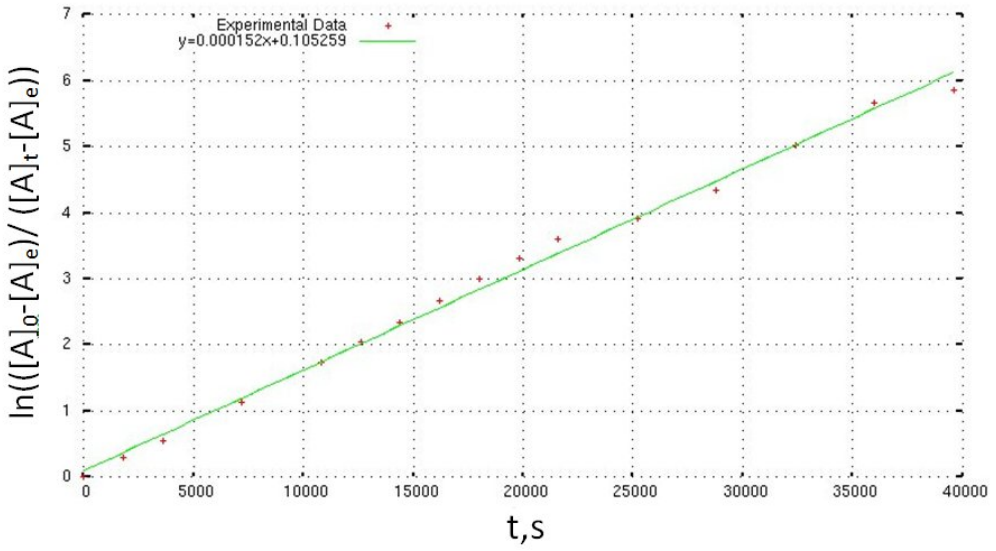

FIGURE 3.13: The plot of $ln(\frac{[A]_0 - [A]_e}{[A]_t - [A]_e})$ value versus time, t (s), using experimental data from Table 3.3.

The slope of the straight line in Figure 3.13 is equal to $1.52 \times 10^{-4}\text{s}^{-1} = k_f + k_b$. Now that we know the sum of both rate constants we can estimate the separate values for the forward and reverse rate constants. To do this, let us write $[A]_e$ as a difference of $[A]_0$ and x, where x should be equal to the concentration of component B at equilibrium ($[B]_e$). Now we can use equation 3.2 to rewrite the concentration of A and B components at equilibrium as follows:

$$[B]_e = \frac{k_f}{k_f + k_b}[A]_0 \tag{3.5}$$

$$[A]_e = \frac{k_r}{k_f + k_b}[A]_0 \tag{3.6}$$

These equations give the values of k_f and k_b as $1.007 \times 10^{-4}\text{s}^{-1}$ and $5.617 \times 10^{-5}\text{s}^{-1}$, respectively, based on the equilibrium concentrations of $[A]_e = 64.2\%$ and $[B]_e = 35.8\%$.

Using the formula for the rate constant as defined by Transition State Theory (Anslyn and Doughtery, 2006);

$$k = \frac{k_b T}{h} e^{-\frac{\Delta G}{RT}} \tag{3.7}$$

where k_b is Boltzmann's constant, h is Planck's constant and R is the ideal gas constant, we can calculate the energy barriers for the forward and reverse reactions at the experiment conditions at 363 K (90^0C). This gives values of energy barriers as 119.0 kJ/mol and 117.3 kJ/mol for ΔG_f and ΔG_r, respectively, assuming that the transmission coefficients are close to unity.

The thermodynamics of the *syn/anti* acetoin oxime equilibrium in Table 3.1 were estimated at 298.15 K (25^oC), which cannot be compared directly to the experimental results for the *anti* to *syn* LIX63 main component interconversion derived at 393 K (90^oC). Using the thermal corrections to the enthalpies extracted from the outputs of frequency calculations of both optimised lowest energy isomers of acetoin oxime, we need to find the values for ΔG^{363} *syn/anti* equilibrium.

It should be noted that in many cases of equilibrium modelling it is very important to consider the effect of solute/solvent interactions for each isomer; however, in this particular case the equilibrium between *syn* and *anti* isomers of LIX63 main component was measured in a non-polar solvent (ShellSol D70). In order to be able to compare experimental *syn/anti* hydroxyoxime equilibrium in a non-polar solvent with gas phase calculations we need to consider the statistical thermodynamics corrections required for vibrational and temperature effects, including the zero-point energy (ZPE). Therefore in order to compare our gas-phase calculations with experimental liquid-phase data we need to calculate ΔG^{363} of *syn/anti* equilibrium as follows;

$$\Delta \mathrm{G}^{363} = (E^o + ZPE_v + G_v^{363})_{anti} - (E^o + ZPE_v + G_v^{363})_{syn} \tag{3.8}$$

where G_v is the vibrational correction to the Gibbs free energy ($G_v^{363} = H_v^{363} - 363 \times S_v^{363}$), ZPE_v is the zero-point vibrational energy and E^o is the total electronic energy. Note that the final values of enthalpy and entropy corrections in most quantum chemical software include three constituents; vibrational, rotational and translational. However, for these calculations we only need the vibrational contribution as gas phase rotational and translational contributions are not appropriate to the liquid state.

The thermodynamics for *syn/anti* acetoin oxime equilibrium calculated at 363K as a function of method and basis set including all the corrections, are given in Table 3.4.

TABLE 3.4: Free energy difference between the lowest energy structures of *anti* and *syn* acetoin oxime isomers at 363K, $\Delta G^{363}_{(Syn/Anti)}$ (kJ/mol), as a function of method and basis set.

Basis Set	Theoretical Method			
	B3LYP	M06	M06-2X	MP2
6-31G	-7.1	-7.3	-5.0	-6.2
6-31G(d,p)	-11.8	-10.9	-12.7	-12.7
6-31G(3df,3pd)	-13.5	-17.1	-15.1	-13.0
6-31++G(d,p)	-13.2	-16.3	-13.5	-11.3
6-31++G(3df,3pd)	-14.0	-18.7	-15.5	-13.2
6-311G	-7.3	-7.9	-4.9	-5.4
6-311G(d,p)	-11.6	-12.3	-12.0	-11.0
6-311G(3df,3pd)	-13.3	-16.2	-16.0	-12.7
6-311++G(d,p)	-13.7	-16.3	-13.9	-12.6
6-311++G(3df,3pd)	-14.2	-18.8	-14.9	-13.7
cc-pVDZ	-10.9	-11.6	-13.5	-10.6
aug-cc-pVDZ	-14.5	-18.4	-14.6	-12.2
cc-pVTZ	-13.2	-17.5	-14.0	-12.7
aug-cc-pVTZ	-14.4	-25.2	-14.6	-12.4

The trends for the ΔG^{363} values determined at the different levels of theory using the corrections described above are the same as the ones for the $\Delta G^{298.15}$ values given in Table 3.1. However, as compared to the MP2/aug-cc-pVTZ results, the B3LYP/6-31G(d,p) and M06-2X/6-31G(d,p) can be chosen as the most favourable methods that give the closest values of ΔG^{363} for *syn/anti* equilibrium at 363K for the lowest computational cost as compared to the MP2/aug-cc-pVTZ calculations. The B3LYP/6-31++G(d,p) and M06-2X/6-31++G(d,p) methods also give reasonably close ΔG^{363} values as compared to those calculated at the MP2/aug-cc-pVTZ level of theory; however, B3LYP/6-31++G(d,p) and M06-2X/6-31++G(d,p) calculations require longer computing times than B3LYP/6-31G(d,p) and M06-2X/6-31G(d,p). It is interesting to note that the B3LYP functional when used with 6-31G(d,p) gives a slight underestimation in the ΔG^{363} value (by 0.6 kJ/mol) compared to the MP2/aug-cc-pVTZ result, and approximately the same magnitude of overestimation (by 0.8 kJ/mol) when used with the 6-31++G(d,p) basis set.

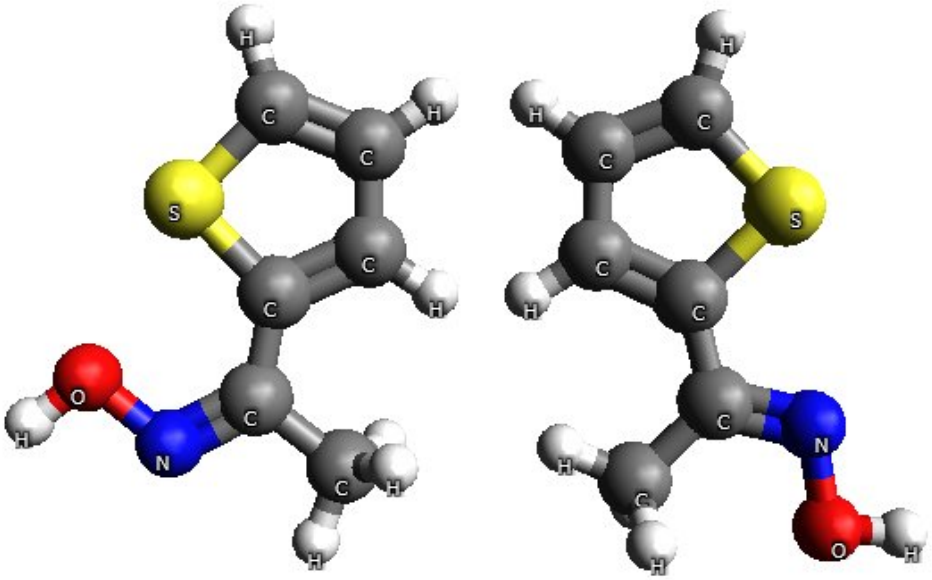

FIGURE 3.14: *Syn* (on the left) and *Anti* (on the right) isomers of 2-acetylthiophene oxime. Atom colours: sulphur (S) - yellow; oxygen (O) - red; nitrogen (N) - dark blue; carbon (C) - grey and hydrogen (H) - white.

Experimental equilibrium concentrations of *syn* and *anti* 5,8-diethyl-7-hydroxy-dodecan-6-oxime at 363 K are equal to 35.8% and 64.2%, respectively, which gives us the value for the equilibrium constant, K_{eq}, equal to 0.57. If we represent the value of K_{eq} as follows;

$$K_{eq} = e^{-\frac{\Delta G^{363}}{RT}} \tag{3.9}$$

we get an experimental value of ΔG^{363} equal to -1.4 kJ/mol. Unfortunately, as can be seen from Table 3.4, the theoretically estimated thermodynamics for *syn/anti* acetoin oxime equilibrium at 363K do not match the experimental data for the equilibrium between the two corresponding isomers of 5,8-diethyl-7-hydroxydodecan-6-oxime. There could be at least two obvious explanations for this. First of all, the assumption that the effect of the size of an R group on equilibrium between two hydroxyoxime isomers is insignificant may be wrong. Secondly, the thermodynamics for this particular system cannot be described accurately by any of the selected methods. In order to test both hypotheses we can calculate the thermodynamics of *syn/anti* equilibrium for a system of a similar nature and size for which experimental data is also known. In their experimental work Conde *et al.* (1985) were focusing on the equilibrium between *syn* and *anti* isomers of 2-acetylthiophene oxime, shown in Figure 3.14. A theoretical study of *syn/anti* equilibrium for 2-acetylthiophene oxime is expected to take approximately the

same amount of time as that of acetoin oxime as it has the same number of atoms - 16. The potential energy surface for each isomer consists of only four conformers; these arise from the case of the hydroxyl group hydrogens pointing up (HONC- torsion angle equal to 180^o) and down (HONC torsion angle equal to 0^o) and with the thiophene group pointing also up (-NCCS- torsion angle equal to 0^o) and down (-NCCS- torsion angle equal to 180^o). Geometrical representations of the lowest energy structures for both *syn* and *anti* isomers of 2-acetylthiophene oxime are depicted in Figure 3.14.
Experimental equilibrium concentrations of *syn* and *anti* isomers of 2-acetyl-thiophene oxime represented in Figure 3.14 are 33% and 67%, respectively (Conde *et al.*, 1985). It is important to note that equilibrium between these two isomers was reached and determined in aqueous solution, which means that in our modelling we need to take into account the effect of solute/solvent interactions. This was achieved via use of the Polarisable Continuum Model (PCM) as implemented in the Gaussian09 program (Frisch *et al.*, 2009) using parameters appropriate to water.

It is interesting to note that in modelling of acetoin oxime *syn/anti* equilibrium all three DFT functionals gave relatively similar results when used with the 6-31G(d,p) basis set as compared to the MP2/aug-cc-pVTZ calculations. It can be seen from the Table 3.4 that the further increase in the size of a basis set in calculations with B3LYP and M06-2X gives only a slight overestimation of ΔG^{363} values as compared to the MP2/aug-cc-pVTZ level of theory and much higher overestimation in the case of the M06 functional. B3LYP and M06-2X DFT functionals have shown virtually identical behaviour for acetoin oxime as they were both parametrised for modelling the same type of systems. However, there is a heavier sulphur atom present in 2-acetylthiophene oxime; therefore M06 is expected to give better results for this particular system according to Zhao and Truhlar (2008) as it was specifically parametrised for modelling systems containing heavier atoms. In order to select the method for the modelling this type of system it would be interesting to see how both B3LYP and M06 functionals perform in modelling equilibrium between *syn* and *anti* isomers of 2-acetylthiophene oxime. The thermodynamic data for *syn/anti* 2-acetylthiophene oxime calculated at different levels of theory in both the non-polar (the gas phase thermodynamics corrected for vibration motion only) and polar (PCM=water) solvents are given in Tables 3.5 and 3.6 respectively. If we compare the equilibrium calculated as a function of method and basis set between *syn* and *anti* isomers of 2-acetylthiophene oxime in water and non-polar solvent we can see that the $\Delta G^{298.15}_{(\mathrm{Syn/Anti})}$ values are virtually identical for both solvents. One possible explanation why the effect of solvent is quite insignificant on the *syn/anti* equilibrium is because the level of interaction between each of the two isomers and the surrounding water could be roughly the same.

The M06/6-311++G(3df,3pd) gives the best thermodynamics for 2-acetylthiophene oxime *syn/anti* equilibrium as compared to the experiment (Conde *et al.*, 1985)

TABLE 3.5: Free energy difference between the lowest energy structures of the *anti* and *syn* 2-acetylthiophene oxime isomers at 298.15K, $\Delta G^{298.15}_{(Syn/Anti)}$ (kJ/mol), in a non-polar solvent as a function of method and basis set. The corresponding fractions of *anti* and *syn* isomers are given.

Basis Set	B3LYP			M06		
	$\Delta G^{298.15}$, $\frac{kJ}{mol}$	[Anti], %	[Syn], %	$\Delta G^{298.15}$, $\frac{kJ}{mol}$	[Anti], %	[Syn], %
6-31G	-8.3	97	3	-4.0	84	16
6-31G(d,p)	-8.0	96	4	-2.2	70	30
6-31G(3df,3pd)	-6.2	93	7	-2.7	75	25
6-31++G(d,p)	-7.1	95	5	-3.6	81	19
6-31++G(3df,3pd)	-6.9	94	6	-5.2	89	11
6-311G	-8.1	96	4	-2.6	74	26
6-311G(d,p)	-7.3	95	5	-1.0	60	40
6-311G(3df,3pd)	-11.1	99	1	-2.1	70	30
6-311++G(d,p)	-6.9	94	6	-1.6	66	34
6-311++G(3df,3pd)	-7.3	95	5	-1.8	67	33
cc-pVDZ	-4.5	86	14	-3.8	82	18
aug-cc-pVDZ	-7.6	96	4	-4.3	85	15
cc-pVTZ	-7.7	96	4	-1.8	68	32
aug-cc-pVTZ	-9.4	98	2	-3.7	82	18

at 298.15 K, however, based on the mean time required for geometry optimisation and frequency calculation of acetoin oxime (16 atom system) (Table 3.2) it can be seen that modelling with the 6-311++G(3df,3pd) basis set is quite expensive. In this case the M06/6-31G(d,p) method gives the closest result to the experimental value of $\Delta G^{298.15}_{(Anti\text{-}Syn)}$ for the least computer resources followed by the M06/6-311G(d,p) and M06/6-311++G(d,p) methods.

One of the main targets of current study is to model metal complexation processes, in other words we will be mainly interested in modelling organometallic complexes formed between transition metals and organic compounds, such as hydroxyoxime and/or carboxylic acid. It is desirable to use a method that will perform equally well for each of these systems separately and when combined in an organometallic complex. Therefore, based on the literature and present results, at this stage it appears to be preferable to use the M06 method with the 6-31G(d,p) basis set for studying thermodynamics of such systems as the best compromise between accuracy and computing time. To conclude

TABLE 3.6: Free energy difference between the lowest energy structures of the *anti* and *syn* 2-acetylthiophene oxime isomers at 298.15K, $\Delta G^{298.15}_{(Syn/Anti)}$ (kJ/mol), in water as a function of method and basis set. The corresponding fractions of *anti* and *syn* isomers are given.

Basis Set	B3LYP			M06		
	$\Delta G^{298.15}$, $\frac{kJ}{mol}$	[Anti], %	[Syn], %	$\Delta G^{298.15}$, $\frac{kJ}{mol}$	[Anti], %	[Syn], %
6-31G	-7.8	96	4	-3.9	83	17
6-31G(d,p)	-6.5	93	7	-2.2	71	29
6-31G(3df,3pd)	-6.4	93	7	-3.2	78	22
6-31++G(d,p)	-6.6	94	6	-4.3	85	15
6-31++G(3df,3pd)	-6.8	94	6	-3.2	79	21
6-311G	-7.5	95	5	-3.2	78	22
6-311G(d,p)	-8.9	97	3	-1.1	61	39
6-311G(3df,3pd)	-8.8	97	3	-2.3	72	28
6-311++G(d,p)	-6.6	94	6	-2.2	71	29
6-311++G(3df,3pd)	-7.4	95	5	-1.9	68	32
cc-pVDZ	-4.2	85	15	-2.7	75	25
aug-cc-pVDZ	-8.2	97	3	-3.3	79	21
cc-pVTZ	-6.6	94	6	-2.4	72	28
aug-cc-pVTZ	-8.4	97	3	-2.5	74	26

this section we can say that the method is not a problem since good agreement with experiment is possible for 2-acetylthiophene oxime. In case of acetoin oxime all methods show relatively similar results, however, the calculated thermodynamics of *syn/anti* acetoin oxime isomerisation do not match experimantal data for the *syn/anti* equilibrium of LIX63 hydroxyoxime. This difference in thermodynamics is most likely to be due to the discrepancy in the size of the hydrocarbon side-chains of these two hydroxyoximes. Unfortunately, LIX63 hydroxyoxime is a large system and due to the limit in both time and computer resources we cannot afford to study the PES for each isomer. Therefore we need to estimate the effect of hydrocarbon side-chains on thermodynamics of equilibrium between two isomers and determine whether this effect is constant or not. However before testing this effect of hydrocarbon side-chains it would be interesting to check if the model of acetoin oxime is suitable for estimating the rate constants of *anti* to *syn* 5,8-diethyl-7-hydroxydodecan-6-oxime isomerisation.

3.3.2 Kinetics of *Syn/Anti* Hydroxyoxime Equilibrium

Three possible mechanisms for *anti* to *syn* hydroxyoxime isomerisation were selected to be of highest priority for consideration in the current study due to a number of reasons. Specifically these are: isomerisation via inversion, via tautomerisation of enamine compounds, and via tautomerisation of nitroso compounds. The reasons for considering only three mechanisms are as follows; first of all, experimental data listed in Table 3.3 corresponds to the *anti* to *syn* isomerisation in non-polar ShellSol D70 solvent, so isomerisation was not considered in the presence of water and/or acid. The presence of acid accelerates the *anti* to *syn* isomerisation of hydroxyoxime (Johnson *et al.*, 2001; Vasiltsov *et al.*, 2009) giving a higher percentage of *syn* isomer, which is the opposite of what is desired. Secondly, the photoisomerisation mechanism was considered irrelevant here because it requires energy in the form of light of a specific frequency in order to excite the hydroxyoxime molecule into the triplet state, which allows easy rotation about C = N double bond. Furthermore, the isomerisation of the oxime anions through C = N bond rotation does not appear to be a general mechanism according to Glaser and Streitwieser (1989) and Nsikabaka *et al.* (2006).

In this section we are going to analyse each of the three mechanisms by using transition state theory. In order to decrease the computational cost of studying the kinetics we have decided to use a similar assumption to that made in the study of the thermodynamics of *syn/anti* isomerisation, which was to use acetoin oxime instead of the LIX63 main component. The experimentally determined value of the rate constant of *anti* to *syn* 5,8-diethyl-7-hydroxydodecan-6-oxime isomerisation (Barnard and co-workers) is $1.007 \times 10^{-4}\text{s}^{-1}$ which corresponds to a value for the free energy of activation ($\Delta G_f^{\ddagger}$) being equal to 119.0 kJ/mol. According to transition state theory, the activation energy barrier can be calculated at a certain temperature by finding the Gibbs free energy difference at that temperature between the corresponding first order saddle point on the potential energy surface and its related minimum. As can be seen in the introduction section of the current chapter, along the paths for the tautomerisation mechanisms via enamine and nitroso compounds there are more than one stationary state and consequently more than one transition state. Therefore in order to estimate the total free energy of activation for *anti* to *syn* acetoin oxime interconversion via tautomerisation mechanisms we need to calculate the Gibbs free energy differences between each transition state and corresponding minimum. Note that after each transition state is optimised it is important to check if there is only one imaginary frequency and that back and forth following this imaginary frequency (IRC calculation) leads us to the stationary points of interest. Schematic reaction profiles for the inversion mechanism, as well as for the tautomerisation mechanisms, of the *anti* to *syn* acetoin oxime isomerisation via nitroso and enamine compounds are shown in Figures 3.15, 3.16 and 3.17,

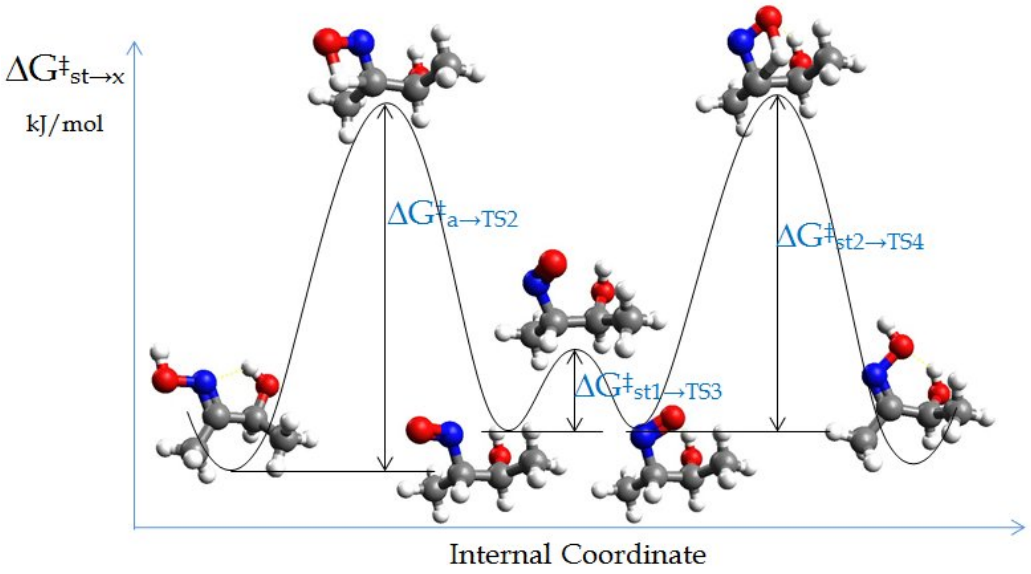

FIGURE 3.16: Reaction profile for the *anti* to *syn* acetoin oxime tautomerisation via nitroso compound. Atom colours: oxygen (O) - red; nitrogen (N) - dark blue; carbon (C) - grey and hydrogen (H) - white.

respectively.

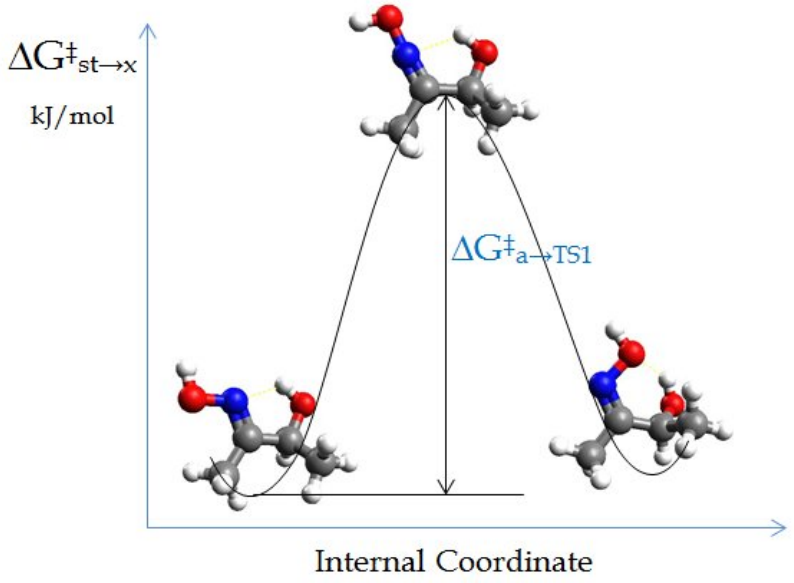

FIGURE 3.15: Reaction profile for the *anti* to *syn* acetoin oxime isomerisation via inversion mechanism. Atom colours: oxygen (O) - red; nitrogen (N) - dark blue; carbon (C) - grey and hydrogen (H) - white.

The $\Delta G^{\ddagger}_{(a \rightarrow TS1)}$ represented in Figure 3.15 corresponds to the Gibbs free energy of activation for the inversion mechanism, which can be calculated taking the difference

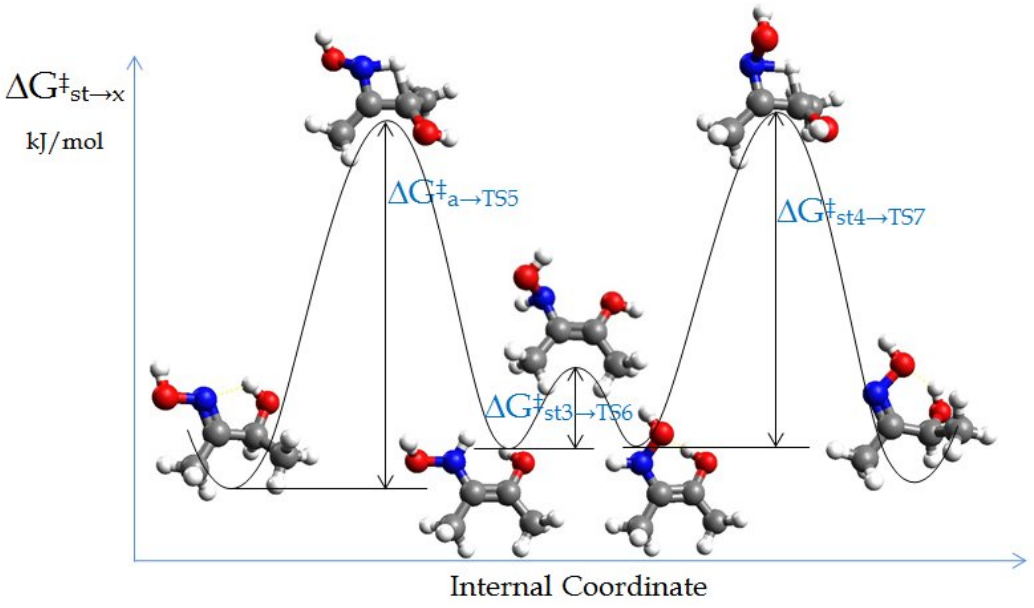

FIGURE 3.17: Reaction profile for the *anti* to *syn* acetoin oxime tautomerisation via enamine compound. Atom colours: oxygen (O) - red; nitrogen (N) - dark blue; carbon (C) - grey and hydrogen (H) - white.

between the Gibbs free energy of the transition state structure depicted at the maximum and the left side minimum of *anti*-acetoin oxime. The $\Delta G^{\ddagger}_{(a\rightarrow TS1)}$ calculated at the B3LYP/6-31G(d,p) level of theory is equal to 217.5 kJ/mol at 363 K. In a similar manner $\Delta G^{\ddagger}_{(a\rightarrow TS2)}$, $\Delta G^{\ddagger}_{(st1\rightarrow TS3)}$ and $\Delta G^{\ddagger}_{(st2\rightarrow TS4)}$ correspond to the Gibbs free energy differences between the transition states and the corresponding stationary structures in tautomerisation via a nitroso compound shown in Figure 3.16, while $\Delta G^{\ddagger}_{(a\rightarrow TS5)}$, $\Delta G^{\ddagger}_{(st3\rightarrow TS6)}$ and $\Delta G^{\ddagger}_{(st4\rightarrow TS7)}$ are those in tautomerisation via enamine compound shown in Figure 3.17. For the tautomerisation mechanism via a nitroso compound the values of $\Delta G^{\ddagger}_{(a\rightarrow TS2)}$, $\Delta G^{\ddagger}_{(st1\rightarrow TS3)}$ and $\Delta G^{\ddagger}_{(st2\rightarrow TS4)}$ calculated at the B3LYP/6-31G(d,p) level of theory for a temperature of 363 K are equal to 312.7, 92.1 and 308.5 kJ/mol, respectively, while the values of $\Delta G^{\ddagger}_{(a\rightarrow TS5)}$, $\Delta G^{\ddagger}_{(st3\rightarrow TS6)}$ and $\Delta G^{\ddagger}_{(st4\rightarrow TS7)}$ for the tautomerisation mechanism via an enamine compound estimated at the same level of theory and temperature are equal to 243.9, 78.7 and 241.2 kJ/mol, respectively. Unfortunately, none of the theoretically estimated free energies of activation using suggested mechanisms for *anti* to *syn* acetoin oxime isomerisation match well with the experimental value of $\Delta G^{\ddagger}_{(a\rightarrow x)}$=119.0 kJ/mol for 5,8-diethyl-7-hydroxydodecan-6-oxime. This could be due to one of several reasons; the B3LYP/6-31G(d,p) method may not be suitable for studying the kinetics of systems of this or a similar nature; neither of the suggested mechanisms for *anti/syn* hydroxyoxime isomerisation describes the way it is occurring in reality well enough, or that the properties derived from acetoin oxime do not correspond to those of the LIX63 main component. At this stage we do not have any alternative

mechanisms to the ones described above. Furthermore, until it is proven that the chosen method is appropriate for estimating the kinetics of *anti/syn* hydroxyoxime isomerisation we cannot conclude that the acetoin oxime model is non-suitable for studying the kinetics of *syn/anti* 5,8-diethyl-7-hydroxydodecan-6-oxime isomerisation.

As in the preceding section we are going to use four methods B3LYP, M06, M06-2X and MP2 in order to select the best compromise between accuracy and computing time for modelling *syn/anti* hydroxyoxime interconversion. Results of the MP2/aug-cc-pVTZ level of theory were chosen to be the reference. When the energy barriers are calculated as a function of method and basis set it is important to consider all types of transition states involved. At the end it would be great to have one method describing all types of transition states equally well for all the stationary points on the reaction profile. Therefore in order to select the most appropriate method we are going to compare the mean unsigned errors given by each method in estimating both kinetics and thermodynamics as compared to the MP2/aug-cc-pVTZ results, taking into account the amount of computer resources required by each method.

It is interesting to note that the shapes of the energy plots for the *anti* to *syn* tautomerisation mechanisms via enamine and nitroso compounds are similar. Both mechanisms include transfers of a hydrogen atom and the functional group rotation around a single C-N bond. This means that the nature of the transition states in both tautomerisations is also similar and therefore the trend of calculated energy barriers as a function of method and basis set is also expected to be similar. This gives us a total of three main types of transition state involved in selected mechanisms, namely: transition state for the inversion mechanism, one for hydrogen transfer, and one for functional group rotation around the C-N single bond. For calculation of $\Delta G^{\ddagger}_{(a \rightarrow x)}$ values involving the second and third types of transition state we are going to use those of the tautomerisation mechanism via a nitroso compound.

For the simplicity of the following let us denote the transition state of the hydrogen atom transfer from the oxime group (=NOH) to the carbon atom bonded to this group as TS1, the transition state for rotation of the -N=O group around the single C-N bond as TS2, and that of the inversion mechanism for *anti/syn* acetoin oxime isomerisation as TS3. The values of the Gibbs free energy differences between TS1, TS2 and TS3 and the *anti* isomer calculated at 363K are given in Tables 3.7, 3.8 and 3.9, respectively, using the B3LYP, M06, M06-2X and MP2 methods.

TABLE 3.7: Free energy difference between transition state TS1 and *anti*-acetoin oxime isomer, $\Delta G^{363}_{(TS1/Anti)}$ (kJ/mol), calculated as a function of method and basis set at 363K and corrected for a non-polar solvent.

Basis Set	Theoretical Method			
	B3LYP	M06	M06-2X	MP2
6-31G	328.9	333.6	351.9	339.9
6-31G(d,p)	312.7	315.1	326.8	317.4
6-31G(3df,3pd)	317.5	319.1	328.6	312.4
6-31++G(d,p)	320.2	322.9	332.1	320.7
6-31++G(3df,3pd)	319.9	320.6	330.4	313.4
6-311G	332.1	334.4	354.1	334.1
6-311G(d,p)	318.5	317.9	330.5	310.9
6-311G(3df,3pd)	322.9	320.8	333.7	315.1
6-311++G(d,p)	324.5	324.8	336.0	317.3
6-311++G(3df,3pd)	323.6	323.4	333.1	314.9
cc-pVDZ	305.1	306.0	321.7	302.7
aug-cc-pVDZ	317.0	318.2	327.2	308.9
cc-pVTZ	320.8	319.5	331.9	312.6
aug-cc-pVTZ	323.7	327.7	334.4	315.4

It can be seen from Table 3.7 that both the B3LYP and M06 methods for each of the considered basis sets provide very similar Gibbs free energy differences between TS1 and the *anti* isomer of acetoin oxime calculated at 363 K, while the value given by M06-2X calculations for the corresponding basis sets seem to be consistently higher. According to Zhao *et. al*, 2004, Hartree-Fock exchange gives higher barriers by reducing self interaction error. As was discussed in Chapter 2, the amount of Hartree-Fock exchange contribution is doubled in the M06-2X functional which could be the reason for this behaviour. It is important to note that this overestimation is particularly significant for cases when the considered transition state includes partially broken bonds and/or unusual bonding arrangements (Blanco *et al.*, 2009). This explains why the barrier height calculated for the transition state - TS1, in which the O-H bond is being broken and the C-H bond is being formed, is overestimated by the M06-2X method as compared to the corresponding MP2 calculations[4]. It is interesting to note that the energy barriers estimated for this type of transition state using the B3LYP, M06, M06-2X and MP2

[4]Note that MP2 is a single reference method and so might have problems too.

TABLE 3.8: Free energy difference between transition state TS2 and *anti*-acetoin oxime isomer, $\Delta G^{363}_{(TS2/Anti)}$ (kJ/mol), calculated as a function of method and basis set at 363K and corrected for a non-polar solvent.

Basis Set	Theoretical Method			
	B3LYP	M06	M06-2X	MP2
6-31G	100.5	101.6	104.3	85.3
6-31G(d,p)	92.1	92.1	92.9	84.6
6-31G(3df,3pd)	96.8	98.8	96.5	91.7
6-31++G(d,p)	100.0	103.1	98.1	91.4
6-31++G(3df,3pd)	100.8	102.3	99.6	95.8
6-311G	105.4	103.9	106.5	85.0
6-311G(d,p)	96.3	94.5	95.7	83.4
6-311G(3df,3pd)	100.7	98.4	98.7	94.4
6-311++G(d,p)	101.2	100.0	98.6	89.3
6-311++G(3df,3pd)	102.2	101.7	98.3	96.2
cc-pVDZ	89.6	89.0	92.7	78.4
aug-cc-pVDZ	98.9	101.1	96.0	89.6
cc-pVTZ	100.0	98.1	98.9	94.3
aug-cc-pVTZ	102.7	107.5	101.3	96.4

methods are very sensitive to the initial increase in the size of the basis sets. Hence the addition of polarization functions "d" and "p" to both heavy atoms and hydrogen, respectively, improves values of $\Delta G^{363}_{(TS1/Anti)}$ calculated using selected DFT methods as compared to the MP2/aug-cc-pVTZ results. However, further increase in the size of the basis sets does not have a significant impact on the free energy of activation calculated for TS1. A similar observation was made by Grein (2003) in his theoretical study of dihedral angle energy barriers of biphenyl. He showed that larger basis sets do not necessarily improve the kinetics estimated by the DFT methods. It is found that for this type of transition state, the basis sets developed by Dunning and co-workers (cc-pVXZ type of basis sets) give better values of activation energy barriers, however optimisation takes longer. Using the results derived at the MP2/aug-cc-pVTZ level of theory as the reference, the B3LYP/6-31G(d,p) and M06/6-31G(d,p) methods can be selected as giving the best possible estimation of $\Delta G^{363}_{(TS1/Anti)}$ for the least computer resources.

Now let us see how the selected functionals perform in studying the kinetics involving the second type of transition state - TS2. According to the results presented

TABLE 3.9: Free energy difference between transition state TS3 and *anti*-acetoin oxime isomer, $\Delta G^{363}_{(TS3/Anti)}$ (kJ/mol), calculated as a function of method and basis set at 363K and corrected for a non-polar solvent.

Basis Set	Theoretical Method			
	B3LYP	M06	M06-2X	MP2
6-31G	214.6	206.6	216.3	252.3
6-31G(d,p)	217.5	205.1	220.9	244.7
6-31G(3df,3pd)	217.7	202.2	221.9	238.6
6-31++G(d,p)	221.4	213.2	223.6	247.1
6-31++G(3df,3pd)	219.6	204.5	222.9	240.0
6-311G	214.5	208.0	217.0	249.3
6-311G(d,p)	217.6	206.0	222.2	239.3
6-311G(3df,3pd)	216.9	202.7	221.4	235.5
6-311++G(d,p)	220.3	210.3	223.8	242.0
6-311++G(3df,3pd)	217.7	205.4	220.3	236.7
cc-pVDZ	218.0	205.6	224.1	239.3
aug-cc-pVDZ	223.6	210.7	226.0	246.4
cc-pVTZ	217.4	204.6	221.1	236.7
aug-cc-pVTZ	218.5	210.0	222.0	239.2

in Table 3.8, at each level of theory the energy barriers for -N=O group rotation about the C-N single bond estimated with all three DFT functionals are overestimated by less than 5 kJ/mol in most cases. As expected, the $\Delta G^{363}_{(TS2/Anti)}$ overestimation is lower with larger basis sets as compared to the corresponding MP2 calculations and a bit larger when the DFT results with smaller basis sets like 6-31G, 6-311G and/or cc-pVDZ are compared. In other words, we can say that the overestimation of $\Delta G^{363}_{(TS2/Anti)}$ values by DFT methods is being decreased when larger basis sets are considered. The least expensive and best reproduction of MP2/aug-cc-pVTZ result can be achieved by any of the three DFT methods for this particular type of transition state using the 6-311G(d,p) basis set. It is also interesting to note that for this particular case all chosen DFT methods in combination with the 6-31G(d,p) basis set also give a good estimate of the energy barrier as compared to the MP2/aug-cc-pVTZ calculations.

The data presented in Table 3.9 corresponds to the values of the activation energy for the inversion mechanism of *anti* to *syn* acetoin oxime isomerisation calculated

TABLE 3.10: Percentage of underestimation of the free energy difference between transition state TS3 and *anti*-acetoin oxime isomer, (%), as compared to the MP2/aug-cc-pVTZ calculations as a function of method and basis set.

Basis Set	Theoretical Method		
	B3LYP	M06	M06-2X
6-31G	10.3	13.6	9.6
6-31G(d,p)	9.1	14.3	7.7
6-31G(3df,3pd)	9.0	15.5	7.2
6-31++G(d,p)	7.4	10.9	6.5
6-31++G(3df,3pd)	8.2	14.5	6.8
6-311G	10.3	13.0	9.3
6-311G(d,p)	9.0	13.9	7.1
6-311G(3df,3pd)	9.3	15.3	7.4
6-311++G(d,p)	7.9	12.1	6.4
6-311++G(3df,3pd)	9.0	14.1	7.9
cc-pVDZ	8.9	14.0	6.3
aug-cc-pVDZ	6.5	11.9	5.5
cc-pVTZ	9.1	14.5	7.6
aug-cc-pVTZ	8.7	12.2	7.2

with the B3LYP, M06, M06-2X and MP2 methods using different basis sets. In contrast to the previous results, the Gibbs free energy differences between this type of transition state (TS3) and *anti*-acetoin oxime calculated using DFT methods are underestimated comparing to the corresponding values of $\Delta G^{363}_{(TS3/Anti)}$ calculated using the MP2 method. The trend for the performance of the M06 functional is also changed in this case. M06 gives the lowest energy barriers for the inversion mechanism of *anti/syn* acetoin oxime isomerisation or, in other words, a greater degree of underestimation of $\Delta G^{363}_{(TS3/Anti)}$ values calculated using MP2, followed by the B3LYP and M06-2X methods. The B3LYP/6-31++G(d,p) and M06-2X/6-31++G(d,p) levels of theory can be recommended as adequate for modelling isomerisation mechanisms occurring via this type of transition state.

In order to make the comparison of the $\Delta G^{363}_{(TS3/Anti)}$ value calculated by each DFT method with the MP2/aug-cc-pVTZ results clearer let us have a look at the percentage underestimation of MP2/aug-cc-pVTZ values of $\Delta G^{363}_{(TS3/Anti)}$ by each DFT method as a function of basis set (Figure 3.10). As can be seen, the percentage of

TABLE 3.11: Mean unsigned error, (kJ/mol), of B3LYP, M06 and M06-2X in estimating the kinetics and thermodynamics of *anti* to *syn* isomerisation as compared to the MP2/aug-cc-pVTZ calculations as a function of method and basis set.

Basis Set	Theoretical Method		
	B3LYP	M06	M06-2X
6-31G	11.9	15.3	18.6
6-31G(d,p)	7.3	10.0	8.4
6-31G(3df,3pd)	6.3	11.9	8.4
6-31++G(d,p)	6.7	11.1	8.8
6-31++G(3df,3pd)	7.5	13.0	9.4
6-311G	13.9	15.6	19.6
6-311G(d,p)	6.4	9.4	8.3
6-311G(3df,3pd)	8.8	11.9	10.5
6-311++G(d,p)	8.5	11.4	9.9
6-311++G(3df,3pd)	9.4	13.4	10.3
cc-pVDZ	10.0	12.8	6.5
aug-cc-pVDZ	5.4	10.5	6.9
cc-pVTZ	7.9	11.4	9.7
aug-cc-pVTZ	9.3	16.3	10.8

underestimation of the reference $\Delta G^{363}_{(TS3/Anti)}$ value is quite constant as a function of basis set, which means that the barrier height does not depend significantly on the size of basis set when estimated by any of the chosen DFT methods. It is important to note that the percentage is slightly lower when diffuse functions are added to the basis set.

Now that we have both kinetics and thermodynamics of *syn/anti* acetoin oxime interconversion estimated by the B3LYP, M06 and M06-2X DFT methods as a function of basis set size, we can calculate the mean unsigned errors given by each of these methods in calculating the Gibbs free energy for *syn/anti* hydroxyoxime equilibrium and barrier heights for *anti* to *syn* interconversion as compared to the MP2/aug-cc-pVTZ results (Table 3.11).

Summarising the results, B3LYP/6-31G(d,p) can be recommended as the best compromise between the quality of barrier estimation involving different types of transition states and computer expense required for studying the kinetics of this particular type of system based on the MP2/aug-cc-pVTZ results as the reference. Unfortunately, the experimental value of the energy of activation for the *anti/syn* 5,8-diethyl-7-hydroxydodecan-6-oxime isomerisation process was not reproduced by any of the considered mechanisms using acetoin oxime as a model. When estimated at the MP2/aug-cc-pVTZ level of theory, the energy barrier (241.4 kJ/mol) for the inversion mechanism is the closest to the experimental activation energy barrier (119.0 kJ/mol) and seems to be the most realistic among the others. However, the difference between the theoretical and experimental barrier heights is too high to make any certain conclusions. As the next stage it would be interesting to see if there is any significant effect of the hydrocarbon side-chains on the estimated free energies of activation in the *anti* to *syn* hydroxyoxime interconversion.

3.4 Conclusions

Based on the results of the thermodynamics and kinetics of *anti/syn* acetoin oxime isomerisation presented in this chapter the B3LYP hybrid functional can be recommended for modelling of this type of system using 6-31G(d,p) and/or 6-31++G(d,p) basis sets.

The B3LYP method gives a good description of the thermodynamics of *syn/anti* acetoin oxime equilibrium and kinetics of *anti* to *syn* isomerisation as compared to the MP2/aug-cc-pVTZ level of theory. It is important to note that although M06 is slightly more expensive than B3LYP, and in some cases yields less accurate results as compared to MP2/aug-cc-pVTZ, it still can also be recommended for modelling both the kinetics and thermodynamics of organic constituents of synergistic solvent extraction systems and metal complexation processes occurring in them. The key reason for this is that in addition to describing well organic systems it is also known to provide good theoretical descriptions of the systems containing heavy elements, in particular transition metals (Zhao and Truhlar, 2008), which is a very important factor in modelling organometallic complexes.

Unfortunately at this stage we cannot select an optimal method based on the second criteria, which is the comparison to the experimental data. The most obvious hypothesis why the equilibrium between *syn* and *anti* isomers of hydroxyoxime was overestimated is that the effect of the R groups on it is not as insignificant as was hoped. Therefore, we have decided to study the effect of the size of the R groups on both the

thermodynamics and kinetics of *syn/anti* hydroxyoxime isomerisation, which is the subject of the next chapter.

3.5 References

Anslyn E.V. and Doughtery D.A. (2006) *Transition State Theory and Related Topics.* In Modern Physical Organic Chemistry University Science Books.

Barnard K.R. (2007) Isolation and characterisation of the LIX63 degradation products 5,8-diethyl-6,7-dodecanedione monooxime (keto-oxime) and 5,8-diethyl-6,7-dodecanediol (diol) and regeneration of oxime from keto-oxime. *Hydrometallurgy* **90**, 147-153.

Barnard K.R. and Urbani (2007) The effect of organic acids on LIX63 stability under harsh strip conditions and isolation of a diketone degradation product. *Hydrometallurgy* **89**, 40-51.

Barnard K.R. (2008) LIX63 stability in the presence of Versatic 10 under proposed commercial extract and strip conditions, part I: operation at high temperature. *Hydrometallurgy* **91**, 1-10.

Barnard K.R. and Turner N.L. (2008) LIX63 stability in the presence of Versatic 10 under proposed commercial extract and strip conditions, part II: oxime isomer interconversion and the effect of oxime degradation products on selected physical properties. *Hydrometallurgy* **91**, 11-19.

Barnard K.R. and Turner N.L. (2008) Reagent stability in synergistic SX systems incorporating LIX63 oxime and Versatic 10, part II: The El Boleo case study, SOLVENT EXTRACTION: Fundamentals to Industrial Applications. *Proceedings of ISEC 2008 International Solvent Extraction Conference*, 119-124.

Barnard K.R., Turner N.L. and Shiers D.W. (2010) LIX63 stability in the presence of Versatic 10 under proposed commercial extract and strip conditions, part III: Effect of manganese and cobalt loading on oxime stability at 30 ^{o}C. *Hydrometallurgy* **104**, 268-277.

Barnard K.R. and Tsuntsaeva M.N. (2012) The effect of hydroxyoxime isomer conformation on metal extraction in the LIX 63/Versatic 10 synergistic system. *Solvent Extraction and Ion exchange* **30** (6), 566-578.

Blanco F., Alkorta I. and Elguero J. (2009) Barriers about double carbon-nitrogen bond in imine derivatives (aldimines, oximes, hydrazones, azines). *Croatica Chemica Acta* **82**, 1-10.

Castresana J.M., Elizalde M.P., Aguilar M. and Cox M. (1988) Synergistic extraction of nickel by mixtures of alpha-hydroxyoximes and carboxylic acids. *Solvent Extraction and Ion exchange* **6**(2), 265-274.

Cheng C.Y. (2006) Solvent extraction of nickel and cobalt with synergistic systems of carboxylic acid and aliphatic hydroxyoxime. *Hydrometallurgy* **84**, 109-117.

Cheng C.Y., Barnard K.R. and Urbani M.D. (2005) Improving plant operations using synergistic solvent extraction technology and organic monitoring. *First Extractive Metallurgy Operators' Conference, Brisbane.* AUSIMM, Victoria, 59-66.

Conde S., Corral C. and Lissavetzky J. (1985) E- and Z-isomerism of 2-acetylthiophene oximes. *Journal of Heterocyclic Chemistry* **22**2, 301-304.

Csaszar A.G., Allen W.D. and Schaefer III H.F. (1998) In pursuit of the ab initio limit for conformational energy prototypes. *Journal of Chemical Physics* **108**, 23.

Ditchfield R, Hehre W.J. and Pople J.A. (1971) Self-Consistent Molecular Orbital Methods. 9. Extended Gaussian-type basis for molecular-orbital studies of organic molecules. *Journal of Chemical Physics* **54**, 724.

Dobashi T.S., Parker D.R. and Grubbs E.J. (1977) Rearrangements of nitrones to O-alkyl oximes via geometrically isomerizing iminoxy radicals. *Journal of the American Chemical Society* **99**(16), 5382-5387.

Dunning Jr.T.H. (1989) Gaussian basis sets for use in correlated molecular calculations. I. The atoms boron through neon and hydrogen. *Journal of Chemical Physics* **90**, 1007-23.

Frisch M.J., Trucks G.W., Schlegel H.B., Scuseria G.E., Robb M.A., Cheeseman J.R., Scalmani G., Barone V., Mennucci B., Petersson G.A., Nakatsuji H., Caricato M., Li X., Hratchian H.P., Izmaylov A.F., Bloino J., Zheng G., Sonnenberg J.L., Hada M., Ehara M., Toyota K., Fukuda R., Hasegawa J., Ishida M., Nakajima T., Honda Y., Kitao O., Nakai H., Vreven T., Montgomery J.A., Jr., Peralta J.E., Ogliaro F., Bearpark M., Heyd J.J., Brothers E., Kudin K.N., Staroverov V.N., Kobayashi R., Normand J., Raghavachari K., Rendell A., Burant J.C., Iyengar S.S., Tomasi J., Cossi M., Rega N., Millam J.M., Klene M., Knox J.E., Cross J.B., Bakken V., Adamo C., Jaramillo J., Gomperts R., Stratmann R.E., Yazyev O., Austin A.J., Cammi R., Pomelli C., Ochterski J.W., Martin R.L., Morokuma K., Zakrzewski V.G., Voth G.A., Salvador

P., Dannenberg J.J., Dapprich S., Daniels A.D., Farkas ., Foresman J.B., Ortiz J.V., Cioslowski J. and Fox D.J. (2009) *Gaussian*, Inc., Wallingford CT.

Georgieva I. and Trendafilova N. (2006) Comprehensive DFT and MO studies on glyoxilic acid oxime and related ions in gas phase and solution: Conformations, basicities and acidities. *Chemical Physycs* **321**, 311-324.

Glaser R., Murmann R.K. and Barnes C.L. (1996) Why do nitroso compounds dimerize while their oxime tautomers do not? A structural study of the *trans*-dimer of 2-chloro-2-methyl-3-nitrosobutane and higher level ab initio study of thermodynamic stabilities and electronic structures of isomers of diazene dioxides. *Journal of Organic Chemistry* **61**, 1047-1058.

Glaser R. and Streitwieser A. (1989) Configurational and conformational preferences in oximes and oxime carbanions. Ab initio study of the *syn* effect in reactions of oxyimine enolate equivalents. *Journal of the American Chemical Society* **111**, 7340-7348.

Goodrow A., Bell A.T. and Head-Gordon M. (2009) Transition state-finding strategies for use with the growing string method. *Journal of Chemical Physics* **130**, 244108(1-14).

Gordon M.S. (1980) The isomers of silacyclopropane. *Chemical Physics Letters* **76**, 163-68.

Grein F. (2003) New theoretical studies on the dihedral angle and energy barriers of biphenyl. *Journal of Molecular Structure (Theochem)* **624**, 23-28.

Halgren T.A. (1996) Merck molecular force field. I. Basis, form, scope, parameterization, and performance of MMFF94. *Journal of Computational Chemistry* **17**, 490-519.

Jennings W.B. and Boyd D.R. (1972) The mechanism of interconversion of (Z)- and (E)-ketimines. *Journal of the American Chemical Society* **94**(20), 7187-7188.

Johnson J.E., Morales N.M., Gorczyca A.M., Dolliver D.D. and McAllister M.A. (2001) Mechanisms of acid-catalized Z/E isomerisation of imines. *Journal of Organic Chemistry* **66**, 7979-7985.

Kendall R.A., Dunning Jr.T.H. and Harrison R.J. (1992) Electron affinities of the first-row atoms revisited. Systematic basis sets and wave functions. *Journal of Chemical Physics* **96**, 6796-806.

Long J.A., Harris N.J. and Lammertsma K (2001) Formaldehyde oxime nitrosomethane tautomerism. *Journal of Organic Chemistry* **66**, 6762-6767.

Maeda S. and Ohno K. (2005) A new approach for finding a transition state connecting a reactant and a product without initial guess: applications of the scaled hypersphere

search method to isomerisation reactions of HCN, (H2O)2, and alanine dipeptide. *Chemical Physics Letters* **404**, 95-99.

Marriott P., Aryusuk K., Shellie R., Ryan D., Krisnangkura K., Schuring V. and Trapp O. (2004) Molecular interpretation behaviour in comprehensive two-dimensional gas chromatography. *Journal of Chromatography A* **1033**, 135-143.

Mueller M. (2002) *Fundamentals of quanrum chemistry. Molecular spectroscopy and modern electronic structure computations.* New York, Boston, Dordrecht, London, Moscow: Kluwer Academic Publishers.

Nagy P.I., Kokosi J., Gergely A. and Racz A. (2003) Theoretical conformational analysis for codienone-6-oximes in gas phase and in solution. *Journal of Physical Chemistry A* **107**, 7861-7868.

Nsikabaka S., Harb W. and Ruiz-Lopes M.F. (2006) The role of water on the acid promoted E/Z isomerisation of oximes in aqueous solution. *Theochem* **764**, 161-166.

Ochterski J.W. 1999 Vibrational Analysis in Gaussian. *Gaussian, Inc*, 1-10.

Ochterski J.W. 2000 Thermochemistry in Gaussian. *Gaussian, Inc*, 2-19.

Padwa A. and Albrecht F. (1974) Concentration effects in the photochemical *syn-anti* isomerisation of an oxime ether. *Journal of Organic Chemistry* **39**(16), 2361-2366.

Padwa A. and Albrecht F. (1974) Photochemical *syn-anti* isomerisation about the carbon-nitrogen double bond. *Journal of the American Chemical Society* **96**(15), 4849-4857.

Peng C., Ayala P.Y., Schlegel H.B. and Frisch M.J. (1996) Using redundant internal coordinates to optimize equilibrium geometries and transition states. *Journal of Computational Chemistry* **17**, 49-56.

Peters B., Heyden A., Bell A.T. and Chakraborty A. (2004) A growing string method for determining transition states: Comparison to the nudged elastic band and string methods. *Journal of Chemical Physics* **120** (17), 7877-7886.

Peterson A.K., Woon D.E. and Dunning T.H.Jr. (1994) Benchmark calculations with correlated molecular wave functions. IV. The classical barrier height of the H+H2 H2+H reaction. *Journal of Chemical Physics* **100**, 7410-15.

Quapp W. (2005) A growing string method for the reaction pathway defined by a Newton trajectory. *The Journal of Chemical Physics* **122**, 174106(1-7).

Quapp W. (2007) Finding the transition state without initial guess: the growing string method for Newton trajectory to isomerisation and enantiomerisation reaction of alanine dipeptide and poly(15)alanine. *Journal of Computational Chemistry* **28**(11), 1834-1847.

Raghavachari K., Binkley J.S., Seeger R. and Pople J.A. (1980) Self-Consistent Molecular Orbital Methods. 20. Basis set for correlated wave-functions. *Journal of Chemical Physics* **72**, 650-54.

Rassolov V.A., Ratner M.A., Pople J.A., Redfern P.C. and Curtiss L. A. (2001) 6-31G* Basis Set for Third-Row Atoms. *Journal of Computational Chemistry* **22**, 976-84.

Ronchin R., Bortoluzzi M. and Vavasori A. (2008) A DFT study on secondary reaction pathways in the acid-catalysed Backmann rearrangement of cyclohexanone oxime in aprotic solvent. *Journal of Molecular Structure* **858**, 46-51.

Rusinska-Roszak D., Lozynski M., Korn M. and Mack H.G. (1995) Ab initio and PM3 calculated molecular structures and energies of acetoin oxime - the LIX63 progenitor. *Journal of Molecular Structure (Theochem)* **331**, 95-107.

Rusinska-Roszak D., Lozynski M. and Mack H.G. (1997) Ab initio and PM3 studies of hydrogen bonding of acetoin (E)- and (Z)-oxime dimers. Cooperativity and competition. *Journal of Molecular Structure (Theochem)* **393**, 177-187.

Schmidt M.W., Baldridge K.K., Boatz J.A., Elbert S.T., Gordon M.S., Jensen J.H., Koseki S., Matsunaga N., Nguyen K.A., Su S.J., Windus T.L., Dupuis M., Montgomery J.A. (1993) General atomic and molecular electronic structure system. *Journal of Computational Chemistry* **14**, 1347-1363.

Stewart J.J.P. (2007) Optimization of parameters for semiempirical methods. V. Modification of NDDO approximations and application to 70 elements. *Journal of Molecular Modelling* **13**, 1173-213.

Usvyat D., Civalleri B., Maschio L., Dovesi R., Pisani C. and Schutz M. (2011) Approaching the theoretical limit in periodic local MP2 calculations with atomic-orbital basis sets: The case of LiH. *Journal of Chemical Physics* **134**, 214105.

Vasiltsov A.M., Zhang K., Ivanov A.V., Ushakov I.A., Afonin A.V., Petrushenko K.B., Li S., Ma J.S., Mikhaleva A.I., Trofimov B.A. and Yang, G. (2009) 1-Vinylpyrrole-2-carbaldehyde oximes: synthesis, isomerisation, and spectral properties. *Monatsh Chemistry* **140**, 1475-1480.

Zhao Y., Pu J., Lynch B.J. and Truhlar D.G. (2004) Tests of second-generation and third-generation density functionals for thermochemical kinetics. *Journal of Chemical Physics* **6**, 673-676.

Zhao Y. and Truhlar D.G. (2008) The M06 suite of density functionals for main group thermochemistry, thermochemical kinetics, noncovalent interactions, excited states, and transition elements: two new functionals and systematic testing of four M06-class functionals and 12 other functionals. *Theoretical Chemistry Account* **120**, 215-241.

Chapter 4

Effect of the Hydrocarbon Side-chains on the *Syn/Anti* Equilibrium and Kinetics of Hydroxyoxime Isomerisation

4.1 Introduction

In the previous chapter the equilibrium between *syn* and *anti* isomers of acetoin oxime has been studied. It was expected that the thermodynamics and the kinetics of acetoin oxime isomerisation would be similar to those of the LIX63 main component. However, it was concluded that although both LIX63 and acetoin oxime have identical functional groups, an assumption on the relative insignificance of the nature of the hydrocarbon R groups on the equilibrium between *anti* and *syn* isomers of aliphatic α-hydroxyoxime is likely to be invalid. In 2009, Rappoport and Liebman showed that the effect of the nature of the R groups (aliphatic, aromatic, halogen-substituted aliphatic and aromatic) on the *syn/anti* equilibrium of oximes is quite significant. In their study the authors considered the *syn/anti* equilibrium of R-CH=NOH oxime with three substituents of a different nature: R=CH_3 (aldoxime), R=CH_2Cl (chloroacetaldoxime) and R=C_6H_5 (benzaldoxime). Rappoport and Liebman also considered the equilibrium between *syn* and *anti* isomers of acetophenone oxime which is obtained by substituting the H atom sitting on the carbon of the oxime group (-CH=NOH) in aldoxime with R=C_6H_5. The equilibrium between *syn* and *anti* isomers of these four oximes were estimated using equation 4.1;

$$K_{eq} = e^{(-\frac{\Delta G^o}{RT})} \tag{4.1}$$

where ΔG^o is the value of the standard Gibbs free energy difference between the *anti* and *syn* oxime isomers, R is the universal gas constant and T is the absolute temperature. The standard Gibbs free energy differences of *anti/syn* equilibrium for all four oximes were estimated at the B3LYP/6-311G(3df,2p) level of theory. The calculated equilibrium constants are as follows: acetaldoxime (R=CH_3) - $K_{ex} = 2.2$, chloroacetaldoxime (R=CH_2Cl) - $K_{ex} = 9.0$, benzaldoxime (R=C_6H_5) - $K_{ex} = 1.7 \times 10^{-2}$ and acetophenone oxime (R=CH_3 R'=C_6H_5) - $K_{ex} = 2.2 \times 10^{-2}$. From this data it can be seen that the stability of the *anti* oxime isomer increases in the following order: benzaldoxime < acetaldoxime < chloroacetaldoxime < acetophenone oxime. Based on this, it is possible that not only the nature but also the size of the R groups has a significant effect on the ratio between *syn* and *anti* hydroxyoxime isomers. In the current chapter it is examined how the size of the R groups affects both the kinetics and thermodynamics of the *syn/anti* hydroxyoxime isomerisation process.

The target molecule of 5,8-diethyl-7-hydroxydodecan-6-oxime has aliphatic R groups equal to C_7H_{15} on both ends as shown in Figure 3.10 and it is of great interest to see how the change of length of the R groups will affect the *syn/anti* equilibrium of hydroxyoxime moving from acetoin oxime to the LIX63 main component. In order to check this, we need to find the global minima for both isomers with R groups on each end of the molecule equal to -C_2H_5, -C_3H_7, -C_4H_9 and so on until the effect no longer varies.

4.2 Methodology

Based on the results of the previous chapter both B3LYP and M06 DFT functionals were selected for modelling the present type of system with the 6-31G(d,p) and 6-31++G(d,p) basis sets. These methods have been shown to be the best compromise between the time required for modelling and accuracy as compared to the performance of the MP2/aug-cc-pVTZ level of theory.

In order to find the global minima for both isomers of hydroxyoximes with R groups of different length, all possible conformers were constructed for each isomer using the Avogadro[1] molecular visualisation software and then optimised. Convergence criteria were chosen to be "tight" for geometry optimisation; that is the maximum and root

[1]Avogadro: an open-source molecular builder and visualization tool. Version 1.0.3/April 25, 2011 http://avogadro.openmolecules.net/

mean square gradient in Cartesian coordinates are set to 0.00001 a.u. and the maximum and root mean square of the Cartesian step to 0.00005 a.u. For practical reasons, all preliminary calculations of the minima have been performed using the semi-empirical PM6 method (Stewart, 2007) as implemented in the Gamess program (Schmidt *et al.*, 1993) and then the resulting structures were re-optimised at higher levels of theory using the Gaussian09 program (Frisch *et al.*, 2009). The Berny algorithm (which is set by default in Gaussian09) was used in geometry optimisation.

Vibrational frequencies were evaluated in order to determine the nature of each stationary point as well as to estimate the thermochemistry (Joseph, 2000). The Intrinsic Reaction Coordinates (IRCs) were computed in order to check if the transition states found connect the desired reactants and products.

4.3 Results and Discussion

In the previous chapter the B3LYP and M06 methods were found to be adequate for modelling E/Z hydroxyoxime equilibrium based on the comparison with the results derived from calculations at the MP2/aug-cc-pVTZ level of theory for acetoin oxime. It was shown that when large basis sets are used with added polarisation and diffuse functions to both hydrogen and heavy atoms, the B3LYP method tends to give very accurate Gibbs free energies for the *syn/anti* acetoin oxime equilibrium, while M06 tends to overestimate the thermodynamics by up to 4 kJ/mol as compared to the MP2/aug-cc-pVTZ value. However, when 6-31G(d,p) and/or 6-31++G(d,p) basis sets are used both methods (B3LYP and M06) give very similar results which are still fairly close to those derived at the MP2/aug-cc-pVTZ level of theory. This gave us a reason to keep both functionals, although this situation may be different when E/Z equilibrium between larger hydroxyoximes is considered.

It is also worth noting that both B3LYP and M06 methods predict similar structures for the global minima for *syn* and *anti*-acetoin oxime. However, this similarity may also be changed when hydroxyoximes with larger hydrocarbon side-chains are considered. Therefore, it is also interesting to see how both of these methods perform in the potential energy surface (PES) scans of hydroxyoxime molecules with R groups of different size in order to see if both of these methods still locate similar global minima on the PES.

4.3.1 Thermodynamics of the *Syn/Anti* Hydroxyoxime Equilibrium

The first step in studying the effect of the size of R groups on the *syn/anti* equilibrium was to scan the potential energy surface of the hydroxyoxime in which the R groups on both ends (oximic and carboxylic) were equal to C_2H_5 leading to the molecule of 4-hydroxyhexane-3-oxime. All possible conformers of *syn*- and *anti*-4-hydroxyhexane-3-oxime can be divided into three groups depending on the value of the -NCCO- torsion angle. Potential energy surface scans were performed for each of these groups changing $-NC(CC)_{R1}-$ and $-NC(CC)_{R2}-$ torsion angles in a systematic manner[2]. The notation of the 4-hydroxyhexan-3-oxime conformers should be interpreted as follows: I-Anti 1-2 means that this conformer is the *anti* isomer of 4-hydroxyhexan-3-oxime which belongs to the first group (structure "a" in Figure 4.1) where first methyl group ($R=CH_3$) is added to position 1 which is coloured black in Figure 4.1 and second methyl group is added to position 2 which is coloured blue in Figure 4.1.

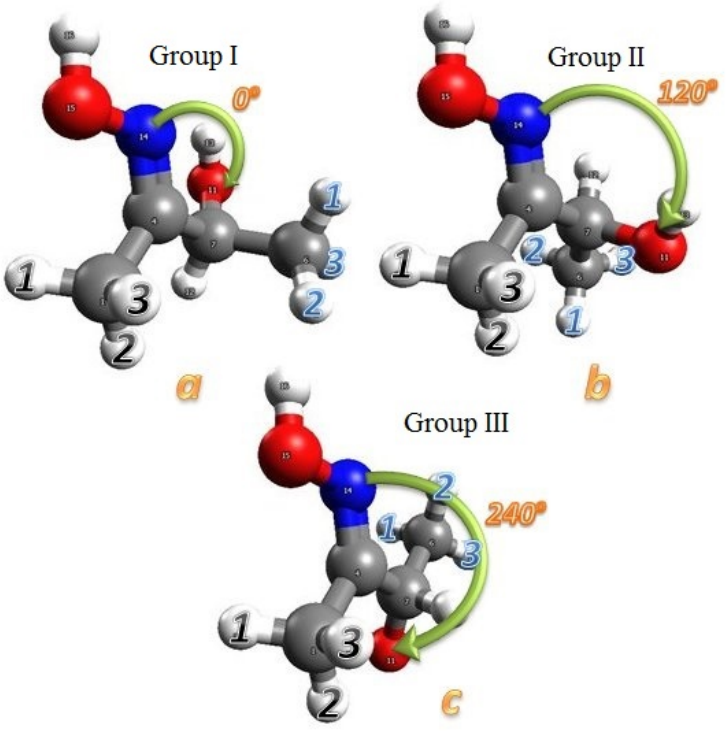

FIGURE 4.1: Example of acetoin oxime conformer division into three groups. Group I (a) - NCCO torsion angle close to 0^o, Group II (b) - NCCO torsion angle close to 120^o and Group III (c) - NCCO $\approx 240^o$. Black numbers correspond to the position of the first methyl group and blue numbers - to that of second one. Atom colours: oxygen (O) - red; nitrogen (N) - dark blue; carbon (C) - grey and hydrogen (H) - white.

[2]Note that -HONC- and -HOCC- torsion angles of a functional group were not considered as variables for this PES scan. Their values corresponding to the lower energy structures were chosen based on the full PES scan of acetoin oxime.

All possible conformers of *syn* and *anti* hydroxyoxime isomers were constructed and then optimised at the B3LYP/6-31G(d,p) and M06/6-31G(d,p) levels of theory. Gibbs free energy and enthalpy differences between each structure and the lowest energy conformer calculated for both isomers at 363 K at the B3LYP/6-31G(d,p) level of theory are given in Tables 4.1, 4.2 and 4.3 for groups I, II and III, respectively. As can be seen from Tables 4.1, 4.2 and 4.3, the I-Anti 1-3 and I-Syn 1-3 conformers of the first group are the lowest energy structures, corresponding to the global minima on the potential energy surface of *anti-* and *syn-* isomers of 4-hydroxyhexan-3-oxime, respectively. The lowest energy I-Anti 1-3 structure is therefore used as the reference configuration for all three groups. If we look at the thermodynamics between the lowest energy conformers of the *anti* and *syn* isomers we see that the Gibbs free energy difference (ΔG^{o}_{363}) of *anti/syn* equilibrium for 4-hydroxyhexan-3-oxime is 4.8 kJ/mol, as compared to 11.8 kJ/mol for acetoin oxime. This corresponds to a 17% vs 83% distribution of *syn* and *anti* isomers, respectively, instead of 2 vs 98%. This demonstrates the importance of the nature of the R groups. It is also interesting to note that *anti* 1-1, 2-3, 3-1, 3-3 and *syn* 1-3, 2-3 of the first group are very close energetically and in reality could possibly co-exist together at 363 K. The ΔG^{o}_{363} between *syn* and *anti* structures and their corresponding conformers of the second and third groups of hydroxyoxime isomers in most cases is greater than, or equal to, 5 kJ/mol, which gives them a low probability of coexistence with the lowest energy structure. Imagine all these conformers of 4-hydroxyhexan-3-oxime are present in the real system. Now having the energetics of any single conformer in the system we can easily calculate their population in solution using the Boltzmann distribution, which can be written as follows;

$$P_i = \frac{e^{-\frac{\Delta G_{i-A}}{RT}}}{\sum_{j=1}^{N_{tot}} e^{-\frac{\Delta G_{j-A}}{RT}}} \tag{4.2}$$

where P_i is the probability of finding the conformer i within the mixture of all conformers; ΔG_{i-A} is the Gibbs free energy difference between conformer i and the lowest energy conformer; R is the molar ideal gas constant and T is the temperature in Kelvin. The denominator of this equation corresponds to the sum from 1 to N_{tot}, where N_{tot} corresponds to the total number of conformers. The calculated populations of all conformers based on the thermodynamics computed at the B3LYP/6-31G(d,p) level of theory are given in Table 4.4. The overall distribution of *syn* and *anti* isomers of 4-hydroxyhexan-3-oxime within this mixture calculated at the B3LYP/6-31G(d,p) level is 13.4 and 86.6%, respectively, which is closer to the experimental data (36.0% of *syn* and 64.0% of *anti* isomers for the main component of LIX63 hydroxyoxime) as compared to 2.0 and 98.0% of *syn* and *anti* isomers calculated for acetoin oxime. This indicates that there is a

TABLE 4.1: Gibbs free energy (ΔG^o_{363}, kJ/mol) and enthalpy (ΔH^o_{363}, kJ/mol) differences relative to the most stable conformer for group-I of 4-hydroxyhexan-3-oxime conformers calculated at the B3LYP/6-31G(d,p) level of theory.

Anti-isomer	B3LYP/6-31G(d,p)		*Syn*-isomer	B3LYP/6-31G(d,p)	
	ΔG^o_{363}, $\frac{kJ}{mol}$	ΔH^o_{363}, $\frac{kJ}{mol}$		ΔG^o_{363}, $\frac{kJ}{mol}$	ΔH^o_{363}, $\frac{kJ}{mol}$
I-Anti 1-1	1.1	1.3	I-Syn 1-1	12.3	9.8
I-Anti 1-2	9.4	9.2	I-Syn 1-2	9.2	6.2
I-Anti 1-3	0.0	0.0	I-Syn 1-3	4.8	2.2
I-Anti 2-1	1.1	1.3	I-Syn 2-1	13.2	11.3
I-Anti 2-2	14.4	15.3	I-Syn 2-2	10.1	7.8
I-Anti 2-3	1.4	3.8	I-Syn 2-3	5.9	3.8
I-Anti 3-1	3.6	1.6	I-Syn 3-1	18.7	15.4
I-Anti 3-2	12.6	11.1	I-Syn 3-2	16.6	13.4
I-Anti 3-3	0.8	-0.1	I-Syn 3-3	8.8	5.6

TABLE 4.2: Gibbs free energy (ΔG^o_{363}, kJ/mol) and enthalpy (ΔH^o_{363}, kJ/mol) differences relative to the most stable conformer for group-II of 4-hydroxyhexan-3-oxime conformers calculated at the B3LYP/6-31G(d,p) level of theory.

Anti-isomer	B3LYP/6-31G(d,p)		*Syn*-isomer	B3LYP/6-31G(d,p)	
	ΔG^o_{363}, $\frac{kJ}{mol}$	ΔH^o_{363}, $\frac{kJ}{mol}$		ΔG^o_{363}, $\frac{kJ}{mol}$	ΔH^o_{363}, $\frac{kJ}{mol}$
II-Anti 1-1	19.7	17.6	II-Syn 1-1	20.3	17.4
II-Anti 1-2	8.3	6.7	II-Syn 1-2	17.4	14.6
II-Anti 1-3	5.4	4.8	II-Syn 1-3	11.0	8.4
II-Anti 2-1	13.7	14.0	II-Syn 2-1	23.6	20.0
II-Anti 2-2	8.3	6.7	II-Syn 2-2	27.2	26.0
II-Anti 2-3	5.4	4.8	II-Syn 2-3	16.7	13.4
II-Anti 3-1	14.9	14.4	II-Syn 3-1	28.6	24.7
II-Anti 3-2	5.2	5.9	II-Syn 3-2	19.2	16.8
II-Anti 3-3	4.2	4.8	II-Syn 3-3	14.4	12.2

TABLE 4.3: Gibbs free energy (ΔG^o_{363}, kJ/mol) and enthalpy (ΔH^o_{363}, kJ/mol) differences relative to the most stable conformer for group-III of 4-hydroxyhexan-3-oxime conformers calculated at the B3LYP/6-31G(d,p) level of theory.

Anti-isomer	B3LYP/6-31G(d,p)		*Syn*-isomer	B3LYP/6-31G(d,p)	
	ΔG^o_{363}, $\frac{kJ}{mol}$	ΔH^o_{363}, $\frac{kJ}{mol}$		ΔG^o_{363}, $\frac{kJ}{mol}$	ΔH^o_{363}, $\frac{kJ}{mol}$
III-Anti 1-1	13.5	12.0	III-Syn 1-1	19.8	17.3
III-Anti 1-2	9.6	8.9	III-Syn 1-2	12.8	12.7
III-Anti 1-3	7.4	6.5	III-Syn 1-3	8.3	7.4
III-Anti 2-1	12.9	12.3	III-Syn 2-1	20.3	18.7
III-Anti 2-2	9.6	8.9	III-Syn 2-2	20.1	18.7
III-Anti 2-3	7.4	6.5	III-Syn 2-3	12.2	10.7
III-Anti 3-1	12.9	12.3	III-Syn 3-1	15.2	14.0
III-Anti 3-2	7.5	8.1	III-Syn 3-2	16.5	15.3
III-Anti 3-3	5.5	5.9	III-Syn 3-3	10.9	9.5

TABLE 4.4: Conformer population (%) computed from a Boltzmann distribution using the Gibbs free energies calculated at the B3LYP/6-31G(d,p) level of theory for each conformer at 363K.

Anti-isomer	B3LYP/6-31G(d,p)			*Syn*-isomer	B3LYP/6-31G(d,p)		
	Group I, %	Group II, %	Group III, %		Group I, %	Group II, %	Group III, %
Anti 1-1	13.2	0.0	0.2	Syn 1-1	0.3	0.0	0.0
Anti 1-2	0.8	1.2	0.8	Syn 1-2	0.9	0.1	0.3
Anti 1-3	19.1	3.2	1.6	Syn 1-3	3.9	0.5	1.2
Anti 2-1	0.0	0.2	0.0	Syn 2-1	0.2	0.0	0.0
Anti 2-2	0.2	0.0	0.0	Syn 2-2	0.7	0.0	0.0
Anti 2-3	12.0	0.0	0.0	Syn 2-3	2.7	0.1	0.3
Anti 3-1	5.8	0.1	0.3	Syn 3-1	0.0	0.0	0.1
Anti 3-2	0.3	3.4	1.6	Syn 3-2	0.1	0.0	0.1
Anti 3-3	14.5	4.8	3.1	Syn 3-3	1.0	0.2	0.5
Sum, %		86.6		Sum, %		13.4	

significant effect of the size of R groups on the overall *syn/anti* hydroxyoxime distribution. Such an effect could be explained by either the steric and/or inductive effects of R groups (Turovtsev and Orlov, 2009). However, in order to reach a definite conclusion a separate study of steric and inductive effects of R groups of various size on *syn/anti* hydroxyoxime equilibrium should be undertaken. For now it is clear that the size of the hydrocarbon side-chains primarily affects the ΔG^o_{363} value between the global minima of the two isomers and, therefore all that is needed in order to get the realistic ratio between the two isomers is to find the lowest limit for the size of R groups beyond which it will not significantly affect the equilibrium ratio between *syn* and *anti* hydroxyoxime isomers.

Before moving forward it is important to say that this effect of the size of hydroxyoxime's R groups on the $\Delta G^o_{s\to a}$ is due to the significant change in enthalpy and moderate change in entropy of isomerisation between *syn* and *anti* isomers of 4-hydroxyhexan-3-oxime as compared to that of acetoin oxime: $\triangle H_{s\to a}$=2.2 kJ/mol and $\triangle S_{s\to a}$=-2.6 kJ/mol for 4-hydroxyhexan-3-oxime versus $\triangle H_{s\to a}$=7.0 kJ/mol and $\triangle S_{s\to a}$=-4.8 kJ/-mol for acetoin oxime. Note that the thermochemistry used for calculating these values of $\triangle H_{s\to a}$ and $\triangle S_{s\to a}$ were estimated at the B3LYP/6-31G(d,p) level of theory at 363 K.

As can be seen from Tables 4.1, 4.2 and 4.3, most of the conformers of *anti*-4-hydroxyhexan-3-oxime were found to be stable according to the B3LYP/6-31G(d,p) calculations. However, it is important to note that I-Anti 1-1 and I-Anti 2-1 conformers have identical values of ΔG^o_{363} and ΔH^o_{363}. This is because during the calculation at the B3LYP/6-31G(d,p) level of theory the initial structure of I-Anti 2-1 4-hydroxyhexan-3-oxime conformer was optimised to the I-Anti 1-1 one. The same thing happened for the II-Anti 2-2, II-Anti 2-3, III-Anti 2-1, III-Anti 2-2 and III-Anti 2-3 structures, which optimised to the II-Anti 1-2, II-Anti 1-3, III-Anti 3-1, III-Anti 1-2 and III-Anti 1-3 4-hydroxyhexan-3-oxime conformers, respectively. According to the B3LYP/6-31G(d,p) calculations this means that these conformations are not stable and revert to the closest minima. Therefore the population for each of these conformers is equal to zero in Table 4.4. However, in case of *syn*-4-hydroxyhexan-3-oxime isomers the situation is different. All possible structures were located at the B3LYP/6-31G(d,p) level of theory and the zero values of *syn*-4-hydroxyhexan-3-oxime conformer populations in the Table 4.4 correspond to the case of large ΔG_{j-A} values.

In the previous chapter we have seen how different levels of theory perform for the thermodynamics and kinetics of the isomerisation process between the lowest energy structures of *syn* and *anti* isomers of acetoin oxime. It was shown that there is no significant difference in the potential energy surface scans of the acetoin oxime molecule performed using either the B3LYP or M06 DFT functionals. Even though there were some minor differences in the relative stabilities of the optimised conformers, the global

minima of *syn* and *anti* acetoin oxime isomers found with the B3LYP method were identical to those found with M06. This, however, may not be the case when the size of the R groups of the hydroxyoxime is increased. Therefore before moving on to study the PES of the hydroxyoxime with R groups equal to C_3H_7 (2,5-dimethyl-4-hydroxyhexan-3-oxime) it is important to make sure that both B3LYP and M06 DFT functionals are suitable to perform the potential energy surface scan of the current system.

The Gibbs free energy differences (ΔG^o_{363}) and enthalpy changes (ΔH^o_{363}) between each conformer in the first group of *syn*/*anti* isomers and the lowest energy structure of 4-hydroxyhexan-3-oxime calculated at the M06/6-31G(d,p) level of theory are given in Table 4.5. The trend of relative stabilities between each group of isomers calculated with M06 is identical to B3LYP giving the first group of isomers as the most stable. The calculated values of ΔG^o_{363} between the conformers of the second/third group and the lowest energy structure of the first group *anti* isomer is greater than, or equal to 5 kJ/mol. Therefore for the purpose of conciseness, we have decided to show here only the relative energetics for the first group's conformers and an interested reader is referred to the Appendix for the full data.

TABLE 4.5: Gibbs free energy (ΔG^o_{363}, kJ/mol) and enthalpy (ΔH^o_{363}, kJ/mol) differences relative to the most stable conformer for group-I of 4-hydroxyhexan-3-oxime conformers calculated at the M06/6-31G(d,p) level of theory.

Anti-isomer	M06/6-31G(d,p)		*Syn*-isomer	M06/6-31G(d,p)	
	ΔG^o_{363}, $\frac{kJ}{mol}$	ΔH^o_{363}, $\frac{kJ}{mol}$		ΔG^o_{363}, $\frac{kJ}{mol}$	ΔH^o_{363}, $\frac{kJ}{mol}$
I-Anti 1-1	1.9	3.1	I-Syn 1-1	15.1	13.6
I-Anti 1-2	10.6	12.0	I-Syn 1-2	10.8	9.6
I-Anti 1-3	2.6	4.8	I-Syn 1-3	8.3	7.7
I-Anti 2-1	5.2	5.8	I-Syn 2-1	16.1	15.4
I-Anti 2-2	14.9	16.6	I-Syn 2-2	12.3	11.9
I-Anti 2-3	4.2	7.5	I-Syn 2-3	8.6	9.8
I-Anti 3-1	0.0	0.0	I-Syn 3-1	20.3	18.4
I-Anti 3-2	14.2	12.7	I-Syn 3-2	17.7	16.4
I-Anti 3-3	0.6	2.0	I-Syn 3-3	11.4	10.3

As can be seen by comparing Tables 4.1 and 4.5, while the conformation of the *syn* isomer global minimum found at the M06/6-31G(d,p) level of theory is identical with the one found using B3LYP/6-31G(d,p), in the case of the *anti* isomers of 4-hydroxyhexan-3-oxime there is a difference. According to the M06 calculations, the I-Anti 3-1 conformer

corresponds to the lowest energy structure and not the I-Anti 1-3 one predicted to be the global minimum by B3LYP calculations. If we look at the geometrical representations of the lowest energy structures found with both B3LYP/6-31G(d,p) and M06/6-31G(d,p) levels of theory, depicted in Figure 4.2, we can see that the R groups in the ground state structure predicted by M06 calculations are in a gauche-gauche-type (GG-type) orientation where the end carbon atoms are pointing towards each other. According to Gruzman *et al.* (2009) when the interactions in GG-type conformers are predicted, this effect could be due to the overestimation of the Coulomb interaction between the carbon atoms, which is a common drawback of the M06 family of functionals. In addition to this, as compared with the MP2 calculations using the same 6-31G(d,p) basis set, the B3LYP hybrid method predicts the correct global minimum for *anti*-4-hydroxyhexan-3-oxime in contrast to M06[3].

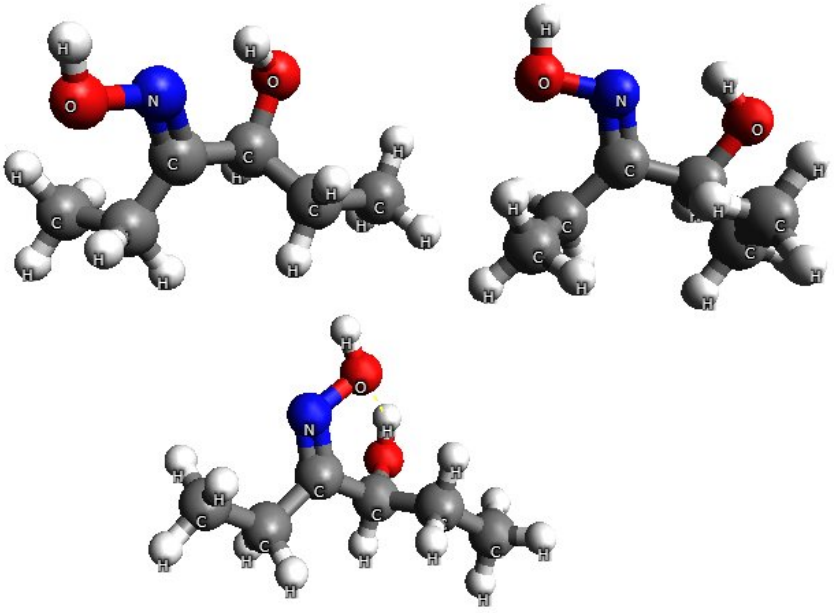

FIGURE 4.2: The lowest energy structures for *syn*- and *anti*-hydroxyoxime with R groups equal to -C_2H_5. Top left corner structure corresponds to I-Anti 1-3, top right - to I-Anti 3-1 and bottom structure is for I-Syn 1-3. Grey coloured atoms represent carbon, red - oxygen, dark blue - nitrogen and white - hydrogen atoms.

It is interesting to note that at the M06/6-31G(d,p) level of theory the ΔG^o_{363} between I-Anti 1-3 and the more stable I-Anti 3-1 conformer is equal to 2.6 kJ/mol, which means that both of these conformers may co-exist in the real mixture. In contrast to M06,

[3]Note that at the MP2/6-31G(d,p) the ΔG^o_{363} value between I-Anti 3-1 and I-Anti 1-3 4-hydroxyhexan-3-oxime conformers is only equal to 0.5 kJ/mol at 363 K, however, this may differ significantly with respect to the basis set size.

B3LYP calculations with the same basis set predict I-Anti 1-3 to be more stable than I-Anti 3-1 by 3.6 kJ/mol. It is clear that the selected DFT functionals predict different geometries for the global minimum of *anti*-4-hydroxyhexan-3-oxime; however, the geometry of the global minimum predicted for the *syn* isomer by B3LYP calculations matches the one found with the M06 functional. Before drawing any conclusion we need to have a look at the population of different conformers of 4-hydroxyhexan-3-oxime predicted by the M06/6-31G(d,p) method. The overall distribution of *syn* and *anti* isomers corresponds to 6.0 and 94.0%, respectively, when considering the equilibria between all possible conformers of 4-hydroxyhexan-3-oxime (Table 4.6). When the results are compared with the overall *syn/anti* isomer distribution estimated for acetoin oxime it is clear that at this stage, in contrast to B3LYP, the effect of a size of R groups on the *syn/anti* 4-hydroxyhexan-3-oxime equilibrium predicted at the M06/6-31G(d,p) level of theory is not as significant.

TABLE 4.6: Conformer population (%) computed from a Boltzmann distribution using the Gibbs free energies calculated at the M06/6-31G(d,p) level of theory for each conformer at 363K.

Anti-isomer	M06/6-31G(d,p)			*Syn*-isomer	M06/6-31G(d,p)		
	Group I, %	Group II, %	Group III, %		Group I, %	Group II, %	Group III, %
Anti 1-1	13.4	0.0	0.1	Syn 1-1	0.2	0.0	0.1
Anti 1-2	0.7	3.2	0.8	Syn 1-2	0.7	0.1	0.0
Anti 1-3	10.7	1.8	0.2	Syn 1-3	1.6	0.3	0.1
Anti 2-1	4.5	0.0	0.0	Syn 2-1	0.1	0.0	0.0
Anti 2-2	0.2	0.0	0.1	Syn 2-2	0.4	0.0	0.0
Anti 2-3	6.3	0.0	0.0	Syn 2-3	1.5	0.3	0.1
Anti 3-1	25.2	0.0	0.0	Syn 3-1	0.0	0.0	0.1
Anti 3-2	0.2	1.8	0.5	Syn 3-2	0.1	0.0	0.0
Anti 3-3	20.4	2.9	0.4	Syn 3-3	0.6	0.0	0.2
Sum, %		93.5		Sum, %		6.5	

It is worth noting that in the first group of *syn* and *anti* isomers of 4-hydroxyhexan-3-oxime there are two types of intramolecular hydrogen bonding: -OH$\cdots$O- in *syn* and -OH$\cdots$N- in *anti* isomers of the hydroxyoxime molecule. Therefore another very important factor to consider when studying the potential energy surface of the systems of this nature is the level of accuracy at which this type of intramolecular interaction is

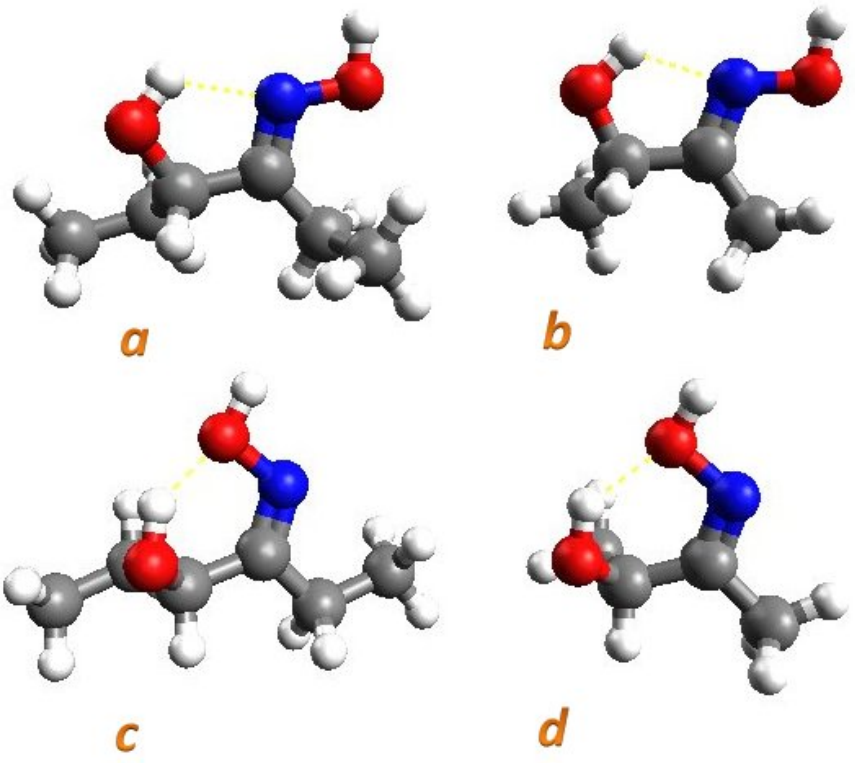

FIGURE 4.3: Intra-molecular hydrogen bonding in the lowest energy conformations of *anti* and *syn* isomers of 4-hydroxyhexan-3-oxime (a and c) and acetoin oxime (b and d) calculated at the B3LYP/6-31G(d,p) level of theory. Values of the lengths (in Angstroms) of the represented hydrogen bonds (yellow dashed line) are as follows: a) 2.020, b) 1.991, c) 1.942 and d) 1.951. Grey coloured atoms represent carbon, red - oxygen, dark blue - nitrogen and white - hydrogen atoms.

described. If we compare the lengths of intramolecular hydrogen bonds in *syn* and *anti* isomers of acetoin oxime with those in the corresponding isomers of 4-hydroxyhexan-3-oxime (Figure 4.3) we see that there is no significant difference in intramolecular hydrogen bonding strength when comparing corresponding isomers of these two molecules, as calculated at the B3LYP/6-31G(d,p) level of theory. According to Csonka *et al.* (1996), hydrogen bonding interactions are better described when diffuse functions are added to the basis set due to the additional variational freedom provided for the electrons remote from the nuclei. Therefore it was also of interest to see if there is any effect of diffuse functions (added to both hydrogen and heavy atoms) on the relative energetics of different conformers.

As was previously discussed, there were some stationary points which could not be located by B3LYP/6-31G(d,p) but were successfully found at the M06/6-31(d,p) level of theory. The addition of diffuse functions may affect not just the relative energetics but also the success in location of these stationary points. Therefore it was decided to use

TABLE 4.7: Gibbs free energy (ΔG^o_{363}, kJ/mol) and enthalpy (ΔH^o_{363}, kJ/mol) differences relative to the most stable conformer for group-I of 4-hydroxyhexan-3-oxime conformers calculated at the B3LYP/6-31++G(d,p) level of theory.

Anti-isomer	B3LYP/6-31++G(d,p)		*Syn*-isomer	B3LYP/6-31++G(d,p)	
	ΔG, $\frac{kJ}{mol}$	ΔH, $\frac{kJ}{mol}$		ΔG, $\frac{kJ}{mol}$	ΔH, $\frac{kJ}{mol}$
I-Anti 1-1	2.5	2.6	I-Syn 1-1	16.2	12.9
I-Anti 1-2	8.6	8.8	I-Syn 1-2	11.5	8.0
I-Anti 1-3	0.0	0.0	I-Syn 1-3	7.5	4.7
I-Anti 2-1	2.2	2.4	I-Syn 2-1	16.6	13.6
I-Anti 2-2	13.6	15.2	I-Syn 2-2	11.6	8.7
I-Anti 2-3	4.1	4.4	I-Syn 2-3	7.6	5.4
I-Anti 3-1	6.6	3.7	I-Syn 3-1	22.6	18.3
I-Anti 3-2	13.1	11.4	I-Syn 3-2	18.1	14.8
I-Anti 3-3	2.9	0.7	I-Syn 3-3	11.3	7.7

manually constructed initial geometries of all possible conformers of 4-hydroxyhexan-3-oxime, as was done previously, and not the structures optimised with the corresponding DFT functional using the 6-31G(d,p) basis set. Gibbs free energy differences (ΔG^o_{363}) and enthalpy changes (ΔH^o_{363}) between the first group of conformers and the global minimum of *anti* isomer calculated at the B3LYP/6-31++G(d,p) and M06/6-31++G(d,p) levels of theory are given in Tables 4.7 and 4.8, respectively[4]. As can be seen, the addition of diffuse functions does not significantly affect the hierarchy in terms of stabilities of *syn* conformers relative to the lowest energy structure of the *anti* isomer. However, the overall picture of the potential energy surface of *anti*-4-hydroxyhexan-3-oxime predicted at the M06/6-31++G(d,p) level of theory is changed a little bit as compared to the M06/6-31G(d,p) one. However, the M06 functional still predicts a different conformation to be the global minimum for *anti*-4-hydroxyhexan-3-oxime as compared to the B3LYP calculations using same basis set. It should be noted that this time M06 predicts the I-Anti 1-1 conformation to be the global minimum of *anti*-4-hydroxyhexan-3-oxime when used with the 6-31++G(d,p) basis set and not the I-Anti 3-1 one that was found to be the lowest energy conformation at the M06/6-31G(d,p) level of theory. However, calculated at the M06/6-31++G(d,p) level of theory, values of the Gibbs free energy differences for I-Anti 1-3 and I-Anti 3-1 relative to the lowest energy conformer (I-Anti

[4]Note that the full potential energy surface of 4-hydroxyhexan-3-oxime was scanned at both B3LYP/6-31++G(d,p) and M06/6-31++G(d,p) levels of theory. However, not to overwhelm the thesis with the large amount of data, the relative stabilities of the second and third groups of *syn* and *anti* hydroxyoxime conformers can be found in the Appendices.

TABLE 4.8: Gibbs free energy (ΔG^o_{363}, kJ/mol) and enthalpy (ΔH^o_{363}, kJ/mol) differences relative to the most stable conformer for group-I of 4-hydroxyhexan-3-oxime conformers calculated at the M06/6-31++G(d,p) level of theory.

Anti-isomer	M06/6-31++G(d,p)		*Syn*-isomer	M06/6-31++G(d,p)	
	ΔG, $\frac{kJ}{mol}$	ΔH, $\frac{kJ}{mol}$		ΔG, $\frac{kJ}{mol}$	ΔH, $\frac{kJ}{mol}$
I-Anti 1-1	0.0	0.0	I-Syn 1-1	14.1	12.2
I-Anti 1-2	3.5	7.1	I-Syn 1-2	10.9	8.2
I-Anti 1-3	0.3	1.5	I-Syn 1-3	8.1	6.3
I-Anti 2-1	5.7	4.3	I-Syn 2-1	15.0	13.6
I-Anti 2-2	14.5	13.8	I-Syn 2-2	15.3	11.4
I-Anti 2-3	1.8	3.9	I-Syn 2-3	8.0	7.8
I-Anti 3-1	0.8	-1.3	I-Syn 3-1	22.1	17.5
I-Anti 3-2	7.3	7.7	I-Syn 3-2	20.0	15.7
I-Anti 3-3	2.1	0.6	I-Syn 3-3	10.4	8.6

1-1) are only equal to 0.3 and 0.8 kJ/mol, respectively. This means that all 3 conformers would co-exist in roughly equal proportions.

One possible reason why the effect of diffuse functions is insignificant in case of studying the potential energy surface of *syn*-4-hydroxyhexan-3-oxime is because the hydrogen bond in the first group of *syn* isomers is more pronounced (stronger) than in the *anti* isomers of the same group and a good description of -OH$\cdots$O- hydrogen bonding can already be obtained with the 6-31G(d,p) basis set. For *anti* isomers, the picture is a little bit different. In order to see this difference let us compare the conformer populations calculated using a Boltzmann distribution based on the thermodynamic data estimated with the 6-31++G(d,p) basis set (Table 4.9 and 4.10) with the population derived from 6-31G(d,p) calculations (Tables 4.4 and 4.6).

TABLE 4.9: Conformer population (%) computed from a Boltzmann distribution using the Gibbs free energies calculated at the B3LYP/6-31++G(d,p) level of theory for each conformer at 363K.

Anti-isomer	B3LYP/6-31++G(d,p)			*Syn*-isomer	B3LYP/6-31++G(d,p)		
	Group I, %	Group II, %	Group III, %		Group I, %	Group II, %	Group III, %
Anti 1-1	10.0	0.0	0.1	Syn 1-1	0.1	0.0	0.1
Anti 1-2	1.3	1.7	0.6	Syn 1-2	0.5	0.2	0.2
Anti 1-3	23.0	5.7	0.9	Syn 1-3	1.9	0.5	0.7
Anti 2-1	11.3	0.0	0.0	Syn 2-1	0.1	0.0	0.0
Anti 2-2	0.3	0.1	0.3	Syn 2-2	0.5	0.2	0.0
Anti 2-3	5.8	0.0	0.6	Syn 2-3	1.9	0.1	0.2
Anti 3-1	2.6	0.2	0.2	Syn 3-1	0.0	0.0	0.1
Anti 3-2	0.3	5.0	2.2	Syn 3-2	0.1	0.1	0.1
Anti 3-3	8.9	7.1	3.0	Syn 3-3	0.5	0.2	0.3
Sum, %		91.5		Sum, %		8.5	

TABLE 4.10: Conformer population (%) computed from a Boltzmann distribution using the Gibbs free energies calculated at the M06/6-31++G(d,p) level of theory for each conformer at 363K.

Anti-isomer	M06/6-31++G(d,p)			*Syn*-isomer	M06/6-31++G(d,p)		
	Group I, %	Group II, %	Group III, %		Group I, %	Group II, %	Group III, %
Anti 1-1	16.8	0.1	0.1	Syn 1-1	0.2	0.0	0.1
Anti 1-2	5.3	5.6	0.7	Syn 1-2	0.5	0.1	0.1
Anti 1-3	15.2	6.6	0.2	Syn 1-3	1.1	0.2	0.2
Anti 2-1	2.5	0.0	0.0	Syn 2-1	0.1	0.0	0.0
Anti 2-2	0.1	0.1	0.2	Syn 2-2	0.1	0.0	0.0
Anti 2-3	9.3	0.0	0.7	Syn 2-3	1.2	0.3	0.1
Anti 3-1	13.0	0.1	0.0	Syn 3-1	0.0	0.0	0.1
Anti 3-2	1.5	1.1	0.8	Syn 3-2	0.0	0.0	0.1
Anti 3-3	8.4	4.7	1.2	Syn 3-3	0.5	0.2	0.2
Sum, %		94.4		Sum, %		5.6	

As can be seen, in contrast to the performance of the M06/6-31G(d,p) (Table 4.6), the M06/6-31++G(d,p) level of theory gives a better description of the PES for *anti*-4-hydroxyhexan-3-oxime as compared to the B3LYP calculations using the same basis set, which is probably due to a better description of the -OH$\cdots$N- hydrogen bond. However, the energetics of the GG-type conformers are still overestimated at the M06/6-31++G(d,p) level of theory.

Populations of *anti* 4-hydroxyhexan-3-oxime isomers calculated at the B3LYP/6-31++G(d,p) level of theory are different from those estimated at the B3LYP/6-31G(d,p) level. The main difference is that the stationary state of the I-Anti 2-1 conformer of 4-hydroxyhexan-3-oxime was successfully optimised at the B3LYP/6-31++G(d,p) level in contrast to the B3LYP method with the 6-31G(d,p) basis set. Another major difference is that the populations of the I-Anti 2-3 and I-Anti 3-3 conformers calculated using B3LYP with a 6-31++G(d,p) basis set were lowered from 12.0 and 14.5 to 5.8 and 8.9%, respectively, as compared to the B3LYP calculations using the 6-31G(d,p) basis set. The M06/6-31G(d,p) calculations, gave I-Anti 3-1 and I-Anti 3-3 4-hydroxyhexan-3-oxime conformers as the most stable ones, followed by I-Anti 1-1 and I-Anti 1-3. In contrast to the M06/6-31G(d,p), M06/6-31++G(d,p) calculations identified the I-Anti 1-1 and I-Anti 1-3 conformers as the most stable ones with nearly equal conformer populations, followed by I-Anti 3-1 4-hydroxyhexan-3-oxime conformer. However, the overall distributions between *syn* and *anti* isomers of 4-hydroxyhexan-3-oxime calculated at the M06/6-31G(d,p) and M06/6-31++G(d,p) levels of theory are nearly identical: 93.5% *anti* vs 6.5% *syn* at the M06/6-31G(d,p) level and 94.4% *anti* vs 5.6% *syn* at the M06/6-31++G(d,p) one. As can be seen, the effect of the diffuse functions on conformer population estimated with the M06 method is more dramatic than it is on the one calculated with the B3LYP functional.

To summarise, we can say that the process of minima location on the potential energy surface depends on the type of DFT functional we choose. It is interesting to note that the inclusion of the diffuse functions for both hydrogen and heavy atoms has a more significant effect on minima location using the M06 functional as compared to that using the B3LYP one which is probably occurred due to the influence of these functions on the meta-GGA part of M06 functional. Therefore, when systems with weak intramolecular interactions via hydrogen bonding are studied with the M06 method, inclusion of diffuse functions in the basis set may be very important in order to get the population/relative energetics right. However in order to make a stronger conclusion regarding the effect of diffuse functions on the description quality of the weak intramolecular interactions we need to compare the lengths of hydrogen bonds calculated for the first group of *anti* conformers of 4-hydroxyhexan-3-oxime optimised using both B3LYP and M06 DFT functionals with the 6-31G(d,p) and 6-31++G(d,p) basis sets (Table 4.11).

TABLE 4.11: Hydrogen bond lengths calculated for the first group of *anti*-4-hydroxyhexan-3-oxime conformers (Å) calculated using B3LYP and M06 DFT functionals with the 6-31G(d,p) and 6-31++G(d,p) basis sets and differences between the lengths of H-bonds calculated using same functional but with two different basis sets (6-31G(d,p) and 6-31++G(d,p)).

Anti-isomer	H bond with B3LYP, Å			H bond with M06, Å		
	6-31G (d,p)	6-31++G (d,p)	Δ	6-31G (d,p)	6-31++G (d,p)	Δ
Anti 1-1	1.991	2.027	0.036	1.993	2.025	0.032
Anti 1-2	2.095	2.176	0.081	2.097	2.164	0.067
Anti 1-3	2.020	2.053	0.033	2.017	2.054	0.037
Anti 2-1	1.990	2.027	0.037	1.972	2.005	0.033
Anti 2-2	2.035	2.142	0.107	2.099	2.188	0.089
Anti 2-3	1.967	1.992	0.025	1.990	2.011	0.021
Anti 3-1	1.991	2.031	0.040	1.999	2.033	0.034
Anti 3-2	1.954	1.988	0.034	1.968	1.997	0.029
Anti 3-3	1.980	2.015	0.035	1.985	2.019	0.034

According to Ramaekers *et al.* (2003) similar types of hydrogen bonding are well described at the B3LYP/6-31++G(d,p) level. Therefore, it is assumed that the values of the hydrogen bond lengths calculated at this level are more trustworthy. However, this assumption needs to be checked and results compared to calculations using full Configuration Interaction (CI) and/or MP2 methods. As can be seen from Table 4.11, the B3LYP/6-31G(d,p) level underestimates intramolecular hydrogen bond lengths for the first group *anti*-isomers of 4-hydroxyhexan-3-oxime or in other words the strength of hydrogen bonding is overestimated at this level of theory. The hydrogen bonding is only one of many factors affecting stabilities of hydroxyoxime conformers and it is hard to draw the analogy between the strength of a hydrogen bond and stability for each first group conformer. However, it is clear that the addition of the diffuse functions has a significant effect on the hydrogen bond lengths of this type and therefore it should be recommended to consider it when studying the potential energy surface of systems with weak intra-molecular interactions.

Even at this stage we can conclude that the size of R groups is a significant effect on the equilibrium between *syn* and *anti* hydroxyoxime. However, it is important not just to prove that the effect exists, but also to find the minimal size of the R groups that will yield a good description of LIX63 system, such that any further increase in size of R groups has negligible effect on the thermodynamics of *anti/syn* hydroxyoxime

isomerisation. Therefore the next step in the current study is to perform the potential energy surface scan for the hydroxyoxime molecule with R groups equal to C_3H_7 on both ends.

In the study of the *syn/anti* equilibrium of 4-hydroxyhexan-3-oxime with B3LYP and M06 methods, it has been shown that the M06 method is very sensitive to the size of basis set (with and without diffuse functions) which results in location of different global minima on the PES. It has also been shown that the stability of GG-type conformers seems to be overestimated. However, in order to make more solid conclusions regarding invalidity of the M06 method for the description of the equilibrium between *syn* and *anti* isomers of LIX63 hydroxyoxime, we need to check its performance in studying the *syn/anti* equilibrium of 2,5-dimethyl-4-hydroxyhexan-3-oxime, where the R group is equal to isopropyl groups (C_3H_7). The Gibbs free energy (ΔG^o_{363}) and enthalpy differences (ΔH^o_{363}) calculated at the B3LYP/6-31G(d,p) and M06/6-31G(d,p) levels of theory between each conformer in the first group of *syn/anti* isomers and the lowest energy structure of the *anti*-2,5-dimethyl-4-hydroxyhexan-3-oxime are given in Tables 4.12 and 4.13.

TABLE 4.12: Gibbs free energy (ΔG^o_{363}, kJ/mol) and enthalpy (ΔH^o_{363}, kJ/mol) differences relative to the most stable conformer for group-I of 2,5-dimethyl-4-hydroxyhexan-3-oxime conformers calculated at the B3LYP/6-31G(d,p) level of theory.

Anti-isomer	B3LYP/6-31G(d,p)		*Syn*-isomer	B3LYP/6-31G(d,p)	
	ΔG, $\frac{kJ}{mol}$	ΔH, $\frac{kJ}{mol}$		ΔG, $\frac{kJ}{mol}$	ΔH, $\frac{kJ}{mol}$
I-Anti 1-1	4.3	7.9	I-Syn 1-1	9.2	6.9
I-Anti 1-2	4.5	3.2	I-Syn 1-2	11.8	9.9
I-Anti 1-3	21.2	19.0	I-Syn 1-3	25.0	23.6
I-Anti 2-1	9.9	11.0	I-Syn 2-1	10.5	8.5
I-Anti 2-2	0.0	0.0	I-Syn 2-2	14.1	11.8
I-Anti 2-3	10.9	10.3	I-Syn 2-3	25.9	26.5
I-Anti 3-1	8.1	8.0	I-Syn 3-1	0.9	0.0
I-Anti 3-2	7.0	7.6	I-Syn 3-2	5.1	4.8
I-Anti 3-3	17.1	18.4	I-Syn 3-3	12.7	10.8

TABLE 4.13: Gibbs free energy (ΔG^o_{363}, kJ/mol) and enthalpy (ΔH^o_{363}, kJ/mol) differences relative to the most stable conformer for group-I of 2,5-dimethyl-4-hydroxyhexan-3-oxime conformers calculated at the M06/6-31G(d,p) level of theory.

Anti-isomer	M06/6-31G(d,p)		*Syn*-isomer	M06/6-31G(d,p)	
	ΔG, $\frac{kJ}{mol}$	ΔH, $\frac{kJ}{mol}$		ΔG, $\frac{kJ}{mol}$	ΔH, $\frac{kJ}{mol}$
I-Anti 1-1	13.5	12.9	I-Syn 1-1	14.5	12.2
I-Anti 1-2	0.0	0.0	I-Syn 1-2	16.4	15.3
I-Anti 1-3	20.7	18.0	I-Syn 1-3	33.8	29.4
I-Anti 2-1	12.1	14.2	I-Syn 2-1	14.9	13.5
I-Anti 2-2	4.4	3.8	I-Syn 2-2	15.5	14.6
I-Anti 2-3	15.5	12.7	I-Syn 2-3	31.5	29.9
I-Anti 3-1	12.7	14.5	I-Syn 3-1	3.8	3.7
I-Anti 3-2	10.1	10.8	I-Syn 3-2	7.1	8.9
I-Anti 3-3	21.3	22.4	I-Syn 3-3	14.6	13.6

As can be seen from Tables 4.12 and 4.13 both B3LYP and M06 yield very similar potential energy surfaces for 2,5-dimethyl-4-hydroxyhexan-3-oxime except for two major differences. Firstly, the I-Anti 2-2 conformer was predicted to be the lowest energy conformer on the PES at the B3LYP/6-31G(d,p) level of theory, while according to the M06 calculations with the same basis set the I-Anti 1-2 structure corresponds to the most stable conformer. Secondly, the I-Anti 1-1 and I-Anti 1-2 group-I isomers were predicted by B3LYP calculations to be of similar stability at 363 K (I-Anti 1-1 is more stable than I-Anti 1-2 by only 0.2 kJ/mol), while the I-Anti 1-2 structure was predicted to be more stable than I-Anti 1-1 by 13.5 kJ/mol according to M06 calculations.

The overall distribution between *syn* and *anti* isomers of 2,5-dimethyl-4-hydroxyhexan-3-oxime is also predicted to be a little bit different by the above two methods. The B3LYP/6-31G(d,p) method predicts 66% of *anti* and 34% of *syn* hydroxyoxime when the R groups on both ends of the molecule correspond to C_3H_7, while according to M06/6-31G(d,p) calculations the distribution is correspondingly 72 to 28%. As can be seen from Table 4.13, the ΔG values between the group-I *syn* isomers of 2,5-dimethyl-4-hydroxyhexan-3-oxime and the lowest energy structure of the *anti* isomer calculated at the M06/6-31G(d,p) level of theory are higher than those estimated at the B3LYP/6-31G(d,p) level of theory. Populations of all possible conformers of 2,5-dimethyl-4-hydroxyhexan-3-oxime calculated using thermodynamic data estimated at the B3LYP/6-31G(d,p) and M06/6-31G(d,p) levels of theory are given in Tables 4.14

and 4.15, respectively.

TABLE 4.14: Conformer population (%) of 2,5-dimethyl-4-hydroxyhexan-3-oxime computed from a Boltzmann distribution using the Gibbs free energies calculated at the B3LYP/6-31G(d,p) level of theory for each conformer at 363K.

Anti-isomer	B3LYP/6-31G(d,p)			*Syn*-isomer	B3LYP/6-31G(d,p)		
	Group I, %	Group II, %	Group III, %		Group I, %	Group II, %	Group III, %
Anti 1-1	6.4	0.3	7.5	Syn 1-1	1.3	0.2	0.0
Anti 1-2	6.1	0.3	0.2	Syn 1-2	0.5	0.0	0.0
Anti 1-3	0.0	0.0	0.2	Syn 1-3	0.0	0.0	0.0
Anti 2-1	1.0	7.0	1.4	Syn 2-1	0.8	0.6	1.2
Anti 2-2	27.1	0.1	0.9	Syn 2-2	0.3	0.1	2.3
Anti 2-3	0.7	0.1	0.1	Syn 2-3	0.0	0.0	0.1
Anti 3-1	1.9	0.2	1.3	Syn 3-1	20.3	0.4	0.3
Anti 3-2	2.6	0.0	0.3	Syn 3-2	4.9	0.1	0.1
Anti 3-3	0.1	0.0	0.0	Syn 3-3	0.4	0.2	0.0
Sum, %		65.9		Sum, %		34.1	

TABLE 4.15: Conformer population (%) of 2,5-dimethyl-4-hydroxyhexan-3-oxime computed from a Boltzmann distribution using the Gibbs free energies calculated at the M06/6-31G(d,p) level of theory for each conformer at 363K.

Anti-isomer	M06/6-31G(d,p)			*Syn*-isomer	M06/6-31G(d,p)		
	Group I, %	Group II, %	Group III, %		Group I, %	Group II, %	Group III, %
Anti 1-1	0.6	0.3	0.6	Syn 1-1	0.4	0.0	0.0
Anti 1-2	48.3	0.0	0.0	Syn 1-2	0.2	0.0	0.0
Anti 1-3	0.1	0.0	0.1	Syn 1-3	0.0	0.0	0.0
Anti 2-1	0.9	5.5	0.5	Syn 2-1	0.3	0.4	0.3
Anti 2-2	11.3	0.1	0.1	Syn 2-2	0.3	0.9	5.7
Anti 2-3	0.3	0.2	0.0	Syn 2-3	0.0	0.0	0.0
Anti 3-1	0.7	0.1	0.3	Syn 3-1	13.6	0.4	0.2
Anti 3-2	1.7	0.0	0.1	Syn 3-2	4.6	0.0	0.0
Anti 3-3	0.0	0.0	0.1	Syn 3-3	0.4	0.1	0.0
Sum, %		72.0		Sum, %		28.0	

Both methods describe the potential energy surface of 2,5-dimethyl-4-hydroxy-hexan-3-oxime very similarly despite the two main differences described above. It is interesting to note that the addition of diffuse functions does not change the overall picture for both B3LYP and M06 methods (the interested reader is referred to the Appendices). The I-Anti 2-2 configuration is still predicted to be the lowest energy structure at the B3LYP/6-31++G(d,p) level, while the I-Anti 1-2 conformer was optimised to be the global minimum at the M06/6-31++G(d,p) level. The overall distribution between *syn* and *anti* isomers calculated at the B3LYP/6-31++G(d,p) level is equal to 34.6 and 65.4%, respectively, and to 20.2% *syn* and 79.8% *anti* at the M06/6-31++G(d,p) level of theory. Based on the results of the potential energy surface scans of three hydroxyoxime molecules, namely: acetoin oxime, 4-hydroxyhexan-3-oxime and 2,5-dimethyl-4-hydroxyhexan-3-oxime, and considering the information about the failure of the M06 method to describe gauche-gauche conformations reported by Gruzman *et al.* (2009) we can conclude that B3LYP is more suitable for modelling this type of system. However, in order to strengthen this conclusion we need to perform additional optimisation of structures, where the relative energetics were described differently by B3LYP and M06, using the MP2 method. Calculated at the MP2/6-31++G(3df,3pd) level of theory the Gibbs free energy difference at 363K between I-Anti 1-2 and I-Anti 2-2 conformers of 2,5-dimethyl-4-hydroxyhexan-3-oxime is equal to 4.9kJ/mol. As can be seen, this corresponds to the finding with the B3LYP method, which supports the preferential choice of this method.

The lowest energy structures for *syn* and *anti* isomers of 2,5-dimethyl-4-hydroxyhexan-3-oxime predicted by B3LYP and M06 methods are represented in Figure 4.4. The experimental equilibrium between *syn* and *anti* isomers of 5,8-diethyl-7-hydroxydodecan-6-oxime (65.9% of *anti* and 34.1% of *syn* isomer) is already well reproduced by modelling 2,5-dimethyl-4-hydroxy-hexan-3-oxime at the B3LYP/6-31G(d,p) level of theory, yielding equilibrium concentrations of *anti* and *syn* isomers equal to 63.0 and 37.0%, respectively. However, in order to prove that this equilibrium between *syn* and *anti* hydroxyoxime isomers will remain the same when the size of the carbon side-chains is increased further we need to show that this finding still holds true for 3,6-dimethyl-5-hydroxyoctan-4-oxime. A conformer of the *anti* isomer of 3,6-dimethyl-5-hydroxyoctan-4-oxime is shown in Figure 4.5. As can be seen from Figure 4.5 there are three chiral centres (sp^3 carbon atoms with four different groups around them) in the 3,6-dimethyl-5-hydroxyoctan-4-oxime molecule[5]. This makes the scan of the potential energy surface a bit more complicated for this system. In order to perform a systematic search for all of

[5]In order to determine the type of the chiral centre (R or S), based on atomic number (according to the Cahn-Ingold-Prelog priority rules (CIP)) one deeds to assign a priority of each of four groups around it. When the lowest priority group is pointed away from the viewer, the centre is labeled R (for Rectus, Latin for right) if the priority of the remaining three groups is decreased in clockwise direction, and S (for Sinister, Latin for left) if the priority is decreased in counter-clockwise direction.

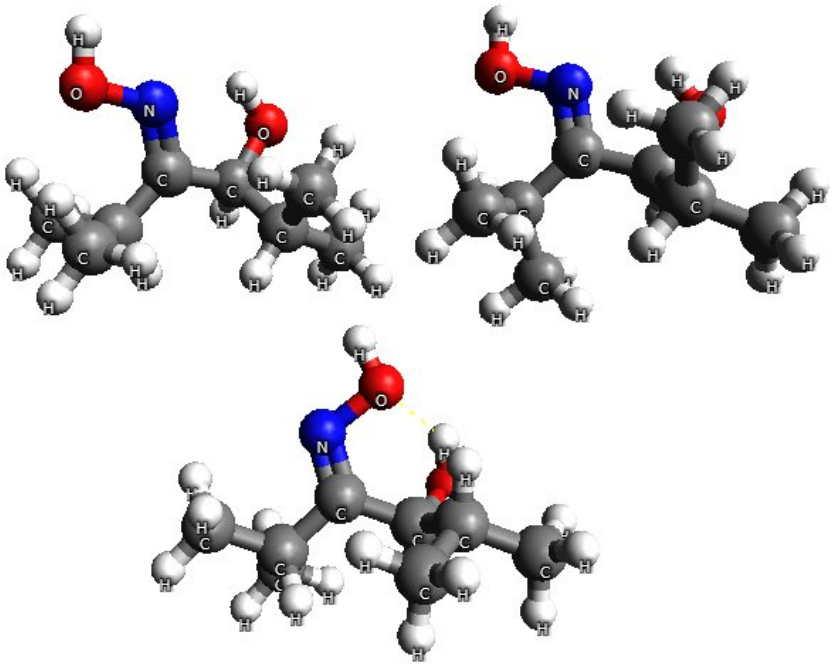

FIGURE 4.4: Representations of the lowest energy structures for *syn*- and *anti*-hydroxyoxime with R groups equal to -C_3H_7. Top left corner structure corresponds to I-Anti 2-2, top right - to I-Anti 1-2 and bottom structure is I-Syn 3-1. Grey coloured atoms represent carbon, red - oxygen, dark blue - nitrogen and white - hydrogen.

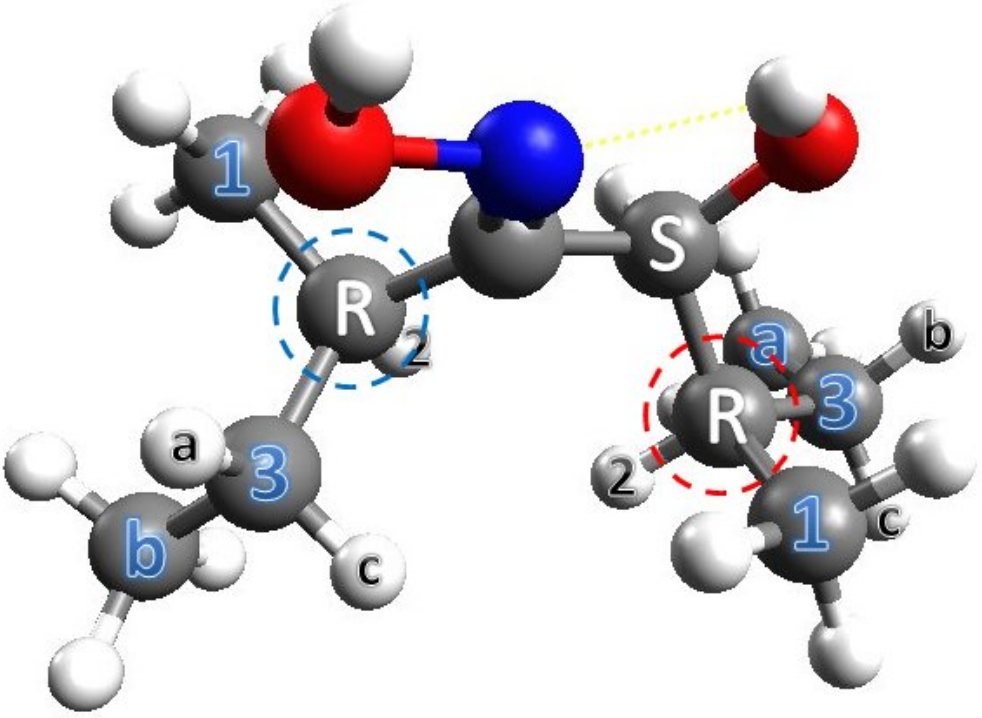

FIGURE 4.5: R3b_R3a conformer of *Anti*-3,6-dimethyl-5-hydroxyoctan-4-oxime. Grey coloured atoms represent carbon, red - oxygen, dark blue - nitrogen and white - hydrogen.

the minima on the PES of molecule with several chiral centres, we first need to define all possible stereo isomers[6] of 3,6-dimethyl-5-hydroxyoctan-4-oxime, each one of which will represent a group where all possible conformers will be constructed and optimised at the B3LYP/6-31G(d,p) level of theory. In contrast to conformers, stereoisomers[7] cannot be inter-converted one to another by simple rotation around a single bond. For simplicity we have created our own nomenclature (an example of the conformer named using this nomenclature is represented in Figure 4.5) which was used in naming all possible conformers of 3,6-dimethyl-5-hydroxyoctan-4-oxime.

In order to construct a new stereoisomer, the hydrogen atom and CH_3 group are exchanged in either one of, or both chiral centres circled with blue and red dashed lines in Figure 4.5. Similar to the PES scans of previous molecules due to the limited time assigned for this research we decided to fix the position and chirality of functional groups of *syn*- and *anti*-3,6-dimethyl-5-hydroxyoctan-4-oxime. These gives us four stereoisomers (SS, RR, SR and RS) or four groups of conformers for each, *syn* and *anti*, isomer of 3,6-dimethyl-5-hydroxyoctan-4-oxime. The name R3b_R3a of the *anti*-3,6-dimethyl-5-hydroxyoctan-4-oxime conformer represented in Figure 4.5 was derived as follows: the first letter R represents the type of chiral centre which is located closer to the oxime group (circled with a blue dashed line). The following number 3 represents the position of hydrogen (blue number around chiral centre R); the following letter b corresponds to the position of CH_3 group around carbon atom number three. The rest of the notation is described in similar manner but for the other end of the hydroxyoxime molecule. In other words, the geometry and allocations of groups around the chiral centre closest to the oxime group are described first, followed by the same for the chiral centre which is located closer to the hydroxyl group.

It is not hard to calculate that the total number of conformers (from all groups of stereoisomers) for both *syn* and *anti* isomers of 3,6-dimethyl-5-hydroxyoctan-4-oxime is 1944; therefore, in order to save space, we will not show the data from the potential energy surface scan performed at the B3LYP/6-31G(d,p) level of theory for the 3,6-dimethyl-5-hydroxyoctan-4-oxime molecule and will only show the PES plot of the SS *syn*- and *anti*- isomers (Figure 4.6). The reason why we are showing the PES plots of SS-3,6-dimethyl-5-hydroxyoctan-4-oxime is because the lowest energy structures of its *syn* and *anti* isomers were found to be more stable than those of other three hydroxyoximes (SR, RS and RR). Most importantly, the overall distribution between *anti* and *syn* isomers are approximately equal to 65 and 35%, respectively, for each group of 3,6-dimethyl-5-hydroxyoctan-4-oxime stereoisomers (64 and 36% for SS conformers; 65 and 35% for RR conformers; 61 and 39% for SR conformers, and 63 and 37% for RS

[6]Note that mirror images are not considered as their total energies are identical.

[7]Note that the type of bonding between the atoms and their connection order are the same in both types of isomers as they do not represent structural isomers.

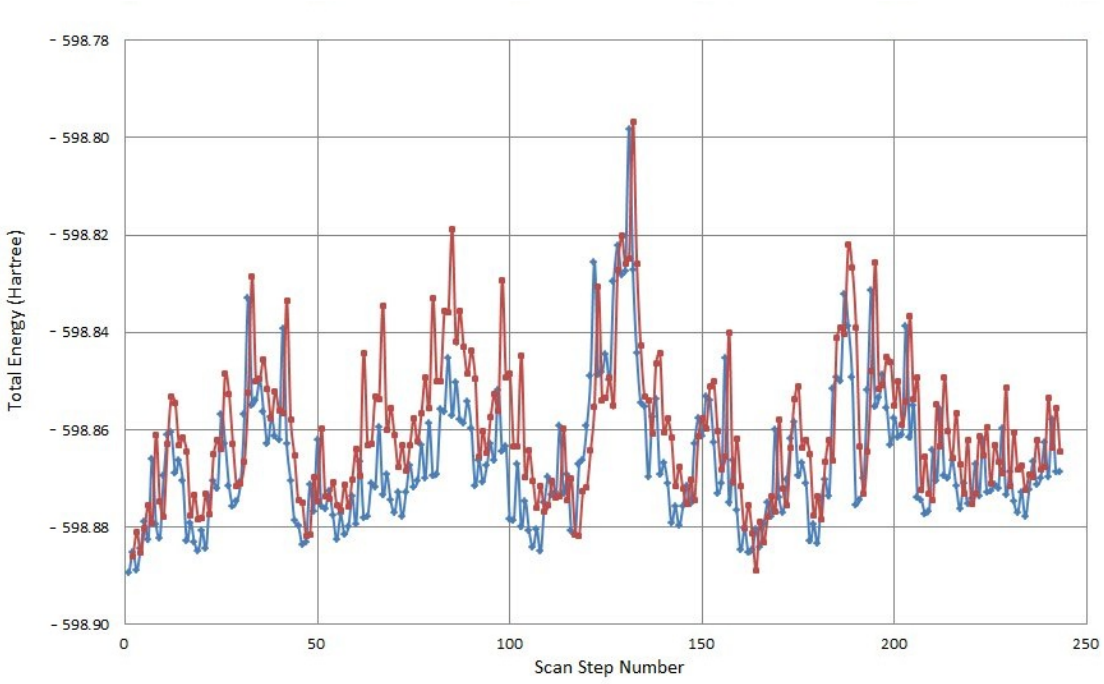

FIGURE 4.6: Potential energy surfaces of RR-*anti*- (blue line) and RR-*syn*-3,6-dimethyl-5-hydroxyoctan-4-oxime (red line). Each scan step number correspond to a different conformer of *syn*- and/or *anti*- isomer of 3,6-dimethyl-5-hydroxyoctan-4-oxime.

3,6-dimethyl-5-hydroxyoctan-4-oxime conformers).

In order to conclude this section we can say that the experimental equilibrium between *syn* and *anti* isomers of the main component of LIX63 - 5,8-diethyl-7-hydroxydodecan-6-oxime is well reproduced by modelling the system of 2,5-dimethyl-4-hydroxyhexan-3-oxime where R groups on both ends of the molecule are equal to C_3H_7 at the B3LYP/6-31G(d,p) level of theory. It can be concluded that there is no significant effect of adding diffuse functions to the basis set in describing intramolecular interactions via hydrogen bonding for hydroxyoximes with R groups bigger or equal to C_3H_7. Some disagreements between the B3LYP and M06 results were found in scans of the potential energy surfaces of different hydroxyoxime molecules. It is recommended to use the B3LYP hybrid DFT functional in order to get the more reliable structure for the global minimum for each isomer (*syn* and *anti*) of the hydroxyoximes considered. However, it is recommended to re-optimise the lowest energy structures found using both B3LYP and M06, along with the MP2 method using largest basis set that can be afforded in order to check the validity of this conclusion.

4.3.2 Kinetics of the *Syn/Anti* Hydroxyoxime Equilibrium

We have successfully determined the minimal size of hydrocarbon side-chain which is required in order to model the equilibrium between *syn* and *anti* isomers of 5,8-diethyl-7-hydroxydodecan-6-oxime (LIX63 main component). It is now the main goal to see if the effect of the size of hydrocarbons side-chains on the kinetics of the *syn/anti* hydroxyoxime isomerisation process is as significant as it is on the thermodynamic equilibrium between the two isomers. Previously it was determined that the experimental activation energy barrier for *syn/anti* hydroxyoxime isomerisation is equal to 119 kJ/mol for the *anti* to *syn* hydroxyoxime interconversion and 117.3 kJ/mol for the *syn* to *anti* isomerisation at 363K. According to transition state theory this barrier can be estimated by calculating the Gibbs free energy difference between the transition state and minimum at 363K. Based on the previous preliminary calculations of the kinetics of *syn/anti* hydroxyoxime isomerisation, three mechanisms including inversion, tautomerisation via an enamine and tautomerisation via nitroso compounds were selected as the most probable according to their energetics. Four different types of transition states were selected from these mechanisms. In order to check the effect of the size of hydrocarbon side-chains on the kinetics of *syn/anti* isomerisation we need to calculate the Gibbs free energy differences between each of these four transition states and corresponding minimum of the *anti* isomer at 363K. The lowest energy *anti* isomers and transition states of hydroxyoxime molecules with the size of hydrocarbon side-chains equal to CH_3, C_2H_5, C_3H_7 and C_4H_9[8] were considered.

Let us review the types of transition states previously identified. Schematic representation of the first type of transition state is the one used in the inversion mechanism. The energy plot for the inversion mechanism is shown in Figure 4.7.

[8]Note that the Gibbs free energy differences between each of these transition states and corresponding minimum of *anti* isomer was already previously calculated for acetoin oxime (R=CH_3).

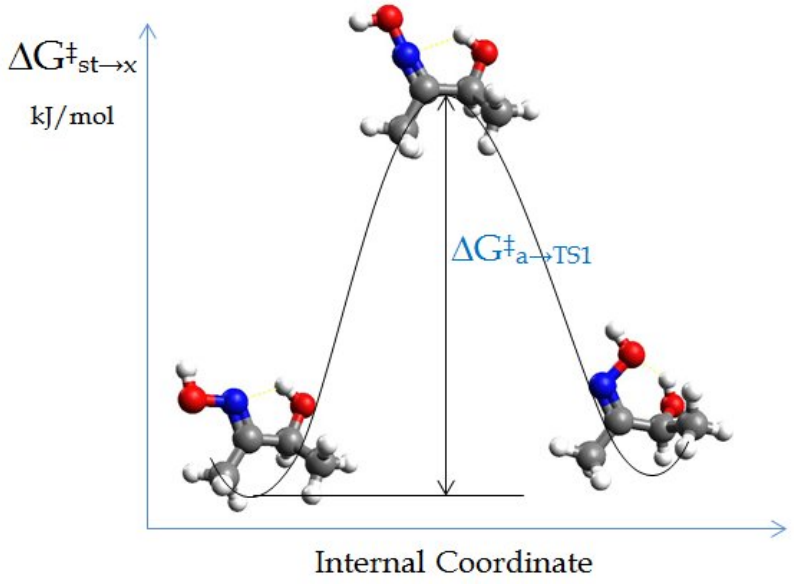

FIGURE 4.7: Reaction profile for the *anti* to *syn* acetoin oxime isomerisation via inversion mechanism. Atom colours: oxygen (O) - red; nitrogen (N) - dark blue; carbon (C) - grey and hydrogen (H) - white.

In order to study the effect of the hydrocarbon side-chains we need to calculate the energy barrier ($\Delta G^{\ddagger}_{(a\rightarrow TS1)}$) between the stable *anti* isomer and transition state, that is depicted in Figure 4.7, for all four hydroxyoximes[9]. The next two types of transition states are those considered in tautomerisation mechanisms, which correspond to either a direct hydrogen atom migration from the oxime group to the carbon atom which is attached to it or the case when hydrogen atom is first migrated to the nitrogen and then to carbon. The last type of transition state is the one which involves an N=O group rotation about a single CN bond. An example of a schematic energy plot for the tautomerisation mechanism of the *anti* to *syn* acetoin oxime isomerisation via a nitroso compound with direct and step-migration of a hydrogen atom are shown in Figures 4.8 and 4.9, respectively.

[9]Note that the structures of minima and transition state depicted in Figure 4.7 are those of acetoin oxime

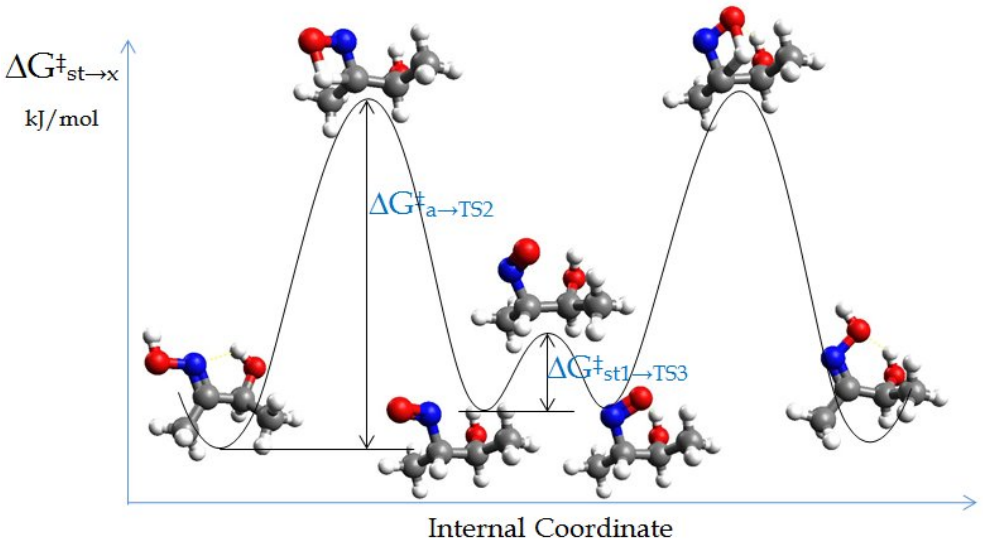

FIGURE 4.8: Reaction profile for the tautomerisation mechanism of the *anti* to *syn* hydroxyoxime isomerisation via a nitroso compound (direct migration of a hydrogen atom). Atom colours: oxygen (O) - red; nitrogen (N) - dark blue; carbon (C) - grey and hydrogen (H) - white.

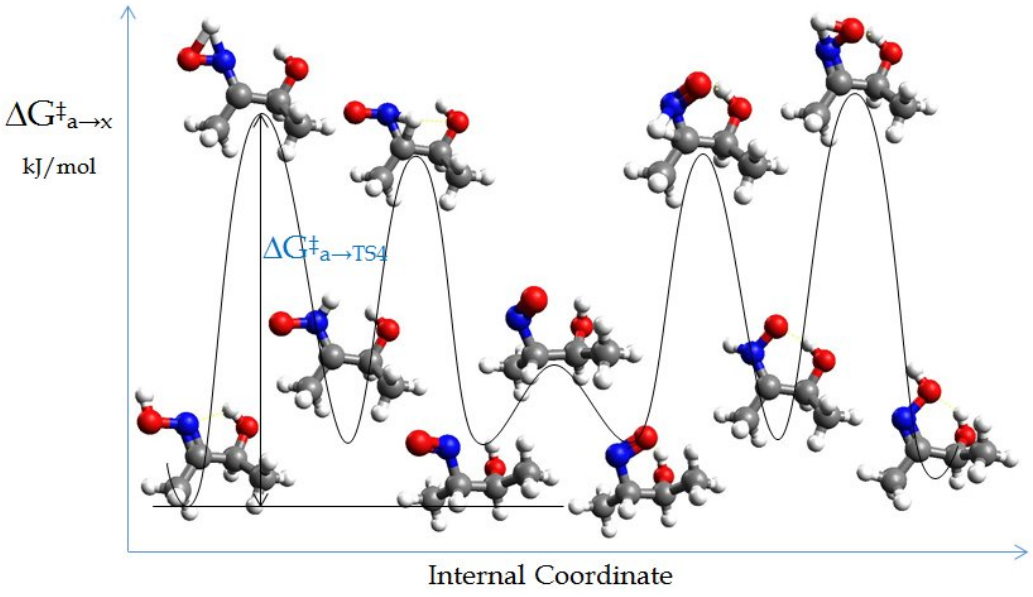

FIGURE 4.9: Reaction profile for the tautomerisation mechanism of the *anti* to *syn* hydroxyoxime isomerisation via a nitroso compound (stepped migration of a hydrogen atom). Atom colours: oxygen (O) - red; nitrogen (N) - dark blue; carbon (C) - grey and hydrogen (H) - white.

Previously, in chapter 3, it was shown that the total energy barrier of the *anti* to *syn* acetoin oxime interconversion via the stepped tautomerisation mechanism shown in Figure 4.9 (when the hydrogen atom is migrated from the oxygen to the nitrogen atom) is

higher than that of isomerisation via direct tautomerisation (when the hydrogen atom is migrated from the oxygen to the carbon atom). However, it is very interesting to see how the size of the hydrocarbon side-chains will affect the energetics of stepped tautomerisation via a nitroso compound[10].

The Gibbs free energy differences between these types of transition state and the lowest energy *anti* isomers ($\Delta G^{\ddagger}_{(a\rightarrow TS1)}$, $\Delta G^{\ddagger}_{(a\rightarrow TS2)}$ and $\Delta G^{\ddagger}_{(a\rightarrow TS3)}$, and $\Delta G^{\ddagger}_{(a\rightarrow TS4)}$ shown in Figures 4.7, 4.8 and 4.9, respectively) need to be estimated for different types of hydroxyoximes and compared in order to see if there is any effect of the size of the hydrocarbon side-chains on the kinetics of the *anti* to *syn* isomerisation process.

The structures of the minima used to calculate the $\Delta G^{363}_{(a\rightarrow i)}$, where i=1, 2, 3 and 4, were those corresponding to the lowest energy *anti* isomers of hydroxyoximes found during the potential energy surface scans at the B3LYP/6-31G(d,p) level of theory. The $\Delta G^{363}_{(a\rightarrow i)}$ values were calculated for hydroxyoximes with R groups on both ends of the molecule equal to CH_3, C_2H_5, C_3H_7 and C_4H_9, for i=1, 2, 3 and 4 respectively. The results are listed in Table 4.16.

TABLE 4.16: Gibbs free energy differences (kJ/mol) between transition states and the global minima of *anti* isomer of acetoin oxime (R=CH_3), 4-hydroxyhexan-3-oxime (R=C_2H_5), 2,5-dimethyl-4-hydroxyhexan-3-oxime (R=C_3H_7) and 3,6-dimethyl-5-hydroxyoctan-4-oxime (R=C_4H_9) calculated at the B3LYP/6-31G(d,p) level of theory.

Anti-isomer	$\Delta G^{363}_{(a\rightarrow TS1)}$	$\Delta G^{363}_{(a\rightarrow TS2)}$	$\Delta G^{363}_{(a\rightarrow TS3)}$	$\Delta G^{363}_{(a\rightarrow TS4)}$
R=CH_3	223.1	328.5	94.7	221.6
R=C_2H_5	211.3	321.3	89.3	218.7
R=C_3H_7	207.8	325.4	95.8	218.1
R=C_4H_9	206.2	327.0	98.5	217.9

As can be seen from Table 4.16 there are no significant changes in the energy barriers when comparing the hydroxyoximes with different sized hydrocarbon side-chains for all four mechanisms of *syn/anti* hydroxyoxime isomerisation, except perhaps for the inversion mechanism. The Gibbs free energy difference taken between the transition state for this mechanism and the corresponding minimum of the *anti* isomer is decreased when the size of the hydroxyoxime R groups is increased; therefore, based on the present data we conclude that the inversion mechanism is energetically the most favourable for *syn/anti*

[10]Note that due to the limited time the $\Delta G^{\ddagger}_{(a\rightarrow TSX)}$ between transition states in tautomerisation via an amine compound and corresponding minimum of *anti* isomer were not considered. The transition states in tautomerisations via an enamin and nitroso compounds are of similar nature, therefore the effect of the size of hydrocarbon side-chains on the $\Delta G^{\ddagger}_{(a\rightarrow TSX)}$-s for these mechanisms is also expected to be similar.

5,8-diethyl-7-hydroxydodecan-6-oxime isomerisation. However, before making any final conclusion it would be interesting to examine the value of $\Delta G^{363}_{(a \rightarrow TS1)}$ calculated for the main component of LIX63. Unfortunately due to time constraints we cannot afford to perform this calculation; therefore, it is recommended for future research.

In order to gain some additional information about LIX63 we have decided to investigate the experimental IR spectrum of *anti*-5,8-diethyl-7-hydroxydodecan-6-oxime and compare it with the one calculated for the *anti*-2,5-dimethyl-4-hydroxyhexan-3-oxime at the B3LYP/6-31G(d,p) level of theory. The experimental IR spectra was measured at Curtin University with the assistance of Dr Matthew Mclldowie, research fellow in the Nanochemistry Research Institute. Experimental and calculated (B3LYP/6-31G(d,p)) IR spectra for *anti*-5,8-diethyl-7-hydroxydodecan-6-oxime (black) and *anti*-2,5-dimethyl-4-hydroxyhexan-3-oxime (blue) are shown in Figure 4.10.

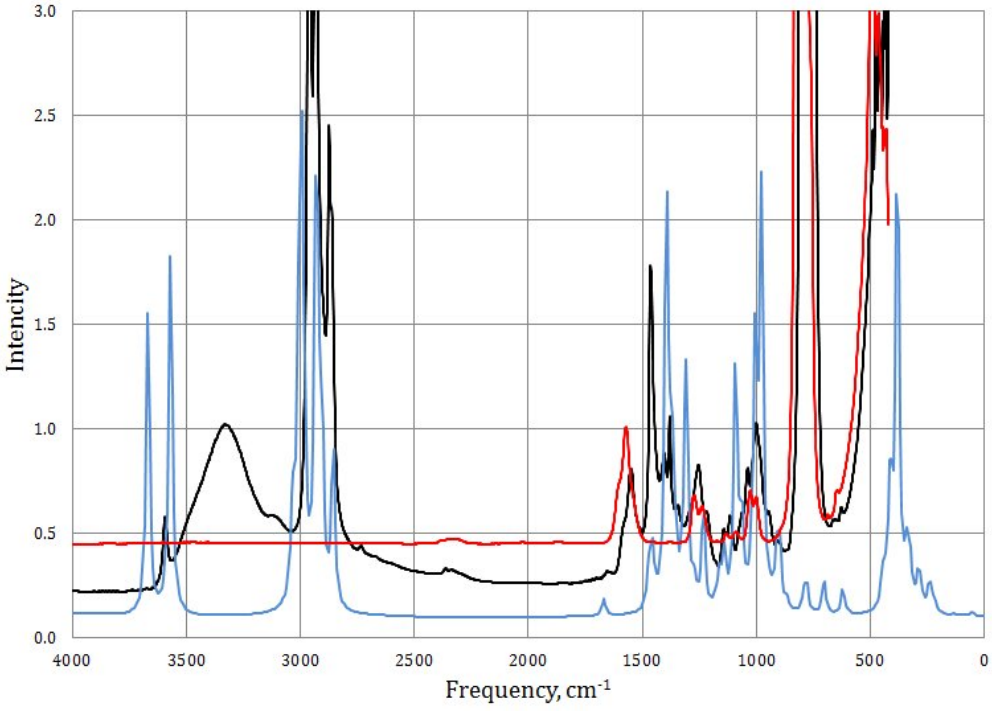

FIGURE 4.10: Experimental IR spectrum of 5,8-diethyl-7-hydroxydodecan-6-oxime measured in tetrachloromethane (black), pure tetrachloromethane (red) and IR spectra of 2,5-dimethyl-4-hydroxyhexan-3-oxime (I Anti 2-2) calculated at the B3LYP/6-31G(d,p) level of theory (blue).

It should be noted that the calculated frequencies in Figure 4.10 were multiplied by the scaling factor of 0.9614 recommended by Arjunan *et al.* (2011) and Gorce and Bahceli (2011) for B3LYP calculations. According to Arjunan *et al.* (2011), this scaling factor is not universal and in order to achieve a better fit with the experimental data

it is recommended to use different scaling factors for the vibration modes of different groups. However, even with this factor it can be seen from the Figure 4.10 that the main difference between the experimental and calculated IR spectra is two broad peaks in the 3200-3500 and 650-850 cm^{-1} frequency intervals. According to Coates and Meyers (2000), these peaks correspond to a strong intermolecular hydrogen bonding interaction. In other words, the main component of LIX63 - 5,8-diethyl-7-hydroxydodecan-6-oxime exists in an oligomeric form. It is important to determine what type of oligomers are present in the system of LIX63 and see if there is any impact of intermolecular hydrogen bonding on the selected mechanisms of *syn/anti* hydroxyoxime isomerisation. The results from the study of different types of hydroxyoxime oligomers and the kinetics of *syn/anti* interconversion are described in the next chapter.

4.4 Conclusions

Based on the results described in this chapter it is recommended to use the B3LYP hybrid density functional with the 6-31G(d,p) basis set for modelling aliphatic α-hydroxyoximes or similar type of systems as the best compromise between accuracy and computational cost. It was shown that even though the addition of diffuse functions to the basis set improves the energetics, it does not affect significantly the process of minima location on the potential energy surface.

Similar to B3LYP, the M06 method was also shown to provide a good approximation in describing the equilibrium between *syn* and *anti* isomers of hydroxyoxime; however, the lowest energy conformers of *anti*-hydroxyoximes located with the M06 method were different from those allocated with B3LYP. As compared to MP2 calculations, the global minima located using the M06 functional were found to be incorrect.

The minimal size of the hydrocarbon side-chains in order to obtain a good description of the experimental equilibrium between *syn* and *anti* isomers of 5,8-diethyl-7-hydroxydodecan-6-oxime was determined to be 2,5-dimethyl-4-hydroxyhexan-3-oxime (R=C_3H_7). It was also shown that a further increase in the size of the hydrocarbon side-chains does not have any significant effect on the thermodynamics of *syn/anti* hydroxyoxime isomerisation.

Studying the effect of the size of the hydrocarbon side-chains on the kinetics of *syn/anti* interconversion it was shown that the energy barrier to the inversion mechanism of the hydroxyoxime isomerisation is lowered when isomerisation is considered between *syn* and *anti* isomers with larger R groups. In order to measure the level of accuracy at which kinetics is described at the B3LYP/6-31G(d,p) level of theory, the

inversion mechanism should be considered between *syn* and *anti* isomers of 5,8-diethyl-7-hydroxydodecan-6-oxime and results compared with experimental data.

According to the measurement of the IR spectra for *anti*-5,8-diethyl-7-hydroxydodecan-6-oxime it appears that the aliphatic α-hydroxyoximes are present in the form of oligomers and it is suggested that other types of mechanisms for the *syn/anti* isomerisation involving hydrogen atoms migration along intermolecular hydrogen bond may be valid when hydroxyoxime oligomers are considered.

4.5 References

Arjunan V., Mythili C.V., Mageswari K. and Mohan S. (2011) Experimental and theoretical investigation of benzamide oxime. *Spectrochimica Acta Part A: Molecular and Biomolecular Spectroscopy* **79**, 245-253.

Coates J. and Meyers R.A. (2000) Interpretation of infrared spectra, a practical approach. *Encyclopedia of Analytical Chemistry*, 10815-10837.

Csonka G.I., Elias K. and Csizmadia I.G. (1996) Relative stability of $^1C_4$ and $^4C_1$ chair forms of -d-glucose: a density functional study. *Chemical Physics Letters* **257**, 49-60(12).

Frisch M.J., Trucks G.W., Schlegel H.B., Scuseria G.E., Robb M.A., Cheeseman J.R., Scalmani G., Barone V., Mennucci B., Petersson G.A., Nakatsuji H., Caricato M., Li X., Hratchian H.P., Izmaylov A.F., Bloino J., Zheng G., Sonnenberg J.L., Hada M., Ehara M., Toyota K., Fukuda R., Hasegawa J., Ishida M., Nakajima T., Honda Y., Kitao O., Nakai H., Vreven T., Montgomery J.A., Jr., Peralta J.E., Ogliaro F., Bearpark M., Heyd J.J., Brothers E., Kudin K.N., Staroverov V.N., Kobayashi R., Normand J., Raghavachari K., Rendell A., Burant J.C., Iyengar S.S., Tomasi J., Cossi M., Rega N., Millam J.M., Klene M., Knox J.E., Cross J.B., Bakken V., Adamo C., Jaramillo J., Gomperts R., Stratmann R.E., Yazyev O., Austin A.J., Cammi R., Pomelli C., Ochterski J.W., Martin R.L., Morokuma K., Zakrzewski V.G., Voth G.A., Salvador P., Dannenberg J.J., Dapprich S., Daniels A.D., Farkas ., Foresman J.B., Ortiz J.V., Cioslowski J. and Fox D.J. (2009) *Gaussian*, Inc., Wallingford CT.

Gorce H. and Bahceli S. (2011) A study on quantum chemical calculations of 3-, 4-nitrobenzaldehyde oximes. *Spectrochimica Acta Part A: Molecular and Biomolecular Spectroscopy* **79**, 1783-1793.

Gruzman D., Karton A. and Martin J. M. L. (2009) Performance of Ab Initio and Density Functional Methods for Conformational Equilibria of CnH2n+2 Alkane Isomers (n = 4-8). *The Journal of Physical Chemistry A* **113**, 1197411983.

Joseph W.O. 2000 Thermochemistry in Gaussian. *Gaussian, Inc*, 2-19.

Ramaekers R., Houben L., Adamowicz L. and Maes G. (2003) Correlations between experimental and DFT(B3LYP)/6-31++G** H-bonding parameters for closed X$\cdots$HO$\cdots$HN (X = N, O or S) H-bonded complexes. *Vibrational Spectroscopy* **32**, 185-197.

Rappoport Z. and Liebman J.F. (2009) *The chemistry of hydroxylamines, oximes and hydroxamic acids. Part 1.* Chichester: John Wiley & Sons Ltd.

Schmidt M.W., Baldridge K.K., Boatz J.A., Elbert S.T., Gordon M.S., Jensen J.H., Koseki S., Matsunaga N., Nguyen K.A., Su S.J., Windus T.L., Dupuis M., Montgomery J.A. (1993) General atomic and molecular electronic structure system. *Journal of Computational Chemistry* **14**, 1347-1363.

Stewart J.J.P. (2007) Optimization of parameters for semiempirical methods. V. Modification of NDDO approximations and application to 70 elements. *Journal of Molecular Modeling* **13**, 1173-213.

Turovtsev V.V. and Orlov Yu.D. (2009) A Quantum-Mechanical Study of Inductive and Steric Effects in Isoalkanes. *Russian Journal of Physical Chemistry A* **84**, 1174-1181.

Chapter 5

DFT Study of Hydroxyoxime Oligomerisation

5.1 Introduction

According to DFT calculations at the B3LYP/6-31G(d,p) level of theory described in the previous chapter, the inversion mechanism was estimated to be the most probable mechanism for the *syn/anti* interconversion of 3,6-dimethyl-5-hydroxyoctan-4-oxime. This was based on it having the lowest activation energy barrier in comparison to the other studied mechanisms. However, it should be noted that the energy barrier for *syn/anti* isomerisation via inversion was derived using the model of 3,6-dimethyl-5-hydroxyoctan-4-oxime with R groups equal to C_4H_9 on both ends of the molecule. The calculated barrier was higher in energy compared to the one determined experimentally for the *syn/anti* isomerisation of 5,8-diethyl-7-hydroxydodecan-6-oxime. This could be due to the limitation of the B3LYP method and/or the limited size of the basis set in this calculation. Another possible explanation is that the chosen model of 3,6-dimethyl-5-hydroxyoctan-4-oxime does not fully describe the kinetics of the *syn/anti* isomerisation of the LIX63 main component. In order to check the latter ideally the activation energy barrier should be calculated for the inversion mechanism using the isomers and transition states of 5,8-diethyl-7-hydroxydodecan-6-oxime. However, due to limited time it was unfortunately not possible. Of course it remains possible that none of the chosen mechanisms for the *syn/anti* hydroxyoxime interconversion considered in earlier chapters describe well the process happening in reality.

In the previous chapter it has been shown that there is a broad peak in the 3600-3400 cm^{-1} frequency interval corresponding to intermolecular hydrogen-bonding. From the literature (Georgieva *et al.*, 2003; Harris *et al.*, 2011) it is known that different

types of oximes, in particular aldoximes and ketoximes tend to oligomerise. It has also been shown by Harris *et al.* (2011) that these types of oximes (aldoximes and ketoximes) form intermolecular hydrogen bonds with different types of modifiers, such as alcohols and esters. In their study Harris *et al.* (2011) described that there is a degree to which oximes tend to oligomerise (dimers, trimers, tetramers and so on), depending on the nature of the solvent. For example, when the solvent is of aromatic nature (i.e. somewhat polar in nature), oxime molecules are predominantly present in monomeric form, while if the solvent is purely aliphatic (i.e. non polar) then oxime molecules tend to oligomerise to a large extent, which can be increased significantly at higher oxime concentrations.

The solvent (ShellSol D70) used in the industrial transition metal extraction by the mixture of LIX63 aliphatic α-hydroxyoxime and Versatic10 carboxylic acid is an aliphatic solvent, which means there is likely to be intermolecular interaction of the polar components in this system (e.g., hydroxyoxime-hydroxyoxime, carboxylic acid-carboxylic acid, and hydroxyoxime-carboxylic acid). It would be interesting to see what types of oligomers (dimers, trimers, tetramers etc.) are formed in the case of hydroxyoxime alone and in the mixture of hydroxyoxime and carboxylic acid. Also it would be quite interesting to see if the barrier to hydrogen atom migration in the tautomerisation mechanisms of *syn/anti* hydroxyoxime interconversion is lowered when the process is considered within hydroxyoxime oligomers.

5.2 Methodology

Based on the results of the previous chapter, the B3LYP hybrid DFT functional was selected for modelling the present type of system with the 6-31G(d,p) and 6-31++G(d,p) basis sets, as they were shown to be a good compromise between the accuracy (as compared to the MP2 calculations using the aug-cc-pVTZ basis set (Kendall *et al.*, 1992)) and computing time.

All possible structures of different types of oligomers formed between *syn* and *anti* isomers of hydroxyoxime (dimers, trimers, tetramer etc.) were constructed using the Avogadro[1] molecular visualisation software and then optimised. The binding energies of acetoin oxime dimers were corrected for Basis Set Superposition Error (BSSE). Convergence criteria were chosen to be "tight" for geometry optimisation, that is: the maximum and root mean square gradient in Cartesian coordinates are set to 0.00001 a.u. and the maximum and root mean square of the Cartesian step - to 0.00005 a.u. For practical reasons, all preliminary calculations of the minima and transition states

[1]Avogadro: an open-source molecular builder and visualization tool. Version 1.0.3/April 25, 2011 http://avogadro.openmolecules.net/

have been performed using the semi-empirical PM6 method (Stewart, 2007) as implemented in the Gamess program (Schmidt *et al.*, 1993) and then the resulting structures were re-optimised at higher levels of theory using the Gaussian09 program (Frisch *et al.*, 2009). The Berny algorithm (which is set by default in Gaussian09) was used in geometry optimisation.

Vibrational frequencies were evaluated in order to determine the nature of each stationary point, as well as to estimate the thermochemistry. Thermal corrections to the enthalpy and Gibbs free energy were used in order to calculate the thermodynamics (Joseph, 2000).

The search for the first-order saddle points was performed by using two different methods. The first approach is based on the eigenvector following algorithm (Peng *et al.*, 1996), while the second method is via the Growing String Method (GSM), (Peters *et al.*, 2004). The main advantage of the GSM is that it allows one to find the transition state without an initial guess if the structures of reagents and products are known. There are a number of papers where a comprehensive description of the GSM and its successful application can be found (Maeda and Ohno, 2005; Quapp, 2005; Quapp, 2007; Goodrow *et al.*, 2009).

In describing the underlying principles of finding the first-order saddle point by eigenvector following algorithm, it should be clarified that an educated guess for the transition state (TS) structure is required (Mueller, 2002); therefore, the general procedure for the TS search was as follows:

1. Locate a TS-like structure by constraining a chosen reaction coordinate during a sequence of energy minimisations;
2. Check whether the constrained optimised structure has an imaginary frequency that looks like the reaction coordinate;
3. If it does, use it as a starting point for the TS search.

The Intrinsic Reaction Coordinates (IRCs) were computed to see how the transition states found connect the reactants and products. IRC computation is analogous to geometry optimisation initiated near the transition state and then following the gradient down-hill leading to products and reactants.

5.3 Results and Discussion

In the modelling of intermolecular hydrogen-bonding we are mostly interested in describing the behaviour of the functional groups; therefore, initially we had to cut down

the R groups as even the modelling of oligomerisation of the previously recommended 2,5-dimethyl-4-hydroxyhexan-3-oxime (with R groups equal to C_3H_7 on both ends of the molecule) would be too costly in terms of the computing time required for complete optimisation.

It is important to note that acetoin oxime *anti-anti* and *syn-syn* dimers were previously studied in 1997 by Rusinska-Roszak *et al.* using the semiempirical PM3 (Stewart, 1989) and *ab initio* Hartree-Fock method with the 6-31G(d,p) basis set. The authors concluded that *syn*-hydroxyoximes tend to form cyclic dimers, while *anti*-isomers are more likely to form linear dimers. In this study we are going to re-optimise acetoin oxime dimers using the B3LYP and M06 methods and see if hydroxyoximes tend to olgomerise to any extent by comparing the Gibbs free energies of dimerisation (from monomers), trimerisation (from dimers) and tetramerisation (from trimers). Furthermore, Rusinska-Roszak *et al.* (1997) used the 6-31G(d,p) basis set, however, according to Georgieva *et al.* (2003), who studied oligomerisation between glyoxilic acid oxime molecules, the effect of the diffuse functions on the strength of hydrogen bonding interactions may be significant. Therefore, another important aspect of this study is to consider this effect as well as the effect of correction for BSSE on the strength of intermolecular interaction via hydrogen bonding between aliphatic α-hydroxyoximes.

5.3.1 Thermodynamics of *Syn/Anti* Aceoin Oxime Dimerisation

Dimerisation between *syn* and *anti* isomers of acetoin oxime is the first process to be described in this chapter. In order to determine whether it is possible or not to form a dimer between two isomers of acetoin oxime in a non-polar solvent we can use thermodynamic data derived from gas-phase calculations as a first approximation. The reaction of acetoin oxime dimerisation can be simply represented by the following equation;

$$A + B \rightleftarrows AB \tag{5.1}$$

where A and B are two monomers of acetoin oxime and AB its dimer. Note that A=B for the case of dimerisation between two *anti* or two *syn* acetoin oxime monomers, and A≠B when dimerisation is occuring between *syn* and *anti* acetoin oximes.

It should be noted that in order to convert the results derived from the gas-phase calculations to those in a non-polar solvent we need to consider the statistical thermodynamics corrections for the temperature effect along with the vibrational and zero-point energy (ZPE). Therefore the ΔG^{363} of the acetoin oxime dimerisation process in a non-polar solvent should be calculated as follows;

$$\Delta G^{363}_{dim-n} = (E^o + ZPE_v + G^{363}_v)_{dimer} - 2 \times (E^o + ZPE_v + G^{363}_v)_{monomer} \quad (5.2)$$

where G_v is the vibrational correction to the Gibbs free energy ($G^{363}_v = H^{363}_v - 363 \times S^{363}_v$); H^{363}_v and S^{363}_v are the vibrational corrections at 363 K to the enthalpy and entropy, respectively; ZPE_v is the zero-point vibrational energy and E^o is the total electronic energy. Note that the final values of enthalpy and entropy corrections in most quantum chemical software include all three constituents: vibrational, rotational and translational. However, for these calculations we only need the vibrational contribution as gas phase rotational and translational contributions are not appropriate to the liquid state.

The energetics of both *syn* and *anti* isomers of acetoin oxime estimated at different levels of theory were presented in the previous chapters of this thesis. If we look at the lowest energy structures of the *syn* and *anti* acetoin oxime isomers shown in Figure 5.1 we can see that there are two donor centres (the hydroxyl group on carbon and the oxime group) and three acceptors (two oxygen atoms and one nitrogen) for hydrogen bonding. This means that there are many different types of dimers that can be formed.

FIGURE 5.1: The lowest energy structures of *anti* (left) and *syn* (right) acetoin oxime isomers optimised at the B3LYP/6-31G(d,p) level of theory. Grey coloured atoms represent carbon, red - oxygen, dark blue - nitrogen and white - hydrogen.

All possible dimers were constructed and divided into three different groups. The first group represents acetoin oxime dimers formed between two *anti* isomers, the second one mixed dimers formed between both *syn* and *anti* isomers, and the third group dimers formed between two *syn* isomers.

In the literature (Georgieva *et al.*, 2003; Gorce and Bahceli, 2011) it is recommended to include diffuse functions for both hydrogen and heavy atoms when studying oligomerisation processes. Therefore, it has been decided to perform calculations at both B3LYP/6-31G(d,p) and B3LYP/6-31++G(d,p) levels of theory. Another important thing to test, according to Bende *et al.* (2001), is the effect of BSSE on the thermodynamics of the intermolecular hydrogen bonding process. Thermodynamic data

estimated at the B3LYP/6-31G(d,p) and B3LYP/6-31++G(d,p) levels of theory corresponding to the process of formation of different types of acetoin oxime dimers between two *anti* isomers are given in Tables 5.1 and 5.2, respectively.

TABLE 5.1: Magnitude of BSSE correction (BSSE), enthalpies ($\Delta H^{BSSE}_{dim\text{-}n}$) and Gibbs free energies ($\Delta G^{BSSE}_{dim\text{-}n}$) in kJ/mol including BSSE correction for the acetoin oxime dimerisation process between two *anti* isomers and free energy differences with BSSE correction in kJ/mol between each optimised acetoin oxime dimer and the lowest energy structure ($\Delta\Delta G^{BSSE}$) calculated at the B3LYP/6-31G(d,p) level of theory at 298.15 K.

Anti-anti dimer	B3LYP/6-31G(d,p)			
	BSSE	$\Delta H^{BSSE}_{dim\text{-}n}$	$\Delta G^{BSSE}_{dim\text{-}n}$	$\Delta\Delta G^{BSSE}$
COH-OC, NOH-N; COH-N	19.9	-4.5	-33.0	18.6
NOH-N; NOH-N	17.0	-14.5	-39.9	6.5
COH-ON; NOH-N	16.8	-10.5	-37.5	11.7
NOH-OC, COH-N; NOH-OC, COH-N	25.5	-12.4	-45.1	14.1
COH-OC	15.4	6.9	-20.1	31.4
NOH-N; NOH-ON	14.0	-1.5	-41.3	10.2
NOH-ON	12.3	0.2	-40.8	10.7
NOH-OC	10.6	-11.1	-51.6	0.0

TABLE 5.2: Magnitude of BSSE correction (BSSE), enthalpies ($\Delta H^{BSSE}_{dim\text{-}n}$) and Gibbs free energies ($\Delta G^{BSSE}_{dim\text{-}n}$) in kJ/mol including BSSE correction for the acetoin oxime dimerisation process between two *anti* isomers and free energy differences with BSSE correction in kJ/mol between each optimised acetoin oxime dimer and the lowest energy structure ($\Delta\Delta G^{BSSE}$) calculated at the B3LYP/6-31++G(d,p) level of theory at 298.15 K.

Anti-anti dimer	B3LYP/6-31++G(d,p)			
	BSSE	$\Delta H^{BSSE}_{dim\text{-}n}$	$\Delta G^{BSSE}_{dim\text{-}n}$	$\Delta\Delta G^{BSSE}$
COH-OC, NOH-N; COH-N	4.4	-8.3	-32.5	13.4
NOH-OC, COH-N; NOH-OC, COH-N	4.1	-13.6	-44.6	1.4
NOH-N; NOH-N	4.0	-17.5	-46.0	0.0
COH-ON; NOH-N	3.4	-8.6	-19.6	26.4
COH-N; NOH-N	4.3	-6.1	-29.8	16.1
NOH-ON	3.3	-12.7	-27.5	18.4
NOH-OC	3.9	-22.8	-34.1	11.9

Eight different types of dimer that could possibly be formed between two *anti* isomers of acetoin oxime were optimised at the B3LYP/6-31G(d,p) level of theory and only seven at the B3LYP/6-31++G(d,p) level. Note that the number of manually constructed *anti-anti* dimers was higher than eight; however, during geometry optimisation some structures were found to lead to one of the other minima represented in Tables 5.1 and 5.2. It should also be noted that the names of dimers are constructed in such a way that if the donor groups (written before the dash sign "-") forming intermolecular hydrogen bond with corresponding acceptors (written after the dash sign "-") belong to the same molecule (isomer), the types of hydrogen bonds in the name of dimer are separated by a comma and by a semicolon if the donor groups are from another molecule. For instance, in a COH-OC, NOH-N; COH-N *anti-anti* acetoin oxime dimer the COH hydroxyl and NOH oxime groups of the first *anti* acetoin oxime isomer form two hydrogen bonds with OC and N acceptors of the second molecule, respectively, while the COH donor group of the second *anti* isomer is bonded to the N acceptor of the first molecule. In the first two types of hydrogen bond both donors belong to the same molecule, therefore, they are separated by a comma, while the donors in the NOH-N and COH-N hydrogen bonds belong to different molecules and, therefore these types of hydrogen bonds are separated by the semicolon.

As can be seen from Tables 5.1 and 5.2, the B3LYP/6-31G(d,p) level predicts the NOH-OC *anti-anti* acetoin oxime dimer to be the lowest energy structure followed by NOH-N; NOH-N, while the NOH-N; NOH-N structure was predicted to be the most stable at the B3LYP/6-31++G(d,p) level followed by NOH-OC, COH-N; NOH-OC, COH-N. It is interesting to note that the Gibbs free energy difference between NOH-OC and NOH-N; NOH-N dimer structures calculated at the B3LYP/6-31G(d,p) level is 6.5 kJ/mol, which gives quite a low probability of co-existence for these two dimers. In contrast, the B3LYP/6-31++G(d,p) level of theory predicts co-existence of NOH-N; NOH-N and NOH-OC, COH-N; NOH-OC, COH-N *anti-anti* acetoin oxime dimers, as the predicted Gibbs free energy difference between them is only 1.4 kJ/mol. Another observation is that if the Gibbs free energy differences between the lowest energy structure and each optimised acetoin oxime dimer are taken without BSSE correction, the B3LYP/6-31G(d,p) level predicts NOH-OC, COH-N; NOH-OC, COH-N to be the lowest energy structure for the *anti-anti* acetoin oxime dimer followed by NOH-N; NOH-N and NOH-OC with just 0.8 kJ/mol difference. Graphical representations of the most stable *anti-anti* acetoin oxime dimers are depicted in Figure 5.2.

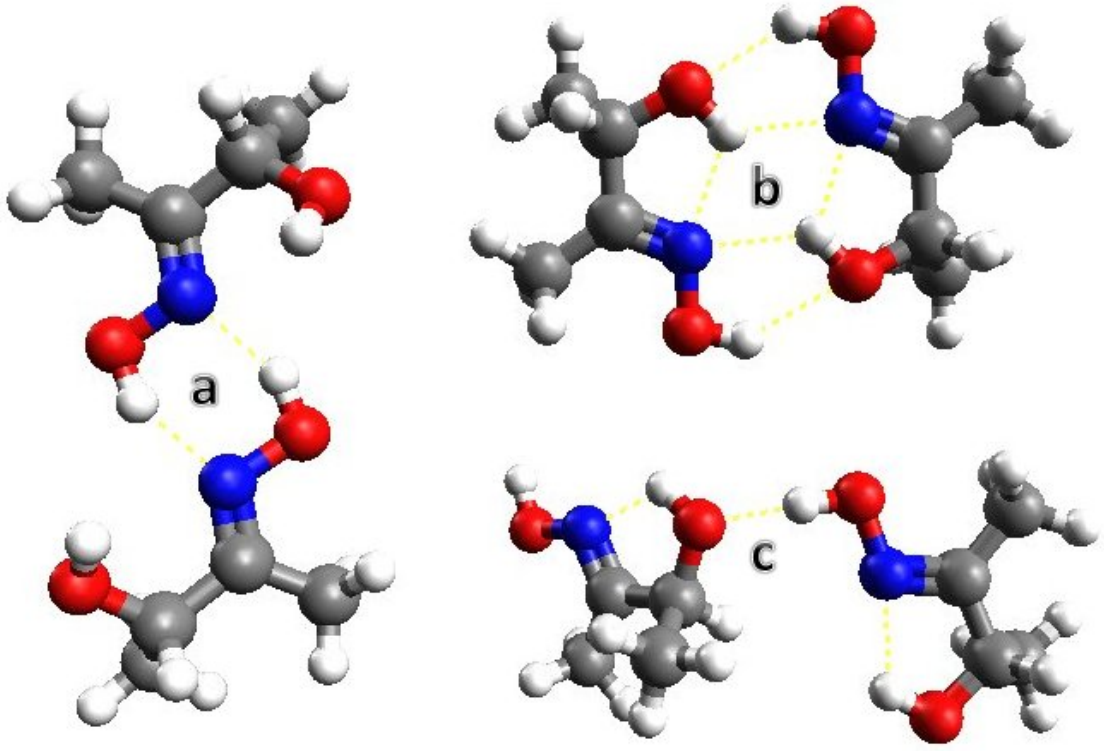

FIGURE 5.2: The lowest energy structures of *anti-anti* acetoin oxime dimers optimised at the B3LYP/6-31++G(d,p) (a and b) and B3LYP/6-31G(d,p) (c) levels of theory. Grey coloured atoms represent carbon, red - oxygen, dark blue - nitrogen and white - hydrogen. Dotted yellow lines represent inter- and intra-molecular hydrogen bonding.

Note that in case of calculations at the B3LYP/6-31++G(d,p) level, the exclusion of the BSSE correction does not change the trend of dimer stabilities shown in Table 5.2. Furthermore, the magnitude of BSSE correction is significantly lower as compared to that at the B3LYP/6-31G(d,p) level. This means that in this instance B3LYP calculations with 6-31++G(d,p) basis set are most likely to be more accurate and therefore more trustworthy.

The first conclusion which can be drawn based on the above results is that the number of intermolecular hydrogen bonds is not the determining factor for the stability of the dimers formed, since if it was then the "COH-OC, NOH-N; COH-N" configuration would be expected to be more stable than both "NOH-OC" and "NOH-N; NOH-N" *anti-anti* acetoin oxime dimers. However, according to the B3LYP/6-31G(d,p) calculations "NOH-OC" is the most stable configuration, while according to the B3LYP/6-31++G(d,p) calculations the lowest energy configuration is the "NOH-N; NOH-N" one. This means that the type of inter-molecular hydrogen bonding is the determining factor for *anti-anti* acetoin oxime dimer stability and not the number of hydrogen bonds. However, it is interesting to note that if the BSSE correction is not considered, both

TABLE 5.3: Magnitude of BSSE correction (BSSE), enthalpies ($\Delta H_{\text{dim-n}}^{\text{BSSE}}$) and Gibbs free energies ($\Delta G_{\text{dim-n}}^{BSSE}$) in kJ/mol including BSSE correction for the acetoin oxime dimerisation process between *anti* and *syn* isomers and free energy differences with BSSE correction in kJ/mol between each optimised acetoin oxime dimer and the lowest energy structure ($\Delta\Delta G^{\text{BSSE}}$) calculated at the B3LYP/6-31G(d,p) level of theory at 298.15 K.

Anti-syn dimer	B3LYP/6-31G(d,p)			
	BSSE	$\Delta H_{\text{dim-n}}^{\text{BSSE}}$	$\Delta G_{\text{dim-n}}^{BSSE}$	$\Delta\Delta G^{\text{BSSE}}$
sNOH-OC	10.5	-16.8	-45.4	9.3
sNOH-N; aNOH-N	14.6	-24.8	-54.7	0.0
sNOH-N; aCOH-N	16.1	-13.8	-42.9	11.8
sNOH-ON	12.5	-2.7	-38.0	16.7
sCOH-N; aCOH-OC, NOH-ON	28.7	10.3	-19.1	35.6
aNOH-ON; sCOH-ON	16.4	8.5	-24.9	29.8
sNOH-OC, COH-N; aNOH-OC	23.5	-3.7	-33.6	21.1
aNOH-OC	18.6	-8.7	-39.1	15.5
sCOH-OC, NOH-N; aCOH-ON	28.6	19.4	-2.5	52.2
aCOH-OC	16.4	8.7	-25.5	29.2

B3LYP/6-31G(d,p) and B3LYP/6-31++G(d,p) methods provide very similar results. Therefore, as compared to the B3LYP/6-31++G(d,p) level of theory, the BSSE correction has an adverse effect on the results provided by B3LYP calculations using the 6-31G(d,p) basis set. However, it is highly recommended in the literature (Bende, 2010) to use BSSE when studying oligomers. This means that the 6-31G(d,p) basis set is not appropriate for studying hydroxyoxime oligomerisation processes, which agrees well with the literature (Sahu, 2004; Papajak and Truhlar, 2010), where it is highly recommended to include diffuse functions for both hydrogen and heavy atoms.

To strengthen this conclusion we are going to look at the thermodynamics of acetoin oxime dimerisation between both *syn* and *anti* isomers and also two *syn*-acetoin oximes calculated using the B3LYP hybrid DFT functional with both 6-31G(d,p) (Tables 5.3 and 5.4) and 6-31++G(d,p) (Tables 5.5 and 5.6) basis sets, with and without BSSE correction[2]. In contrast to acetoin oxime dimerisation between two *anti* isomers, when the *syn*-acetoin oxime is introduced to the system the relative (to the lowest energy structure) energetics of different types of formed dimers between *syn* and *anti* and/or two *syn* isomers are similarly described using both 6-31G(d,p) and 6-31++G(d,p) basis

[2]Note that "s" and "a" letters standing before the donor groups in notations of dimers in Tables 5.3 and 5.5 indicate the isomers (*syn* and *anti*, respectively) to which they belong.

TABLE 5.4: Magnitude of BSSE correction (BSSE), enthalpies ($\Delta H_{dim\text{-}n}^{BSSE}$) and Gibbs free energies ($\Delta G_{dim\text{-}n}^{BSSE}$) in kJ/mol including BSSE correction for the acetoin oxime dimerisation process between two *syn* isomers and free energy differences with BSSE correction in kJ/mol between each optimised acetoin oxime dimer and the lowest energy structure ($\Delta\Delta G^{BSSE}$) calculated at the B3LYP/6-31G(d,p) level of theory at 298.15 K.

Syn-Syn dimer	B3LYP/6-31G(d,p)			
	BSSE	$\Delta H_{dim\text{-}n}^{BSSE}$	$\Delta G_{dim\text{-}n}^{BSSE}$	$\Delta\Delta G^{BSSE}$
NOH-N	13.0	-9.5	-46.4	19.7
NOH-OC; NOH-N	19.3	-10.7	-41.4	24.7
NOH-ON; COH-ON	18.4	10.6	-23.7	42.4
NOH-OC; NOH-OC	27.5	-6.2	-32.6	33.5
COH-OC	19.5	9.1	-26.7	39.4
NOH-ON; COH-N	16.9	-0.5	-41.0	25.2
NOH-N; NOH-N	12.2	-35.1	-66.1	0.0
NOH-OC	11.6	-14.5	-51.5	14.6

TABLE 5.5: Magnitude of BSSE correction (BSSE), enthalpies ($\Delta H_{dim\text{-}n}^{BSSE}$) and Gibbs free energies ($\Delta G_{dim\text{-}n}^{BSSE}$) in kJ/mol including BSSE correction for the acetoin oxime dimerisation process between two *syn* isomers and free energy differences with BSSE correction in kJ/mol between each optimised acetoin oxime dimer and the lowest energy structure ($\Delta\Delta G^{BSSE}$) calculated at the B3LYP/6-31++G(d,p) level of theory at 298.15 K.

Anti-syn dimer	B3LYP/6-31++G(d,p)			
	BSSE	$\Delta H_{dim\text{-}n}^{BSSE}$	$\Delta G_{dim\text{-}n}^{BSSE}$	$\Delta\Delta G^{BSSE}$
sNOH-OC	3.8	-25.0	-34.8	16.1
sNOH-N; aNOH-N	3.8	-22.5	-50.9	0.0
sNOH-N; aCOH-N	4.0	-13.6	-41.3	9.6
sNOH-ON; aNOH-N	2.9	-24.5	-28.4	22.5
sCOH-N; aCOH-OC, NOH-ON	4.4	5.0	-23.5	27.4
aNOH-OC	3.9	-10.0	-43.3	7.6
sCOH-OC; aCOH-ON	4.5	11.8	-24.2	26.7
aCOH-OC	2.2	0.9	-22.8	28.1

TABLE 5.6: Magnitude of BSSE correction, enthalpies and Gibbs free energies (kJ/mol) for the acetoin oxime dimerisation process between two *syn* isomers and free energy differences between each optimised acetoin oxime dimer and the lowest energy structure of this type calculated at the B3LYP/6-31++G(d,p) level of theory at 298.15 K with BSSE correction.

Syn-syn dimer	B3LYP/6-31++G(d,p)			
	ΔBSSE	$\Delta H_{\text{dim-n}}^{\text{BSSE}}$	$\Delta G_{\text{dim-n}}^{BSSE}$	$\Delta\Delta G^{\text{BSSE}}$
NOH-N	2.6	-23.3	-34.0	21.3
NOH-ON; COH-ON	4.6	10.3	-21.6	33.7
COH-OC	2.2	2.1	-34.2	21.0
NOH-ON; COH-N	4.6	0.8	-28.6	26.7
NOH-N; NOH-N	3.5	-40.6	-55.3	0.0
NOH-OC	3.6	-16.5	-44.8	10.4

sets. As can be seen from Tables 5.3, 5.4, 5.5 and 5.6, the NOH-N; NOH-N type of dimer was estimated to be the most stable configuration for both *anti/syn* and *syn/syn* combinations according to the calculation at both levels of theory. The NOH-OC dimer was predicted to be the next most stable configuration. However, it is interesting to note that according to the B3LYP/6-31G(d,p) calculations this type of intermolecular bonding is stronger if the NOH donor group of *syn*-acetoin oxime is bonded to the OC acceptor of the *anti* isomer, while the B3LYP/6-31++G(d,p) calculations show us that the NOH-OC dimer will be stronger if the NOH donor group in it belongs to the *anti*-acetoin oxime. It can be seen that the inclusion of BSSE correction still gives a very significant effect on the stabilities of some *anti/syn* and *syn/syn* dimer configurations calculated at the B3LYP/6-31G(d,p) level of theory.

It would be informative if we answered the question of why the magnitude of BSSE correction estimated at the B3LYP/6-31G(d,p) level of theory is higher for some acetoin oxime dimers and lower for others? To answer this question we should first look at the hydrogen bond distances of the dimers for which the BSSE correction has the lowest and highest values at the B3LYP/6-31G(d,p) level of theory and compare them with the distances of the corresponding dimers calculated at the B3LYP/6-31++G(d,p) level. From Table 5.1 it can be seen that the NOH-OC, COH-N; NOH-OC, COH-N structure of the *anti/anti*-acetoin oxime has the largest value for the BSSE. The lowest BSSE value calculated at the B3LYP/6-31G(d,p) level of theory corresponds to the NOH-OC *anti/anti* dimer. The structures of these two afore-mentioned dimers, with the lengths of intermolecular hydrogen bonds are shown in Figure 5.3. In the *anti/syn* group of acetoin oxime dimers the sNOH-OC has the lowest and sCOH-N; aCOH-OC,

NOH-ON the highest magnitude of BSSE calculated at the B3LYP/6-31G(d,p) level of theory (Figure 5.4). In the *syn/syn* group of acetoin oxime dimers the NOH-OC has the lowest and NOH-OC; NOH-OC the highest magnitude of BSSE calculated at the B3LYP/6-31G(d,p) level of theory. However, it should be noted that NOH-OC; NOH-OC dimer was not optimised at the B3LYP/6-31++G(d,p) level of theory (NOH-OC minimum was located after relaxed optimisation of NOH-OC; NOH-OC configuration). Therefore we are taking COH-OC structure instead as it has the highest value of BSSE next to the NOH-OC; NOH-OC structure. The structures of the COH-OC and NOH-OC dimers with the lengths of intermolecular hydrogen bonds estimated using the B3LYP hybrid method with both 6-31G(d,p) and 6-31++G(d.p) basis sets are shown in Figure 5.5.

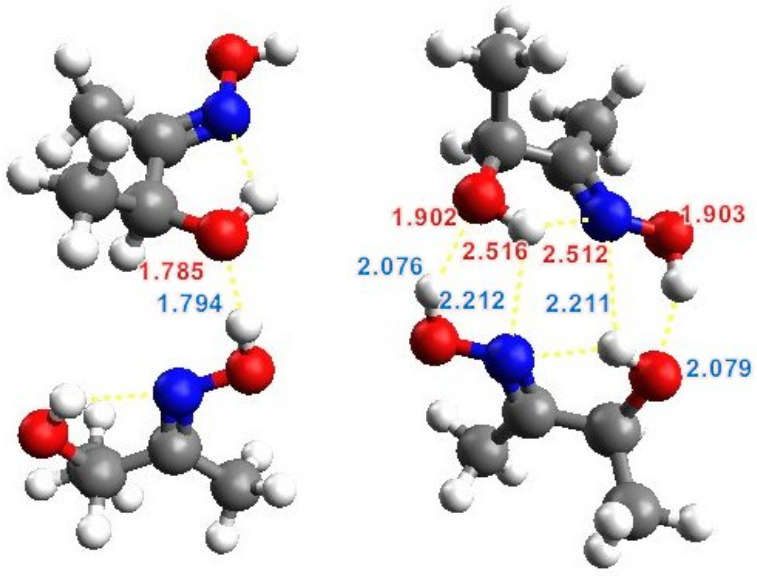

FIGURE 5.3: Graphical representation of NOH-OC (left) and NOH-OC, COH-N; NOH-OC, COH-N (right) *anti/anti*-acetoin oxime dimers with hydrogen bond distances in angstroms (Å) calculated at the B3LYP/6-31G(d,p) (red numbers) and B3LYP/6-31++G(d,p) (blue numbers) levels of theory. Grey coloured atoms represent carbon, red - oxygen, dark blue - nitrogen and white - hydrogen. Dotted yellow lines represent inter- and intra-molecular hydrogen bonding.

It looks like the B3LYP/6-31G(d,p) method gives similar results with the B3LYP/6-31++G(d,p) one in case when the dimers are formed via single inter-molecular hydrogen bond[3]. However, when the dimer is formed with multiple hydrogen bonds the situation is more complicated and it becomes a bit more challenging to explain why the

[3]Except the case of COH-OC *syn/syn* dimer where the intra-molecular bond in donor (when forming dimer) monomer is significantly overestimated as compared to the B3LYP/6-31++G(d,p) results.

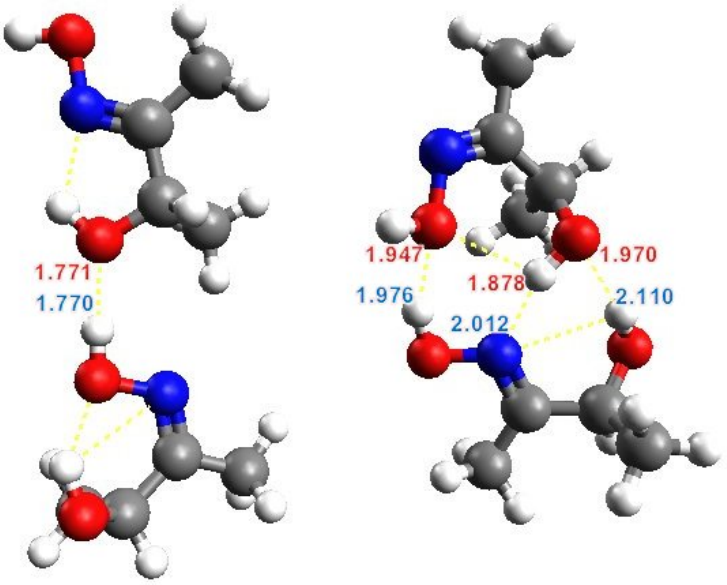

FIGURE 5.4: Graphical representation of sNOH-OC (left) and sCOH-N; aCOH-OC, NOH-ON (right) *anti/syn*-acetoin oxime dimers with hydrogen bond distances in angstroms (Å) calculated at the B3LYP/6-31G(d,p) (red numbers) and B3LYP/6-31++G(d,p) (blue numbers) levels of theory. Grey coloured atoms represent carbon, red - oxygen, dark blue - nitrogen and white - hydrogen. Dotted yellow lines represent inter- and intra-molecular hydrogen bonding.

B3LYP/6-31G(d,p) method gives worse description of these systems as compared to the B3LYP/6-31++G(d,p) one. According to Jeffrey (1997), the hydrogen bond interaction is considered strong if the bond length is less than or equal to 2.2 Å, and weak if the length is more than 2.2 Å. As can be seen from Figures 5.3, 5.4 and 5.5, the B3LYP/6-31G(d,p) method underestimates the hydrogen bond distances for strong interaction (when donor acceptor distances are less than or equal to 2.2Å) and overestimates them, respectively, in case of weak hydrogen bond interaction (when the donor-acceptor distances are higher than 2.2Å) as compared to the B3LYP/6-31++G(d,p) calculations. It is interesting to note that this was found to be the case for inter-molecular hydrogen bonding when the number of hydrogen bonds is more than one. However, for all the intra- and inter-molecular interactions where an oligomer is formed by binding monomers with a single hydrogen bond, the length of these bonds are nearly equal in both B3LYP/6-31G(d,p) and B3LYP/6-31++G(d,p) methods. By looking at the overall picture of acetoin oxime dimerisation estimated at the B3LYP/6-31G(d,p) level of theory it seems like the BSSE value is higher for those dimers in which the hydroxyl group on a carbon atom (-COH) plays the role of donor in the intermolecular interaction. This means that the accuracy in modelling of the oligomerisation process using B3LYP/6-31G(d,p) highly depends on the nature (types of intra-/inter-molecular interactions) of the oligomers formed and therefore is not recommended for this purpose. The

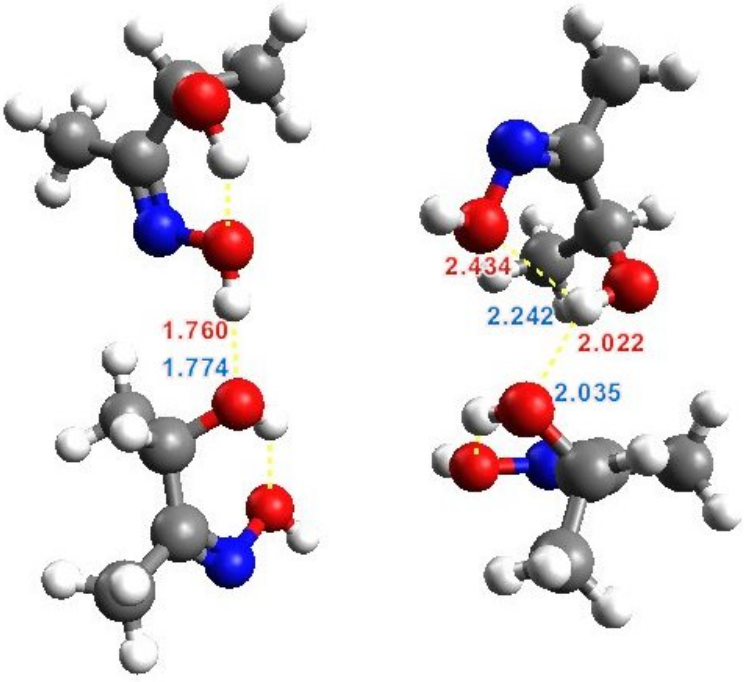

FIGURE 5.5: Graphical representation of NOH-OC (left) and COH-OC (right) *syn/syn*-acetoin oxime dimers with hydrogen bond distances in angstroms (Å) calculated at the B3LYP/6-31G(d,p) (red numbers) and B3LYP/6-31++G(d,p) (blue numbers) levels of theory. Grey coloured atoms represent carbon, red - oxygen, dark blue - nitrogen and white - hydrogen. Dotted yellow lines represent inter- and intra-molecular hydrogen bonding.

magnitude of the BSSEs in B3LYP/6-31++G(d,p) calculations are significantly lower than those for B3LYP/6-31G(d,p). Therefore we choose to continue our modelling of hydroxyoxime oligomerisation using only the B3LYP/6-31++G(d,p) method.

In the study of the effect of the size of hydrocarbon side-chains on the *syn/anti* hydroxyoxime equilibrium it was shown that the experimentally measured *syn/anti* equilibrium of the LIX63 main component is better described by modelling the equilibrium between *syn* and *anti* isomers of 2,5-dimethyl-4-hydroxy-hexan-3-oxime, where the R groups are equal to C_3H_7 on both ends of the molecule. The effect of the size of hydrocarbon side-chains on the dimerisation process may also be significant and although we are limited in computer resources for modelling of higher order oligomers (trimers, tertramers etc.) formed between 2,5-dimethyl-4-hydroxy-hexan-3-oxime molecules, it is of great interest to examine this effect at least for the case of the dimerisation process. Thermodynamic data for the dimerisation process between different isomers of 2,5-dimethyl-4-hydroxy-hexan-3-oxime calculated at the B3LYP/6-31++G(d,p) level of theory are shown in Tables 5.7, 5.8 and 5.9. As can be seen, the relative energetics of *anti/anti*, *syn/anti* and *syn/syn* dimers, as well as the thermodynamics of 2,5-dimethyl-4-hydroxy-hexan-3-oxime dimerisation are very similar to those of acetoin oxime (as

TABLE 5.7: Magnitude of BSSE correction, enthalpies, Gibbs free energies (kJ/mol) for the 2,5-dimethyl-4-hydroxy-hexan-3-oxime dimerisation process between two *anti* isomers and free energy differences between each optimised 2,5-dimethyl-4-hydroxy-hexan-3-oxime dimer and the lowest energy structure of this type calculated at the B3LYP/6-31++G(d,p) level of theory at 298.15 K with BSSE correction.

Anti-anti dimer	B3LYP/6-31++G(d,p)			
	BSSE	$\Delta H^{BSSE}_{dim\text{-}n}$	$\Delta G^{BSSE}_{dim\text{-}n}$	$\Delta\Delta G^{BSSE}$
COH-OC, NOH-N; COH-N	3.8	-6.4	-39.8	10.1
NOH-OC, COH-N; NOH-OC, COH-N	4.4	-10.5	-49.7	2.7
NOH-N; NOH-N	3.1	-19.5	-56.1	0.0
COH-ON; NOH-N	4.2	-9.4	-27.6	24.5
COH-N; NOH-N	4.1	-6.1	-31.8	14.1
NOH-ON	3.9	-9.5	-32.3	17.1
NOH-OC	4.4	-24.9	-38.9	10.5

TABLE 5.8: Magnitude of BSSE correction, enthalpies, Gibbs free energies (kJ/mol) for the 2,5-dimethyl-4-hydroxy-hexan-3-oxime dimerisation process between *anti* and *syn* isomers and free energy differences between each optimised 2,5-dimethyl-4-hydroxy-hexan-3-oxime dimer and the lowest energy structure of this type calculated at the B3LYP/6-31++G(d,p) level of theory at 298.15 K with BSSE correction.

Anti-syn dimer	B3LYP/6-31++G(d,p)			
	BSSE	$\Delta H^{BSSE}_{dim\text{-}n}$	$\Delta G^{BSSE}_{dim\text{-}n}$	$\Delta\Delta G^{BSSE}$
sNOH-OC	4.4	-22.1	-39.1	14.1
sNOH-N; aNOH-N	3.5	-20.5	-54.0	0.0
sNOH-N; aCOH-N	3.9	-15.7	-42.6	10.2
sNOH-ON; aNOH-N	5.0	-21.8	-32.4	21.4
sCOH-N; aCOH-OC, NOH-ON	3.8	9.1	-25.1	23.8
aNOH-OC	4.4	-8.4	-48.6	8.1
sCOH-OC; aCOH-ON	4.2	15.1	-26.0	24.6
aCOH-OC	3.7	3.2	-24.6	25.0

TABLE 5.9: Magnitude of BSSE correction, enthalpies, Gibbs free energies (kJ/mol) for the 2,5-dimethyl-4-hydroxy-hexan-3-oxime dimerisation process between two *syn* isomers and free energy differences between each optimised 2,5-dimethyl-4-hydroxy-hexan-3-oxime dimer and the lowest energy structure of this type calculated at the B3LYP/6-31++G(d,p) level of theory at 298.15 K with BSSE correction.

Syn-syn dimer	B3LYP/6-31++G(d,p)			
	ΔBSSE	$\Delta H^{BSSE}_{dim\text{-}n}$	$\Delta G^{BSSE}_{dim\text{-}n}$	$\Delta\Delta G^{BSSE}$
NOH-N	3.1	-20.0	-36.2	19.0
NOH-ON; COH-ON	5.2	14.1	-25.1	29.8
COH-OC	4.2	5.4	-38.2	20.1
NOH-ON; COH-N	3.5	3.2	-31.8	25.4
NOH-N; NOH-N	4.4	-37.1	-57.2	0.0
NOH-OC	3.9	-11.5	-48.7	9.2

compared to the data shown in Tables 5.2, 5.5 and 5.6). Moreover, similar to acetoin oxime, the NOH-N; NOH-N structure was found to be the minimum for each type of 2,5-dimethyl-4-hydroxy-hexan-3-oxime dimer (*anti/anti*, *syn/anti* and *syn/syn*). Therefore at this stage we can conclude that there is no significant effect of the size of a hydrocarbon side-chains on the thermodynamics of hydroxyoxime oligomerisation.

It is clear from this study that hydroxyoximes easily form the dimers at 298.15 K when present in a non-polar solution at high concentrations and therefore our next step is to see whether oligomerisation continues to a larger extent or if the dimers are the most favourable form of hydroxyoximes at these conditions.

5.3.2 Thermodynamics of Formation of Acetoin Oxime Trimers

According to calculations at the B3LYP/6-31++G(d,p) level of theory, the most stable acetoin oxime dimers are those in which isomers are bonded via NOH-N and NOH-OC intermolecular hydrogen bonding. In particular the NOH-N; NOH-N acetoin oxime dimer was shown to be the most stable for each of three combinations between *syn* and *anti* isomers: *anti/anti*, *anti/syn* and *syn/syn*. The NOH-OC configuration has the closest energetics with the NOH-N; NOH-N acetoin oxime dimer amongst the others. As can be seen from Tables 5.2, 5.5 and 5.6, the Gibbs free energy differences for acetoin oxime dimerisation at the B3LYP/6-31++G(d,p) level of theory have large exothermic values (greater than or equal to 19.6 kJ/mol). This shows that at normal conditions *syn* and *anti* acetoin oxime tends to form the dimers (predominantly those of NOH-N; NOH-N and NOH-OC types) to a large extent. As a next step it would be interesting

to see if hydroxyoximes exist in the form of wholly as dimers at normal conditions or tend to form trimers and/or even higher order oligomers.

The possibility of trimer formation at 298.15 K can be determined in a similar way as was estimated for the dimers in the previous subsection by calculating the difference in Gibbs free energies of trimer and a sum of three corresponding monomers. To see if the trimers of acetoin oxime are more stable than its dimers we need to estimate the Gibbs free energy for acetoin trimer formation from its dimers. Note that the trimer can also be formed by adding one monomer to a dimer. However, in this case we want to compare the stabilities of dimers and trimers, therefore we are going to consider the process of acetoin oxime trimerisation as follows;

$$3\mathrm{AA} \rightleftarrows 2\mathrm{AAA} \tag{5.3}$$

where A is an acetoin oxime isomer (*syn* or *anti*), AA is a dimer of acetoin oxime and AAA is its trimer. Note that a mixture of trimers with various combinations of *syn* and *anti* isomers could be a product of the above reaction. Therefore in order to esimate the probability of the presence of each type of acetoin oxime trimer in a mixture we need to consider all possible combinations between *syn* and *anti* isomers that could be used to form the trimer. In total there are four groups of acetoin oxime trimers which can be constructed. These groups include: trimers formed from *anti* isomers only; from one *syn* and two *anti* acetoin oxime isomers, from one *anti* and two *syn* isomers, and from *syn*-acetoin oximes only.

Due to time and computer constraints, we were not able to study the whole potential energy surface for each group of trimers (as we did for dimers). Therefore, we assumed that if the trimers are formed from the most stable NOH-N; NOH-N and NOH-OC dimer types, the resulting structures should be expected to be analogous - NOH-N; NOH-N; NOH-N and NOH-OC; NOH-OC; NOH-OC[4]. As before, in order to convert the results derived from the gas-phase calculations to the corresponding data in a non-polar solvent we have to consider the statistical thermodynamics corrections for the effect of temperature along with the vibrational zero-point energy (ZPE).

In the study of the thermodynamics of acetoin oxime dimerisation it was shown that B3LYP/6-31++G(d,p) gives a better description of intermolecular hydrogen bonding than B3LYP/6-31G(d,p). Therefore it was decided to perform all following calculations of higher order oligomers using the B3LYP hybrid method with the 6-31++G(d,p) basis set. It was also shown that the magnitude of the BSSE correction is quite significant in some cases; therefore, it is also very important to include it in studying the thermodynamics of trimer formation from acetoin oxime dimers. The Gibbs free energy

[4]Note that both types of acetoin oxime trimers have cyclic structure.

TABLE 5.10: Free energy differences between the lowest energy structure and each optimised acetoin oxime trimer (kJ/mol), Gibbs free energies of trimer formation from acetoin oxime monomers, mixture of monomers and dimers, and pure dimers calculated at the B3LYP/6-31++G(d,p) level of theory at 298.15 K (kJ/mol). Note that all values were corrected for BSSE.

Trimer	B3LYP/6-31++G(d,p)			
	$\Delta\Delta G$	$\Delta G^{mon}_{\text{trim-n}}$	$\Delta G^{mon+dim}_{\text{trim-n}}$	$\Delta G^{dim}_{\text{trim-n}}$
aNOH-N; aNOH-N; aNOH-N	33.1	-75.8	-29.8	-13.7
aNOH-OC; aNOH-OC; aNOH-OC	0.0	-108.9	-64.3	-84.0
sNOH-N; aNOH-N; aNOH-N	32.2	-89.2	-38.3	-30.6
sNOH-OC; aNOH-OC; aNOH-OC	15.9	-105.5	-62.2	-88.3
sNOH-N; sNOH-N; aNOH-N	29.3	-104.6	-53.7	-52.1
sNOH-OC; sNOH-OC; aNOH-OC	24.6	-109.2	-74.4	-85.1
sNOH-N; sNOH-N; sNOH-N	27.7	-118.6	-63.3	-71.4
sNOH-OC; sNOH-OC; sNOH-OC	49.8	-96.6	-51.7	-58.6

differences corrected for BSSE between acetoin oxime trimers and the lowest energy structure, and thermodynamics (also corrected for BSSE) of trimerisation from the corresponding monomers, combination of dimers and monomers, and from dimers only at 298.15 K are shown in Table 5.10. As can be seen, no matter in which form the initial concentrated mixture of *syn* and *anti* acetoin oximes is taken (the mixture of monomers and/or dimers), the trimers are most likely to be formed at normal conditions in a non-polar aliphatic solvent. If we look at the first column of Table 5.10, which shows the Gibbs free energy differences between each conformer and the lowest energy structure, we will see that in contrast to acetoin oxime dimers, trimers with NOH-OC intermolecular hydrogen bonding are more stable for each group of trimers except the one in which the acetoin oxime trimer is constructed from three *syn* isomers (sNOH-OC; sNOH-OC; sNOH-OC). For the *syn/syn/syn* group of trimers, the sNOH-N; sNOH-N; sNOH-N structure is significantly more stable than corresponding trimer with the NOH-OC type of inter-molecular hydrogen bonding. In other words, the presence of the *syn* isomer increases the stability of the NOH-N; NOH-N; NOH-N type of trimer and decreases the stability of the NOH-OC; NOH-OC; NOH-OC trimer. A graphical representation of the minima for NOH-N; NOH-N; NOH-N and NOH-OC; NOH-OC; NOH-OC types of acetoin oxime trimers are shown in Figure 5.6.

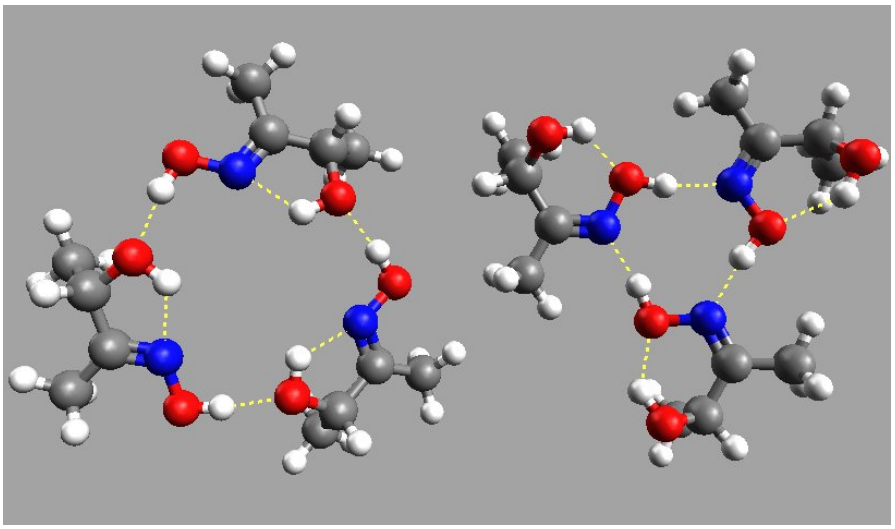

FIGURE 5.6: Graphical representation of aNOH-OC; aNOH-OC; aNOH-OC (left) and sNOH-N; sNOH-N; sNOH-N (right) acetoin oxime trimers optimised at the B3LYP/6-31++G(d,p) levels of theory. Grey coloured atoms represent carbon, red - oxygen, dark blue - nitrogen and white - hydrogen. Dotted yellow lines represent inter- and intra-molecular hydrogen bonding.

According to the results of the current modelling, the above structures are the lowest energy structures of *anti/anti/anti* and *syn/syn/syn* acetoin oxime trimers. However, it may not be possible to form these structures in the real system of LIX63 hydroxyoxime as the R groups of 5,8-diethyl-7-hydroxydodecan-6-oxime are quite large (equal to C_7H_{15} on both ends of the molecule) and therefore inter-molecular repulsion forces arising between these groups may prevent the formation of these structures. Unfortunately, we cannot afford to optimise the *anti/anti/anti* and *syn/syn/syn* trimers of 5,8-diethyl-7-hydroxydodecan-6-oxime at the B3LYP/6-31++G(d,p) level of theory, however at this point we are interested in estimation of the possibility of formation of these trimers and not in their relative energetics and/or thermodynamics of their formation from dimers and or monomers. Therefore, we can use a semi-empirical method like PM6 to perform these calculations. When optimised with PM6, the NOH-N; NOH-N; NOH-N and NOH-OC; NOH-OC; NOH-OC structures of *anti/anti/anti* and *syn/syn/syn* 5,8-diethyl-7-hydroxydodecan-6-oxime trimers are shown in Figure 5.7. Note that the PM6 method predicts relatively similar energetics for NOH-N; NOH-N; NOH-N and NOH-OC; NOH-OC; NOH-OC structures of *anti/anti/anti* and *syn/syn/syn* 5,8-diethyl-7-hydroxydodecan-6-oxime trimers with the magnitude of the Gibbs free energy difference not exceeding 2.5 kJ/mol. Although, the thermodynamics estimated at the PM6 level of theory are not expected to be reliable, it can be seen from Figure 5.7 that NOH-N; NOH-N; NOH-N and NOH-OC; NOH-OC; NOH-OC structures can be formed between *syn* and/or *anti* isomers of LIX63 hydroxyoxime.

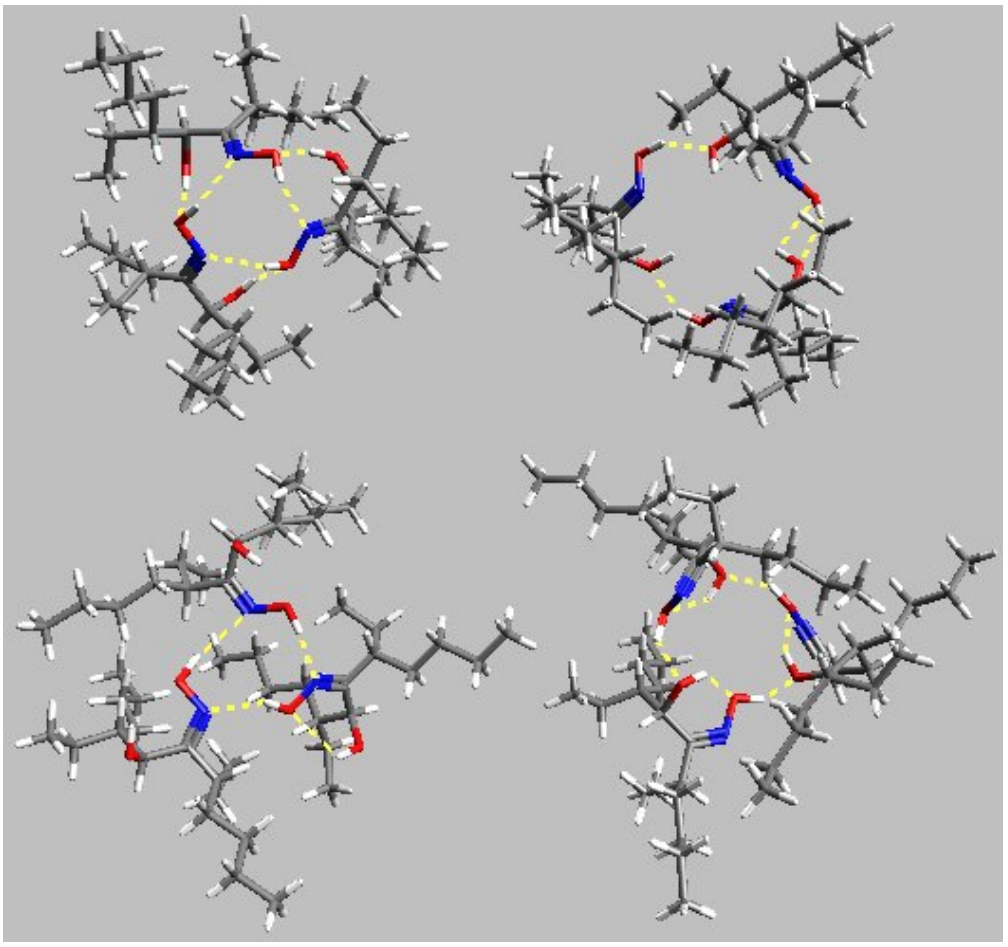

FIGURE 5.7: Graphical representation of aNOH-N; aNOH-N; aNOH-N (a), aNOH-OC; aNOH-OC; aNOH-OC (b), sNOH-N; sNOH-N; sNOH-N (c) and sNOH-OC; sNOH-OC; sNOH-OC (d) LIX63 trimers optimised with PM6 semi-empirical method. Grey coloured atoms represent carbon, red - oxygen, dark blue - nitrogen and white - hydrogen. Dotted yellow lines represent inter- and intra-molecular hydrogen bonds.

Even though it is clear at this stage that hydroxyoximes tend to oligomerise to a large extent we need to see if there is an increase in binding energy going from trimers to tetramers and if so we need to determine how significant this is. This will be examined in the next section.

5.3.3 Thermodynamics of Formation of Aceoin Oxime Tetramers

In order to understand if the tetramers of acetoin oxime are more stable than its trimers we need to estimate the Gibbs free energy for their formation. The tetramer can be formed by adding a monomer to a trimer or from two dimers or by combining four monomers. In addition to these reactions we also want to compare the relative stabilities of trimers and tetramers. Therefore we are also going to estimate the thermodynamics

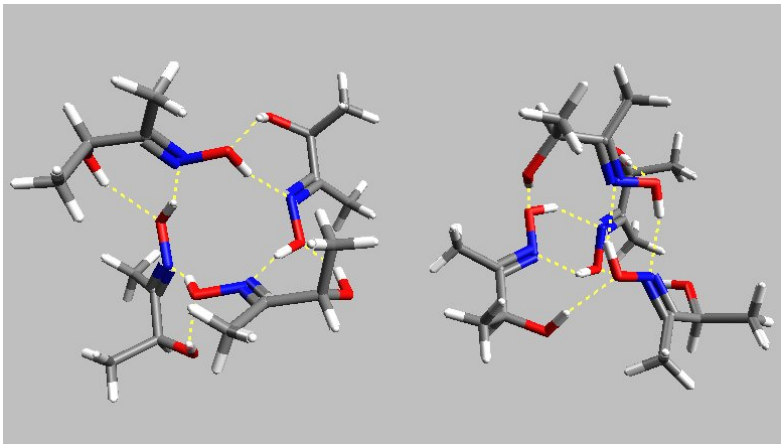

FIGURE 5.8: Graphical representation of (1)aNOH-N; aNOH-N; aNOH-N; aNOH-N (left) and (2)aNOH-N; aNOH-N; aNOH-N; aNOH-N (right) acetoin oxime tetramers. Grey coloured atoms represent carbon, red - oxygen, dark blue - nitrogen and white - hydrogen. Dotted yellow lines represent inter- and intra-molecular hydrogen bonding.

of the process given below;

$$4\text{AAA} \rightleftarrows 3\text{AAAA} \tag{5.4}$$

where A is acetoin oxime isomer (*syn* or *anti*), AAA is a trimer of acetoin oxime and AAAA is its tetramer. Note that a mixture of both *syn* and *anti* acetoin oxime isomers would be present in the real mixture. This means that tetramers containing both isomers could be formed and therefore, similar to the previous subsection, we must consider all possible combinations between *syn* and *anti* isomers that could be used to form the tetramer in order to estimate the probability of the presence of each type of acetoin oxime tetramer. In total, there are five different combinations of *syn* and *anti* isomers of acetoin oxime to look at: 1) 4 *anti* isomers of acetoin oxime, 2) 3 *anti* and 1 *syn* isomer, 3) 2 *anti* and 2 *syn* isomers, 4) 1 *anti* and 3 *syn* isomers and 5) 4 *syn* isomers of acetoin oxime.

Two types of intermolecular hydrogen binding similar to those used to form the trimers of acetoin oxime, namely NOH-N and NOH-OC, were used to construct the tetramers between two isomers of acetoin oxime. All possible combinations between *syn* and *anti* isomers were used to form these two types of tetramers. It is interesting to note that the aNOH-N; aNOH-N; aNOH-N; aNOH-N type of tetramer may exist in two different forms: (1) and (2). If we look at Figure 5.8 where the structures of *anti*-acetoin oximes are shown, it can be seen how these two forms can be easily inter-converted between one another by breaking the NOH$\cdots$N hydrogen bond with the neighbouring molecule and forming the same type of hydrogen bond with the opposite one, leading to two NOH-N; NOH-N dimers (where one is lying one on top of another) connected via COH-ON inter-molecular hydrogen bonding. Thermodynamic data for the acetoin

TABLE 5.11: Magnitude of BSSE correction, free energy differences between the lowest energy structure and each optimised acetoin oxime tetramer, enthalpies and Gibbs free energies of tetramers formation from acetoin oxime trimers calculated at the B3LYP/6-31++G(d,p) level of theory at 298.15 K.

Tetramer	B3LYP/6-31++G(d,p)			
	$\Delta\Delta G$	$\Delta G^{dim}_{\text{trim-n}}$	$\Delta G^{tr+mon}_{\text{trim-n}}$	$\Delta G^{trim}_{\text{trim-n}}$
(1) aNOH-N; aNOH-N; aNOH-N; aNOH-N	50.4	-22.4	-38.6	-39.9
aNOH-OC; aNOH-OC; aNOH-OC; aNOH-OC	0.0	-75.5	-55.8	-58.5
(2) aNOH-N; aNOH-N; aNOH-N; aNOH-N	53.8	-19.0	-35.1	-29.5
(1) sNOH-N; aNOH-N; aNOH-N; aNOH-N	48.8	-31.5	-39.2	-41.8
sNOH-OC; aNOH-OC; aNOH-OC; aNOH-OC	6.7	-82.6	-65.0	-86.0
(2) sNOH-N; aNOH-N; aNOH-N; aNOH-N	49.4	-30.9	-38.6	-40.0
(1) sNOH-N; sNOH-N; aNOH-N; aNOH-N	47.2	-40.7	-37.9	-39.8
sNOH-OC; sNOH-OC; aNOH-OC; aNOH-OC	19.0	-84.1	-61.4	-82.5
(2) sNOH-N; sNOH-N; aNOH-N; aNOH-N	48.2	-39.7	-36.9	-36.8
(1) sNOH-N; aNOH-N; sNOH-N; aNOH-N	51.2	-36.6	-33.9	-27.8
sNOH-OC; aNOH-OC; sNOH-OC; aNOH-OC	20.7	-82.5	-59.8	-77.5
(2) sNOH-N; aNOH-N; sNOH-N; aNOH-N	54.2	-33.7	-30.9	-18.8
(1) sNOH-N; sNOH-N; sNOH-N; aNOH-N	45.9	-50.0	-37.6	-36.3
sNOH-OC; sNOH-OC; sNOH-OC; aNOH-OC	30.8	-83.2	-40.9	-89.8
(2) sNOH-N; sNOH-N; sNOH-N; aNOH-N	47.6	-48.3	-35.9	-31.2
(1) sNOH-N; sNOH-N; sNOH-N; sNOH-N	39.1	-64.9	-56.9	-52.1
sNOH-OC; sNOH-OC; sNOH-OC; sNOH-OC	44.7	-80.2	-73.3	-123.4
(2) sNOH-N; sNOH-N; sNOH-N; sNOH-N	41.9	-62.1	-54.1	-43.7

oxime tetramers calculated at the B3LYP/6-31++G(d,p) level of theory is given in Table 5.11. As can be seen from Table 5.11, the NOH-OC type of intermolecular hydrogen bonding still produces the lowest energy structure of the acetoin oxime tetramer as compared to its trimer. Similar to the trimers, the stability of the NOH-N; NOH-N; NOH-N; NOH-N type of tetramer is increased when the number of *syn*-isomers present in the system is increased. For the case when the tetramer is constructed from *syn*-isomers only, the NOH-N; NOH-N; NOH-N; NOH-N structure is more stable than the NOH-OC; NOH-OC; NOH-OC; NOH-OC one. A graphical representation of the lowest energy aNOH-OC; aNOH-OC; aNOH-OC; aNOH-OC and sNOH-N; sNOH-N; sNOH-N;

sNOH-N structures of *anti/anti/anti/anti* and *syn/syn/syn/syn* acetoin oxime tetramers optimised with the B3LYP/6-31++G(d,p) method is shown in Figure 5.9.

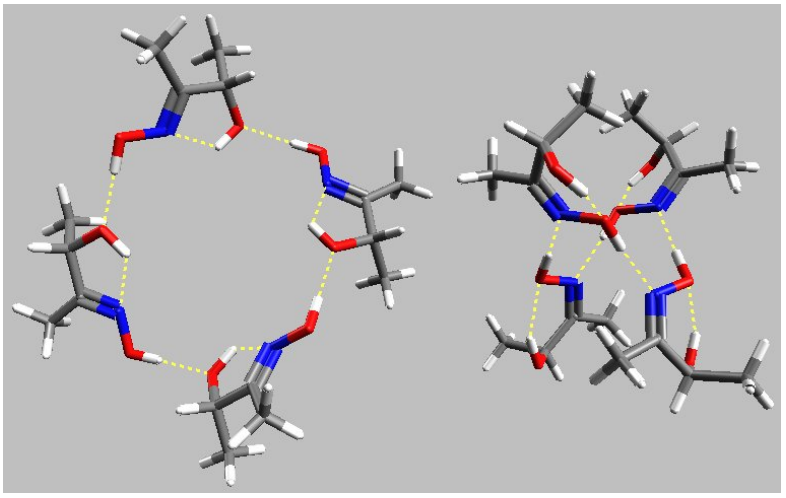

FIGURE 5.9: Graphical representation of (1)aNOH-OC; aNOH-OC; aNOH-OC; aNOH-OC (left) and sNOH-N; sNOH-N; sNOH-N; sNOH-N (right) lowest energy structures of *anti/anti/anti/anti* and *syn/syn/syn/syn* acetoin oxime tetramers, respectively, optimised at the B3LYP/6-31++G(d,p) levels of theory. Grey coloured atoms represent carbon, red - oxygen, dark blue - nitrogen and white - hydrogen. Dotted yellow lines represent inter- and intra-molecular hydrogen bonding.

As can be seen from Table 5.11, the Gibbs free energy of acetoin oxime tetramerisation from dimers, trimers and a mixture of trimers and monomers have large negative values, which shows that at normal conditions *syn* and *anti* isomers of acetoin oxime tend to form higher order oligomers with NOH-N and NOH-OC types of intermolecular interactions. As before it would be also quite useful to check whether it is possible to construct these structure types using *syn* and *anti* isomers of LIX63 hydroxyoxime. Optimised with PM6, the NOH-N; NOH-N; NOH-N; NOH-N and NOH-OC; NOH-OC; NOH-OC; NOH-OC structures of *anti/anti/anti/anti* and *syn/syn/syn/syn* 5,8-diethyl-7-hydroxydodecan-6-oxime tetramers are shown in Figure 5.10. As can be seen, it is sterically possible to form these types of tetramers using the real molecules of *syn* and *anti* LIX63 hydroxyoxime.

It would be interesting to see the further equilibrium between acetoin oxime tetramers and its pentamers. The Gibbs free energy for adding monomer to dimer is more negative than adding to trimer and it could be further increased for the case of adding monomer to the tetramer that would indicate the extant to which acetoin oximes tend to oligomerise at certain conditions, but unfortunately we are note able to perform this calculation as part of the current study. However, it should be noted that the shift of equilibrium between higher and lower order oligomers to the side of higher order acetoin

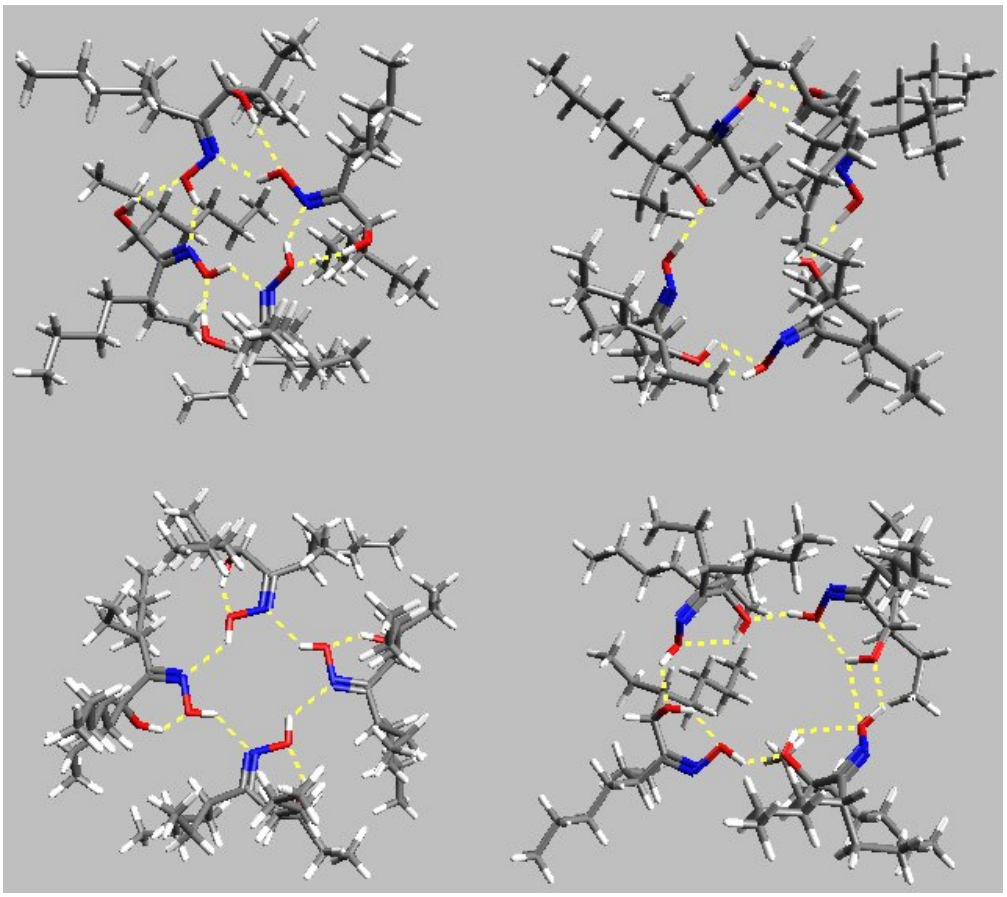

FIGURE 5.10: Graphical representation of aNOH-N; aNOH-N; aNOH-N; aNOH-N (a), aNOH-OC; aNOH-OC; aNOH-OC; aNOH-OC (b), sNOH-N; sNOH-N; sNOH-N; sNOH-N (c) and sNOH-OC; sNOH-OC; sNOH-OC; sNOH-OC (d) LIX63 tetramers optimised with PM6 semi-empirical method. Grey coloured atoms represent carbon, red - oxygen, dark blue - nitrogen and white - hydrogen. Dotted yellow lines represent inter- and intra-molecular hydrogen bonds.

oxime oligomers is consistent for each of the three considered equilibria: Monomers $\rightleftarrows$ Dimers, Dimers $\rightleftarrows$ Trimers and Trimers $\rightleftarrows$ Tetramers. This could be an indicator that hydroxyoximes exist as a mixture of a long chain/circles oligomers bonded composed of molecules of *syn* and/or *anti* isomers bonded via NOH-N and NOH-OC intermolecular interactions.

Previously it was shown experimentally by studying the IR spectra of *anti* - 5,8-diethyl-7-hydroxydodecan-6-oxime in hexane (Figure 4.10) that hydroxyoximes exhibit strong intermolecular interactions via hydrogen bonding in a non-polar aliphatic solvent. It is now of interest to compare the experimental spectra of *anti*-5,8-diethyl-7-hydroxydodecan-6-oxime with the computationally derived IR spectra of three *anti*-acetoin oxime tetramers. The experimental IR spectra were measured at Curtin University with the assistance of Dr Matthew Mclldowie, research fellow at the Nanochemistry

Research Institute. Experimental IR spectra for *anti*-5,8-diethyl-7-hydroxydodecan-6-oxime and those for different types of *anti*-acetoin oxime tetramers, are shown in Figure 5.11.

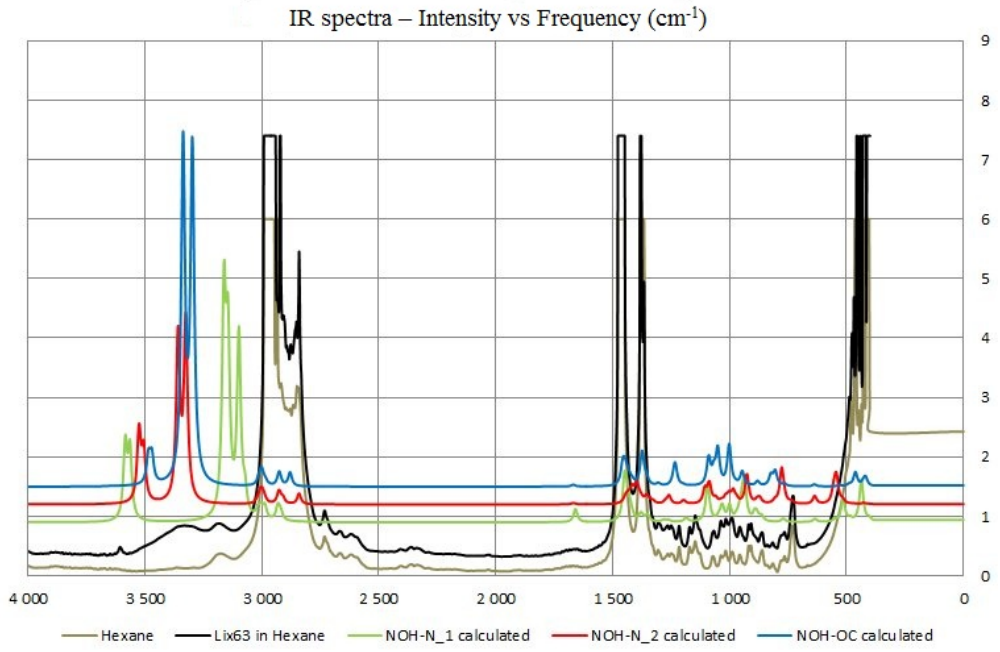

FIGURE 5.11: Experimental IR spectra of pure hexane (brown line), 0.1M *anti* isomer of LIX63 main component diluted in hexane (black line) and calculated at the B3LYP/6-31++G(d,p) level of theory IR spectra of (1)aNOH-N; aNOH-N; aNOH-N; aNOH-N (green line), (2)aNOH-N; aNOH-N; aNOH-N; aNOH-N (red line) and aNOH-OC; aNOH-OC; aNOH-OC; aNOH-OC (blue line).

It should be noted that the calculated frequencies in Figure 5.11 were multiplied by the scaling factor of 0.9614 recommended by Arjunan *et al.* (2011) and Gorce and Bahceli (2011) for B3LYP calculations. This scaling factor is not universal and in order to achieve a better fit to experimental data it is recommended to use different scaling factors for the vibrational modes of different groups. However, even with this single factor it can be seen from the Figure 5.11 that in contrast to the calculated IR spectra of *anti*-2,5-dimethyl-4-hydroxyhexan-3-oxime (shown in Figure 4.10), the IR spectra of (2) aNOH-N; aNOH-N; aNOH-N; aNOH-N and aNOH-OC; aNOH-OC; aNOH-OC; aNOH-OC tetramers match more closely to the experimental results. In particular, the maximum of the experimental broad peak in the 3300-3600cm^{-1} frequency interval is located at approximatelly 3400cm^{-1}, which corresponds to the location of two peaks for O-H bond stretching along the intermolecular hydrogen bond in (2) aNOH-N; aNOH-N; aNOH-N; aNOH-N and aNOH-OC; aNOH-OC; aNOH-OC; aNOH-OC acetoin oxime tetramers. According to Coates and Meyers (2000), this broad experimental

peak also corresponds to a strong intermolecular hydrogen bonding interaction. In other words, based on the current study it is most likely that the main component of LIX63 - 5,8-diethyl-7-hydroxydodecan-6-oxime exists in an oligomeric form with NOH-OC and NOH-N intermolecular interactions.

5.3.4 Kinetics of *Syn/Anti* Isomerisation of Hydroxyoxime Oligomers

In aliphatic non-polar solvents such as ShellSolD70 which is used in SSX of transition metal cations, hydroxyoximes exist in the form of oligomers where both types of hydrogen bonding, represented in Figure 5.10 are possible. Therefore, alternative routes for the *syn/anti* interconversion should be considered using oligomeric forms of hydroxyoxime. Previously it was suggested that the barrier for the hydrogen atom migration, which is an intermediate stage in the tautomerisation mechanisms via enamine and/or nitroso compounds, can be lowered significantly if the transfer takes place along the intermolecular hydrogen bond connecting two hydroxyoxime molecules. At the B3LYP/6-31++G(d,p) level of theory the energy barrier for simultaneous hydrogen transfer along two intermolecular NOH-N; NOH-N hydrogen bonds forming an *anti-anti* acetoin oxime dimer is depicted in Figure 5.12.

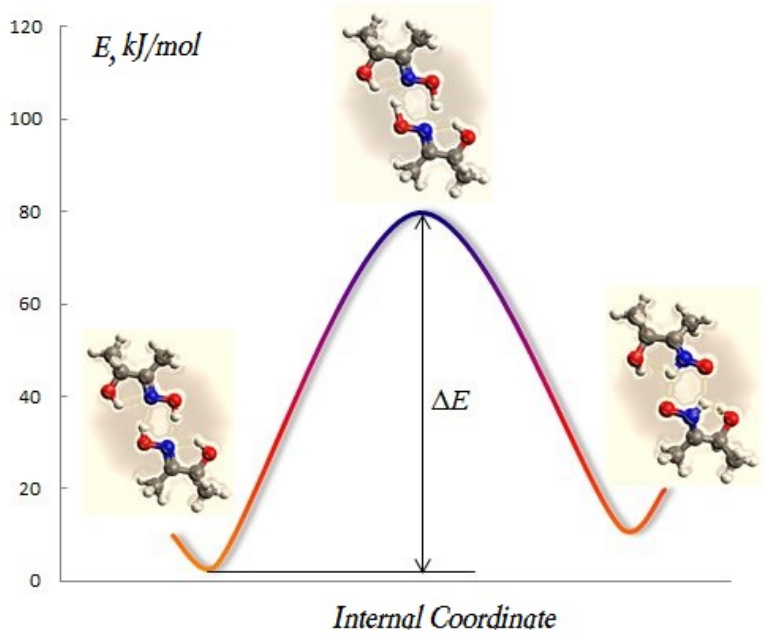

FIGURE 5.12: Reaction profile of a simultaneous migration of a hydrogen atom from oxygen to nitrogen along two NOH-N intermolecular hydrogen bonds. Green coloured atoms represent carbon, red - oxygen, dark blue - nitrogen and white - hydrogen.

In order to estimate this barrier we need to know the energy of the minimum (*anti-anti* acetoin oxime dimer) and that of the transition state which is depicted in Figure 5.12. This barrier estimated at the B3LYP/6-31++G(d,p) level of theory has a value of 68.4 kJ/mol at 363 K, which is significantly lower than the barrier for hydrogen atom migration in *anti*-acetoin oxime monomer (221.7 kJ/mol at 363K estimated at the same level of theory). This leads us to the conclusion that in an environment where hydroxyoxime oligomerisation is possible, the *syn/anti* hydroxyoxime isomerisation may occur via at least two different routes, the first corresponding to the inversion mechanism and the second corresponding to the tautomerisation mechanism via enamine and nitroso compounds. According to the energetics the second mechanism appears far more likely mechanism. However, it should be noted that the introduction of a polar carboxylic acid is likely to affect the hydrogen bonding interactions, and this study is also of fundamental interest.

5.3.5 Conclusion

In the study of acetoin oxime oligomerisation at the B3LYP/6-31++G(d,p) level of theory it was shown that energetically it is more favourable for acetoin oxime to exist in forms of long chain/cyclic oligomers where the *syn* and/or *anti* isomers of hydroxyoxime interact with each other via NOH-OC and NOH-N types of intermolecular hydrogen bonding.

Calculated at the B3LYP/6-31++G(d,p) level of theory IR spectra of (2) aNOH-N; aNOH-N; aNOH-N; aNOH-N and aNOH-OC; aNOH-OC; aNOH-OC; aNOH-OC acetoin oxime tetramers correspond well to the experimental IR spectra of *anti*-5,8-diethyl-7-hydroxydodecan-6-oxime which also support the conclusion that acetoin oxime exists in oligomeric form where the *syn* and/or *anti* isomers of hydroxyoxime interact with each other via NOH-OC and NOH-N types of intermolecular hydrogen bonding.

Calculated at the B3LYP/6-31++G(d,p) level of theory energy barrier for hydogen migration is significantly lower when considered inside the oligomer as compared to the monomeric form, which increases the probability of *syn/anti* hydroxyoxime interconversion via tautomerisation mechanisms as compared to the inversion mechanism.

It was shown that even though the magnitude for BSSE correction is lowered significantly when the diffuse functions are added for both hydrogen and heavy atoms, it is highly recommended to include it when studying oligomerisation processes as it effect remains quite significant.

5.4 References

Arjunan V., Mythili C.V., Mageswari K. and Mohan S. (2011) Experimental and theoretical investigation of benzamide oxime. *Spectrochimica Acta Part A: Molecular and Biomolecular Spectroscopy* **79**, 245-253.

Bende A., Vibok A., Halasz G.J. and Suhai S. (2001) BSSE-Free Description of the Formamide Dimers *International Journal of Quantum Chemistry* **84**, 617-622.

Bende A. (2010) Hydrogen bonding in the urea dimers and adeninethymine DNA base pair: anharmonic effects in the intermolecular H-bond and intramolecular H-stretching vibrations. *Theoretical Chemistry Accounts* **125**, 253-268.

Coates J. and Meyers R.A. (2000) Interpretation of infrared spectra, a practical approach. *Encyclopedia of Analytical Chemistry*, 10815-10837.

Frisch M.J., Trucks G.W., Schlegel H.B., Scuseria G.E., Robb M.A., Cheeseman J.R., Scalmani G., Barone V., Mennucci B., Petersson G.A., Nakatsuji H., Caricato M., Li X., Hratchian H.P., Izmaylov A.F., Bloino J., Zheng G., Sonnenberg J.L., Hada M., Ehara M., Toyota K., Fukuda R., Hasegawa J., Ishida M., Nakajima T., Honda Y., Kitao O., Nakai H., Vreven T., Montgomery J.A., Jr., Peralta J.E., Ogliaro F., Bearpark M., Heyd J.J., Brothers E., Kudin K.N., Staroverov V.N., Kobayashi R., Normand J., Raghavachari K., Rendell A., Burant J.C., Iyengar S.S., Tomasi J., Cossi M., Rega N., Millam J.M., Klene M., Knox J.E., Cross J.B., Bakken V., Adamo C., Jaramillo J., Gomperts R., Stratmann R.E., Yazyev O., Austin A.J., Cammi R., Pomelli C., Ochterski J.W., Martin R.L., Morokuma K., Zakrzewski V.G., Voth G.A., Salvador P., Dannenberg J.J., Dapprich S., Daniels A.D., Farkas ., Foresman J.B., Ortiz J.V., Cioslowski J. and Fox D.J. (2009) *Gaussian*, Inc., Wallingford CT.

Georgieva I., Binev D., Trendafilova N. and Bauer G. (2003) DFT study of hydrogen-bonded dimers and tetramer of glyoxilic acid oxime. *Chemical Physics* **286**, 205-217.

Georgieva I., Trendafilova N. and Binev D. (2003) Vibrational properties of glyoxilic acid oxime dimers and tetramer. Ab initio and DFT study. *Vibrational Spectroscopy* **31**, 143-154.

Gorce H. and Bahceli S. (2011) A study on quantum chemical calculations of 3-, 4-nitrobenzaldehyde oximes. *Spectrochimica Acta Part A: Molecular and Biomolecular Spectroscopy* **79**, 1783-1793.

Harris D.J., Roach B.D. and Tasker P.A. (2011) Diffusion-NMR elucidation of modifier-oxime interactions. *19th International Solvent Extraction Conference*, 1-8.

Jeffrey G.A. (1997) *An introduction to hydrogen bonding.* Oxford: University Press.

Joseph W.O. 2000 Thermochemistry in Gaussian. *Gaussian, Inc*, 2-19.

Kendall R.A., Dunning Jr.T.H. and Harrison R.J. (1992) Electron affinities of the first-row atoms revisited. Systematic basis sets and wave functions. *Journal of Chemical Physics* **96**, 6796-806.

Papajak E. and Truhlar D.G. (2010) Efcient Diffuse Basis Sets for Density Functional Theory. *Journal of Chemical Theory and Computation* **6**, 597-601.

Peng C., Ayala P.Y., Schlegel H.B. and Frisch M.J. (1996) Using redundant internal coordinates to optimize equilibrium geometries and transition states. *Journal of Computational Chemistry* **17**, 49-56.

Peters B., Heyden A., Bell A.T. and Chakraborty A. (2004) A growing string method for determining transition states: Comparison to the nudged elastic band and string methods. *Journal of Chemical Physics* **120** (17), 7877-7886.

Rusinska-Roszak D., Lozynski M. and Mack H.G. (1997) Ab initio and PM3 studies of hydrogen bonding of acetoin (E)- and (Z)-oxime dimers. Cooperativity and competition. *Journal of Molecular Structure (Theochem)* **393**, 177-187.

Sahu P.K., Chaudhari A. and Lee S.L. (2004) Theoretical investigation for the hydrogen bond interaction in THFwater complex. *Chemical Physics Letters* **386**, 351-355.

Schmidt M.W., Baldridge K.K., Boatz J.A., Elbert S.T., Gordon M.S., Jensen J.H., Koseki S., Matsunaga N., Nguyen K.A., Su S.J., Windus T.L., Dupuis M., Montgomery J.A. (1993) General atomic and molecular electronic structure system. *Journal of Computational Chemistry* **14**, 1347-1363.

Stewart J.J.P. (1989) Optimization of parameters for semiempirical methods. I. Method. *Journal of Computational Chemistry* **10**, 209-220.

Stewart J.J.P. (2007) Optimization of parameters for semiempirical methods. V. Modification of NDDO approximations and application to 70 elements. *Journal of Molecular Modeling* **13**, 1173-213.

Chapter 6

Modelling Metal Complexation in Solvent Extraction Systems

6.1 Introduction

Solvent extraction (SX) is a hydrometallurgical process used industrially to purify and concentrate metal ions of interest from an aqueous solution. It relies on the mixing and subsequent separation of immiscible organic and aqueous phases. The organic phase is typically kerosene-based, and contains a reagent (extractant) which permits selective extraction via formation of organometallic complexes with the desired metal ions in preference to other metal ions (Rydberg *et al.*, 2004). These ions are removed from the organic phase in a subsequent stripping stage using a different aqueous solution. The organic is continually recycled between the extract and strip stages.

Utilizing a single extractant is often not sufficiently selective and intermediate releach and precipitation steps are required in order to reach the desired selectivity of the process. As was previously discussed in chapter 3, newly proposed synergistic solvent extraction (SSX) system consisting of Versatic10 (a C10 carboxylic acid) and 5,8-diethyl-7-hydroxydodecan-6-oxime (main component of LIX63) metal extractants (Figure 3.1) has the potential to extract Cu, Co, Ni and Zn over Mn, Mg and Ca from nickel laterite leach solutions via direct solvent extraction avoiding intermediate precipitation/releach processes (Cheng and Urbani, 2005ab). It is of interest to interpret the fundamental chemistry of this system in order to better understand how this synergistic system works. Experimental investigation of the coordination chemistry for the different metals is currently being undertaken at CSIRO Minerals (now known as CSIRO Process Science and Engineering). In addition to this, computational modelling is desirable as many different coordination environments are possible in these multiple extractant

systems. Developing and validating a theoretical model of this system using the available laboratory-generated data from CSIRO Minerals, kindly provided by Dr. Barnard, would increase our understanding of this intriguing system. It would also permit the extension into conceptual experiments whereby subtle alterations in extractant (ligand) structure can be undertaken and the theoretically predicted effects of these changes on metal complexation (e.g. metal selectivity, metal binding constants) assessed. If successful, this would open the way for the *ab initio* optimisation of SX systems to enhance selectivity for the removal of specific metal ions and thereby potentially increase yields operational efficiency.

Barnard *et al.* (2010) in their crystallographic study of Ni-α-hydroxyoxime-carboxylic acid synergist complexes have determined the structure of the Ni complex that may form in the synergistic solvent extraction mixture consisting of LIX63 and Versatic10. An equivalent structure has also been crystallographically determined for the cobalt complex (Barnard *et al.*, 2011). According to the X-ray crystal structure of the experimentally determined complex, hydroxyoxime is a synergist and the carboxylic acid plays the role of the extractant (being deprotonated). This contradicts both the proposed structure of the Ni complex and the roles played by the ligands suggested earlier by Castresana *et al.* (1988) who predicted that in SSX of a nickel cation hydroxyoxime molecules are deprotonated and the carboxylic acid plays the role of the synergist.

Recent experimental results (Barnard *et al.*, 2010; Barnard and Turner, 2011) indicate that the formation of tris-oxime metal complexes in solution with a $M(OxH)_3(Ac)_2$ stoichiometry, where two molecules of carboxylic acid (Ac) are deprotonated and three molecules of hydroxyoxime (OxH) stay neutral, is also possible. Indeed, an X-ray crystal structure for nickel tris hydroxyoxime cation counterbalanced by inorganic nitrate salts has also been obtained (Barnard, 2012, personal comment). Modelling metal complexation using Density Functional Theory is known to be a useful tool for studying the stabilities of various geometries of organometallic complexes of different stoichiometries with ligands of a similar nature (Kamilla *et al.*, 2005; Mehdi *et al.*, 2011). Using this technique it should also be possible to see what role the synergist plays in the stability of the complexes formed between molecules of an extractant and each transition metal cation.

6.1.1 Coordination Chemistry of The Transition Metal-Hydroxyoxime-Carboxylic Acid Complexes

The spin multiplicity of metal centres is a very important factor to consider when constructing organometallic complexes. According to ligand field theory (Schläfer and Gliemann, 1969), if the transition metal complex has an octahedral structure, the d-orbitals of the transition element are split as shown in Figure 6.1.

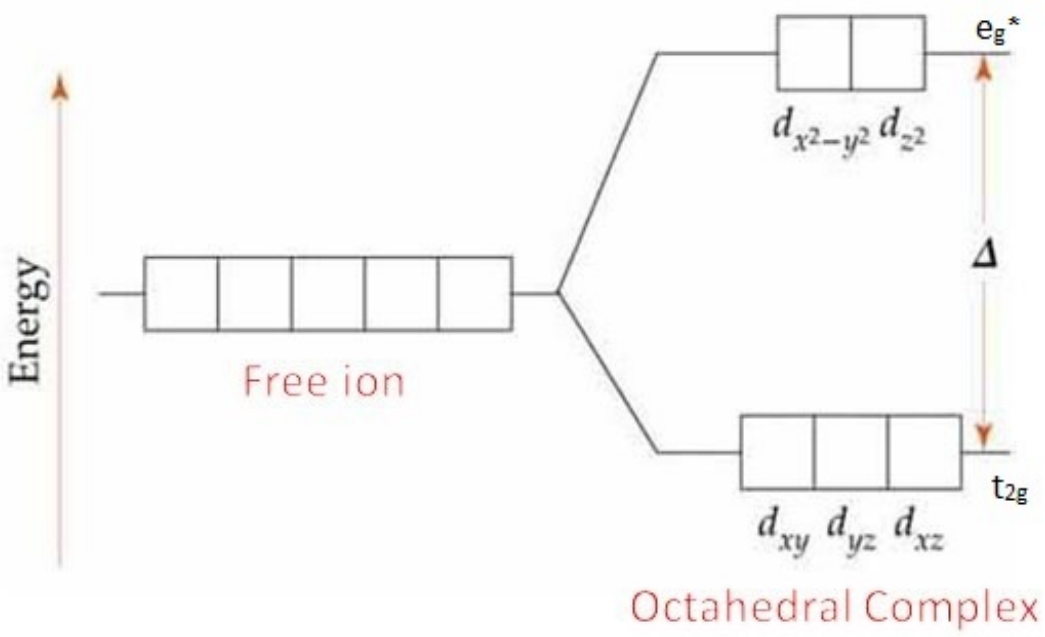

FIGURE 6.1: Splitting of the d-orbitals of a transition metal in an octahedral complex.

This energy difference between d_{xy}, d_{xz}, d_{yz} and d_{z^2}, $d_{x^2-y^2}$ orbitals varies depending on the nature of the ligands forming the octahedral transition metal complex. Low and high spin configurations have different spin multiplicities when the number of electrons in the d-orbitals are greater than or equal to 4 and less than or equal to 7. In Figure 6.2 it is shown how for a specific case of d^4 the strong field ligands (i.e. those that give rise to a large value for Δ) lead to a low spin configuration, while the weak field ligands tend to form high spin metal complexes.

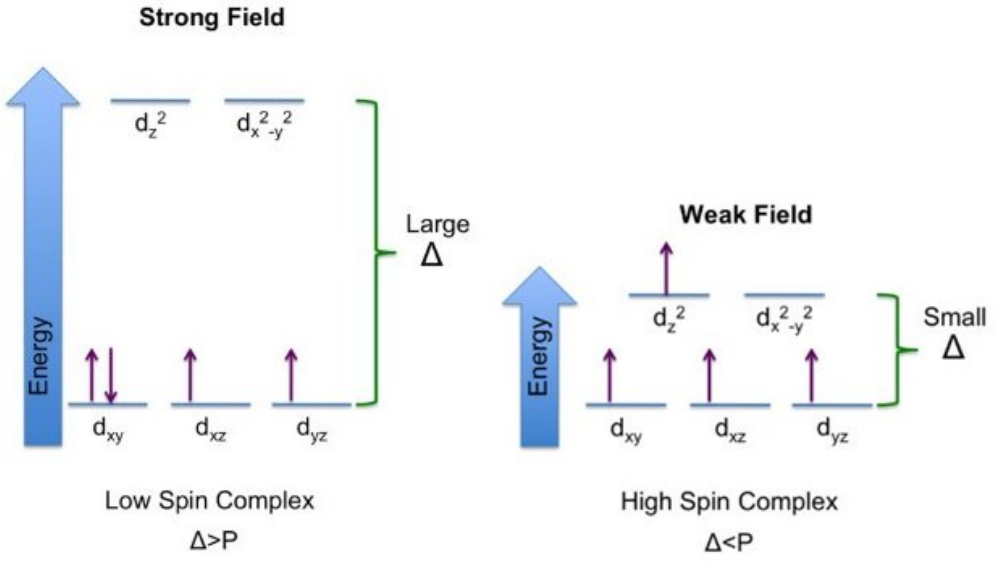

FIGURE 6.2: Splitting of the d-orbitals of a transition metal for a d^4 configuration in an octahedral complex formed with strong (left) or weak (right) field ligands. P - is the pairing energy (i.e. the energy required to add an electron to an orbital already occupied by another electron).

Generally, the magnitude of the d-orbital splitting depends on the binding strength of the ligand (π ligands generally bind stronger than σ ones). Depending on the nature of the ligands, the magnitude of the d-orbital splitting decreases in following order: $CN^- > CO > NO_2^- >$ en $> NH_3 > H_2O > OH^- > F^- > Cl^- > Br^- > I^-$. In some cases the magnitude of the d-orbital splitting is comparable to the pairing energy and therefore both high and low spin configurations are not very different energetically. This leads to co-existence of both spin states for an octahedral metal complex.

In our modelling we will be considering a system of organometallic complexes where the transition element is charged 2+. Before going to the construction of different types of transition metal complexes and studying their potential energy surfaces, let us first determine the multiplicity for each metal centre in its high and low spin configuration. It should be noted that the energetic order of atomic orbitals for a metal cation is different from that in the neutral atom so that the 4s level is higher in energy than the 3d one[1]. This is a very important factor to consider when estimating the multiplicity, because when the transition element is oxidised the first electrons to leave are the ones located in the s-orbital, followed by those in the d-orbital. Electronic configurations for high- and low-spin metal complexes are represented in Figure 6.3. As can be seen, only Co^{2+} and Mn^{2+} of these transition metal cations have the potential to exist as both low- and/or high-spin complexes.

Note that in some cases distortions in octahedral metal complexes (metal-ligand

[1]Note that the copper cation is an exception where the d-orbital is higher in energy then the s one.

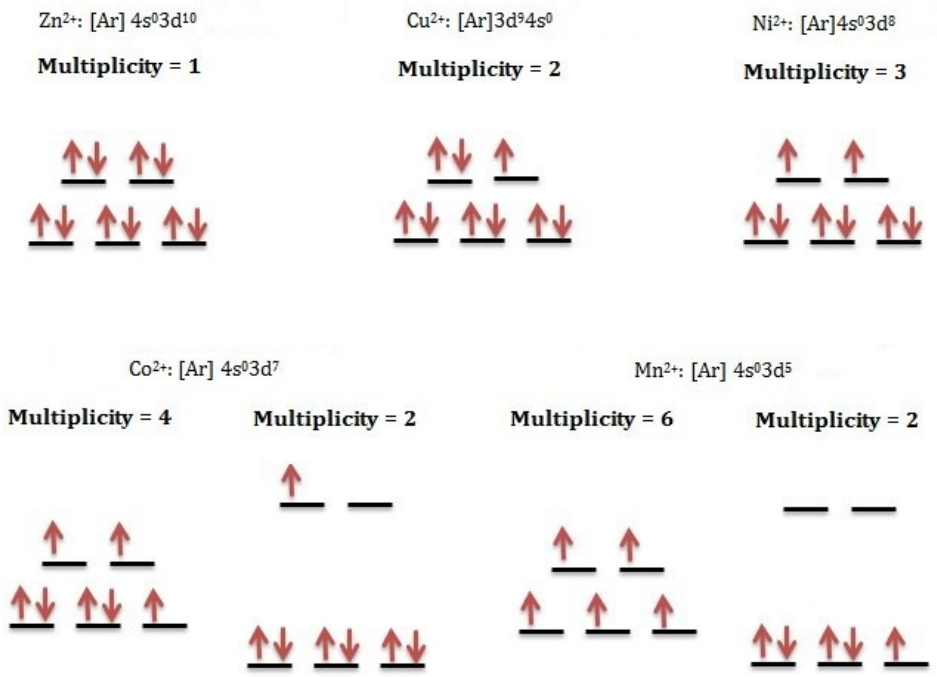

FIGURE 6.3: Valence d electron configurations of Zn^{2+}, Cu^{2+}, Ni^{2+}, Co^{2+} and Mn^{2+} transition metal cations.

bond length) are possible (Jahn and Teller, 1937; Maja *et al.*, 2010; Victor, 2007). This distortion is known as the Jahn-Teller effect. A strong Jahn-Teller effect is expected for complexes with Co^{2+} in its low-spin configuration and with Cu^{2+} according to Jahn and Teller (1937). Conversely a weak Jahn-Teller effect is expected for complexes with Co^{2+} in its high-spin configuration and for Mn^{2+} in its low-spin configuration. The energetics of low- and high-spin Co^{2+} and Mn^{2+} transition metal complexes will be compared during calculations. However, it should be noted that most DFT methods tend to underestimate HOMO-LUMO gaps which leads to a higher spin than expected in some cases (Ojanen and Rantala, 2009; Garcia-Suarez, 2011). Therefore it is recommended for the future work to compare the energetics of low- and high-spin Co^{2+} and Mn^{2+} transition metal complexes calculated using more accurate post-Hartree-Fock methods with well converged basis sets.

6.2 Methodology

According to Zhao and Truhlar (2008) the M06 functional was specifically parameterised for modelling organometallic complexes and therefore was chosen as the main method for the current study. Based on the results of the previous chapters it was decided to use the

6-31G(d,p) basis set to describe the atomic orbitals of the main group elements. In the literature (Yang *et al.*, 2009) it is recommended to use the LanL2DZ pseudo-potential and basis set to describe the atomic orbitals of the transition elements. Therefore it was decided to use the M06 functional with a combination of two basis sets: 6-31G(d,p) - for the main group elements and LanL2DZ - for the first row transition metals.

All possible structures of different types (stoichiometries) of Ni^{2+}, Co^{2+}, Cu^{2+}, $Mn^{2+}$and Zn^{2+} transition metal complexes with aliphatic α-hydroxyoxime and carboxylic acid were constructed using the Avogadro[2] molecular visualisation software and then optimised. Convergence criteria were chosen to be "tight" for geometry optimisation, that is: the maximum and root mean square gradient in Cartesian coordinates are set to 0.00001 a.u. and the maximum and root mean square of the Cartesian step to 0.00005 a.u. For practical reasons, all preliminary calculations of the minima have been performed using the semi-empirical PM6 method (Stewart, 2007) as implemented in the Gamess program (Schmidt *et al.*, 1993) and then the resulting structures were re-optimised at higher levels of theory using the Gaussian09 program (Frisch *et al.*, 2009). The Berny algorithm (which is set by default in Gaussian09) was used in geometry optimisation.

All the experimental studies of the transition metal complexes were undertaken in a non-polar aliphatic solvent. Therefore in order to convert the results derived from the gas-phase calculations to those in a non-polar solvent we had to consider the statistical thermodynamics corrections for the effect of temperature along with the vibrational zero-point energy (ZPE) (Joseph, 2000). Vibrational frequencies were also evaluated in order to determine the nature of each stationary point. Note that the final values of enthalpy and entropy corrections in most quantum chemical software, including Gaussian09, comprise all three components: vibrational, rotational and translational. However, for these calculations we only need the vibrational contribution, as the gas phase rotational and translational contributions are not appropriate to the liquid state.

6.3 Results and Discussion

In order to determine which stoichiometry of each transition metal (TM) complex is the most favourable we need to compare the energetics of the lowest energy conformations between each type of TM complex. To determine the minimum for each stoichiometry of transition metal complex we must scan their potential energy surfaces. The actual target molecules of the LIX63 main component and Versatic10 (Figure 3.1) consist of a

[2]Avogadro: an open-source molecular builder and visualization tool. Version 1.0.3/April 25, 2011 http://avogadro.openmolecules.net/

large number of atoms. Therefore, the scanning of the potential energy surface of different types of TM complexes with these reagents using the M06 method would require an enormous amount of time and computer resource. Even if using ligands with the optimal compromise size of the hydrocarbon side-chains equal to -C_3H_7, as determined previously, this would still be hardly possible. In order to decrease the computational cost of this theoretical investigation we are going to use the LIX63 progenitor - acetoin oxime and acetic acid instead of Versatic10 carboxylic acid. The relevant functional groups of the LIX63 and acetoin oxime molecules are identical (as are the functional groups of Versatic10 and acetic acid), which implies that the simplified molecules should have similar properties to the target molecules with respect to metal complexation. As was discussed earlier, the metal complexes with hydroxyoxime molecules are formed via chelation of the hydroxyoxime functional group with the metal cation. Therefore it would be reasonable to suggest the stabilities of different types of organometallic complexes with hydroxyoxime and a carboxylic acid mostly depend on the way in which the functional groups of the ligands are located around the metal centre. However, it is proposed for future investigations to compute the formation of the lowest energy structures of organometallic complexes with carboxylic acids and hydroxyoximes that are closer in size to the real system.

6.3.1 Thermodynamics of $M(OxH)_2(Ac)_2$ and $M(Ox)_2(AcH)_2$ Transition Metal Complexes with Acetoin Oxime and Acetic Acid for M = Ni^{2+}, Co^{2+}, Cu^{2+}, Mn^{2+} and Zn^{2+}

Two different types of stoichiometry for the transition metal complexes that could possibly be formed in a system of LIX63 and Versatic10 were suggested based on the experimental results derived recently by Barnard and co-workers (Barnard *et al.*, 2010; Barnard and Turner, 2011). These stoichiometries are as follows: $M(OxH)_3(Ac)_2$ and $M(OxH)_2(Ac)_2$, where M - corresponds to a metal cation (2+), OxH - corresponds to a neutral molecule of hydroxyoxime and Ac - stands for an anion of a carboxylic acid. It appears that in both cases the carboxylic acid plays the role of the extractant (i.e. it is deprotonated) while the hydroxyoxime appears to be the synergist and that this does not seem to be pH dependant according to Barnard *et al.*. This observation contradicts the earlier study of Flett *et al.* (1974)[3] and Castresana *et al.* (1988). Therefore, one of the main goals of a current study is to see which hypothesis is valid from a theoretical perspective. To answer this question we need to estimate the relative stabilities

[3]Note that Flett and Titmuss (1969) originally suspected that the carboxylic acid was the anion.

of organometallic complexes of each of the two stoichiometries considering two different scenarios; first where the hydroxyoxime is deprotonated and the carboxylic acid is neutral, and second - vice-versa, where the hydroxyoxime ligands are neutral and the carboxylic acid molecules are deprotonated.

First of all, to be able to compare the binding energies between different types of organometallic complexes and estimate the probability of their co-existence in the liquid phase of a non-polar solvent, we need to locate the global minimum for each type of transition metal complex. In order to do this we need to perform a potential energy scan for each case. It is hard to visualise the structures of transition metal complexes by looking at the name constructed using the traditional way of labelling organometallic compounds. Therefore for better understanding we have decided to label the 3D structures for each stoichiometry of metal complexes formed in SSX mixture of hydroxyoxime and carboxylic acid using the sequential numbering of the displayed structures first and then also label each structure using standard nomenclature.

It should be noted that acetoin oxime has one chiral centre, so that each S-type conformer has its mirror image R-conformer. When we calculate the energy of each S and R monomer of acetoin oxime separately their energetics will be identical. However, when both S and R conformers are present in the same system the energetics of such a system will be different for the system containing the same stereo-isomers (RR or SS) and the system containing two different stereo-isomers of acetoin oxime (R and S). Therefore when studying the potential energy surfaces of transition metal complexes it is important to take into account both scenarios. All possible geometries of M-α-hydroxyoxime-carboxylic acid complexes of $M(Ox)_2(AcH)_2$ stoichiometry where two acetoin oxime molecules correspond to S and R stereoisomers are depicted in Figure 6.4. All possible geometries of M(II)-α-hydroxyoxime-carboxylic acid complexes of $M(Ox)_2$ AcH_2 stoichiometry where two acetoin oxime molecules are of the same stereochemistry (S) are depicted in Figure 6.5. Note that it is possible to construct other geometries by rotating the carboxylic acid ligand around the O-M bond; however, due to the limited time it was decided to optimise only those geometries that have a higher number of intra-molecular hydrogen bonds, assuming they would have lower energies. Moreover, using preliminary calculations with the PM6 semi-empirical method it was also determined that the metal complexes are more stable when the ends of carboxyl groups (which are intra-molecularly bonded to the oxime/hydroxyl groups via hydrogen bonding) are pointing towards opposite directions. Now that we have 3D structures of our complexes displayed it is easier to write traditional labels for each structure shown in Figures 6.4 and 6.5, as given in Table 6.1:

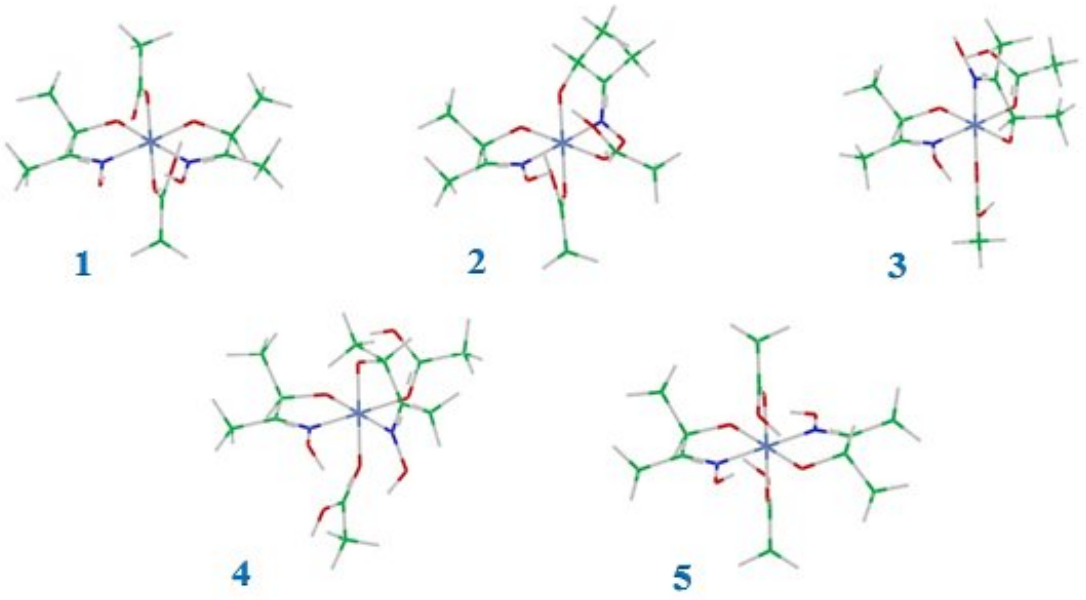

FIGURE 6.4: Initial structures for studying the potential energy surface of M(II)-α-hydroxyoxime-carboxylic acid complexes of $M(Ox)_2(AcH)_2$ stoichiometry where the two hydroxyoxime molecules correspond to different stereo-isomers. Green coloured atoms represent carbon, red - oxygen, dark blue - nitrogen, purple - metal centre (M) and white - hydrogen atoms and bonding.

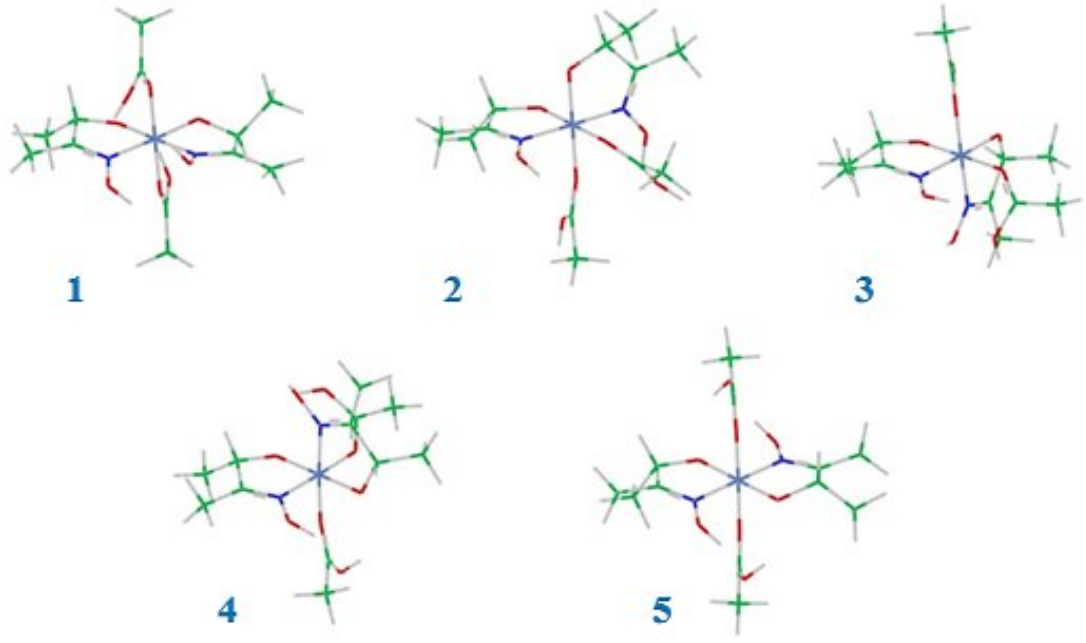

FIGURE 6.5: Initial structures for studying the potential energy surface of M(II)-α-hydroxyoxime-carboxylic acid complexes of $M(Ox)_2(AcH)_2$ stoichiometry where the two hydroxyoxime molecules correspond to the same S-stereo-isomers. Green coloured atoms represent carbon, red - oxygen, dark blue - nitrogen, purple - metal centre (M) and white - hydrogen atoms and bonding.

TABLE 6.1: Traditional labelling of metal complexes from Figures 6.4 and 6.5.

RS Metal Complexes		SS Metal Complexes	
Fig. 6.4	Traditional Labels	Fig. 6.5	Traditional Labels
1	Trans-Ox(NN-90^o,OO-90^o)	1	Trans-Ox(NN-90^o,OO-90^o)
2	Cis-Ox(NN-180^o,OO-90^o)	2	Cis-Ox(NN-180^o,OO-90^o)
3	Cis-Ox(NN-90^o,OO-180^o)	3	Cis-Ox(NN-90^o,OO-90^o)
4	Cis-Ox(NN-90^o,OO-90^o)	4	Cis-Ox(NN-90^o,OO-180^o)
5	Trans-Ox(NN-180^o,OO-180^o)	5	Trans-Ox(NN-180^o,OO-180^o)

It is interesting to note that in all structures, except complex number 4 (RS-Cis-Ox(NN-90^o,OO-90^o)) in Figure 6.4, changing the chirality of the ligands (R to S and S to R) will lead to the mirror images of the initial structure, as each hydroxyoxime ligand is bonded to a different carboxylic acid within the complex. However, in RS-Cis-Ox(NN-90^o,OO-90^o) both acetoin oximes are hydrogen bonded to the same acetic acid, which means that if we freeze the structure of the complex and change the chirality of an R-acetoin oxime to S and S-oxime to R we will get a different complex. Therefore we have calculated the energetics of a total of six complexes of $M(Ox)_2(AcH)_2$ stoichiometry, including the RS-Cis-Ox(NN-90^o,OO-90^o) and SR-Cis-Ox(NN-90^o,OO-90^o) structures.

Gibbs free energy differences and enthalpy changes between each complex and the lowest energy structure of $M(Ox)_2(AcH)_2$ for Ni^{2+}, Co^{2+} (doublet), Co^{2+} (quartet), Cu^{2+} (doublet), Mn^{2+} (doublet), Mn^{2+} (sextet) and Zn^{2+} transition metal cations (with multiplicity in parenthesis) are given in Tables 6.2, 6.3, 6.4, 6.5, 6.6, 6.7 and 6.8, respectively. All energetics are from gas phase calculations at the M06/6-31G(d,p)/LanL2DZ level of theory including only vibrational parts of the enthalpy and entropy (so that the energetics would correspond to those in a non-polar solvent) at 298.15 K.

TABLE 6.2: Gibbs free energy ($\Delta G^o_{298.15}$, kJ/mol) and enthalpy ($\Delta H^o_{298.15}$, kJ/mol) differences relative to the most stable structure of $Ni(Ox)_2(AcH)_2$ complex at the M06/6-31G(d,p)/LanL2DZ level of theory. Note that "S" stands for spin multiplicity.

$Ni(Ox)_2(AcH)_2$ ($Ni^{2+}S = 3$)	M06/6-31G(d,p)/LanL2DZ	
	ΔG, $\frac{kJ}{mol}$	ΔH, $\frac{kJ}{mol}$
RS-Trans-Ox(NN-90^o,OO-90^o)	162.5	175.3
RS-Cis-Ox(NN-180^o,OO-90^o)	10.7	13.5
RS-Cis-Ox(NN-90^o,OO-180^o)	13.8	14.9
RS-Cis-Ox(NN-90^o,OO-90^o)	108.1	115.6
SR-Cis-Ox(NN-90^o,OO-90^o)	135.2	143.4
RS-Trans-Ox(NN-180^o,OO-180^o)	13.2	19.6
SS-Trans-Ox(NN-90^o,OO-90^o)	130.9	136.1
SS-Cis-Ox(NN-180^o,OO-90^o)	11.7	15.0
SS-Cis-Ox(NN-90^o,OO-90^o)	135.5	137.9
SS-Cis-Ox(NN-90^o,OO-180^o)	0.0	0.0
SS-Trans-Ox(NN-180^o,OO-180^o)	17.8	28.5

TABLE 6.3: Gibbs free energy ($\Delta G^o_{298.15}$, kJ/mol) and enthalpy ($\Delta H^o_{298.15}$, kJ/mol) differences relative to the most stable structure of $Co(Ox)_2(AcH)_2$ (with spin multiplicity equal to 2 for Co^{2+}) complex at the M06/6-31G(d,p)/LanL2DZ level of theory. Note that "S" stands for spin multiplicity.

$Co(Ox)_2(AcH)_2$ ($Co^{2+}S = 2$)	M06/6-31G(d,p)/LanL2DZ	
	ΔG, $\frac{kJ}{mol}$	ΔH, $\frac{kJ}{mol}$
RS-Trans-Ox(NN-90^o,OO-90^o)	156.6	125.9
RS-Cis-Ox(NN-180^o,OO-90^o)	43.3	13.7
RS-Cis-Ox(NN-90^o,OO-180^o)	28.0	-0.6
RS-Cis-Ox(NN-90^o,OO-90^o)	106.8	77.7
SR-Cis-Ox(NN-90^o,OO-90^o)	84.8	60.8
RS-Trans-Ox(NN-180^o,OO-180^o)	0.0	0.0
SS-Trans-Ox(NN-90^o,OO-90^o)	120.5	96.8
SS-Cis-Ox(NN-180^o,OO-90^o)	22.2	-2.8
SS-Cis-Ox(NN-90^o,OO-90^o)	69.4	52.0
SS-Cis-Ox(NN-90^o,OO-180^o)	53.9	29.6
SS-Trans-Ox(NN-180^o,OO-180^o)	14.5	6.0

TABLE 6.4: Gibbs free energy ($\Delta G^{o}_{298.15}$, kJ/mol) and enthalpy ($\Delta H^{o}_{298.15}$, kJ/mol) differences relative to the most stable structure of $Co(Ox)_2(AcH)_2$ (with spin multiplicity equal to 4 for Co^{2+}) complex at the M06/6-31G(d,p)/LanL2DZ level of theory. Note that "S" stands for spin multiplicity.

$Co(Ox)_2(AcH)_2$ ($Co^{2+}S = 4$)	M06/6-31G(d,p)/LanL2DZ	
	ΔG, $\frac{kJ}{mol}$	ΔH, $\frac{kJ}{mol}$
RS-Trans-Ox(NN-90^o,OO-90^o)	142.1	155.8
RS-Cis-Ox(NN-180^o,OO-90^o)	14.0	13.8
RS-Cis-Ox(NN-90^o,OO-180^o)	12.0	20.7
RS-Cis-Ox(NN-90^o,OO-90^o)	103.1	110.2
SR-Cis-Ox(NN-90^o,OO-90^o)	102.3	112.0
RS-Trans-Ox(NN-180^o,OO-180^o)	18.3	25.3
SS-Trans-Ox(NN-90^o,OO-90^o)	118.5	121.8
SS-Cis-Ox(NN-180^o,OO-90^o)	12.3	14.4
SS-Cis-Ox(NN-90^o,OO-90^o)	82.4	80.6
SS-Cis-Ox(NN-90^o,OO-180^o)	0.0	0.0
SS-Trans-Ox(NN-180^o,OO-180^o)	5.7	9.6

TABLE 6.5: Gibbs free energy ($\Delta G^{o}_{298.15}$, kJ/mol) and enthalpy ($\Delta H^{o}_{298.15}$, kJ/mol) differences relative to the most stable structure of $Cu(Ox)_2(AcH)_2$ complex at the M06/6-31G(d,p)/LanL2DZ level of theory. Note that "S" stands for spin multiplicity.

$Cu(Ox)_2(AcH)_2$ ($Cu^{2+}S = 2$)	M06/6-31G(d,p)/LanL2DZ	
	ΔG, $\frac{kJ}{mol}$	ΔH, $\frac{kJ}{mol}$
RS-Trans-Ox(NN-90^o,OO-90^o)	127.6	130.0
RS-Cis-Ox(NN-180^o,OO-90^o)	12.4	18.8
RS-Cis-Ox(NN-90^o,OO-180^o)	3.9	6.7
RS-Cis-Ox(NN-90^o,OO-90^o)	58.8	54.2
SR-Cis-Ox(NN-90^o,OO-90^o)	86.1	85.7
RS-Trans-Ox(NN-180^o,OO-180^o)	8.1	26.3
SS-Trans-Ox(NN-90^o,OO-90^o)	104.2	104.8
SS-Cis-Ox(NN-180^o,OO-90^o)	28.3	20.5
SS-Cis-Ox(NN-90^o,OO-90^o)	54.8	56.8
SS-Cis-Ox(NN-90^o,OO-180^o)	0.0	0.0
SS-Trans-Ox(NN-180^o,OO-180^o)	20.0	32.0

TABLE 6.6: Gibbs free energy ($\Delta G^{o}_{298.15}$, kJ/mol) and enthalpy ($\Delta H^{o}_{298.15}$, kJ/mol) differences relative to the most stable structure of $Mn(Ox)_2(AcH)_2$ (with spin multiplicity equal to 2 for Mn^{2+}) complex at the M06/6-31G(d,p)/LanL2DZ level of theory. Note that "S" stands for spin multiplicity.

$Mn(Ox)_2(AcH)_2$ ($Mn^{2+}S = 2$)	M06/6-31G(d,p)/LanL2DZ	
	ΔG, $\frac{kJ}{mol}$	ΔH, $\frac{kJ}{mol}$
RS-Trans-Ox(NN-90^o,OO-90^o)	134.2	146.2
RS-Cis-Ox(NN-180^o,OO-90^o)	36.4	47.3
RS-Cis-Ox(NN-90^o,OO-180^o)	21.3	25.8
RS-Cis-Ox(NN-90^o,OO-90^o)	105.8	117.7
SR-Cis-Ox(NN-90^o,OO-90^o)	78.9	88.0
RS-Trans-Ox(NN-180^o,OO-180^o)	0.0	0.0
SS-Trans-Ox(NN-90^o,OO-90^o)	114.6	126.0
SS-Cis-Ox(NN-180^o,OO-90^o)	21.5	29.5
SS-Cis-Ox(NN-90^o,OO-90^o)	54.6	66.6
SS-Cis-Ox(NN-90^o,OO-180^o)	8.5	16.9
SS-Trans-Ox(NN-180^o,OO-180^o)	10.5	21.6

TABLE 6.7: Gibbs free energy ($\Delta G^{o}_{298.15}$, kJ/mol) and enthalpy ($\Delta H^{o}_{298.15}$, kJ/mol) differences relative to the most stable structure of $Mn(Ox)_2(AcH)_2$ (with spin multiplicity equal to 6 for Mn^{2+}) complex at the M06/6-31G(d,p)/LanL2DZ level of theory. Note that "S" stands for spin multiplicity.

$Mn(Ox)_2(AcH)_2$ ($Mn^{2+}S = 6$)	M06/6-31G(d,p)/LanL2DZ	
	ΔG, $\frac{kJ}{mol}$	ΔH, $\frac{kJ}{mol}$
RS-Trans-Ox(NN-90^o,OO-90^o)	156.7	155.2
RS-Cis-Ox(NN-180^o,OO-90^o)	9.3	-0.1
RS-Cis-Ox(NN-90^o,OO-180^o)	9.7	8.8
RS-Cis-Ox(NN-90^o,OO-90^o)	122.0	112.7
SR-Cis-Ox(NN-90^o,OO-90^o)	122.3	122.5
RS-Trans-Ox(NN-180^o,OO-180^o)	15.8	10.3
SS-Trans-Ox(NN-90^o,OO-90^o)	125.0	120.1
SS-Cis-Ox(NN-180^o,OO-90^o)	0.0	0.0
SS-Cis-Ox(NN-90^o,OO-90^o)	114.5	113.9
SS-Cis-Ox(NN-90^o,OO-180^o)	9.1	4.7
SS-Trans-Ox(NN-180^o,OO-180^o)	8.6	3.7

TABLE 6.8: Gibbs free energy ($\Delta G^o_{298.15}$, kJ/mol) and enthalpy ($\Delta H^o_{298.15}$, kJ/mol) differences relative to the most stable structure of $Zn(Ox)_2(AcH)_2$ complex at the M06/6-31G(d,p)/LanL2DZ level of theory. Note that "S" stands for spin multiplicity.

$Zn(Ox)_2(AcH)_2$ ($Zn^{2+}S = 1$)	M06/6-31G(d,p)/LanL2DZ	
	ΔG, $\frac{kJ}{mol}$	ΔH, $\frac{kJ}{mol}$
RS-Trans-Ox(NN-90^o,OO-90^o)	160.2	164.9
RS-Cis-Ox(NN-180^o,OO-90^o)	5.4	5.4
RS-Cis-Ox(NN-90^o,OO-180^o)	4.0	-0.1
RS-Cis-Ox(NN-90^o,OO-90^o)	114.7	113.3
SR-Cis-Ox(NN-90^o,OO-90^o)	129.4	134.7
RS-Trans-Ox(NN-180^o,OO-180^o)	16.5	17.6
SS-Trans-Ox(NN-90^o,OO-90^o)	131.1	129.6
SS-Cis-Ox(NN-180^o,OO-90^o)	3.8	7.1
SS-Cis-Ox(NN-90^o,OO-90^o)	136.5	137.8
SS-Cis-Ox(NN-90^o,OO-180^o)	0.0	0.0
SS-Trans-Ox(NN-180^o,OO-180^o)	32.3	35.1

As previously described, the spin multiplicity of Co^{2+} and Mn^{2+} can be different depending on the nature of the ligands. If we calculate the Gibbs free energy difference between the low and high spin complexes of Co and Mn we get a positive average value of approximately 50 kJ/mol in case of Co complexes and nearly 300 kJ/mol for Mn complexes of $M(Ox)_2(AcH)_2$ stoichiometry. According to Zhao and Truhlar, the M06 functional should be expected to give fairly good thermodynamics of transition metal complexes. Therefore, in this instance the results are expected to be reliable. The fact that the high spin complexes of Co and Mn cations are significantly more stable than the low ones leads us to the conclusion that hydroxyoxime and carboxylic acid are weak field ligands at least for the specific molecules considered here. This agrees well with the conclusion made by Vostrikova (2008) in her studies of high-spin metal complexes.

As can be seen from Tables 6.2, 6.4, 6.5, 6.7 and 6.8, SS-Cis-Ox(NN-90^o,OO-180^o) corresponds to the lowest energy structure of Ni, Co, Cu and Zn metal complexes, while for Mn the SS-Cis-Ox(NN-180^o,OO-90^o) complex is estimated to be the most stable at the M06/6-31G(d,p)/LanL2DZ level of theory[4]. The lowest energy structures of $M(Ox)_2(AcH)_2$ complexes are depicted in Figure 6.6 for Ni, Co, Cu, Mn and Zn.

[4]As can be noted from Tables 6.2 - 6.8 some structures of the $M(Ox)_2(AcH)_2$ metal complexes have significantly higher Gibbs Free energies than corresponding lowest energy ones. To ensure that all these structures correspond to stationary points, the frequency analysis has been performed which showed that neither of represented structures has imaginary frequencies. Therefore it could only mean that all of these structures are just significantly less stable than corresponding lowest energy complexes.

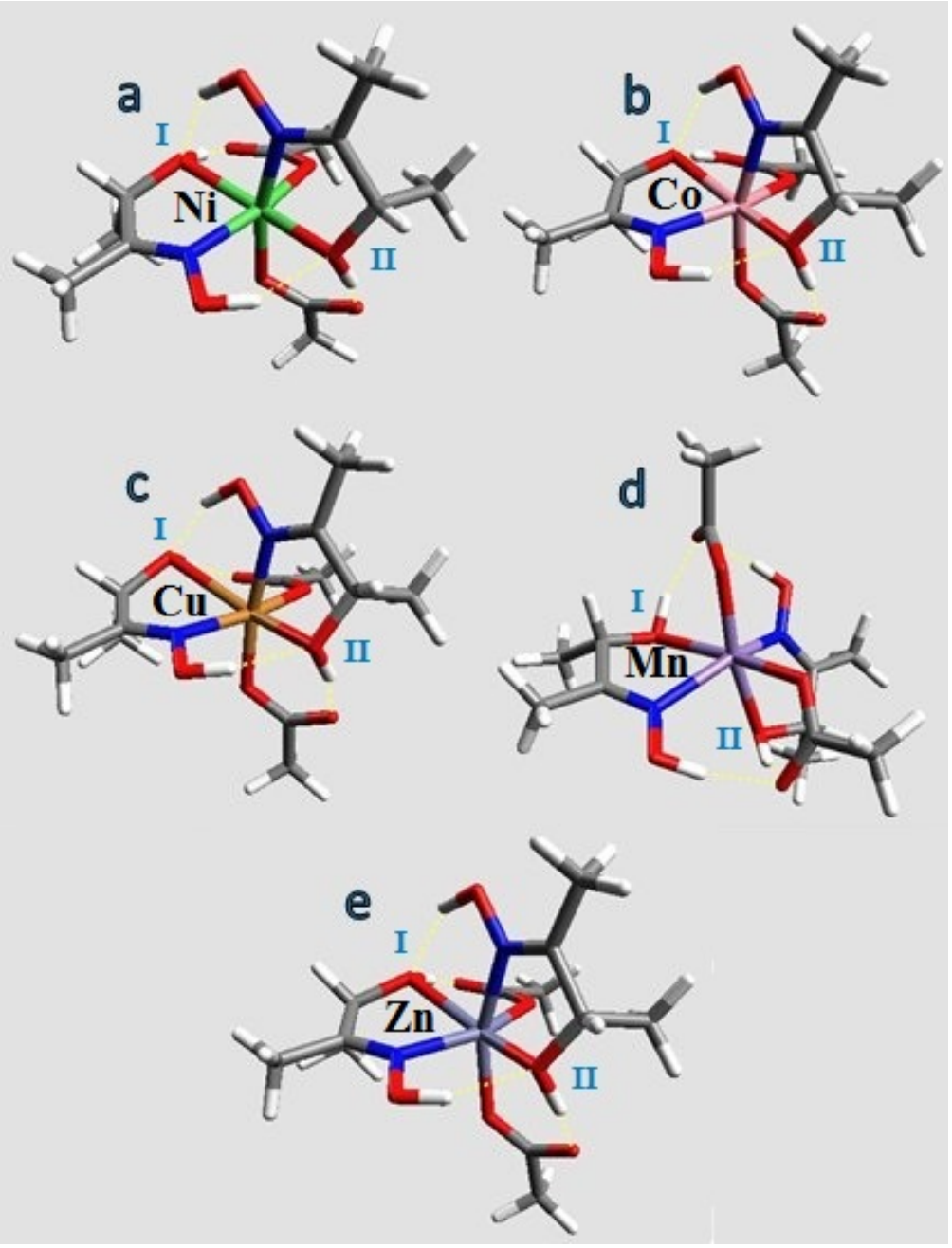

FIGURE 6.6: Schematic representations of the lowest energy structures of Ni, Co, Cu, Mn and Zn transition metal complexes with acetoin oxime and acetic acid optimized for the $M(Ox)_2(AcH)_2$ stoichiometry: a) SS-Cis-Ox(NN-90^o,OO-180^o) structure of Ni^{2+} complex; b) SS-Cis-Ox(NN-90^o,OO-180^o) structure of Co^{2+} complex; c) SS-Cis-Ox(NN-90^o,OO-180^o) structure of Cu^{2+} complex; d) SS-Cis-Ox(NN-90^o,OO-180^o) structure of Mn^{2+} complex and e) SS-Cis-Ox(NN-90^o,OO-180^o) structure of Zn^{2+} complex. Grey coloured atoms represent carbon, red - oxygen, dark blue - nitrogen, white - hydrogen, green - nickel, pink - cobalt, orange - copper, purple - manganese and dark purple - zinc.

If we compare the initial structures of the metal complexes shown in Figure 6.4 with the optimised lowest energy structures for the corresponding metal species shown in Figure

6.6, we will see that the initial structures have a $M(Ox)_2(AcH)_2$ stoichiometry with protonated acid ligands and deprotonated oxime ligands; however, during the optimisation the stoichiometry of some metal complexes has changed to either MOx(OxH)Ac(AcH) or $M(OxH)_2(Ac)_2$. For instance, the most stable structures for Ni^{2+}, Zn^{2+}, Cu^{2+} and Mn^{2+} complexes have the $M(OxH)_2(Ac)_2$ stoichiometry while in the lowest energy structure of the Co^{2+} complex only one molecule of acetic acid is deprotonated[5]. It should be noted that the full optimisation of the structures shown in Figures 6.4 and 6.6 was performed. However, in order to check the energetics of $M(Ox)_2(AcH)_2$ structures and see if they may be minima that were missed during optimisation routine, we constrained the stoichiometry to $M(Ox)_2(AcH)_2$ by fixing the O-H bond lengths in the acetic acid ligand. The optimisation was converged slowly using the Berny algorithm and the resulting structures were significantly less stable (higher in energy). This could be an indication of a synergistic effect of hydroxyoxime in synergistic solvent extraction of Ni^{2+}, Zn^{2+}, Cu^{2+} and Mn^{2+} cations, while in case of Co^{2+} complexation, hydroxyoxime may play the role of an extractant. In order to see this more clearly let us compare the O-H bond distances in COH groups and also the lengths of OH$\cdots$O hydrogen bonds (Table 6.9).

TABLE 6.9: The O-H (in COH group) and OH$\cdots$O hydrogen bond distances in the lowest energy Ni^{2+}, Co^{2+}, Zn^{2+}, Cu^{2+} and Mn^{2+} complexes calculated at the M06/6-31G(d,p)/LanL2DZ level of theory.

Labels of Metal Complexes	Ligand I (Fig. 6.6)		Ligand II (Fig. 6.6)	
	O-H, Å	OH$\cdots$O, Å	O-H, Å	OH$\cdots$O, Å
Ni^{2+} SS-Cis-Ox(NN-90^o,OO-180^o)	1.185	1.214	1.184	1.215
Co^{2+} SS-Cis-Ox(NN-90^o,OO-180^o)	1.195	1.206	1.192	1.209
Zn^{2+} SS-Cis-Ox(NN-90^o,OO-180^o)	1.134	1.275	1.135	1.274
Cu^{2+} SS-Cis-Ox(NN-90^o,OO-180^o)	1.006	1.607	1.006	1.607
Mn^{2+} SS-Cis-Ox(NN-180^o,OO-90^o)	0.992	1.710	0.992	1.710

It should be noted that the frequency analysis at the M06/6-31G(d,p)/LanL2DZ level of theory has shown that all structures listed in Table 6.9 correspond to minima on the potential energy surface and not saddle points (i.e. they do not have any imaginary frequencies). The equilibrium value of the CO-H bond distance in the *anti*-acetoin oxime monomer calculated at the M06/6-31G(d,p) level of theory is equal to 0.969 Å, and to 0.990 Å in the (Ac)OH$\cdots$OC(Ox) acetic acid - acetoin oxime dimer. As can

[5]Note that the graphical representation of the Zn^{2+} lowest energy complex is identical to the Ni^{2+} one

be seen from Table 6.9, the CO-H bonds in Ni^{2+}, Co^{2+} and Zn^{2+} complexes are longer by approximately 0.2 Å than its equilibrium length in the (Ac)OH$\cdots$OC(Ox) dimer, while in Mn^{2+} complexes the length of CO-H bond is nearly identical with the one in (Ac)OH$\cdots$OC(Ox) dimer. This could be an indication of a balanced situation between $M(Ox)_2(AcH)_2$ and $M(OxH)_2(Ac)_2$ stoichiometries for the Ni^{2+}, Co^{2+} and Zn^{2+} complexes, which means that both acetic acid and aliphatic α-hydroxyoxime can play the role of an extractant in the synergistic solvent extraction of these transition metal cations. However, before making any final conclusions we need to make sure that the optimisation of Ni^{2+}, Co^{2+}, Zn^{2+}, Cu^{2+} and Mn^{2+} metal complexes of $M(OxH)_2(Ac)_2$ stoichiometry leads to the same structures as optimisation of complexes of $M(Ox)_2(AcH)_2$ stoichiometry.

Initial structures for studying the potential energy surface of the $M(OxH)_2(Ac)_2$ metal complexes are identical to the $M(Ox)_2(AcH)_2$ ones, with the only difference being that the hydroxyoxime ligands are deprotonated instead of the carboxylic acid ones. Gibbs free energy differences and enthalpy changes between each complex and the lowest energy structure of $M(OxH)_2(Ac)_2$ for Ni^{2+} (triplet), Co^{2+} (quartet), Cu^{2+} (doublet), Mn^{2+} (sextet) and Zn^{2+} (singlet) transition metal cations are given in Tables 6.10, 6.11, 6.12, 6.13 and 6.14 respectively. All energetics are from gas phase calculations at the M06/6-31G(d,p)/LanL2DZ level of theory including only vibrational contributions to the enthalpy and entropy at 298.15 K.

TABLE 6.10: Gibbs free energy ($\Delta G^o_{298.15}$, kJ/mol) and enthalpy ($\Delta H^o_{298.15}$, kJ/mol) differences relative to the most stable structure of $Ni(OxH)_2(Ac)_2$ complex at the M06/6-31G(d,p)/LanL2DZ level of theory.

$Ni(OxH)_2(Ac)_2$ ($Ni^{2+}S = 3$)	M06/6-31G(d,p)/LanL2DZ	
	ΔG, $\frac{kJ}{mol}$	ΔH, $\frac{kJ}{mol}$
RS-Trans-Ox(NN-90^o,OO-90^o)	24.9	20.7
RS-Cis-Ox(NN-180^o,OO-90^o)	0.0	0.0
RS-Cis-Ox(NN-90^o,OO-180^o)	9.4	6.9
RS-Cis-Ox(NN-90^o,OO-90^o)	6.9	5.2
SR-Cis-Ox(NN-90^o,OO-90^o)	8.8	6.9
RS-Trans-Ox(NN-180^o,OO-180^o)	19.4	17.8
SS-Trans-Ox(NN-90^o,OO-90^o)	18.9	17.5
SS-Cis-Ox(NN-180^o,OO-90^o)	0.9	1.5
SS-Cis-Ox(NN-90^o,OO-90^o)	2.2	0.3
SS-Cis-Ox(NN-90^o,OO-180^o)	6.5	3.8
SS-Trans-Ox(NN-180^o,OO-180^o)	25.7	28.6

TABLE 6.11: Gibbs free energy ($\Delta G^o_{298.15}$, kJ/mol) and enthalpy ($\Delta H^o_{298.15}$, kJ/mol) differences relative to the most stable structure of $Co(Ox)_2(AcH)_2$ (with multiplicity equal to 4 for Co^{2+}) complex at the M06/6-31G(d,p)/LanL2DZ level of theory.

$Co(Ox)_2(AcH)_2$ ($Co^{2+}S = 4$)	M06/6-31G(d,p)/LanL2DZ	
	ΔG, $\frac{kJ}{mol}$	ΔH, $\frac{kJ}{mol}$
RS-Trans-Ox(NN-90^o,OO-90^o)	27.8	29.3
RS-Cis-Ox(NN-180^o,OO-90^o)	9.6	7.1
RS-Cis-Ox(NN-90^o,OO-180^o)	22.1	20.6
RS-Cis-Ox(NN-90^o,OO-90^o)	3.5	1.6
SR-Cis-Ox(NN-90^o,OO-90^o)	3.3	5.3
RS-Trans-Ox(NN-180^o,OO-180^o)	19.3	20.2
SS-Trans-Ox(NN-90^o,OO-90^o)	24.8	23.1
SS-Cis-Ox(NN-180^o,OO-90^o)	11.3	1.9
SS-Cis-Ox(NN-90^o,OO-90^o)	14.2	11.1
SS-Cis-Ox(NN-90^o,OO-180^o)	0.0	0.0
SS-Trans-Ox(NN-180^o,OO-180^o)	15.5	13.9

TABLE 6.12: Gibbs free energy ($\Delta G^{o}_{298.15}$, kJ/mol) and enthalpy ($\Delta H^{o}_{298.15}$, kJ/mol) differences relative to the most stable structure of $Cu(Ox)_2(AcH)_2$ complex at the M06/6-31G(d,p)/LanL2DZ level of theory.

$Cu(Ox)_2(AcH)_2$ ($Cu^{2+}S = 2$)	M06/6-31G(d,p)/LanL2DZ	
	ΔG, $\frac{kJ}{mol}$	ΔH, $\frac{kJ}{mol}$
RS-Trans-Ox(NN-90^o,OO-90^o)	5.2	11.7
RS-Cis-Ox(NN-180^o,OO-90^o)	4.8	8.4
RS-Cis-Ox(NN-90^o,OO-180^o)	0.0	0.0
RS-Cis-Ox(NN-90^o,OO-90^o)	4.7	5.5
SR-Cis-Ox(NN-90^o,OO-90^o)	6.4	3.5
RS-Trans-Ox(NN-180^o,OO-180^o)	10.1	9.2
SS-Trans-Ox(NN-90^o,OO-90^o)	33.8	34.6
SS-Cis-Ox(NN-180^o,OO-90^o)	16.7	17.6
SS-Cis-Ox(NN-90^o,OO-90^o)	2.9	1.1
SS-Cis-Ox(NN-90^o,OO-180^o)	9.1	-1.0
SS-Trans-Ox(NN-180^o,OO-180^o)	7.2	3.8

TABLE 6.13: Gibbs free energy ($\Delta G^{o}_{298.15}$, kJ/mol) and enthalpy ($\Delta H^{o}_{298.15}$, kJ/mol) differences relative to the most stable structure of $Mn(Ox)_2(AcH)_2$ (with multiplicity equal to 6 for Mn^{2+}) complex at the M06/6-31G(d,p)/LanL2DZ level of theory.

$Mn(Ox)_2(AcH)_2$ ($Mn^{2+}S = 6$)	M06/6-31G(d,p)/LanL2DZ	
	ΔG, $\frac{kJ}{mol}$	ΔH, $\frac{kJ}{mol}$
RS-Trans-Ox(NN-90^o,OO-90^o)	16.7	20.9
RS-Cis-Ox(NN-180^o,OO-90^o)	10.0	6.1
RS-Cis-Ox(NN-90^o,OO-180^o)	0.0	0.0
RS-Cis-Ox(NN-90^o,OO-90^o)	3.3	5.8
SR-Cis-Ox(NN-90^o,OO-90^o)	8.9	6.0
RS-Trans-Ox(NN-180^o,OO-180^o)	42.8	40.3
SS-Trans-Ox(NN-90^o,OO-90^o)	44.6	42.0
SS-Cis-Ox(NN-180^o,OO-90^o)	0.7	6.2
SS-Cis-Ox(NN-90^o,OO-90^o)	7.6	10.9
SS-Cis-Ox(NN-90^o,OO-180^o)	0.1	-5.1
SS-Trans-Ox(NN-180^o,OO-180^o)	10.7	9.7

TABLE 6.14: Gibbs free energy ($\Delta G^o_{298.15}$, kJ/mol) and enthalpy ($\Delta H^o_{298.15}$, kJ/-mol) differences relative to the most stable structure of $Zn(Ox)_2(AcH)_2$ complex at the M06/6-31G(d,p)/LanL2DZ level of theory.

$Zn(Ox)_2(AcH)_2$ ($Zn^{2+}S = 1$)	M06/6-31G(d,p)/LanL2DZ	
	ΔG, $\frac{kJ}{mol}$	ΔH, $\frac{kJ}{mol}$
RS-Trans-Ox(NN-90^o,OO-90^o)	25.0	32.0
RS-Cis-Ox(NN-180^o,OO-90^o)	10.7	9.7
RS-Cis-Ox(NN-90^o,OO-180^o)	8.9	7.7
RS-Cis-Ox(NN-90^o,OO-90^o)	7.1	10.6
SR-Cis-Ox(NN-90^o,OO-90^o)	10.5	6.9
RS-Trans-Ox(NN-180^o,OO-180^o)	46.3	45.0
SS-Trans-Ox(NN-90^o,OO-90^o)	41.4	43.2
SS-Cis-Ox(NN-180^o,OO-90^o)	6.2	11.0
SS-Cis-Ox(NN-90^o,OO-90^o)	8.3	14.0
SS-Cis-Ox(NN-90^o,OO-180^o)	0.0	0.0
SS-Trans-Ox(NN-180^o,OO-180^o)	17.3	19.6

As can be seen from Tables 6.10, 6.11, 6.12, 6.13 and 6.14, the relaxed optimization of $M(OxH)_2Ac_2$ metal complexes leads to the same lowest energy structures for Co^{2+} (SS-Cis-Ox(NN-90^o,OO-180^o)), Cu^{2+} (RS-Cis-Ox(NN-90^o,OO-180^o)) and Zn^{2+} (SS-Cis-Ox(NN-90^o,OO-180^o)) metal cations as an unconstrained optimisation of $M(Ox)_2(AcH)_2$ metal complexes where hydroxyoxime ligands are deprotonated instead of carboxylic acid ones. However, for Ni^{2+} and Mn^{2+} $M(OxH)_2(Ac)_2$ complexes the RS-Cis-Ox(NN-180^o,OO-90^o) and RS-Cis-Ox(NN-90^o,OO-180^o) structures, respectively, were found to be the most stable instead of SS-Cis-Ox(NN-90^o,OO-180^o) and SS-Cis-Ox(NN-180^o,OO-90^o) ones, which were predicted to be the lowest energy structures when the starting geometries were of $M(Ox)_2(AcH)_2$ stoichiometry. It is important to note that the Gibbs free energy difference between SS-Cis-Ox(NN-180^o,OO-90^o) and RS-Cis-Ox(NN-90^o,OO-180^o) structures of the $Mn(OxH)_2(Ac)_2$ complex is only 0.7 kJ/mol, which means that both these structures may coexist in the real mixture (Table 6.13) with a high probability. The probability of coexistence of SS-Cis-Ox(NN-90^o,OO-180^o) and RS-Cis-Ox(NN-180^o,OO-90^o) structures of $Ni(OxH)_2Ac_2$ complex is significantly lower as the value of $\triangle$G between these two structures is 6.5 kJ/mol (Table 6.10).

The lowest energy structures of Ni^{2+}, Co^{2+}, Cu^{2+}, Mn^{2+} and Zn^{2+} $M(OxH)_2Ac_2$ complexes are shown in Figure 6.7. In all structures represented in Figure 6.7, acetic acid ligands are deprotonated, which can be clearly seen if we compare the O-H bond

distances in COH groups of hydroxyoxime and also the lengths of OH$\cdots$O hydrogen bonding (Table 6.15).

TABLE 6.15: The O-H (in COH group) and OH$\cdots$O hydrogen bond distances (Å) in the lowest energy Ni^{2+}, Co^{2+}, Zn^{2+}, Cu^{2+} and Mn^{2+} complexes (Fig. 6.7) calculated at the M06/6-31G(d,p)/LanL2DZ level of theory.

Labels of Metal Complexes	Ligand I (Fig. 6.7)		Ligand II (Fig. 6.7)	
	O-H, Å	OH$\cdots$O, Å	O-H, Å	OH$\cdots$O, Å
Ni^{2+} RS-Cis-Ox(NN-180^o,OO-90^o)	0.997	1.676	0.994	1.718
Co^{2+} SS-Cis-Ox(NN-90^o,OO-180^o)	0.996	1.662	0.996	1.662
Zn^{2+} SS-Cis-Ox(NN-90^o,OO-180^o)	0.993	1.681	0.993	1.680
Cu^{2+} RS-Cis-Ox(NN-90^o,OO-180^o)	0.983	1.756	0.981	1.789
Mn^{2+} RS-Cis-Ox(NN-90^o,OO-180^o)	0.993	1.685	0.992	1.708

It is interesting to note that the lowest energy structures for Co^{2+}, Cu^{2+} and Zn^{2+} depicted in Figure 6.7 are very similar to those shown in Figure 6.6, except for the type of intra-molecular hydrogen bonding, which results in different lengths of the O-H (in COH group) and OH$\cdots$O hydrogen bond distances. If we compare the stabilities between the metal complexes represented in Figures 6.6 and 6.7 it can be seen that the structures with (Oxime)NOH$\cdots$OC(Oxime) intra-molecular hydrogen bonding are more stable. When we studied the thermodynamics of hydroxyoxime oligomerisation (see the previous chapter), this type of hydrogen bonding was shown to be one of the most favourable energetically and it seems to have a significant impact on the stabilities of metal complexes for all metal cations except Mn^{2+}. The lowest energy structure (RS-Cis-Ox(NN-90^o,OO-180^o)) of the $Mn(OxH)_2(Ac)_2$ metal complex (Fig. 6.7) does not have this type of hydrogen bonding and both COH and NOH functional groups of acetoin oxime are connected via hydrogen bonding with an oxygen in the CO functional group of the carboxylic acid. Unfortunately, at this stage we cannot make any final conclusions regarding the effect of the type of intra-molecular interaction on the stability of different metal complexes as we have not performed the full scan of their potential energy surfaces. Therefore, in a future study it would be interesting to investigate the stabilities of different metal complexes as a function of different values of COMN torsion angles (where M - is a metal centre, N is a nitrogen from NOH oxime group and CO is a part of functional group of acetic acid bonded to the metal centre) that specify the location of the C=O functional group of the carboxylic acid with respect to an NOH functional group of hydroxyoxime.

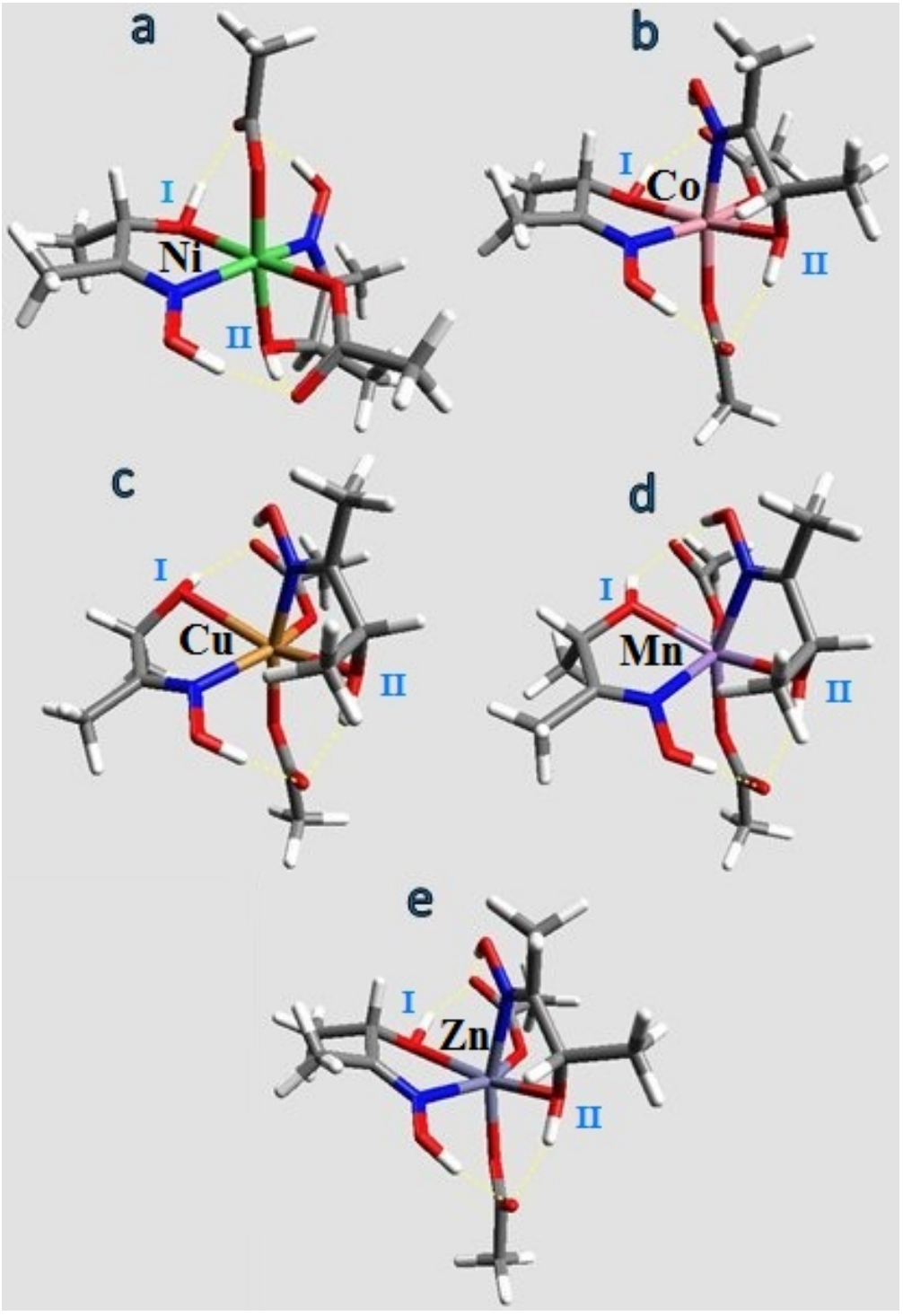

FIGURE 6.7: Schematic representation of the lowest energy structures of Ni, Co, Cu, Mn and Zn transition metal complexes with acetoin oxime and carboxylic acid optimized for the $M(OxH)_2(Ac)_2$ stoichiometry: a) RS-Cis-Ox(NN-180^o,OO-90^o) structure of Ni^{2+} complex; b) SS-Cis-Ox(NN-90^o,OO-180^o) structure of Co^{2+} complex; c) RS-Cis-Ox(NN-90^o,OO-180^o) structure of Cu^{2+} complex; d) RS-Cis-Ox(NN-90^o,OO-180^o) structure of Mn^{2+} complex and e) SS-Cis-Ox(NN-90^o,OO-180^o) structure of Zn^{2+} complex. Grey coloured atoms represent carbon, red - oxygen, dark blue - nitrogen, white - hydrogen, green - nickel, pink - cobalt, orange - copper, purple - manganese and dark purple - zinc.

Now that we have the lowest energy structures of the $M(OxH)_2(Ac)_2$ metal complex for each metal cation, it is interesting to estimate the Gibbs free energy and enthalpy for metal complexation starting from the mixture of carboxylic acid and hydroxyoxime. There are several techniques available in the literature (Ramalho *et al.*, 2004; Pesonen *et al.*, 2007; Xia *et al.*, 2011) to estimate the thermodynamics of formation of organometallic complexes. The model which we are going to use is as follows;

$$M(H_2O)^{2+}_{6(aq)} + 2OxH_{(o)} + 2Ac^{-}_{(aq)} \rightleftharpoons M(OxH)_2Ac_{2(o)} + 6H_2O_{(aq)} \tag{6.1}$$

where $M(H_2O)^{2+}_{6(aq)}$ is an aqueous phase octahedral metal aquo complex of charge 2+, OxH is a neutral molecule of hydroxyoxime dissolved in organic phase, $Ac^{-}_{(o)}$ is an aqueous phase anion of a carboxylic acid, $M(OxH)_2(Ac)_{2(aq)}$ is a transition metal complex with carboxylic acid and hydroxyoxime dissolved in the organic phase and $H_2O_{(aq)}$ is an aqueous phase water molecule. As discussed previously in the background section on extractive metallurgy, for an M^{2+} cation dissolved in water the binding strength between the water molecules of the second solvation shell may not be as strong as for the water molecules in the first solvation shell. This may lead to a certain level of disorder in the hydrogen bonding between the water molecules of the first and second solvation shells (Atta-Fynn *et al.*, 2011). Therefore we decided to calculate the energetics of the $M(H_2O)^{2+}_{6(aq)}$ aquo complexes with only the first explicit solvent shell and account for the interaction of these complexes with the bulk water via the Polarisable Continuum Model (PCM-Water) as implemented in the Gaussian09 software (Frisch *et al.* 2009). Note that the successful application of PCM in modelling aqueous phase complexes was previously shown by Allen *et al.* (2006) in their study of urate interaction with various metal cations, including divalent Be^{2+}, Mg^{2+} and Ca^{2+}. Interaction of a single water molecule with the bulk water was also accounted for via the PCM-Water model. As described in the methodology, in order to convert the data derived from the gas phase calculations to the organic phase data we used only the vibrational contributions to the thermodynamics of each component present in the liquid phase.

According to calculations of Cu^{2+} and Mn^{2+} metal complexes at the M06/6-31G(d,p)/LanL2DZ level of theory, the carboxylic acid is deprotonated during the metal complexation. However, it is interesting to note that for the lowest energy structures of Ni^{2+}, Co^{2+} and Zn^{2+} acetoin oxime-acetic acid $M(OxH)_2(Ac)_2$ metal complexes (Figure 6.6) the lengths of the O-H covalent and $OH\cdots O$ hydrogen (between acetoin oxime and acetic acid ligands) bonds are nearly identical. Therefore it is hard to say for these particular complexes, which of the two different ligands is deprotonated. However, in order to calculate the $\triangle H^{363}$ and $\triangle G^{363}$ values for the equation 6.1 we need to understand which ligand is deprotonated during metal complexation. To clarify this ambiguity we performed a gas phase calculation of two acetoin oxime-acetic acid heterodimers, where

in the first case hydroxyoxime was deprotonated and in the second case it was neutral. At the M06/6-31G(d,p) level of theory, the dimer in which hydroxyoxime loses its proton appears to be significantly less stable than the dimer with a deprotonated carboxylic acid. The Gibbs free energy difference between the OxH$\cdots$Ac and Ox$\cdots$AcH heterodimers was estimated to be equal to 50 kJ/mol. This means that carboxylic acid/hydroxyoxime anionic heterodimer is more stable in the case when the carboxylic acid is deprotonated and hydroxyoxime stays neutral. Moreover, when we performed optimisation of metal complexes with constrained O-H covalent and OH$\cdots$O hydrogen bond distances, the results show that the metal complexes with the deprotonated carboxylic acid are significantly more stable. Therefore in order to calculate the $\triangle H^{363}$ and $\triangle G^{363}$ values for the equation 6.1 we are going to use the enthalpies and the Gibbs free energies of neutral acetoin oxime and deprotonated acetic acid.

In studying the thermodynamics of the hydroxyoxime oligomerisation process it was shown that it is energetically favourable for hydroxyoximes to form inter-molecular hydrogen bonds. It is well known that the water molecules also tend to form inter-molecular hydrogen bonds. In equation 6.1 six water molecules are released. In order to find the lowest energy six-water cluster we have performed the potential energy scan of the $(H_2O)_6$ oligomer at the M06/6-31G(d,p) level of theory. The structure of the most stable 6-water cluster was found to be in good agreement with the one optimised by Silva *et al.* (2006). As it is more likely for the water molecules and hydroxyoximes to be present in oligomeric forms, we decided to use the energetics of a $(H_2O)_6$ water cluster and $(OxH)_2$ hydroxyoxime dimer instead of the sum of the energetics of single molecules in studying the thermodynamics of equation 6.1 (Figure 6.8).

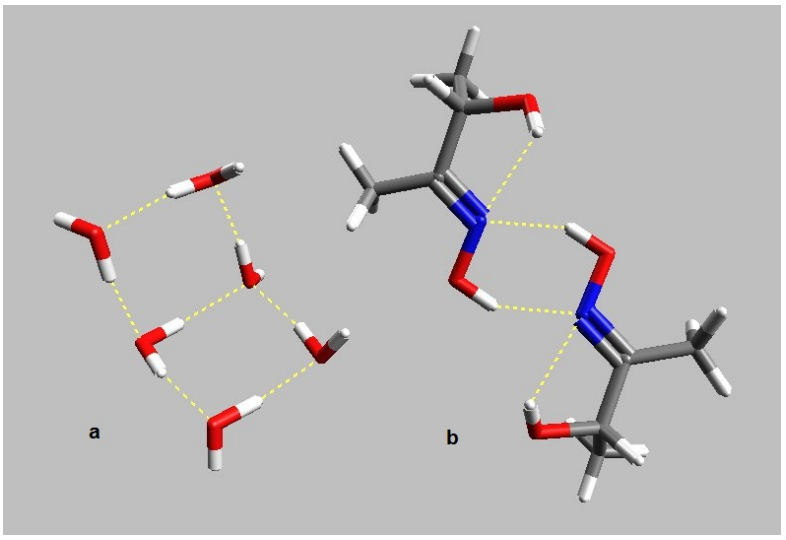

FIGURE 6.8: Lowest energy structures of $(H_2O)_6$ water cluster (a) and $(OxH)_2$ hydroxyoxime dimer (b) optimised at the M06/6-31G(d,p) level of theory. Grey coloured atoms represent carbon, red - oxygen, dark blue - nitrogen and white - hydrogen. Dotted yellow lines represent inter- and intra-molecular hydrogen bonds.

The Gibbs free energy and enthalpy changes at 313 K calculated for equation 6.1 at the M06/6-31G(d,p)/LanL2DZ level of theory are given in Table 6.16[6].

TABLE 6.16: Gibbs free energy (ΔG^o_{313}, kJ/mol) and enthalpy (ΔH^o_{313}, kJ/mol) changes for complexation of Ni^{2+}, Co^{2+}, Cu^{2+}, Mn^{2+} and Zn^{2+} transition metal cations with acetic acid anions and acetoin oxime molecules calculated at the M06/6-31G(d,p)/LanL2DZ level of theory for the case when the formed metal complexes are of $M(OxH)_2(Ac)_2$ stoichiometry.

Lowest energy $M(OxH)_2Ac_2$ complex	M06/6-31G(d,p)/LanL2DZ	
	ΔG^{313}, $\frac{kJ}{mol}$	ΔH^{313}, $\frac{kJ}{mol}$
Ni^{2+} SS-Cis-Ox(NN-90^o,OO-180^o)	-387.2	-340.6
Co^{2+} SS-Cis-Ox(NN-90^o,OO-180^o)	-364.1	-323.1
Cu^{2+} SS-Cis-Ox(NN-90^o,OO-180^o)	-409.6	-364.5
Mn^{2+} RS-Cis-Ox(NN-90^o,OO-180^o)	-337.4	-297.8
Zn^{2+} SS-Cis-Ox(NN-90^o,OO-180^o)	-341.3	-288.3

[6]Note that most of the experimental data on synergistic solvent extraction with LIX63 and Versatic10 was derived at 313 K (Cheng, 2006), therefore, theoretically estimated thermodynamics are also taken at this temperature.

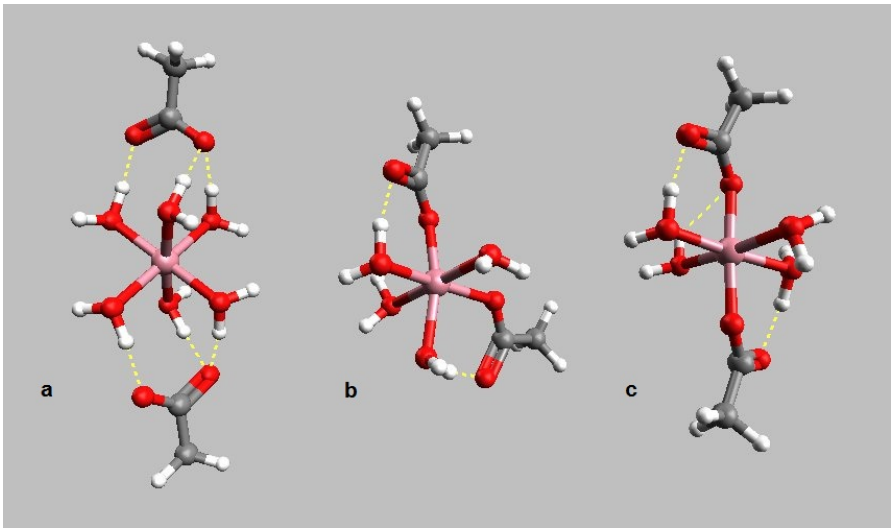

FIGURE 6.9: Graphical representation of $M(H_2O)_6(Ac)_2$ (a) and $M(H_2O)_4(Ac)_2$ (cis - b and trans - c) structures optimised at the M06/6-31G(d,p) level of theory. Grey coloured atoms represent carbon, red - oxygen and white - hydrogen. Dotted yellow lines represent inter- and intra-molecular hydrogen bonds.

As can be seen from the above Table, the Gibbs free energy and enthalpy changes for the formation of organometallic complexes of a carboxylic acid anionic and neutral hydroxyoxime ligands with each of the considered metal cations are very exothermic. This signifies that all these transition metals are readily extracted by the mixture of hydroxyoxime and carboxylic acid at the considered conditions. The magnitude of the Gibbs free energy difference for the copper complexation is the largest, which indicates that the Cu^{2+} metal complex is the most stable, followed by Ni^{2+}, Co^{2+}, Zn^{2+} and Mn^{2+} complexes.

In order to estimate the synergistic effect we can analyse this equilibrium shown in equation 6.1 in two steps. The first step corresponds to the addition of an acetic acid anion to the $M(H_2O)_6^{2+}$ metal aquo complex and the second step is the attachment of the acetoin oxime ligands to the first step product complex. Interaction between the metal aquo complex and deprotonated acetic acid may result in formation of one of the three (a and b or c) complexes shown in Figure 6.9. Note that the $M(H_2O)_4(Ac)_2$ complex may exist in two isomers (cis and trans - b and c in Figure 6.9, respectively). To estimate the probability of formation of each complex we have calculated the thermodynamics of the following reactions at the M06/6-31G(d,p)/LanL2DZ level of theory:

$$M(H_2O)^{2+}_{6(aq)} + 2Ac^-_{(aq)} \rightleftharpoons M(H_2O)_6(Ac)_{2(aq)} \tag{6.2}$$

$$M(H_2O)^{2+}_{6(aq)} + 2Ac^-_{(aq)} \rightleftharpoons M(H_2O)_4(Ac)_{2(aq)} + 2H_2O_{(aq)} \tag{6.3}$$

Gibbs free energies and enthalpies of the above equilibria for $M(H_2O)_6(Ac)_2$ and $M(H_2O)_4$

$(Ac)_2$ complex formation are shown in Table 6.17:

TABLE 6.17: Thermodynamics of formation of $M(H_2O)_6(Ac)_2$ and $M(H_2O)_4(Ac)_2$ metal complexes calculated at the M06/6-31G(d,p)/LanL2DZ level of theory at 313 K. Note that (a), (b) and (c) are the complexes from Figure 6.9.

Metal Ions	$M(H_2O)_6(Ac)_2$ (a)		$M(H_2O)_4(Ac)_2$ (b)		$M(H_2O)_4(Ac)_2$ (c)	
	ΔG, $\frac{kJ}{mol}$	ΔH, $\frac{kJ}{mol}$	ΔG, $\frac{kJ}{mol}$	ΔH, $\frac{kJ}{mol}$	ΔG, $\frac{kJ}{mol}$	ΔH, $\frac{kJ}{mol}$
Ni^{2+}	-340.4	-303.7	-276.1	-267.8	-281.4	-269.2
Co^{2+}	-330.9	-298.8	-265.5	-264.5	-275.4	-270.7
Cu^{2+}	-352.0	-320.6	-294.3	-283.7	-310.0	-294.4
Mn^{2+}	-312.7	-285.4	-239.2	-235.5	-247.0	-243.1
Zn^{2+}	-314.1	-272.6	-241.6	-225.2	-251.2	-233.0

As can be seen from Table 6.17, the formation of the trans (c) acetic acid aquo complex is energetically more favourable as compared to the cis (b) one for each metal cation. However, if we compare the Gibbs free energies of the two equilibria shown in equation 6.2 and 6.3 we can see that according to our calculation the $M(H_2O)_6(Ac)_2$ metal complex is much more likely to be formed in this system. If we compare the thermodynamics for the overall equilibrium (equation 6.1) of metal complexation with both acetic acid and acetoin oxime shown in Table 6.16 with that of $M(H_2O)_6(Ac)_2$ metal complex formation (Table 6.17) we can see that all the metal cations are more likely to be fully transferred to the organic phase via formation of $M(OxH)_2(Ac)_2$ complexes which is in good agreement with the experiment. If we compare the Gibbs free energies for the complexation of different metals, we will see that theoretically estimated order at which the metals are extracted at 313 K is also in good agreement with the experimental one (Cheng, 2006).

Now that we have the thermodynamics of both equilibria (shown in equation 6.1 and 6.2) calculated for each metal cation, we can estimate the synergistic effect of acetoin oxime addition on the selectivity of metal complexation. In order to do this we should compare the thermodynamics between metal cations for each of the two equilibria. As can be seen from Table 6.18 the addition of acetoin oxime to the system increases the differences in Gibbs free energies of metal complexation for each metal cation with respect to the favoured formation of copper complex. This could mean that the metal cations shown in Table 6.18 can be separated by varying process parameters (pH of the solution, for instance) with higher selectivity when the hydroxyoxime oxime is present in the system. This conclusion agrees well with experimental observations (Barnard *et al.* (2010)).

TABLE 6.18: Thermodynamics of metal complexation from equations 6.1 and 6.2 for each metal ion relative to the formation of corresponding complexes of the copper cation, which was shown to be the most favourable process according to the calculation at the M06/6-31G(d,p)/LanL2DZ level of theory at 313 K.

Metal Ions	$M(OxH)_2(Ac)_2$		$M(H_2O)_6(Ac)_2$	
	$\Delta G, \frac{kJ}{mol}$	$\Delta H, \frac{kJ}{mol}$	$\Delta G, \frac{kJ}{mol}$	$\Delta H, \frac{kJ}{mol}$
Ni^{2+}	22.3	24.0	11.7	16.9
Co^{2+}	45.5	41.5	21.1	21.8
Cu^{2+}	0.0	0.0	0.0	0.0
Mn^{2+}	72.1	66.7	39.3	35.2
Zn^{2+}	68.3	76.3	38.0	48.0

In the current study, the lowest energy structure of the $Ni(OxH)_2(Ac)_2$ complex (Fig. 6.6) looks closer to the crystallographically determined structure of the $Ni(OxH)_2$ $(Ac)_2$ complex of Barnard *et al.* (2010) than to the structure of the Ni complex of the same stoichiometry suggested by Castresana *et al.* (1988). These structures are shown in Figure 6.10. Note that hydrocarbon side chains of CH_3 were used for all three structures in order to make clearer representation of the way in which organic ligands are bonded to the metal cation. However, the R groups in the structures determined by Barnard *et al.* (2010) and Castresana *et al.* (1988) are different from those represented in Figure 6.10.

As can be seen from Figure 6.10, the lowest energy structure determined at the M06/6-31G(d,p)/LanL2DZ level of theory generally represents itself as the mirror image of the one determined by Barnard *et al.* (2010) with only minor differences in intra-molecular hydrogen bonding between the ligands. Note that the stereo-chemistry of the two hydroxyoxime ligands in the experimental structure is identical (both of R chirality), while in the theoretically determined structure the stereo-chemistry of each hydroxyoxime ligand is different (S and R). These minor differences could be due to the difference in the environment for the two cases as the experimentally determined structure corresponds to the solid phase complex, while the structure determined theoretically corresponds to that in organic solvent. As was mentioned earlier, there were some assumptions made based on the experimental results of Barnard *et al.* (2011) that in solution three molecules of hydroxyoxime and two molecules of carboxylic acid are required to form an organometallic complex. In order to check this hypothesis we need to calculate the thermodynamics of $M(OxH)_3(Ac)_2$ complex formation and compare this with the thermodynamics of metal complexation in which $M(OxH)_2(Ac)_2$ is formed.

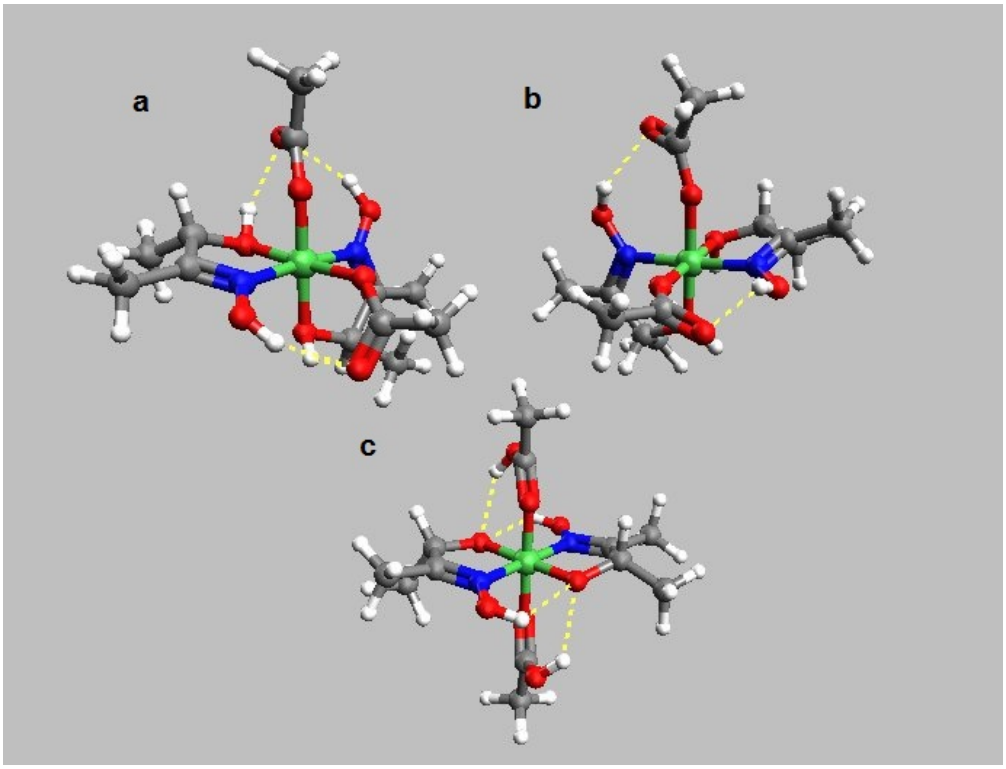

FIGURE 6.10: Graphical representation of the lowest energy $Ni(OxH)_2$ $(Ac)_2$ complex optimised at the M06/6-31G(d,p)/LanL2DZ level of theory (a), crystallographically determined structure of $Ni(OxH)_2$ $(Ac)_2$ (b) (Barnard *et al.*, 2010) and $Ni(Ox)_2$ $(AcH)_2$ structure suggested by Castresana *et al.* (1988) (c). Grey coloured atoms represent carbon, red - oxygen, dark blue - nitrogen and white - hydrogen. Dotted yellow lines represent inter- and intra-molecular hydrogen bonds.

6.3.2 Thermodynamics of $M(OxH)_3Ac_2$ Transition Metal Complexes with Acetoin Oxime and Acetic Acid for M = Ni^{2+}, Co^{2+}, Cu^{2+}, Mn^{2+} and Zn^{2+}

As was shown previously for the hydroxyoxime-carboxylic acid system, the system is more stable when the carboxylic acid molecules are deprotonated and all the hydroxyoxime molecules are left neutral. Therefore in this study we are going to consider only organometallic systems in which the acetic acid is the extractant (deprotonated) and acetoin oxime is the synergist (protonated).

In $M(OxH)_3Ac_2$ metal complexes three oxime ligands are in the inner sphere of the metal complex and bonded directly to the metal cation by a covalent bond. Two carboxylic acid molecules are then located in the outer sphere and attached to the tris-oxime metal complex via intermolecular hydrogen bonding. Therefore, in order to determine the minimum for this stoichiometry we need to study first the PES of the tris-oxime metal complex ($M(OxH)_3^{2+}$), prior to modelling the PES of the $M(OxH)_3Ac_2$ metal complex. The strategy for naming $M(OxH)_3^{2+}$ metal complexes is represented in

Figure 6.11.

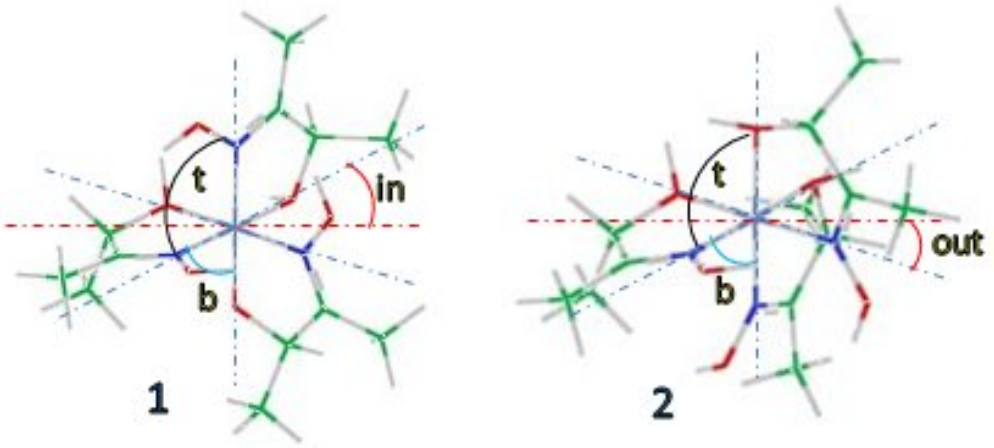

FIGURE 6.11: Graphical representation of the naming of SRR-NN-t(in)-NO-b(out) (1) and SRR-NO-t(out)-NN-b(in)(2) structures of $M(OxH)_3^{2+}$ metal complexes with one S and two R hydroxyoxime stereo-isomers. "in" - corresponds to the location into the viewer's plane and "out" - to that out of the viewer's plane. The 90^o angle "t" - means top angle and "b" - is the bottom 90^o angle. Green coloured atoms represent carbon, red - oxygen, dark blue - nitrogen, purple - metal centre (M) and white - hydrogen.

The name of the first $M(OxH)_3^{2+}$ complex in Figure 6.11 (SRR-NN-t(in)-NO-b(out)) is constructed in such way so that the first three letters represent the stereo-chemistry of the left (S), top (R) and bottom (R) ligands. The next part (NN-t(in)) tells us that the 90^o "t" angle is formed between nitrogen of the left and nitrogen of the top acetoin oxime ligands, where the latter is located within ("in") the viewer's plane. The last part (NO-b(out)) tells us that the 90^o "b" angle is formed between nitrogen of the left and oxygen of the bottom acetoin oxime ligands, where the latter is located out ("out") of the viewer's surface. The names of all SRR and SSS $M(OxH)_3^{2+}$ metal complexes which were constructed are given in Tables 6.19 and 6.20, respectively.

TABLE 6.19: Labels for the structures of SRR $M(OxH)_3^{2+}$ metal complex.

Number	Complex Label	Number	Complex Label
1	NN-t(in)-NO-b(out)	5	NO-t(in)-NO-b(out)
2	NO-t(out)-NN-b(in)	6	NN-t(out)-NN-b(in)
3	NN-t(in)-NN-b(out)	7	NN-t(out)-NO-b(in)
4	NO-t(in)-NN-b(out)	8	NO-t(out)-NO-b(in)

TABLE 6.20: Labels for the structures of SSS $M(OxH)_3^{2+}$ metal complex.

Number	Complex Label	Number	Complex Label
1	NN-t(in)-NN-b(out)	3	NN-t(in)-NO-b(out)
2	NO-t(out)-NO-b(in)	4	NO-t(out)-NN-b(in)

All of these structures were constructed using the Avogadro molecular visualisation software and pre-optimised using the UFF force field (Rappe *et al.*, 1992). The graphical representation of the tris-oxime metal complexes for the $M(OxH)_3^{2+}$ stoichiometry with one S and two R acetoin oxime stereo-isomers are depicted in Figure 6.12.

Gibbs free energy differences and enthalpy changes between each complex and the lowest energy structure of $M(OxH)_3^{2+}$ for Ni^{2+}, Co^{2+}, Cu^{2+}, Mn^{2+} and Zn^{2+} transition metal cations are given in Tables 6.21, 6.22, 6.23, 6.24 and 6.25, respectively. Gas phase geometry optimisation and frequency calculations of each complex were performed at the M06/6-31G(d,p)/LanL2DZ level of theory. To calculate the relative energetics of metal complexes, only the vibration parts of enthalpy and entropy were included along with zero point energy and thermal corrections at 298.15 K. All possible geometries of the tris-oxime metal complexes of $M(OxH)_3^{2+}$ stoichiometry with three S acetoin oxime stereo-isomers are depicted in Figure 6.13.

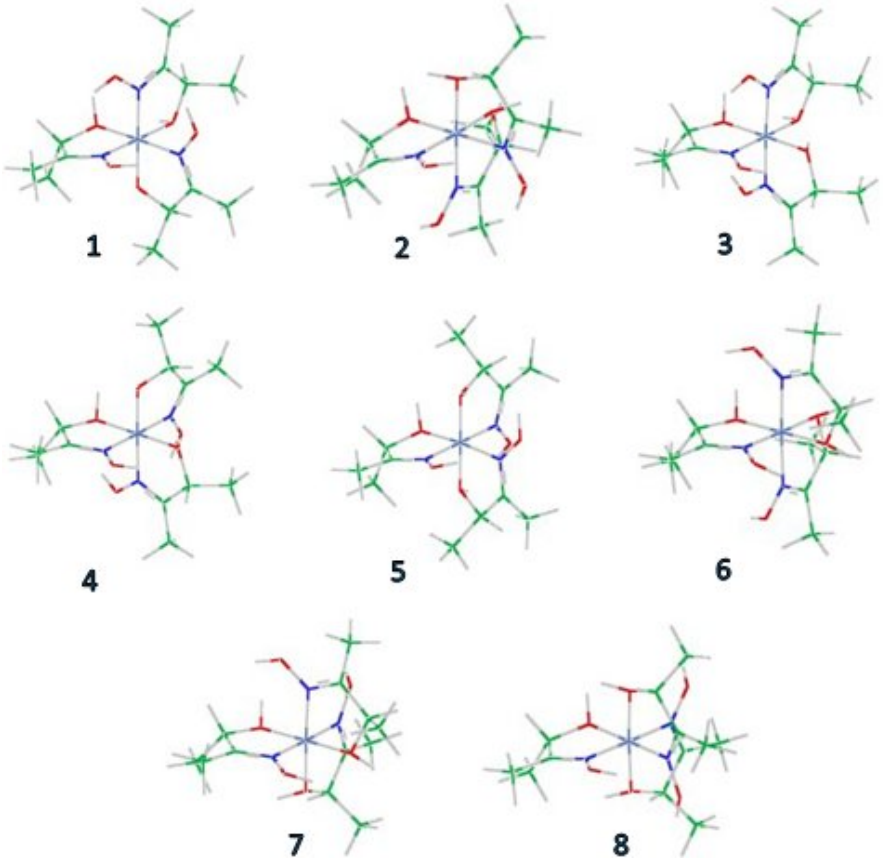

FIGURE 6.12: Initial structures for studying the potential energy surface of M(II)-α-hydroxyoxime complexes of $M(OxH)_3^{2+}$ stoichiometry with one S and two R hydroxyoxime stereo-isomers. Green coloured atoms represent carbon, red - oxygen, dark blue - nitrogen, purple - metal centre (M) and white - hydrogen atoms and bonding.

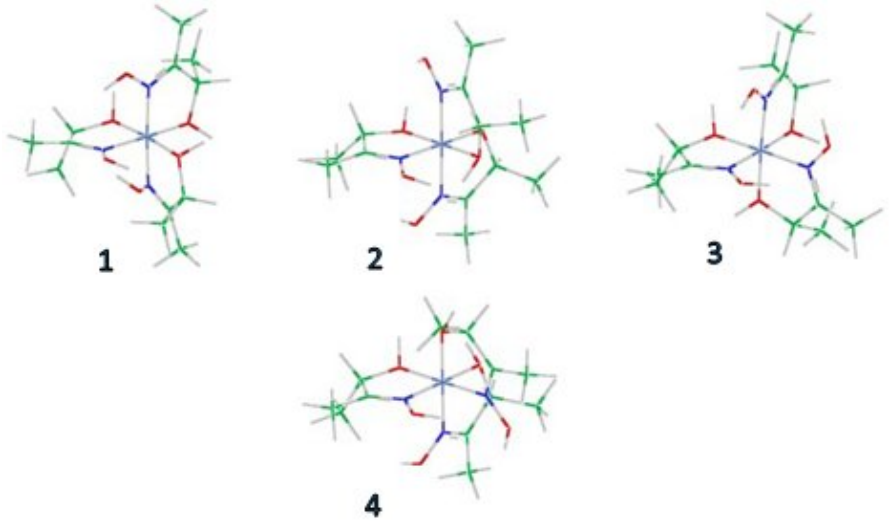

FIGURE 6.13: Initial structures for studying the potential energy surface of M(II)-α-hydroxyoxime complexes of $M(OxH)_3^{2+}$ stoichiometry with three S hydroxyoxime stereo-isomers. Green coloured atoms represent carbon, red - oxygen, dark blue - nitrogen, purple - metal centre (M) and white - hydrogen atoms and bonding.

TABLE 6.21: Gibbs free energy ($\Delta G^o_{298.15}$, kJ/mol) and enthalpy ($\Delta H^o_{298.15}$, kJ/mol) differences relative to the most stable structure of the $Ni(OxH)^{2+}_3$ complex at the M06/6-31G(d,p)/LanL2DZ level of theory.

$Ni(OxH)^{2+}_3$ ($Ni^{2+}S = 3$)	M06/6-31G(d,p)/LanL2DZ	
	ΔG, $\frac{kJ}{mol}$	ΔH, $\frac{kJ}{mol}$
SRR NN-t(in)-NO-b(out)	7.3	-0.8
SRR NO-t(out)-NN-b(in)	2.9	-0.5
SRR NN-t(in)-NN-b(out)	13.5	2.4
SRR NO-t(in)-NN-b(out)	0.0	0.0
SRR NO-t(in)-NO-b(out)	7.6	-3.0
SRR NN-t(out)-NN-b(in)	8.8	1.7
SRR NN-t(out)-NO-b(in)	3.9	-1.4
SRR NO-t(out)-NO-b(in)	2.3	-1.1
SSS NN-t(in)-NN-b(out)	7.5	1.5
SSS NO-t(out)-NO-b(in)	7.3	0.4
SSS NN-t(in)-NO-b(out)	5.4	3.6
SSS NO-t(out)-NN-b(in)	23.0	18.3

TABLE 6.22: Gibbs free energy ($\Delta G^o_{298.15}$, kJ/mol) and enthalpy ($\Delta H^o_{298.15}$, kJ/mol) differences relative to the most stable structure of the $Co(OxH)^{2+}_3$ complex at the M06/6-31G(d,p)/LanL2DZ level of theory.

$Co(OxH)^{2+}_3$ ($Co^{2+}S = 4$)	M06/6-31G(d,p)/LanL2DZ	
	ΔG, $\frac{kJ}{mol}$	ΔH, $\frac{kJ}{mol}$
SRR NN-t(in)-NO-b(out)	0.0	0.0
SRR NO-t(out)-NN-b(in)	86.3	77.4
SRR NN-t(in)-NN-b(out)	12.5	3.0
SRR NO-t(in)-NN-b(out)	8.1	10.5
SRR NO-t(in)-NO-b(out)	14.1	5.8
SRR NN-t(out)-NN-b(in)	12.9	10.4
SRR NN-t(out)-NO-b(in)	49.8	40.2
SRR NO-t(out)-NO-b(in)	9.0	7.7
SSS NN-t(in)-NN-b(out)	21.2	12.4
SSS NO-t(out)-NO-b(in)	12.3	8.1
SSS NN-t(in)-NO-b(out)	8.5	3.8
SSS NO-t(out)-NN-b(in)	4.1	0.5

TABLE 6.23: Gibbs free energy ($\Delta G^{o}_{298.15}$, kJ/mol) and enthalpy ($\Delta H^{o}_{298.15}$, kJ/mol) differences relative to the most stable structure of the $Cu(OxH)^{2+}_{3}$ complex at the M06/6-31G(d,p)/LanL2DZ level of theory.

$Cu(OxH)^{2+}_{3}$ ($Cu^{2+}S = 2$)	M06/6-31G(d,p)/LanL2DZ	
	ΔG, $\frac{kJ}{mol}$	ΔH, $\frac{kJ}{mol}$
SRR NN-t(in)-NO-b(out)	28.9	29.7
SRR NO-t(out)-NN-b(in)	34.3	32.8
SRR NN-t(in)-NN-b(out)	6.0	0.7
SRR NO-t(in)-NN-b(out)	3.9	1.8
SRR NO-t(in)-NO-b(out)	20.3	15.1
SRR NN-t(out)-NN-b(in)	6.6	2.3
SRR NN-t(out)-NO-b(in)	8.0	1.7
SRR NO-t(out)-NO-b(in)	8.0	2.7
SSS NN-t(in)-NN-b(out)	0.0	0.0
SSS NO-t(out)-NO-b(in)	10.7	2.5
SSS NN-t(in)-NO-b(out)	23.8	32.3
SSS NO-t(out)-NN-b(in)	41.4	40.7

TABLE 6.24: Gibbs free energy ($\Delta G^{o}_{298.15}$, kJ/mol) and enthalpy ($\Delta H^{o}_{298.15}$, kJ/mol) differences relative to the most stable structure of the $Mn(OxH)^{2+}_{3}$ complex at the M06/6-31G(d,p)/LanL2DZ level of theory.

$Mn(OxH)^{2+}_{3}$ ($Mn^{2+}S = 6$)	M06/6-31G(d,p)/LanL2DZ	
	ΔG, $\frac{kJ}{mol}$	ΔH, $\frac{kJ}{mol}$
SRR NN-t(in)-NO-b(out)	8.5	1.7
SRR NO-t(out)-NN-b(in)	10.1	3.3
SRR NN-t(in)-NN-b(out)	17.9	12.9
SRR NO-t(in)-NN-b(out)	27.3	20.8
SRR NO-t(in)-NO-b(out)	25.0	18.9
SRR NN-t(out)-NN-b(in)	21.8	19.3
SRR NN-t(out)-NO-b(in)	21.1	15.3
SRR NO-t(out)-NO-b(in)	23.9	17.1
SSS NN-t(in)-NN-b(out)	21.5	17.5
SSS NO-t(out)-NO-b(in)	27.2	17.7
SSS NN-t(in)-NO-b(out)	0.0	0.0
SSS NO-t(out)-NN-b(in)	11.3	4.6

TABLE 6.25: Gibbs free energy ($\Delta G^{o}_{298.15}$, kJ/mol) and enthalpy ($\Delta H^{o}_{298.15}$, kJ/mol) differences relative to the most stable structure of the $Zn(OxH)^{2+}_{3}$ complex at the M06/6-31G(d,p)/LanL2DZ level of theory.

$Zn(OxH)^{2+}_{3}$ ($Zn^{2+}S = 1$)	M06/6-31G(d,p)/LanL2DZ	
	ΔG, $\frac{kJ}{mol}$	ΔH, $\frac{kJ}{mol}$
SRR NN-t(in)-NO-b(out)	0.0	0.0
SRR NO-t(out)-NN-b(in)	26.8	27.4
SRR NN-t(in)-NN-b(out)	43.1	43.3
SRR NO-t(in)-NN-b(out)	39.1	34.3
SRR NO-t(in)-NO-b(out)	28.7	27.6
SRR NN-t(out)-NN-b(in)	14.7	14.3
SRR NN-t(out)-NO-b(in)	11.5	11.7
SRR NO-t(out)-NO-b(in)	12.1	12.1
SSS NN-t(in)-NN-b(out)	8.6	11.1
SSS NO-t(out)-NO-b(in)	19.1	13.8
SSS NN-t(in)-NO-b(out)	4.3	4.9
SSS NO-t(out)-NN-b(in)	8.6	8.9

As can be seen from the data presented above, each transition metal cation favours a different configuration for the tris-oxime complex, except for Co^{2+} and Zn^{2+} where the lowest energy structures are of the same geometry. It is interesting to note that there are many structures, especially in case of the $Ni(OxH)^{2+}_{3}$ and $Cu(OxH)^{2+}_{3}$ metal complexes, for which the values of $\triangle$G relative to the corresponding lowest energy structure are within the range of 2.3-8.8 kJ/mol. This means that in the real solution all these complexes may be found with a certain level of probability. However, due to the limited time of this project we are not able to perform optimisation of each $M(OxH)_3(Ac)_2$ metal complex considering all these tris-oxime structures. Therefore it has been decided to use only the lowest energy structures of $M(OxH)^{2+}_{3}$ (M = Ni, Co, Cu, Mn and Zn) to estimate the thermodynamics of formation of the $M(OxH)_3(Ac)_2$ metal complexes. Graphical representations of the lowest energy structures of $M(OxH)^{2+}_{3}$ tris-oxime complexes optimised at the M06/6-31G(d,p)/LanL2DZ level of theory are given in Figure 6.14.

To calculate the thermodynamics of $M(OxH)_3Ac_2$ metals complex formation for Ni^{2+}, Co^{2+}, Cu^{2+}, Mn^{2+} and Zn^{2+} transition metal cations with the mixture of carboxylic acid and hydroxyoxime, the following equilibrium was considered;

$$M(H_2O)^{2+}_{6(aq)} + (OxH)_{3(o)} + 2Ac^{-}_{(aq)} \rightleftharpoons M(OxH)_3(Ac)_{2(o)} + (H_2O)_{6(aq)} \qquad (6.4)$$

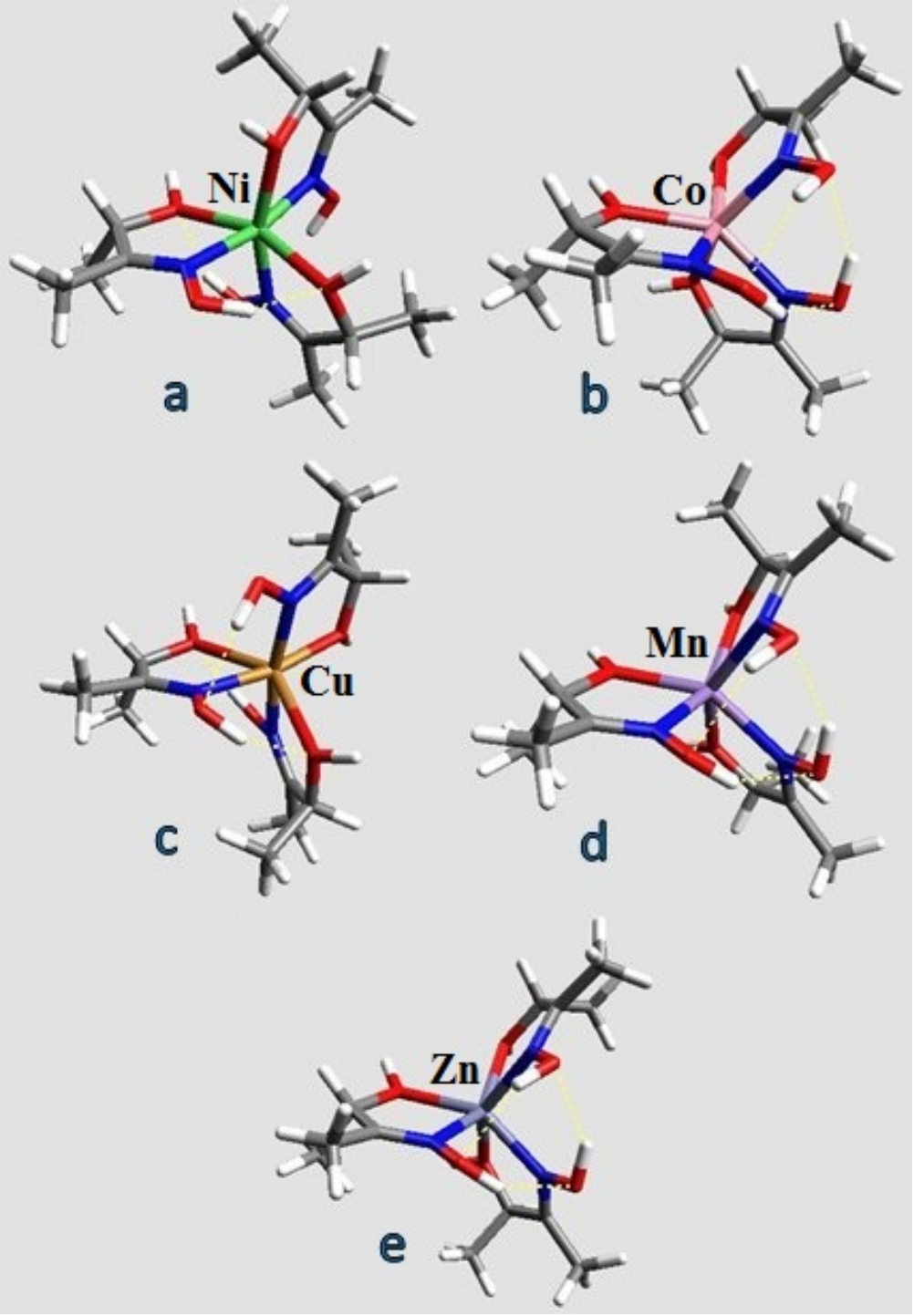

FIGURE 6.14: Graphical representation of the lowest energy structures of the $M(OxH)_3^{2+}$ metal complexes with acetoin oxime: a) SRR NO-t(in)-NN-b(out) structure of Ni^{2+} complex; b) SRR NN-t(in)-NO-b(out) structure of Co^{2+} complex; c) SSS NN-t(in)-NN-b(out) structure of Cu^{2+} complex; d) SSS NN-t(in)-NO-b(out) structure of Mn^{2+} complex and e) SRR NN-t(in)-NO-b(out) structure of Zn^{2+} complex. Grey coloured atoms represent carbon, red - oxygen, dark blue - nitrogen, white - hydrogen, green - nickel, pink - cobalt, orange - copper, purple - manganese and dark purple - zinc.

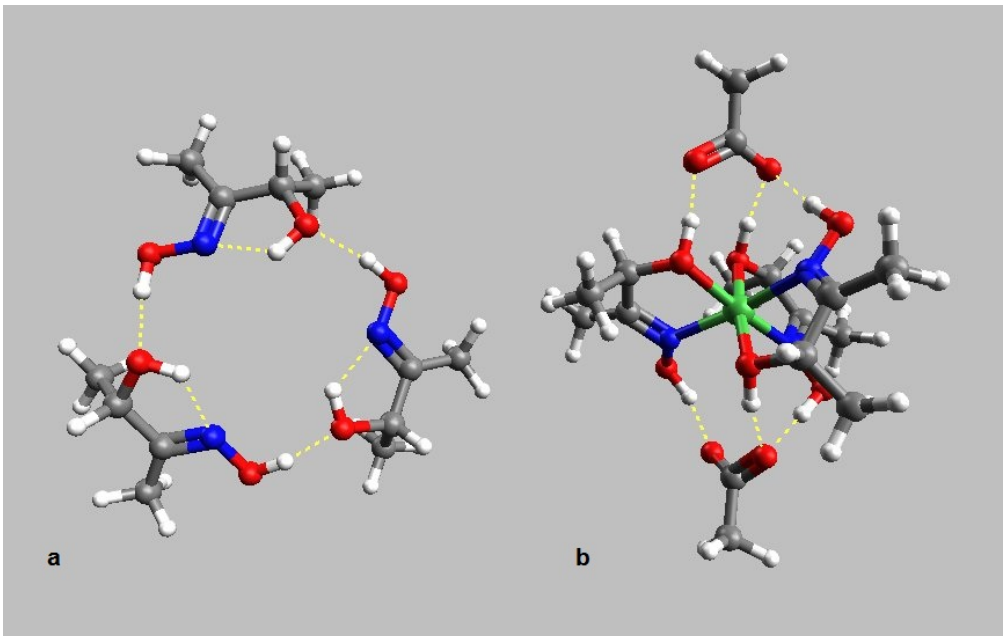

FIGURE 6.15: Lowest energy structures of the acetoin oxime trimer (a) and $Ni(OxH)_3(Ac)_2$ (b) optimised at the M06/6-31G(d,p)/LanL2DZ level of theory. Grey coloured atoms represent carbon, red - oxygen, dark blue - nitrogen and white - hydrogen. Dotted yellow lines represent inter- and intra-molecular hydrogen bonds.

where $M(H_2O)^{2+}_{6(aq)}$ is an aqueous phase octahedral metal aquo complex of charge 2+, $(OxH)_{3(o)}$ is an organic phase acetoin oxime trimer, $Ac^{-}_{(aq)}$ is an aqueous phase acetic acid anion, $M(OxH)_3\ Ac_{2(o)}$ is a transition metal complex with carboxylic acid anions and hydroxyoxime dissolved in the organic phase and $(H_2O)_{6(aq)}$ is an aqueous phase water cluster consisting of six water molecules. Note that the lowest energy structure of the acetoin oxime trimer determined in the previous chapter was used. To estimate the energetics of the $M(OxH)_3(Ac)_{2(o)}$ complex for each metal cation we added two acetic acid anions to each lowest energy structure of tris-oxime metal complex and re-optimised the whole system at the M06/6-31G(d,p)/LanL2DZ level of theory[7]. The structures of the acetoin oxime trimer and $Ni(OxH)_3(Ac)_2$ complex optimised at the M06/6-31G(d,p)/LanL2DZ level of theory are shown in Figure 6.15.

Now that we have all constituents of equation 6.4, we can easily calculate the Gibbs free energy and enthalpy changes for the complexation of Ni^{2+}, Co^{2+}, Cu^{2+}, Mn^{2+} and Zn^{2+} cations with acetic acid and acetoin oxime for the case when the $M(OxH)_3(Ac)_{2(o)}$ metal complex is formed (Table 6.26). Note that most of the experimental data on synergistic solvent extraction with LIX63 and Versatic10 was derived at 313 K. Therefore, theoretically estimated thermodynamics are also taken at this temperature.

[7]Note that different positions of acetic acid anions were tested with the different number of intermolecular (between acetic acid anion and the tris-oxime metal complex) hydrogen bonds and only lowest energy structures were used to calculate the thermodynamics of $M(OxH)_3(Ac)_{2(o)}$ complex formation.

TABLE 6.26: Gibbs free energy (ΔG^{o}_{313}, kJ/mol) and enthalpy (ΔH^{o}_{313}, kJ/mol) changes for complexation of Ni^{2+}, Co^{2+}, Cu^{2+}, Mn^{2+} and Zn^{2+} transition metal cations with acetic acid anions and acetoin oxime molecules calculated at the M06/6-31G(d,p)/LanL2DZ level of theory for the case when the formed metal complexes are of $M(OxH)_3Ac_2$ stoichiometry.

Lowest energy $M(OxH)_3Ac_2$ complexes	M06/6-31G(d,p)/LanL2DZ	
	ΔG^{313}, $\frac{kJ}{mol}$	ΔH^{313}, $\frac{kJ}{mol}$
Ni^{2+} SRR NO-t(in)-NN-b(out)-Ac2	-425.3	-354.3
Co^{2+} SRR NN-t(in)-NO-b(out)-Ac2	-348.7	-307.8
Cu^{2+} SSS NN-t(in)-NN-b(out)-Ac2	-437.2	-390.5
Mn^{2+} SSS NN-t(in)-NO-b(out)-Ac2	-355.3	-310.9
Zn^{2+} SRR NN-t(in)-NO-b(out)-Ac2	-329.4	-274.1

As can be seen by comparing the data in Tables 6.16 and 6.26, the process of formation of nickel-, copper- and manganese-tris-acetoin oxime-di-acetic acid complexes is energetically more favourable than the process of formation of the corresponding di-acetoin oxime-di-acetic acid complexes. According to our calculations, we can conclude at this point that the probability of formation of $M(OxH)_3Ac_2$ metal complexes in a non-polar aliphatic solvent is significantly higher for Ni^{2+}, Cu^{2+} and Mn^{2+} than that of the corresponding organometallic complexes with $M(OxH)_2Ac_2$ stoichiometry.

As before, in order to estimate the synergistic effect we need to compare the thermodynamics of each metal complexation reaction, which were estimated using the equilibrium shown in equation 6.4, with the most favourable one (Table 6.27).

TABLE 6.27: Thermodynamics (kJ/mol) of metal complexation using the equations 6.1, 6.2 and 6.4 for each metal ion relative to the formation of corresponding complexes of the copper cation, which was shown to be the most favourable process according to the calculation at the M06/6-31G(d,p)/LanL2DZ level of theory at 313 K.

Metal Ions	$M(OxH)_3(Ac)_2$		$M(OxH)_2(Ac)_2$		$M(H_2O)_6(Ac)_2$	
	$\Delta\Delta G$	ΔH	$\Delta\Delta G$	ΔH	$\Delta\Delta G$	ΔH
Ni^{2+}	11.9	36.2	22.3	24.0	11.7	16.9
Co^{2+}	88.5	82.7	45.5	41.5	21.1	21.8
Cu^{2+}	0.0	0.0	0.0	0.0	0.0	0.0
Mn^{2+}	81.9	79.6	72.1	66.7	39.3	35.2
Zn^{2+}	107.8	116.4	68.3	76.3	38.0	48.0

TABLE 6.28: Thermodynamics of metal complexation of equation 6.1 and 6.4 for each metal ion using the sum of the energies of acetoin oxime monomers calculated at the M06/6-31G(d,p)/LanL2DZ level of theory at 313 K.

Metal Ions	$M(OxH)_2(Ac)_2$		$M(OxH)_3(Ac)_2$	
	ΔG, $\frac{kJ}{mol}$	ΔH, $\frac{kJ}{mol}$	ΔG, $\frac{kJ}{mol}$	ΔH, $\frac{kJ}{mol}$
Ni^{2+}	-450.5	-365.5	-542.4	-410.7
Co^{2+}	-427.3	-348.0	-465.9	-364.1
Cu^{2+}	-472.8	-389.5	-554.3	-446.9
Mn^{2+}	-400.7	-322.8	-472.4	-367.3
Zn^{2+}	-404.5	-313.2	-446.5	-330.5

As compared to both $M(OxH)_2(Ac)_2$ and $M(H_2O)_6(Ac)_2$ metal complexes, the synergistic effect in $M(OxH)_3(Ac)_2$ metal complexes is significantly higher, especially in the case of Co^{2+}, Mn^{2+} and Zn^{2+} complexation. However, according to the energetics calculated here, the $M(OxH)_2(Ac)_2$ stoichiometry is more stable for Co^{2+} and Zn^{2+} metal cations.

In the real system when the transition metal cations are separated by means of synergistic solvent extraction (SSX), the extractant and synergist are quite dilute (0.5 M Versatic 10 versus 0.35 M of LIX63 in Shellsol 2046 according to Cheng (2006)) plus the whole aqueous/organic system is being stirred continuously throughout the process. This means that during SSX of metal cations the hydroxyoxime molecules may exist in monomeric forms. If we estimate the thermodynamics of metal complexation for $M(OxH)_2(Ac)_2$ (equation 6.1) and $M(OxH)_3(Ac)_2$ (equation 6.4) using the sum of the energies of acetoin oxime monomers instead of dimers/trimers (Table 6.28) we can see that the formation of tris-oxime metal complexes becomes more favourable for all metal cations. This means that concentration of the reactants in SSX has a significant impact on selectivity of metal complexation as the synergistic effect in tris-oxime complexes is higher than that in bis-oxime ones that were shown to be the most energetically favourable for Co^{2+} and Zn^{2+} metal ions at high concentrations of hydroxyoxime. However, it should be noted the order in which metal cations are extracted (which we can get if we compare the thermodynamics of metal complexation for each metal cation with the most energetically favourable copper extraction) agrees well with the experimental data (Barnard and Tsuntsaeva, 2012) only in the case where the metal complexes of $M(OxH)_2(Ac)_2$ stoichiometry are formed (Cu^{2+} followed by Ni^{2+}, Co^{2+}, Zn^{2+} and Mn^{2+}) and not for the case of $M(OxH)_3(Ac)_2$ complex formation (Cu^{2+} followed by Ni^{2+}, Mn^{2+}, Co^{2+}, Zn^{2+}). This could mean either one of two things: 1) the potential energy surface of $M(OxH)_3(Ac)_2$ metal complexes was not fully scanned, therefore, previously located minima may not correspond to the true lowest energy structures, which may significantly affect relative energetics of metal complexes; 2) the potential energy

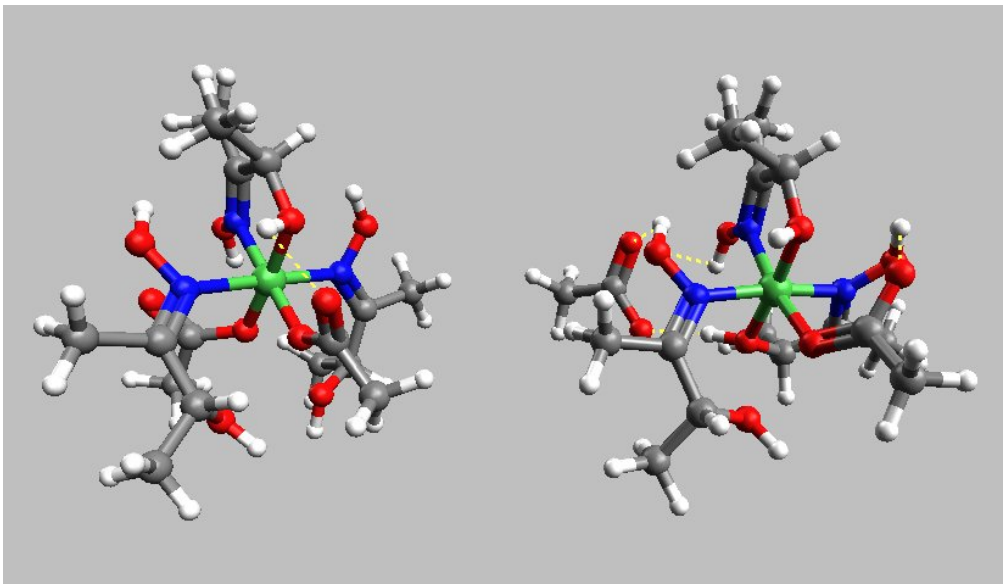

FIGURE 6.16: Suggested structures of tris-oxime metal complexes for the future study. Grey coloured atoms represent carbon, red - oxygen, dark blue - nitrogen and white - hydrogen. Dotted yellow lines represent inter- and intra-molecular hydrogen bonds.

surfaces of some other tris-oxime metal complexes (like the ones shown in Figure 6.16) should be investigated.

In order to draw more solid conclusions regarding complex stabilities it is also recommended to study the potential energy surfaces of the metal complexes with the ligands having larger hydrocarbon side-chains. Furthermore, along with the considered equilibria it would be informative to estimate the thermodynamics of the following ones:

$$M(H_2O)_6SO_{4(aq)} + (AcH)_{6(o)} \rightleftharpoons M(AcH)_4(Ac)_{2(o)} + (H_2O)_{6(aq)} + H_2SO_{4(aq)} \quad (6.5)$$

$$M(AcH)_4(Ac)_{2(o)} + (OxH)_{2(o)} \rightleftharpoons M(OxH)_2(Ac)_{2(o)} + (AcH)_{4(o)} \quad (6.6)$$

$$M(AcH)_4(Ac)_{2(o)} + (OxH)_{3(o)} \rightleftharpoons M(OxH)_3(Ac)_{2(o)} + (AcH)_{4(o)} \quad (6.7)$$

In addition, it would be also quite useful to estimate and compare the energetics of formation of two $M(OxH)_3Ac_2$ metal complexes bonded together via inter-molecular hydrogen bonding with the formation of two $M(OxH)_2Ac_2$ metal complexes, and the case when metal complexes of both stoichiometries are formed in the same system.

6.3.3 Conclusion

In this study modelling of metal complexation in the synergistic solvent extraction system of acetoin oxime and acetic acid was performed at the M06/6-31G(d,p)/LanL2DZ

level of theory. It was shown that both hydroxyoxime and carboxylic acid ligands exhibit a weak field nature which contributes to the formation of high-spin metal complexes for Co^{2+} and Mn^{2+} cations. This derivation agrees well with conclusions made by Vostrikova (2008) in her study of high-spin metal complexes of organic free radicals.

Based on the comparison of the energetics of the two types of complex (where in the first case acetoin oxime ligands were deprotonated and acetic acid ligands were neutral and vice versa in the second case) it was concluded that hydroxyoxime plays the role of the synergist (neutral ligand in the metal complex) and the carboxylic acid extracts the metal cations (anionic ligand in metal complexes). Moreover, this conclusion was strengthened when we compared the energetics of the hydroxyoxime-acetic acid anion hetero-oligomer with that of hydroxyoxime anion-acetic acid one, which showed that the system is significantly more stable when hydroxyoxime molecules stay neutral.

The thermodynamics of formation of two types of metal complexes was estimated, which showed that the formation of $M(OxH)_3(Ac)_2$ transition metal complexes is energetically more favourable than that of complexes with $M(OxH)_2Ac_2$ stoichiometry if the system of carboxylic acid/ hydroxyoxime is diluted so that both reagents are present in monomeric form. However, if hydroxyoxime oligomers are formed it was shown that the formation of the $M(OxH)_3(Ac)_2$ complex is more energetically favourable only for Ni^{2+}, Cu^{2+} and Mn^{2+} metal cations, while the $M(OxH)_2(Ac)_2$ complex is more likely to be formed in case of Co^{2+} and Zn^{2+} metal ions. It is interesting to point out that the synergistic shift is more significant in the case where $M(OxH)_3(Ac)_2$ metal complexes are formed.

For future studies it is recommended to estimate the thermodynamics of formation of different types of multi-complex systems, in particular the formation of $M(OxH)_3(Ac)_2 \cdots M(OxH)_3(Ac)_2$; $M(OxH)_2(Ac)_2 \cdots M(OxH)_2(Ac)_2$ and $M(OxH)_3(Ac)_2 \cdots M(OxH)_2(Ac)_2$ systems. It would be also interesting to estimate the thermodynamics of the equilibria shown in equations 6.5, 6.6 and 6.7. Furthermore, the study of the effect of the size of hydrocarbon side-chains would give us a broader picture of what is happening in the real system

6.4 References

Allen R.N., Shukla M.K., Burda J.V. and Leszezynski J. (2006) Theoretical Study of Interaction of Urate with Li^+, Na^+, K^+, Be^{2+}, Mg^{2+}, and Ca^{2+} Metal Cations. *Journal of Physical Chemistry A* **110**, 6139-6144.

Atta-Fynn R., Bylaska E.J., Schenter G.K. and de Jong W.A. (2011) Hydration shell structure and dynamics of curium(III) in aqueous solution: first principles and empirical studies. *Journal of Physical Chemistry A* **115**, 4665-4677.

Barnard K.R., Turner N.L. and Shiers D.W. (2010) LIX63 stability in the presence of Versatic 10 under proposed commercial extract and strip conditions, part III: Effect of manganese and cobalt loading on oxime stability at 30 ^{o}C. *Hydrometallurgy* **104**, 268-277.

Barnard K.R. and Turner N.L. (2011) The effect of temperature on hydroxyoxime stability in the LIX 63-Versatic 10-tributyl phosphate synergistic solvent extraction system under synthetic nickel laterite conditions. *Hydrometallurgy* **109**, 245-251.

Barnard K.R., Nealon G.L., Ogden M.I. and Skelton B.W. (2010) Crystallographic determination of three Ni-α-hydroxyoxime-carboxylic acid synergist complexes. *Solvent Extraction and Ion exchange* **28**, 778-792.

Barnard K.R., McIldowie M., Nealon G.L., Ogden M.I. and Skelton B.W. (2011) X-Ray Crystal Structures of Nickel and Cobalt Alpha-Hydroxyoxime-Carboxylic Acid Synergist Complexes. *In Proceedings of the 19th International Solvent Extraction Conference ISEC 2011*, Eds F. Valenzuela L., B.A. Moyer, Gecamin Ltda., Santiago, Chile, 161.

Barnard K.R. and Tsuntsaeva M.N. (2012) The effect of hydroxyoxime isomer conformation on metal extraction in the LIX 63/ Versatic 10 synergistic system. *Solvent Extraction and Ion exchange* **30**, 566-578.

Castresana J.M., Elizalde M.P., Aguilar M. and Cox M. (1988) Synergistic extraction of nickel by mixtures of alpha-hydroxyoximes and carboxylic acids. *Solvent Extraction and Ion exchange* **6**(2), 265-274.

Cheng C.Y. and Urbani M.D. (2005a) *Solvent extraction process for separation cobalt and/or manganese from impurities in leach solutions.* Patent Application No PCT/AU2005/000088 and Patent Publication No. WO 2005/073415 A1.

Cheng C.Y. and Urbani M.D. (2005b) *Solvent extraction process for separation cobalt and/or nickel from impurities in leach solutions.* Patent Application No PCT/AU2005/000099 and Patent Publication No. WO 2005/073416 A1.

Cheng C.Y. (2006) Solvent extraction of nickel and cobalt with synergistic systems consisting of carboxylic acid and aliphatic hydroxyoxime. *Hydrometallurgy* **84**, 109-117.

Silva E.S.A., Duarte H.A. and Belchior J.C. (2006) An approach based on genetic algorithms and DFT for studying clusters: $(H2O)_n$ $(2 \leqslant n \geqslant 13)$ cluster analysis. *Journal of Chemical Physics* **323**, 553-562.

Flett D.S. and Titmuss S. (1969) Synergistic effect of LIX63 on the extraction of copper and cobalt by naphthenic acid. *Journal of Inorganic and Nuclear Chemistry* **31** (8), 2612-2613.

Flett D.S., Cox M., and Heels J.D. (1974) Extraction of nickel by a-hydroxy oxime/lauric acid mixtures. *Society of Chemical Industry* **3**, 2560-2575.

Frisch M.J., Trucks G.W., Schlegel H.B., Scuseria G.E., Robb M.A., Cheeseman J.R., Scalmani G., Barone V., Mennucci B., Petersson G.A., Nakatsuji H., Caricato M., Li X., Hratchian H.P., Izmaylov A.F., Bloino J., Zheng G., Sonnenberg J.L., Hada M., Ehara M., Toyota K., Fukuda R., Hasegawa J., Ishida M., Nakajima T., Honda Y., Kitao O., Nakai H., Vreven T., Montgomery J.A., Jr., Peralta J.E., Ogliaro F., Bearpark M., Heyd J.J., Brothers E., Kudin K.N., Staroverov V.N., Kobayashi R., Normand J., Raghavachari K., Rendell A., Burant J.C., Iyengar S.S., Tomasi J., Cossi M., Rega N., Millam J.M., Klene M., Knox J.E., Cross J.B., Bakken V., Adamo C., Jaramillo J., Gomperts R., Stratmann R.E., Yazyev O., Austin A.J., Cammi R., Pomelli C., Ochterski J.W., Martin R.L., Morokuma K., Zakrzewski V.G., Voth G.A., Salvador P., Dannenberg J.J., Dapprich S., Daniels A.D., Farkas ., Foresman J.B., Ortiz J.V., Cioslowski J. and Fox D.J. (2009) *Gaussian*, Inc., Wallingford CT.

Jahn H. and Teller E. (1937) Stability of Polyatomic Molecules in Degenerate Electronic States. I. Orbital Degeneracy. *Proceedings of the Royal Society of London. Series A, Mathematical and Physical Sciences (1934-1990)* **161**(905), 220-235.

Joseph W.O. 2000 Thermochemistry in Gaussian. *Gaussian, Inc*, 2-19.

Garcia-Suarez V. and Lambert C.J. (2011) First-principles scheme for spectral adjustment in nanoscale transport. *Condensed Matter/Mesoscale and Nanoscale Physics* **2**, 1-8.

Georgieva I., Binev D., Trendafilova N. and Bauer G. (2003) DFT study of hydrogen-bonded dimers and tetramer of glyoxilic acid oxime. *Chemical Physics* **286**, 205-217.

Georgieva I., Trendafilova N. and Binev D. (2003) Vibrational properties of glyoxilic acid oxime dimers and tetramer. Ab initio and DFT study. *Vibrational Spectroscopy* **31**, 143-154.

Kamilla M., Henryk K. and Leonard M. P. (2005) Interaction of Na(I), Ni(II) and Cu(II) with 2-cyano- 2-(hydroxyimino)acetic acid: Spectroscopic and theoretical studies. *Polyhedron* **24**, 1175-1184.

Maja G.P., Matija Z., Carl-Wilhelm S. and Claude D. (2010) DFT study of the JahnTeller effect in Cu(II) chelate complexes. *Journal of Molecular Structure (Theochem)* **954**, 80-85.

Mehdi B., Moritz von H., Sadegh S. and Gernot F. (2011) Energy decomposition analysis of the metaleoxime bond in [MRC(NOH)C(NO) R2] (M=Ni(II), Pd(II), Pt(II), R=CH3, H, F, Cl, Br, Ph, CF3). *Journal of Organometallic Chemistry* **696**, 2976-2984.

Nedeljkovic Z. (1998) *Andrew Forrest : a key to Murrin Murrin's past and future.* Mining chronicle: West Perth, W.A.

Ojanen J. and Rantala T.T. (2009) Electronic Structure and Absorption Spectrum of Disperse Red 1: Comparison of Computational Approaches. *The Open Chemical Physics Journal.* **2**, 37-46.

Peters B., Heyden A., Bell A.T. and Chakraborty A. (2004) A growing string method for determining transition states: Comparison to the nudged elastic band and string methods. *Journal of Chemical Physics.* **120**(17), 7877-7886.

Pesonen H., Aksela R. and Laasonen K. (2007) Density functional complexation study of metal ions with amino polycarboxylic acid ligands: EDDHA and HBED in comparison to EDTA, EDDS, ODS, and ISA. *Journal of Molecular Structure: THEOCHEM* **804**, 101-110.

Ramalho T.C., da Cunha E.F.F. and de Alencastro R.B. (2004) A density functional study on the complexation of ethambutol with divalent cations. *Journal of Molecular Structure (Theochem).* **676**, 149-153.

Rappe A.K., Casewit C.J., Colwell K.S., Goddard W.A. and Skiff W.M. (1992) UFF, a full periodic table force field for molecular mechanics and molecular dynamics simulations. *Journal of the American Chemical Society.* **114**(25), 1002410035.

Rydberg J., Cox M., Musikas C. and Choppin G.R. (2004) *Solvent extraction principles and practice.* New York: Taylor and Francis Press.

Schläfer H.L. and Gliemann G. (1969) *Basic Principles of Ligand Field Theory.* Wiley Interscience: New York.

Schmidt M.W., Baldridge K.K., Boatz J.A., Elbert S.T., Gordon M.S., Jensen J.H., Koseki S., Matsunaga N., Nguyen K.A., Su S.J., Windus T.L., Dupuis M., Montgomery J.A. (1993) General atomic and molecular electronic structure system. *Journal of Computational Chemistry* **14**, 1347-1363.

Stewart J.J.P. (2007) Optimization of parameters for semiempirical methods. V. Modification of NDDO approximations and application to 70 elements. *Journal of Molecular Modeling* **13**, 1173-213.

Victor P. (2010) The band JahnTeller effect: A new perspective on an old problem. *Journal of Molecular Structure* **838**, 13-19.

Vostrikova K.E/ (2008) High-spin molecules based on metal complexes of organic free radicals. *Coordination Chemistry Reviews* **252**, 14091419.

Xia Y., Wang X., Zhang Y. and Luo B. (2011) Complexation of alkalimetal cations by conformationally rigid, stereoisomeric calix[4]arene crown ethers: A density functional theory study. *Computational and Theoretical Chemistry.* **967**, 235-242.

Yang Y., Weaver M.N. and Merz K.M.Jr. (2009) Assessment of the "6-31+G** + LANL2DZ" mixed basis set coupled with density functional theory methods and the effective core potential: prediction of heats of formation and ionization potentials for first-row-transition-metal complexes. *Journal of Physical Chemistry A* **113**(36), 9843-9851.

Zhao Y. and Truhlar D.G. (2008) The M06 suite of density functionals for main group thermochemistry, thermochemical kinetics, noncovalent interactions, excited states, and transition elements: two new functionals and systematic testing of four M06-class functionals and 12 other functionals. *Theoretical Chemistry Accounts* **120**, 215-241.

Chapter 7

Conclusions

The main goal of the current research was to evaluate theoretical models for metal complexation in the synergistic solvent extraction (SSX) system consisting of LIX63 hydroxyoxime and Versatic10 carboxylic acid. In addition to this main goal it was also interesting to develop theoretical models for studying the physical and chemical properties of the main components of the SSX system and key processes occurring in it. Theoretical models were selected from the methods available in Density Functional Theory (DFT). The selection process was based on the comparison of the results derived from calculations using different DFT methods with those obtained with post-Hartree-Fock methods, as well as against experimental data from CSIRO. This study is valuable from both a scientific and industrial perspective as it identifies a model that shows good agreement with experiment and can be used for further study of the properties of the SSX system. Furthermore, it can be used to define the structures of metal complexes in various environments and at different conditions. This knowledge can be used in order to improve the selectivity of metal separation by LIX63 hydroxyoxime and Versatic10 carboxylic acid. In this chapter the main conclusions from the study are considered and recommendations for the future research are given.

Theoretical Investigation of *Syn/Anti* Acetoin Oxime Isomerisation

In order to save computing time, acetoin oxime was chosen to describe the properties of the actual target molecule (LIX63 main component). Initially it seemed reasonable to expect that the thermodynamics of equilibrium between *syn* and *anti* isomers of acetoin oxime would be similar to those of LIX63 *syn/anti* isomerisation. Based on a review of the literature (Georgieva and Trendafilova, 2006; Ronchin *et al.*, 2008; Zhao and Truhlar, 2008) a range of methods was selected for studying the potential energy surface (PES) and thermodynamics of equilibrium between the lowest energy structures of *syn*

and *anti* acetoin oxime isomers. Explicit theoretical study of the *syn/anti* acetoin oxime equilibrium with each of the selected methods has shown that the B3LYP DFT functional provides the best overall results in modelling of this type of system in combination with the 6-31G(d,p) and/or 6-31++G(d,p) basis sets as this gives the closest results to the MP2/aug-cc-vVTZ method with the lowest demand for computer resources.

The M06 method also gives a good description of *syn/anti* acetoin oxime equilibrium and kinetics of *anti* to *syn* isomerisation when used with the same 6-31G(d,p) and/or 6-31++G(d,p) basis sets as compared to the MP2/aug-cc-pVTZ level of theory and therefore also can be used for modelling organic constituents of the SSX system. Both B3LYP and M06 locate the same global minima for *syn* and *anti* isomers of acetoin oxime. Bond lengths, bond angles and dihedral angles of the lowest energy acetoin oxime isomers optimised with these two methods are very similar. However, it should be noted that the optimisation process from the same starting point takes a bit longer with M06 than with B3LYP and in some cases the energetics calculated using M06 methods are less accurate as compared to the MP2/aug-cc-pVTZ results.

The main advantage of M06 over B3LYP for this particular study is that in addition to reasonably good kinetics and thermodynamics for organic systems it is also known to provide good theoretical descriptions of the systems containing heavy elements (Zhao and Truhlar, 2008), such as organometallic complexes of Ni^{2+}, Co^{2+}, Cu^{2+}, Mn^{2+} and Zn^{2+} with hydroxyoxime and carboxylic acid. As was shown for the example of the 2-acetylthiophene system that contains a sulphur atom, the thermodynamics of equilibrium between *syn* and *anti* isomers of this compound is well described by the M06 method as compared to experiment, while B3LYP method is shown to have poor performance. In this sense, it is very convenient to have one method which is suitable for studying not only systems containing heavy atoms like 2-acetylthiophene or organometallic complexes, for instance, but also the properties of organic systems like the hydroxyoxime/carboxylic acid synergistic solvent extraction system.

Unfortunately, theoretically estimated thermodynamics for the *syn/anti* equilibrium of acetoin oxime did not match the experimental equilibrium distribution between *syn* and *anti* isomers of the LIX63 main component. Furthermore, theoretically estimated barriers for *syn*$\rightleftharpoons$*anti* acetoin oxime isomerisation using mechanisms selected from the literature, also did not match the corresponding values found experimentally for *syn*/*anti* LIX63 hydroxyoxime interconversion. Based on the results it was concluded that the effect of R groups on the *syn/anti* hydroxyoxime equilibrium are in fact significant. The spatial orientation of the hydrocarbon side-chains in the R groups of the lowest energy *syn* and *anti* structures of LIX63 may be different, which may in turn affect their relative stabilities and, as a result, the equilibrium distribution. In the case of acetoin oxime both isomers are identical with respect to the spatial orientation of R groups. Therefore, as the next step it was decided to study the effect of hydrocarbon

side-chains on the equilibrium between *syn* and *anti* isomers of hydroxyoxime.

Theoretical investigation of the Effect of the Hydrocarbon Side-chains on the *Syn/Anti* Equilibrium and Kinetics

The potential energy surface scan for hydroxyoximes with hydrocarbon side-chains equal to C_2H_5-, C_3H_7- and C_4H_9- has been performed using both M06 and B3LYP methods in combination with 6-31G(d,p) and 6-31++G(d,p) basis sets. It was shown that the addition of diffuse functions to the basis set improves the energetics as compared to both the experimental and calculated MP2/aug-cc-pVTZ thermodynamics. It was also shown that the process of minima location on the potential energy surface was not significantly affected by the addition of the diffuse functions to the basis set and the same conformations were found to be the lowest energy structures with both 6-31G(d,p) and 6-31++G(d,p) basis sets.

When we compared the potential energy surfaces of different hydroxyoximes calculated with the M06 and B3LYP methods, it was found that the lowest energy conformers of *anti*-hydroxyoximes located with the M06 method were different from those located with B3LYP. As compared to the MP2 calculations, the global minima located using the M06 functional were found to be incorrect. The supposed explanation for this is that the Coulombic interaction between the carbon atoms in gauche-gauche oriented (GG) R groups is overestimated by the M06 functional. This actually is known to be quite a common drawback of the M06 family functionals (Gruzman *et al.*, 2009). Therefore, the M06 method cannot be recommended for studying the potential energy surfaces of hydroxyoximes or any similar type of system.

Based on the results described in this chapter it is recommended to use the B3LYP hybrid density functional with the 6-31G(d,p) basis set for modelling aliphatic α-hydroxyoximes or similar types of systems as the best compromise between accuracy and computational cost. However, the overall equilibrium between *syn* and *anti* isomers of hydroxyoxime was also well described by the M06 method. This means that this method can also be used for studying the thermodynamics of hydroxyoximes if the global minima are known for both isomers.

During this study it was determined that the thermodynamics of interconversion between *syn* and *anti* isomers of 2,5-dimethyl-4-hydroxyhexan-3-oxime (R=C_3H_7) is in good agreement with experimental equilibrium between *syn* and *anti* isomers of 5,8-diethyl-7-hydroxydodecan-6-oxime. It was also shown that a further increase in the size of the hydrocarbon side-chains does not have any significant effect on the thermodynamics of the *syn/anti* hydroxyoxime equilibrium.

The effect of the size of the hydrocarbon side-chains on the kinetics of the

syn/anti interconversion has also been studied. It was shown that the energy barriers for the hydrogen atom migration and rotation of the functional group about a single C-N bond in tautomerisation mechanisms via enamine and nitroso compounds are not changed significantly when the size of the hydrocarbon side-chains is increased from R=CH_3 to R=C_4H_9. However, the energy barrier for *syn/anti* hydroxyoxime interconversion calculated via the inversion mechanism is systematically lowered when isomerisation is considered between *syn* and *anti* isomers with larger R groups. This leads us to the conclusion that the inversion mechanism is the most probable mechanism for 5,8-diethyl-7-hydroxydodecan-6-oxime *syn/anti* isomerisation. However, it should be noted that even though the barrier for the inversion mechanism was significantly lower for the system with R=C_4H_9 than that with R=CH_3 it is still overestimated as compared to the experimental value. Therefore, further estimation of the energy barriers for the inversion mechanism as a function of size of hydrocarbon side-chains (for the systems with R groups larger than C_4H_9 on both ends of the molecule) is required to strengthen the choice of the mechanism for the *syn/anti* hydroxyoxime isomerisation.

DFT Study of Hydroxyoxime Oligomerisation

The IR spectra of the *anti* isomer of LIX63 hydroxyoxime has been measured experimentally and compared with the IR spectra of 2,5-dimethyl-4-hydroxyhexan-3-oxime (R=C_3H_7) calculated at the B3LYP/6-31G(d,p) level of theory. Based on this comparison, *anti*-5,8-diethyl-7-hydroxydodecan-6-oxime (main component of LIX63) appears likely to be present in oligomeric form in the environment of a non-polar aliphatic solvent. This suggests an alternative mechanism for *syn/anti* isomerisation involving hydrogen atom migration along intermolecular hydrogen bonds.

Various structures of acetoin oxime dimers with different types and numbers of inter-molecular hydrogen bonds have been optimised at the B3LYP/6-31G(d,p) and B3LYP/6-31++G(d,p) levels of theory. Acetoin oxime dimerisation was considered between 2 *anti*, 2 *syn* and a pair of *syn* and *anti* isomers. The most stable structures of *anti-syn* and *syn-syn* acetoin oxime dimers predicted by both B3LYP/6-31G(d,p) and B3LYP/6-31++G(d,p) methods were identical. However, the lowest energy structure of the *anti-anti* acetoin oxime dimer found with the B3LYP/6-31G(d,p) method was different from that predicted by calculations at the B3LYP/6-31++G(d,p) level. The magnitude for the BSSE correction is significantly lower when the diffuse functions (for both hydrogen and heavy atoms) are added. Therefore it is expected that more reliable results will be achieved with calculations at the B3LYP/6-31++G(d,p) level of theory. During this study of the acetoin oxime oligomerisation process it was found that the magnitude for the BSSE correction is higher for the dimers in which -COH hydroxyl group plays the role of the donor when forming inter-molecular hydrogen bonds between

two monomers.

As compared to the B3LYP/6-31++G(d,p) calculations, the lengths of hydrogen bonds are overestimated by the B3LYP/6-31G(d,p) method if there is a strong interaction between two monomers forming the dimer and underestimated if this intermolecular interaction is weak. This agrees well with information found in the literature (Jeffrey, 1997). It is interesting to note that the description of acetoin oxime dimers in which there is only one inter-molecular hydrogen bond is very similar according to both these methods. Intra-molecular hydrogen bonds are also equally well described by both B3LYP/6-31G(d,p) and B3LYP/6-31++G(d,p) methods.

Comparing the thermodynamics of different oligomerisation processes it was shown that energetically it is more favourable for acetoin oxime to exist in the form of long chain/cyclic oligomers where the *syn* and/or *anti* isomers of hydroxyoxime interact with each other via NOH-OC and NOH-N types of intermolecular hydrogen bonding. The IR spectra of the lowest energy *anti-anti* acetoin oxime tetramers were calculated at the B3LYP/6-31++G(d,p) level of theory and compared with the experimental data of *anti*-5,8-diethyl-7-hydroxydodecan-6-oxime IR spectra. It was shown that the calculated IR spectra of acetoin oxime tetramers correspond well to the experimental IR spectra of *anti* isomer of the LIX63 main component. This supports our conclusion that hydroxyoximes exist in oligomeric form where the *syn* and/or *anti* isomers of hydroxyoxime interact with each other via different types of intermolecular hydrogen bonding.

The kinetics of the *syn*$\rightleftarrows$*anti* acetoin oxime isomerisation between *syn-syn* and *anti-anti* acetoin oxime dimers with NOH-N type of inter-molecular hydrogen bonding were estimated at the B3LYP/6-31++G(d,p) level of theory using the tautomerisation mechanism via a nitroso compound. In this mechanism hydrogen atoms are migrated from NOH groups to the nitrogen atoms of the opposite molecule simultaneously along the NOH$\cdots$N hydrogen bonds. The calculated energy barrier for this type of hydrogen migration (when considered inside the oligomer) is significantly lower than the barrier of a hydrogen migration within a monomer. This increases the probability of *syn/anti* hydroxyoxime interconversion via tautomerisation mechanisms as compared to the inversion mechanism when hydroxyoxime is present in oligomeric form.

Modelling Metal Complexation in Synergystic Solvent Extraction

Based on a literature review the M06 functional was chosen to study metal complexation in the synergistic solvent extraction system of acetoin oxime and acetic acid as, according to Zhao and Truhlar (2008), it was specifically parametrised for modelling organometallic systems. For the main group elements, the 6-31G(d,p) basis set was chosen as it gives one of the best descriptions of organic systems like hydroxyoximes and carboxylic acids (including intra-molecular interactions via hydrogen bonding) with the

lowest demand for computer resources. In accordance with recommendations of Yang *et al.* (2009), the LanL2DZ pseudo-potential basis set was chosen to describe the atomic orbitals of transition metals.

It is a well known fact (Schläfer and Gliemann, 1969) that with respect to the nature of ligands, Co^{2+} and Mn^{2+} cations may form both high and low spin organometallic complexes. Therefore it was of interest to determine the strength of binding of hydroxyoxime and carboxylic acid ligands to the metal cation. Comparing the energetics of Co^{2+} and Mn^{2+} carboxylic acid-hydroxyoxime complexes with metal centres having different multiplicities, it was shown that both hydroxyoxime and carboxylic acid ligands have a weak field nature which contributes to the formation of a high-spin metal complexes for Co^{2+} and Mn^{2+} cations.

In modelling metal complexes of $M(Ox)_2AcH_2$ and $M(OxH)_2Ac_2$ stoichiometries it was shown that in the lowest energy structures of Ni^{2+}, Co^{2+} and Zn^{2+} complexes, the lengths of O-H covalent bonds and $OH\cdots O$ hydrogen bonds (between acetoin oxime and acetic acid ligands) are nearly identical. Therefore for these complexes it is not clear which ligand is getting deprotonated during metal complexation. Unfortunately due to limited time the potential energy surfaces of metal complexes were not fully scanned and so more stable complexes may be located in which it is clearer which of the ligands is deprotonated. For example, in the lowest energy structures of $Cu(OxH)_2Ac_2$ and $Mn(OxH)_2Ac_2$ complexes it is clear that acetic acid is deprotonated and acetoim oxime ligands stay neutral. In order to see which of the two ligands is more likely to get deprotonated an additional study of hydroxyoxime-acetic acid oligomers was performed, where in the first case acetoin oxime was neutral and acetic acid deprotonated and vice versa in the second case. When the energetics were compared it was clear that the system of these two ligands is significantly more stable when hydroxyomime molecules stay neutral and carboxylic acids are deprotonated.

In this study it was also shown that the lowest energy structure of the $Ni(OxH)_2Ac_2$ complex (Fig. 6.6) optimised at the M06/6-31G(d,p)/LanL2DZ level of theory agreed well with the crystallographically determined structure of the $Ni(OxH)_2Ac_2$ complex by Barnard *et al.* (2010) and not with the proposed structure of the Ni complex of the same stoichiometry suggested by Castresana *et al.* (1988).

In order to understand which stoichiometry is more favourable for metal complexes, the potential energy surfaces of $M(OxH)_2Ac_2$ and $M(OxH)_3Ac_2$ (where M corresponds to either Ni, Co, Cu, Mn or Zn metal centres) were first scanned at the M06/6-31G(d,p)/LanL2DZ level of theory and then the Gibbs free energies of metal complexation were estimated using the lowest energy structures of each metal complex. For the case when *anti*-hydroxyoximes are present as oligomers before the complex is formed, we have found that the complex of $M(OxH)_2Ac_2$ stoichiometry is more likely to be formed during the extraction of Co^{2+} and Zn^{2+} cations while the $M(OxH)_3Ac_2$

metal complexes are more energetically favourable for the other three metal cations.

In the case when hydroxyoxime is dilute and its molecules are present as monomers surrounded by molecules of an aliphatic non-polar solvent, it gave a significant increase in $\triangle$G magnitude (the precess became more exothermic) of metal complexation (relative to the value of $\triangle$G for hydroxyoxime dimerisation from monomers in case of $M(OxH)_2Ac_2$ metal complexes and relative to the value of $\triangle$G for hydroxyoxime trimerisation from monomers in the case of $M(OxH)_3Ac_2$ metal complexes). In this case the probability of formation of $M(OxH)_3Ac_2$ metal complexes was shown to be significantly higher than the probability of $M(OxH)_2Ac_2$ complex formation for all metal cations. Experimentally it was found that 1:3:2 metal:hydroxyoxime:carboxylic acid stoichiometry is more likely to be correct (Barnard *et al.*, 2010; Barnard and Tsuntsaeva, 2012).

Recommendations

As we had both finite time and computer resources during this project, not every single goal that we wanted to achieve was accomplished. Therefore, here we present a list of future work recommendations for those who are interested in this topic:

1) The DFT methods selection for studying hydroxyoxime isomerisation and oligomerisation was primarily based on comparison of thermodynamics of acetoin oxime Z/E interconversion derived by each considered method with the results derived at the MP2/aug-cc-pVTZ level of theory. Due to the reasons highlighted above the latter method was not considered in further studies and the level of its accuracy regarding modelling hydroxyoxime interconversion and oligomerisation was not determined by comparing its results with experimental data. The model hydroxyoxime with the minimal size of the hydrocarbon side-chains capable of giving a good description of the experimental equilibrium between *syn* and *anti* isomers of LIX63 hydroxyoxime was determined at the B3LYP/6-31G(d,p) level of theory and it would be interesting to see if thermodynamics of this model hydroxyoxime Z/E interconversion estimated at the MP2/aug-cc-pVTZ level of theory also agrees well with the experimental data of LIX63 hydroxyoxime *syn*/*anti* isomerisation.

2) It was shown that an increase in size of hydrocarbon side-chains of hydroxyoximes has a significant effect on equilibrium between *syn* and *anti* isomers when R groups on both sides of the molecule are equal to CH_3 and/or C_2H_5. However, it would be also interesting to see how this equilibrium is changed if the R groups on both ends of the molecule have a different size. Furthermore it could be tested if the *syn/anti* equilibrium is affected when the hydrogen atom on carbon in -C(H)R-OH functional group of hydroxyoxime is substituted with CH_3 and/or a larger size R group.

3) The effect of further increases in the size of hydrocarbon side-chains on the energy barrier for the *syn/anti* hydroxyoxime interconversion via an inversion mechanism should be investigated.

4) As it was shown by Harris *at al.* (2011) that when the solvent is of aromatic nature hydroxyoximes are most likely to be present in monomeric form. Theoretically, at the B3LYP/6-31G(d,p) level of theory it was shown that when the *syn/anti* hydroxyoxime isomerisation is considered between monomers, it is most likely to occur via an inversion mechanism. However, when isomerisation is considered within hydroxyoxime oligomers tautomerisation via nitroso compound becomes more favourable. Experimental data for the kinetics of *syn* to *anti* and *anti* to *syn* 5,8-diethyl-7-hydroxydodecan-6-oxime interconversion, kindly provided to us by Dr. Barnard, was measured in an

aliphatic solvent and we believe that for better understanding of the *syn/anti* hydroxyoxime interconversion process it would also be interesting to measure the rate constants of this in the environment of an aromatic solvent.

5) A comprehensive scan of the potential energy surface of acetoin oxime dimers was performed at the B3LYP/6-31G(d,p) and B3LYP/6-31++G(d,p) levels of theory, where the latter method was recommended as the method providing better description of an inter-molecular interaction via hydrogen bonding. However, due to constraints of time the PES scans of hydroxyoxime trimers and tetramers have not been performed. It is recommended to perform these scans as the lowest energy structures for hydroxyoxime dimers and trimers may be different from those that we found, which may affect the final conclusions. A very important factor to consider in this case is that the main component of LIX63 (5,8-diethyl-7-hydroxydodecan-6-oxime) is quite bulky (with R=R'=C_7H_{15} in R-C(NOH)-CH(OH)-R'). Therefore it is important to use the model of hydroxyoxime with largest possible R groups (depending on the available computer resources) on each side of a molecule as it may not be possible to form some structures of acetoin oxime oligomers using hydroxyoximes with larger R groups due to the repulsion between hydrocarbon side chains. As an alternative to *ab initio* modelling it would also be reasonable to consider the use of a QM/MM method where the bulky R groups of hydroxyoxime are optimised using molecular mechanics and the functional groups are treated with quantum mechanics. This would allow the study of the potential energy surfaces of 5,8-diethyl-7-hydroxydodecan-6-oxime oligomers.

6) Another very interesting aspect to look at in the study of hydroxyoxime oligomerisation would be the effect of the size of the hydrocarbon side chains on the energy barrier of *syn/anti* isomerisation considered via a tautomerisation mechanism within hydroxyoxime oligomers.

7) In studying the potential energy surfaces of $M(OxH)_2Ac_2$ and $M(Ox)_2AcH_2$ metal complexes at the M06/6-31G(d,p)/LanL2DZ level of theory we made an assumption and inspected only those structures in which there is the largest number of intramolecular hydrogen bonds formed between acetic acid and acetoin oxime ligands, expecting these structures to be lower in energy than those with less of this type of intramolecular interaction. This may not be the case and therefore, in order to check it, it is recommended to perform the PES scan for each structure of $M(OxH)_2Ac_2$ and $M(Ox)_2AcH_2$ metal complexes presented in this study by rotating the carboxylic acid ligand around the O-M bond, where O - is an oxygen of a carboxylic acid ligand. It also should be of great interest to perform these scans using ligands with hydrocarbon side-chains larger than R=CH_3 as it will give a certain limit to the amount of structures which could possibly be formed due to the repulsion between hydrocarbon side chains.

Ideally, if the time and computer resources would allow to do so, the ligands should be the structures of LIX63 hydroxyoxime and Versatic10 carboxylic acid. Development of an appropriate QM/MM method could also be considered in this instance.

8) The same principle (choosing the structure with the highest number of intramolecular hydrogen bonds) was used in studying the potential energy surfaces of $M(OxH)_3Ac_2$ acetic acid-acetoin oxime metal complexes; therefore, it is also required to perform the PES scan of each $M(OxH)_3Ac_2$ structure with respect to the position of a carboxylic acid ligand, using the ligands with a size of the hydrocarbon side-chains as close to the real molecules of hydroxyoxime and carboxylic acid as possible. In addition, it was shown that the selectivity shift of hydroxyoxime addition is higher for the case when $M(OxH)_3Ac_2$ metal complexes are formed. However, in contrast to $M(OxH)_2Ac_2$, the order in which metal cations are extracted is not well reproduced for the $M(OxH)_3Ac_2$ stoichiometry, which means the potential energy surface of this and/or similar 1:3:2 metal:hydroxyoxime:carboxylic acid complexes requires further investigation. Furthermore, in order to draw better conclusions regarding the stabilities of metal complexes of different stoichiometries, other equilibria (like those shown in 6.5, 6.6 and 6.7) should be considered.

9) It will also be interesting to estimate the thermodynamics of formation of different types of multi-complex systems; in particular the formation of $M(OxH)_3Ac_2\cdots M(OxH)_3Ac_2$; $M(OxH)_2Ac_2\cdots M(OxH)_2Ac_2$ and $M(OxH)_3Ac_2\cdots\cdots M(OxH)_2Ac_2$ systems as it will provide some insights for better understanding of the metal complexation process with LIX63 hydroxyoxime and Versatic10 carboxylic acid.

7.1 References

Barnard K.R., Nealon G.L., Ogden M.I. and Skelton B.W. (2010) Crystallographic determination of three Ni-α-hydroxyoxime-carboxylic acid synergist complexes. *Solvent Extraction and Ion exchange* **28**, 778-792.

Barnard K.R., Turner N.L. and Shiers D.W. (2010) LIX63 stability in the presence of Versatic 10 under proposed commercial extract and strip conditions, part III: Effect of manganese and cobalt loading on oxime stability at 30 ^{o}C. *Hydrometallurgy* **104**, 268-277.

Barnard K.R. and Tsuntsaeva M.N. (2012) The effect of hydroxyoxime isomer conformation on metal extraction in the LIX 63/ Versatic 10 synergistic system. *Solvent Extraction and Ion exchange* **30**, 566-578.

Castresana J.M., Elizalde M.P., Aguilar M. and Cox M. (1988) Synergistic extraction of nickel by mixtures of alpha-hydroxyoximes and carboxylic acids. *Solvent Extraction and Ion exchange* **6**(2), 265-274.

Georgieva I. and Trendafilova N. (2006) Comprehensive DFT and MO studies on glyoxilic acid oxime and related ions in gas phase and solution: Conformations, basicities and acidities. *Journal of Chemical Physics* **321**, 311-324.

Gruzman D., Karton A. and Martin J. M. L. (2009) Performance of Ab Initio and Density Functional Methods for Conformational Equilibria of CnH2n+2 Alkane Isomers (n = 4-8). *The Journal of Physical Chemistry A* **113**, 1197411983.

Harris D.J., Roach B.D. and Tasker P.A. (2011) Diffusion-NMR elucidation of modifier-oxime interactions. *19th International Solvent Extraction Conference*, 1-8.

Jeffrey G.A. (1997) *An introduction to hydrogen bonding.* Oxford: University Press.

Ronchin R., Bortoluzzi M. and Vavasori A. (2008) A DFT study on secondary reaction pathways in the acid-catalysed Backmann rearrangement of cyclohexanone oxime in aprotic solvent. *Journal of Molecular Structure* **858**, 46-51.

Schläfer H.L. and Gliemann G. (1969) *Basic Principles of Ligand Field Theory.* Wiley Interscience: New York.

Yang Y., Weaver M.N. and Merz K.M.Jr. (2009) Assessment of the "6-31+G** + LANL2DZ" mixed basis set coupled with density functional theory methods and the effective core potential: prediction of heats of formation and ionization potentials for first-row-transition-metal complexes. *Journal of Physical Chemistry A* **113**(36), 9843-9851.

Zhao Y. and Truhlar D.G. (2008) The M06 suite of density functionals for main group thermochemistry, thermochemical kinetics, noncovalent interactions, excited states, and transition elements: two new functionals and systematic testing of four M06-class functionals and 12 other functionals. *Theoretical Chemistry Accounts* **120**, 215-241.

Appendix A

CD content

List of documents Microsoft Excel:

1. 1-Acetoin Oxime PES as a function of method and basis set.xlsx
2. 2-Acetoin Oxime Thermodynamics and Kinetics.xlsx
3. 3-Acetoin Oxime PES at the B3LYP 6-31G(d,p). Thermodynamics.xlsx
4. 4-Thermodynamics of 4-hydroxyhexane-3-oxime.xlsx
5. 5-Thermodynamics of 2,5-dimethyl-4hydroxyhexan-3-oxime.xlsx
6. 6-Thermodynamics of Acetoin Oxime Dimers.xlsx
7. 7-Thermodynamics of Acetoin Oxime Trimers.xlsx
8. 8-Thermodynamics of Acetoin Oxime Tetramers.xlsx
9. 9-Thermodynamics of M(Ox)2(AcH)2 metal complexes.xlsx
10. 10-Thermodynamics of M(OxH)2(Ac)2 metal complexes.xlsx
11. 11-Thermodynamics of M(Ox)2(OxH) metal complexes.xlsx
12. 12-Thermodynamics of M(OxH)3(2+) metal complexes.xlsx
13. 13-Metal complexation in SSX.xlsx
14. 14-Full Data.xlsx

List of folders containing molecular structures:

1. a-AcetoinOxime-PES
2. b-AcetoinOximeThermodynamicsKinetics
3. c-4-HydroxyHexane-3-Oxime
4. d-2,5-Dimethyl-4-HydroxyHexan-3-Oxime

5. e-AcetoinOximeDimers
6. f-AcetoinOximeTrimers
7. g-AcetoinOximeTetramers
8. h-M(OxH)_2(Ac)_2 MetalComplexes
9. i-M(OxH)_3(2+) MetalComplexes

Intellectual Property Clearance and Research Partners Interests:

Keith Barnard Approval.pdf

Comments:

Thermochemistry (in particular: total electronic energies; vibrational Gibbs free energy, entropy, enthalpy and zero-point energy corrections at 298.15 K and Basis Set Superposition Errors if applicable) represented in each file was calculated using quantum chemical software described earlier in this thesis. Both thermodynamics and kinetics were estimated using the mathematical tools available in Microsoft Excel.

Optimised molecular structures containing in the folders listed above can be viewed using Avogadro an open-source molecular builder and visualization tool, the latest version of which can be freely downloaded at http://avogadro.openmolecules.net/.